

**NOVEL GROUP 3/LANTHANIDE COMPLEXES  
AND THEIR APPLICATION TO  
INTRAMOLECULAR HYDROAMINATION AND  
RING-OPENING POLYMERISATION**

**Stacey D. Bennett MChem (Hons.)**



Thesis submitted to the University of Cardiff, Wales,  
for the degree of Doctor of Philosophy, December 2013.

## DECLARATION

This work has not been submitted in substance for any other degree or award at this or any other university or place of learning, nor is being submitted concurrently in candidature for any degree or other award.

Signed ..... (candidate)      Date .....

## STATEMENT 1

This thesis is being submitted in partial fulfillment of the requirements for the degree of PhD.

Signed ..... (candidate)      Date .....

## STATEMENT 2

This thesis is the result of my own independent work/investigation, except where otherwise stated. Other sources are acknowledged by explicit references. The views expressed are my own.

Signed ..... (candidate)      Date .....

## STATEMENT 3

I hereby give consent for my thesis, if accepted, to be available for photocopying and for inter-library loan, and for the title and summary to be made available to outside organisations.

Signed ..... (candidate)      Date .....

## STATEMENT 4: PREVIOUSLY APPROVED BAR ON ACCESS

I hereby give consent for my thesis, if accepted, to be available for photocopying and for inter-library loans **after expiry of a bar on access previously approved by the Academic Standards & Quality Committee.**

Signed ..... (candidate)      Date .....

**NOTICE OF SUBMISSION OF THESIS: POSTGRADUATE RESEARCH DEGREES****SECTION A: TO BE COMPLETED BY THE CANDIDATE AND SUBMITTED WITH THE THESIS**

CANDIDATE'S LAST NAME	BENNETT		
CANDIDATE'S FIRST NAME(S)	STACEY, DANIELLE		
CANDIDATE'S ID NUMBER	0511465		
SCHOOL	CHEMISTRY		
TITLE OF DEGREE	PhD		
FULL TITLE OF THESIS	NOVEL GROUP 3/LANTHANIDE COMPLEXES AND THEIR APPLICATION TO INTRAMOLECULAR HYDROAMINATION AND RING-OPENING POLYMERISATION		
IS THIS A RESUBMISSION?	YES		
THESIS SUBMITTED FOR EXAMINATION IN	Permanent Binding <input type="checkbox"/> Temporary binding <input type="checkbox"/>		
CANDIDATE SIGNATURE		DATE	

## SUMMARY OF THESIS: POSTGRADUATE RESEARCH DEGREES

### SECTION A: TO BE COMPLETED BY THE CANDIDATE AND SUBMITTED WITH THE THESIS

<b>Student ID Number:</b>	0511465
<b>Title:</b>	Miss
<b>Surname:</b>	BENNETT
<b>First Names:</b>	STACEY, DANIELLE
<b>School:</b>	CHEMISTRY
<b>Title of Degree:</b>	PhD
<b>Full Title of Thesis</b>	NOVEL GROUP 3/LANTHANIDE COMPLEXES AND THEIR APPLICATION TO INTRAMOLECULAR HYDROAMINATION AND RING-OPENING POLYMERISATION



<b>Student ID Number:</b>	<b>0511465</b>
---------------------------	----------------

This thesis describes the synthesis, characterisation and reactivity studies of a range of Group 3/Lanthanide complexes supported by bis(oxazoliny)phenyl amide (BOPA).

**Chapter 1:** Provides an introduction to the properties of the Lanthanides. Their application in asymmetric catalysis is reviewed, including catalysts supported by oxazoline ligands.

**Chapter 2** Describes density functional theory on a series of Group 3 BOPA complexes, the synthesis and characterisation of a new scandium amide-chloride precursor, thirty Group 3/lanthanide compounds supported by BOPA, six cation compounds supported by BOPA and three lithium BOPA compounds along with a discussion of the reactivity of compounds.

**Chapter 3:** Describes the application of compounds described in Chapter 2 to the intermolecular hydroamination reaction of aminoolefins.

**Chapter 4:** Describes a brief introduction to ring-opening polymerisation of *rac*-lactide and the application of compounds described in Chapter 2 to the ring-opening polymerisation of *rac*-lactide.

**Chapter 5:** A brief introduction to luminescence is provided and the photophysical properties of a selection of diamagnetic complexes and all paramagnetic complexes discussed in Chapters 2 are described. Also, the synthesis, characterisation and photophysical properties of five Group 3/lanthanide compounds supported by *pseudo*-substrate ligands are described.

**Chapter 6:** Details full experimental procedures and contains characterising data for all new compounds.

**Appendices A-B:** Full tables of crystallographic data for all new crystallographically characterised compounds described herein are provided in Appendix A. Publications from this thesis are provided in Appendix B.

## Acknowledgements

Firstly I would like to thank Dr Benjamin. D. Ward for his support, patience and the opportunity to work within his research group, for not only being a good boss but also a good friend. His help has been invaluable to me and I'm going to miss the coffee and cake! I would also like to thank Professor Philip Mountford and Dr Simon J. A. Pope for their help with some applications of the complexes made throughout this thesis.

Secondly, I would like to thank the rest of the group, past and present; Drs Andy J. Hallett and Tracy D. Nixon for leading the way and setting an example (if not always good)! In particular, I would like to thank Dr James. S. Wixey for the warm welcome when I joined the group and teaching me the true meaning of sharing! I am also indebted to Thomas M. O'Brian, I would like to thank him for his pearls of wisdom, long gossips and making the last two years more enjoyable. I would also like to thank Dr Paul Newman 'Woody', Dr Angelo J. Amoroso, Professor Pete Edwards, Dr Ian Fallis, Dr Nancy Dervisi, Steve, Owen, Kate, Dr Becky, Tim, Brendan and Ollie.

The technical staff at Cardiff have helped me enormously throughout the last three years, in particular Dr Rob Jenkins for the help with NMR experiments. I would also like to acknowledge the support from Robin, JC, Gaz, Simon, Terrie, Alison, Matt and finally Mal, who never fails to raise a smile.

I am lucky to have a very close and supportive family. I would first like to thank Lynn, Dave, Ann, John, Lisa and Mark for welcoming me into their warm family, you have made the past three years a lot easier. I am also greatly indebted to

my parents; you are the best parents I could wish for, thank-you for your love and support, I am lucky to have you.

Last but not least, I would like to thank Huw, he has been my rock for the past three years and has made me happier than I could ever imagine; dw i'n dy garu di.

# Abbreviations

## General

Ar	aryl
Ar <sup>F</sup>	C <sub>6</sub> F <sub>5</sub>
Bn	benzyl
<sup>n</sup> Bu	<i>normal</i> -butyl
<sup>t</sup> Bu	<i>tert</i> -butyl
Cp	cyclopentadienyl
Cy	cyclohexyl
DCM	dichloromethane
ET	electronic transfer
GPC	gel permeation chromatography
ISC	inter-system crossing
MALDI-Tof	matrix assisted laser desorption/ionisation – time of flight
Me	methyl
<i>Mer</i>	meridional
OTf	CF <sub>3</sub> SO <sub>3</sub>
PDI	polydispersity index
Ph	phenyl
iPr	<i>iso</i> -propyl
ROP	Ring-opening polymerisation
THF	tetrahydrofuran
Tol	toluene

## Nuclear Magnetic Resonance spectroscopic data

br	broad
$^{13}\text{C}\{^1\text{H}\}$	proton-decoupled $^{13}\text{C}$
COSY	Correlation SpectroscopY
d	doublet
$\delta$	chemical shift in ppm
J	coupling constant
HMBC	Heteronuclear Multiple Bond Connectivity
HSQC	Heteronuclear Multiple Quantum Coherence
m	multiplet
NMR	Nuclear Magnetic Resonance
s	singlet
t	triplet

## Infrared spectroscopic data

br	broad
IR	Infrared
m	medium
$\nu$	frequency
s	strong
w	weak

## **Note about numbering of literature compounds described in this thesis**

Literature compounds described in this thesis are numbered **1.x, 2.x, 3.x, 4.x** according to the Chapter in which they occur. The new compounds described in this thesis are numbered **1 – 17**.

## Contents

<b>Chapter 1 – Introduction</b> .....	1
1.1 General introduction .....	2
1.2 Hydroamination Catalysis .....	4
1.2.1 Cyclopentadienyl systems .....	9
1.2.2 Non cyclopentadienyl systems .....	10
1.3 Lanthanides bearing oxazoline ligands .....	21
1.3.1 Bis and trisoxazolines .....	21
1.4 Summary .....	41
1.5 References for Chapter 1 .....	44
<b>Chapter 2 - Coordination chemistry of BOPA supported Group 3/lanthanide complexes</b> .....	50
2.1 Introduction .....	51
2.2 Density Functional Theory .....	53
2.3 Ligand synthesis .....	58
2.3.1 Spectroscopic characterisation of <b>2.1a-c</b> .....	59
2.4 Preparation and Characterisation of Scandium Complexes .....	62
2.4.1 Synthesis of [Sc{N(SiMe <sub>3</sub> ) <sub>2</sub> } <sub>2</sub> Cl(THF)] ( <b>1</b> ) .....	62
2.4.1.1 X-ray crystal structure of [Sc{N(SiMe <sub>3</sub> ) <sub>2</sub> } <sub>2</sub> Cl(THF)] ( <b>1</b> )	63
2.4.1.2 Spectroscopic characterisation of ( <b>1</b> ) .....	65
2.4.2 Synthesis of [Sc(R-BOPA){N(SiMe <sub>3</sub> ) <sub>2</sub> }Cl] ( <b>2a-c</b> ) .....	66
2.4.2.1 Spectroscopic Characterisation of <b>2a</b> .....	67
2.4.2.2 Spectroscopic Characterisation of <b>2b-c</b> .....	70
2.4.3 Synthesis of [Sc(R-BOPA)(OC <sub>6</sub> H <sub>4</sub> Me)Cl] ( <b>3a-c</b> ) .....	72
2.4.3.1 Spectroscopic Characterisation of <b>3a-c</b> .....	73

2.4.4 Synthesis of [Sc(R-BOPA)N(SiMe <sub>3</sub> ) <sub>2</sub> ]OTf ( <b>4a-c</b> ) .....	74
2.4.4.1 Spectroscopic Characterisation of <b>4a-c</b> .....	75
2.4.5 Synthesis of [Sc(R-BOPA)(CH <sub>2</sub> SiMe <sub>2</sub> Ph) <sub>2</sub> ] ( <b>5a-c</b> ) .....	77
2.4.5.1 Spectroscopic Characterisation of <b>5a-c</b> .....	77
2.4.6 Synthesis of [Sc(R-BOPA)(CH <sub>2</sub> SiMe <sub>2</sub> Ph)][B(C <sub>6</sub> F <sub>5</sub> ) <sub>4</sub> ] ( <b>6a-c</b> ) ...	79
2.4.6.1 Spectroscopic Characterisation of <b>6a-c</b> .....	81
2.4.7 Further Reactions of [Sc(R-BOPA)(CH <sub>2</sub> SiMe <sub>2</sub> Ph) <sub>2</sub> ] ( <b>5</b> ) .....	82
2.5 Preparation and Characterisation of Yttrium Complexes .....	82
2.5.1 Preparation of Yttrium Silylamide Complexes .....	83
2.5.2 Spectroscopic Characterisation of <b>7a-c</b> .....	84
2.5.3 Synthesis of [Y(R-BOPA)(CH <sub>2</sub> SiMe <sub>2</sub> Ph) <sub>2</sub> ] ( <b>8a-c</b> ) .....	85
2.5.4 Spectroscopic Characterisation of <b>8a-c</b> .....	86
2.5.5 Synthesis of [Y(R-BOPA)(CH <sub>2</sub> SiMe <sub>2</sub> Ph)][B(C <sub>6</sub> F <sub>5</sub> ) <sub>4</sub> ] ( <b>9a-c</b> ) ...	88
2.5.6 Spectroscopic Characterisation of <b>9a-c</b> .....	89
2.6 Preparation and Characterisation of Lanthanum Complexes .....	90
2.6.1 Synthesis of [La(R-BOPA){N(SiMe <sub>3</sub> ) <sub>2</sub> ] <sub>2</sub> ] ( <b>10a-c</b> ) .....	90
2.6.2 Spectroscopic Characterisation of <b>10a-c</b> .....	91
2.7 Preparation and Characterisation of Paramagnetic Complexes .....	92
2.7.1 Synthesis of [Ln(R-BOPA){N(SiMe <sub>3</sub> ) <sub>2</sub> ] <sub>2</sub> ] ( <b>11 - 13</b> ) .....	92
2.7.2 X-ray crystal structure of [Nd(Ph-BOPA){N(SiMe <sub>3</sub> ) <sub>2</sub> ] <sub>2</sub> ] ( <b>12a</b> ) and [Sm(Ph-BOPA){N(SiMe <sub>3</sub> ) <sub>2</sub> ] <sub>2</sub> ] ( <b>13a</b> ) .....	94
2.7.3 Spectroscopic Characterisation of 11-13 .....	97
2.8 Synthesis and characterisation of Li(R-BOPA) ( <b>14a-c</b> ) .....	100
2.8.1 Spectroscopic Characterisation of <b>14a-c</b> .....	101



2.9 Relative Proportion of Isomers .....	101
2.10 Summary .....	104
2.11 References .....	106
<b>Chapter 3 – Intramolecular Hydroamination Reaction with BOPA Supported</b>	
<b>Catalysts.....</b>	<b>111</b>
3.1 Introduction .....	112
3.2 Asymmetric hydroamination/cyclisation catalysis using Group 3 and lanthanide complexes.....	115
3.2.1 Hydroamination catalysis with scandium complexes.....	115
3.2.2 Hydroamination catalysis with yttrium complexes.....	118
3.2.3 Hydroamination catalysis with lanthanum complexes.....	122
3.2.4 Hydroamination catalysis with paramagnetic lanthanide complexes	125
3.3 Summary and conclusions.....	132
3.4 References for Chapter 3.....	134
<b>Chapter 4 – Ring Opening Polymerisation of <i>rac</i>-lactide with BOPA supported catalysts.....</b>	
4.1 Introduction .....	137
4.2 Results and Discussion .....	140
4.2.1 Ring-opening polymerisation of lactide using lanthanide BOPA complexes.....	140
4.3 Summary and conclusions .....	156
4.4 References for Chapter 4.....	158
<b>Chapter 5 – Photophysical properties of trivalent Group 3 and lanthanide BOPA complexes .....</b>	
	160

5.1 Introduction .....	161
5.2 Density Functional Theory (DFT) Calculations .....	164
5.3 Preparation and Characterisation of [Ln(R-BOPA){NHCH <sub>2</sub> C(Ph) <sub>2</sub> C <sub>3</sub> H <sub>7</sub> } <sub>2</sub> ] (Ln = La 15, Pr 16, Nd 17) .....	167
5.3.1 Synthesis of the <i>pseudo</i> substrate <b>5.1</b> .....	168
5.3.2 Spectroscopic Characterisation of [La(iPr- BOPA){NHCH <sub>2</sub> C(Ph) <sub>2</sub> C <sub>3</sub> H <sub>7</sub> } <sub>2</sub> ] ( <b>15</b> ) .....	168
5.3.3 Spectroscopic Characterisation of [Ln(R-BOPA){NHCH <sub>2</sub> C(Ph) <sub>2</sub> C <sub>3</sub> H <sub>7</sub> } <sub>2</sub> ] (Ln = Pr <b>16</b> , Nd <b>17</b> ) .....	169
5.4 Photophysical Measurements .....	170
5.4.1 Diamagnetic complexes <b>2a-c</b> , <b>5a-c</b> and <b>10a-c</b> .....	170
5.4.2 Paramagnetic complexes <b>11a-c</b> , <b>12a-c</b> and <b>13a-c</b> .....	173
5.4.3 Photophysical properties of complexes <b>16</b> and <b>17a-c</b> .....	176
5.5 Summary .....	181
5.6 References for Chapter 6 .....	182
<b>Chapter 6 – Experimental and Characterising data</b> .....	184
6.1 General Methods and Instrumentation .....	185
6.1.1 Literature preparations .....	187
6.2 Chapter 2 .....	187
6.3 Chapter 3 .....	232
6.4 Chapter 4 .....	233
6.5 Chapter 5 .....	233
6.6 References for Chapter 6 .....	239

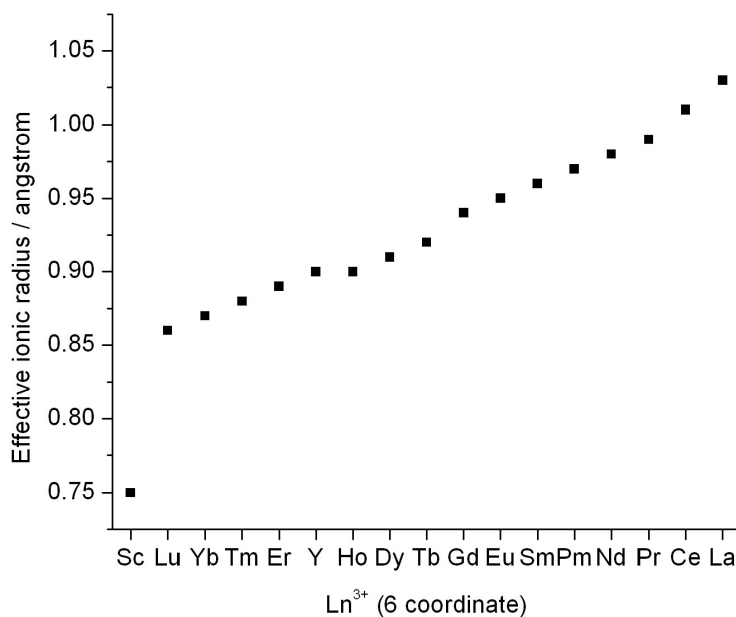
# **CHAPTER 1**

## **Introduction**

## 1.1 General Introduction

The lanthanide elements have found many applications in functional metal complexes, including catalysis. Research into the lanthanides usually includes the Group 3 elements in addition to the  $4f$  block; many comparisons have been drawn between Group 3 and the lanthanides, since they have many properties in common, such as their oxidation state. Although the chemical properties of the Group 3 and lanthanide metals are similar, metal complexes of these elements exhibit reactivity trends that are influenced by their ionic radius. Lanthanum has the largest ionic radius of the series (1.03 Å for a 6-coordinate  $\text{La}^{3+}$  ion) and scandium the smallest (0.75 Å). The radii of the remaining lanthanides lie within this range, whereby they decrease in size with increasing atomic number (Fig. 1).<sup>1</sup> This is the result of the  $f$ -electrons' ineffective shielding of the other valence electrons from the nuclear charge. This poor shielding ability of the  $f$ -electrons is the main result of the orbitals high angular nodality. The  $f$ -orbitals are responsible for many characteristics of these elements, such as photophysical properties and their coordination chemistry.

The coordination chemistry of the lanthanides is largely dominated by the +3 oxidation state. The fourth ionisation energy is sufficiently large that the +4 oxidation state is rarely observed for these metals, whilst the third ionisation energy is often low enough to preclude the +2 oxidation state. Nevertheless, there are some notable exceptions. For example, tetravalent cerium complexes and divalent ytterbium and europium complexes are well known. The cerium(IV) complexes are the result of the poor stabilisation of the  $f$ -orbitals at the beginning of the series and the divalent complexes are accessible due to the relatively large third ionisation energies of ytterbium and europium. A more detailed discussion of lanthanides in oxidation states other than +3 lies beyond the scope of this thesis.



**Fig. 1** Effective ionic radii for 6 coordinate Ln<sup>3+</sup> ions<sup>1</sup>

With little geometrical preference in their coordination complexes (compared to transition metals), steric repulsion between ligands is a significant contributor to the coordination chemistry found for lanthanides (*i.e.* geometry, coordination number). It is therefore unsurprising that the ionic radius of a lanthanide ion can have a profound effect on its coordination chemistry. For example, a metal with a larger radius will show a preference for a higher coordination number, which may be manifested in the incorporation of solvent molecules into the coordination sphere. Additionally, in catalytically active complexes, larger coordination numbers can afford complexes that are less defined with respect to substrate coordination, thereby leading to lower selectivity levels. After giving due consideration to these factors, complexes bearing multidentate ligands are overwhelmingly used in functional metal complexes incorporating Group 3 or lanthanide metal ions. The general coordination chemistry of the lanthanides has been reviewed, and the reader is directed to these articles for a detailed treatment of the area.<sup>2-4</sup>

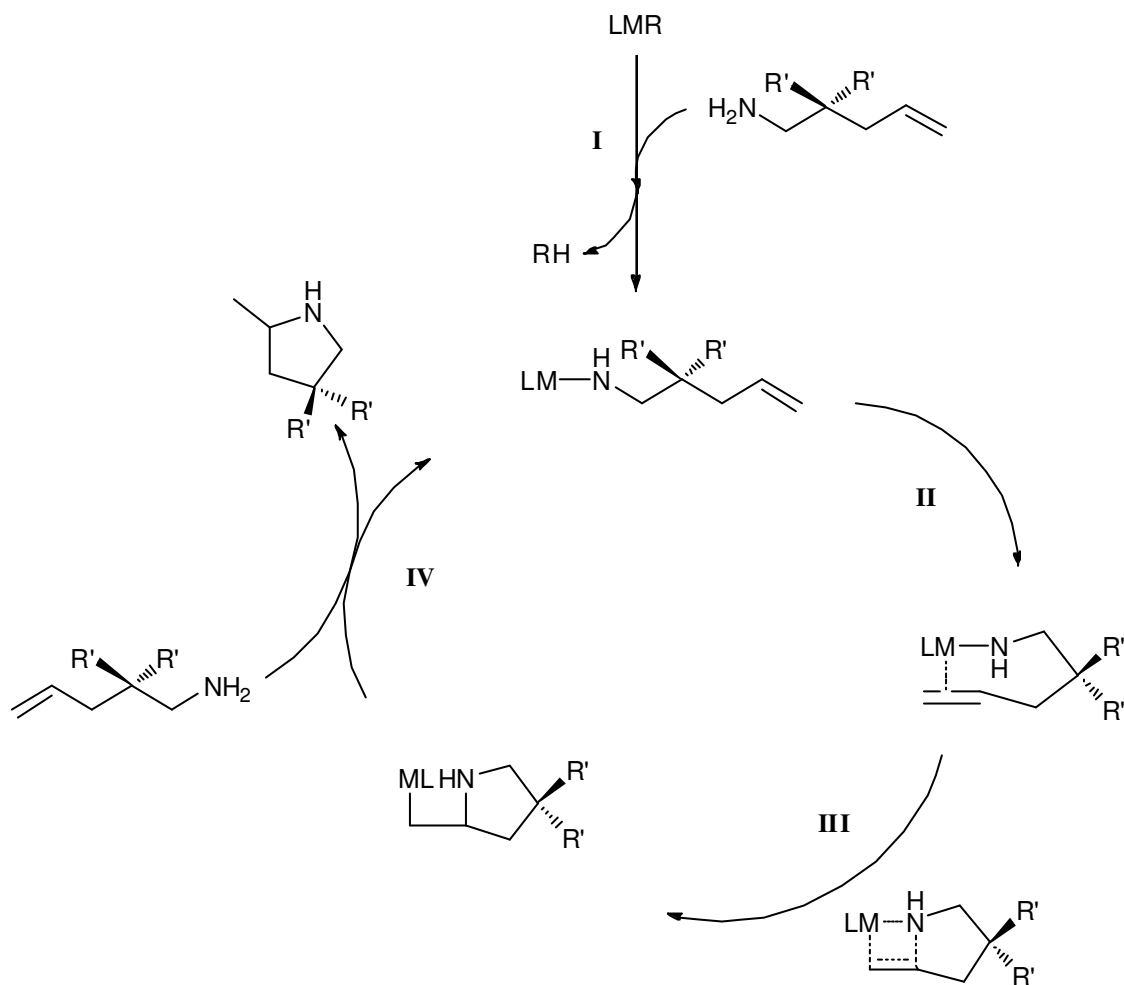
The choice of ligand can have a significant influence on the subsequent reactivity and selectivity on a catalytically active complex, and the supporting ligand must be chosen to

provide the necessary control for any further applications. Several factors need to be considered when designing a ligand: the steric bulk offered by the ligand periphery; the number of donor atoms; the nature of the coordinating atoms; the bite angle; and the nature of any co-ligands. Specific considerations pertinent to this thesis are related to organometallic alkyl complexes, which become increasingly thermally unstable when coordinated to lanthanides with larger ionic radii. Therefore alkyl complexes of the larger lanthanides are often less accessible and amide ligands can be employed; amide complexes are suitable alternatives for the catalytic applications discussed herein.

The coordination chemistry of the lanthanides has been reviewed extensively, and the reader is directed for a general treatment of the area, whilst this chapter describes specific examples of chiral complexes that are relevant to the research discussed in Chapters 2-5. Some of the most successful Group 3 and lanthanide complexes in asymmetric catalysis are supported by binaphyl and oxazoline derived ligands.<sup>5-12</sup> Complexes supported by these ligands, and their catalytic applications, will be discussed.

## 1.2 Hydroamination Catalysis

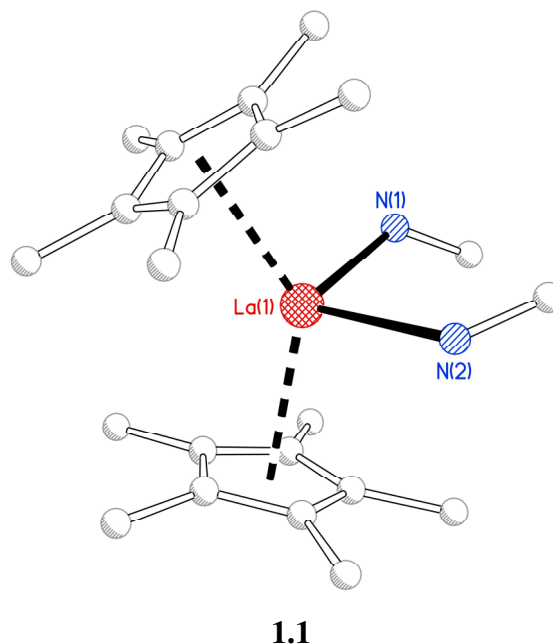
Hydroamination can be performed asymmetrically with the aid of a suitable catalyst. It is an atom efficient reaction where a catalyst enables the reaction between olefins and amines. A widely accepted mechanism for the lanthanide-catalysed intramolecular hydroamination of aminoolefins is shown in Scheme 1.<sup>13-15</sup>



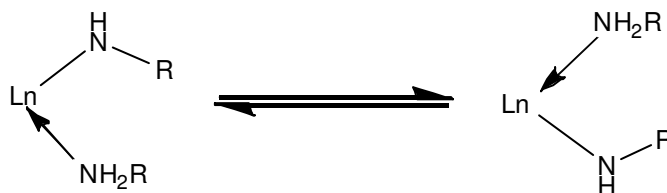
**Scheme 1** The widely accepted mechanism for Ln/Group 3 metal-catalysed intramolecular hydroamination

The first step of this mechanism (I) involves the formation of an amide bond *via* the protonolysis of a co-ligand by the amine substrate. Insertion of the olefin into the metal-N<sub>amide</sub> bond follows and occurs *via* a four-membered transition state (III). This is the rate determining step, thus rendering the reaction zero order in substrate.<sup>14</sup> The resulting metal alkyl species will either react with a second aminoolefin (protonation of the resulting M-C bond), releasing the heterocyclic product (IV), or rearrange to give the N-bound heterocycle. This can remain coordinated to the catalyst or react with a second aminoolefin.

The X-ray crystal structure of  $[\text{Cp}_2'\text{LaNHCH}_3(\text{H}_2\text{NCH}_3)]$  (**1.1**) (Fig. 2) has been obtained, suggesting that the catalyst resting state is in fact a Ln-amine/amido species. This species is present even in low amine concentrations.<sup>13</sup>



**Fig. 2** Molecular structure of  $[\text{Cp}_2'\text{LaNHCH}_3(\text{H}_2\text{NCH}_3)]$  (**1.1**). H atoms omitted for clarity

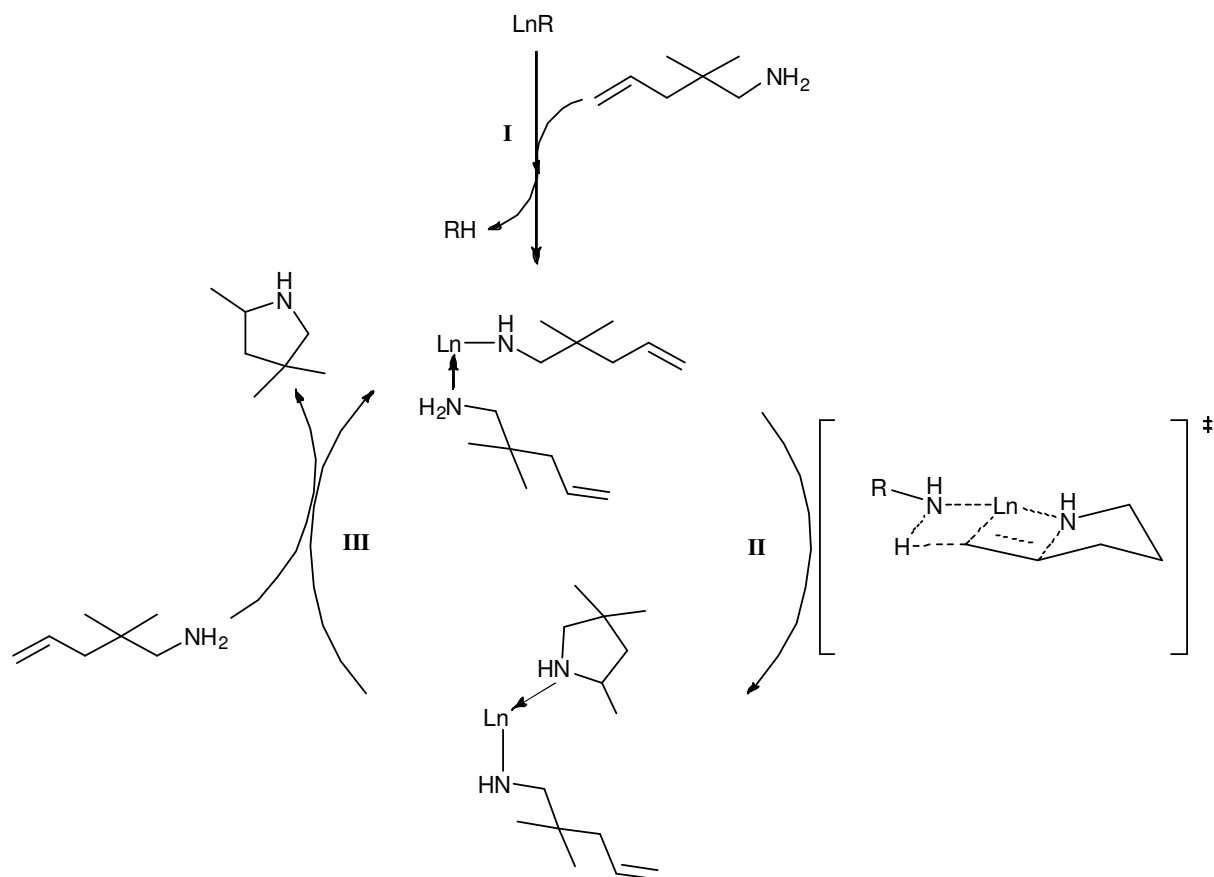


**Scheme 2** The proton exchange between amine and amido ligands

In conjunction with evidence obtained from other mechanistic studies, the reaction pathway may be more complicated. Kinetic isotope experiments show that a deuterium transfers specifically to a  $\beta$ -carbon, indicating that a proton is transferred between amine and olefin. As well as evidence of the rapid proton exchange between amine and amido ligands (Scheme 2),



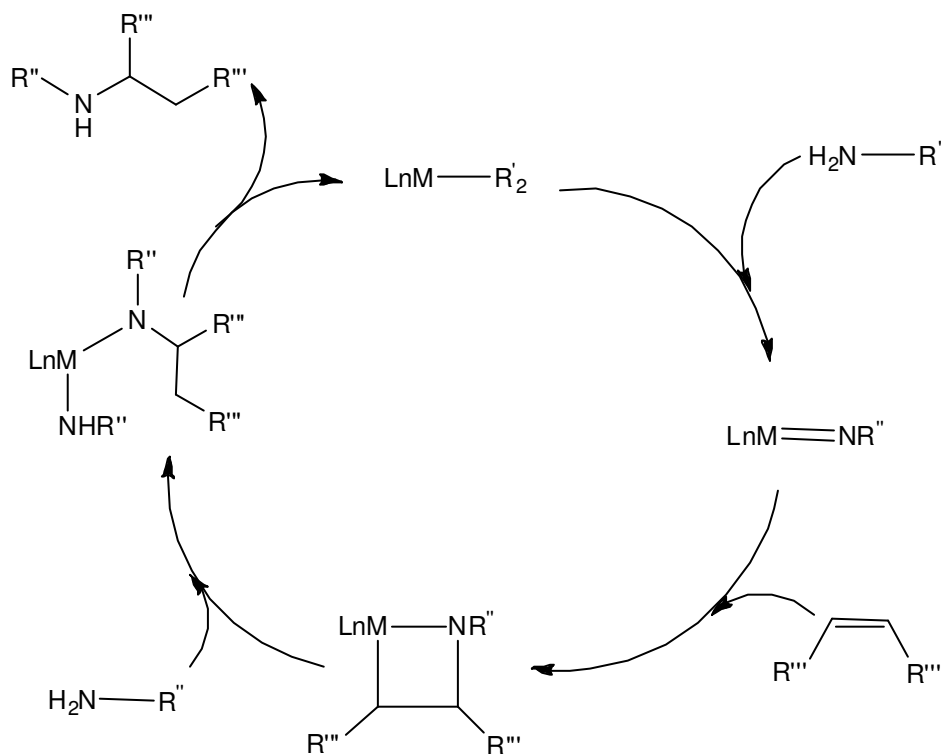
there is evidence for exchange with free amine but not product. This has led to an alternative mechanism being proposed (Scheme 3).<sup>13</sup>



**Scheme 3** Alternative mechanism incorporating Ln-amine/amido species

This mechanism illustrates a chair-like, highly ordered transition state consistent with the calculated enthalpic and entropic parameters. The concerted transfer of a proton to the Ln-C bond as it is being formed stabilises the charge build up and ensures that the insertion is irreversible (consistent with experimental data). This mechanism involves a catalyst resting state more akin to the model resting state shown in Fig. 2 and is well-supported, by detailed mechanistic studies, and therefore should not be disregarded in any interpretation of catalytic data.

Whilst a similar mechanism has been proposed for some cationic zirconium complexes, a different mechanism has been proposed for neutral Group 4 catalysts, involving an imido intermediate (Scheme 4).<sup>16-20</sup>



**Scheme 4** A reaction mechanism for the Group 4 catalysed intermolecular hydroamination

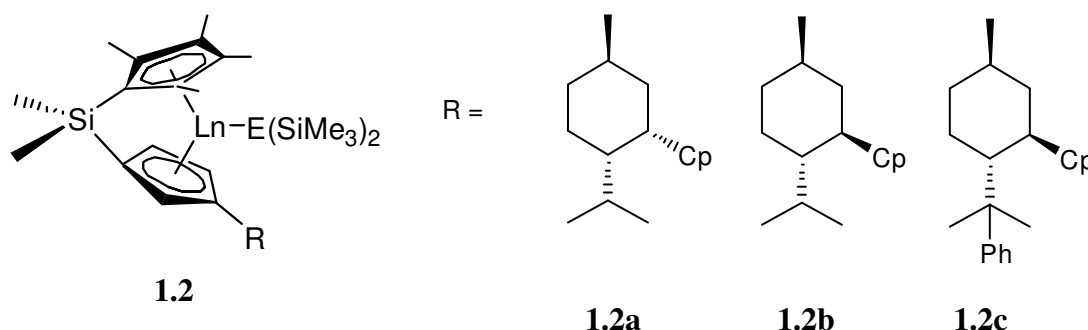
In Scheme 4 a [2+2] cycloaddition follows the formation of the imido species. However, the imido species is sometimes considered to be in equilibrium with a dimeric species incorporating two bridging  $\mu^2$ -imido ligands, and the formation of the terminal imido is often considered the rate-determining step.

The hydroamination reaction has been extensively studied; early and late transition metals (Groups 3-5 and 8-10) have been commonly used, as well as the lanthanides.<sup>12, 21, 22</sup> There are fewer examples of lanthanide catalysed intermolecular hydroamination when compared to intramolecular hydroamination.<sup>15, 23-26</sup> Lanthanide catalysts are highly sensitive to air and water, however, lanthanide-metallocene systems have been highly successful.

Recent research has concentrated on moving this research area into the applications of non-metallocene catalysts.

### 1.2.1 Cyclopentadienyl systems

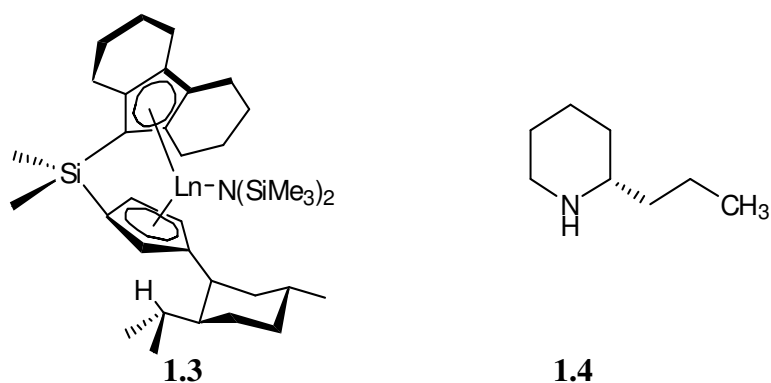
The first asymmetric hydroamination reaction with lanthanides was reported with complexes supported by *ansa*-cyclopentadienyl ligands.<sup>27-29</sup> Three derivatives of the chiral  $C_1$ -symmetric catalyst were synthesised (Fig. 3); the catalytic activity increased with lanthanide ionic radius.



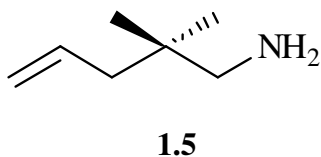
**Fig. 3** Lanthanide cyclopentadienyl catalysts. Ln = La, Nd, Sm, Y, Lu. E = N, CH

Varying the cyclopentadienyl substituent R had little effect on enantioselectivities, but it was reported that the Cp ligands did partially dissociate, *via* protonation of one Cp ring, and thus statistically inverting the chirality at the metal centre. The differences in selectivities are reported as being a result of the lanthanide ionic radius. The highest selectivities were obtained with the samarium catalyst with 2,2-dimethyl-pent-4-enylamine (**1.5**, Fig.5), up to 74% ee.

Complexes **1.3** (Fig. 4) and **1.2** are both supported by Cp derived ligands. However, **1.3** is supported by a more sterically demanding ligand than **1.2**.<sup>30</sup> When coordinated to samarium or yttrium, higher enantioselectivities were obtained for a geminal dimethyl-substituted aminoolefin (**1.5**, Fig. 5). The successful studies involving **1.3** resulted in the catalyst being employed in the synthesis of (+)-coniine (91%, 63% ee).<sup>31</sup>



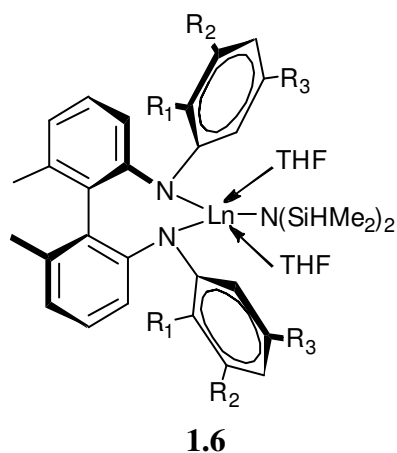
**Fig. 4** Left: Lanthanide catalyst used to synthesise (+)-coniine. Right: (+)-coniine



**Fig. 5** Geminal dimethyl aminoolefin used in hydroamination catalysis

### 1.2.2 Non-cyclopentadienyl systems

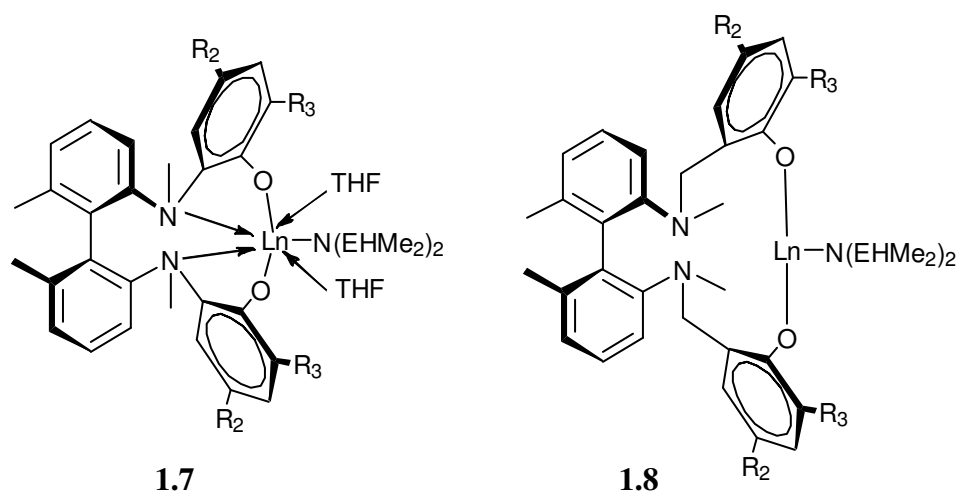
A decade ago several groups began reporting complexes bearing alternatives to the ubiquitous cyclopentadienyl ligands.<sup>32-34</sup> Several bisarylamido supported complexes were synthesised and their catalytic activity studied (Fig. 6).<sup>35</sup>



**Fig. 6** Chiral bisarylamido catalyst. Ln = La, Sm, Y. R<sub>1</sub> = H, Et, Cy, Me. R<sub>2</sub> = <sup>t</sup>Bu, H. R<sub>3</sub> = <sup>t</sup>Bu, H

The enantioselectivities obtained for the hydroamination reaction when catalysed by **1.6** decreased with increasing ionic radius of the metal ion (Y 50%, Sm 33% and La 18% ee), and moreover these catalysts showed only low activities. This was rationalised by the low basicity of  $\text{HN}(\text{SiHMe}_2)_2$  ( $\text{pK}_a = 22.8$ ),<sup>36</sup> causing the initiation step to be slow, (as the equilibrium will lie towards the precatalysts).<sup>37, 38</sup> When a significantly more basic coligand was used the rate of reaction increased, however, there was no increase in enantioselectivity.

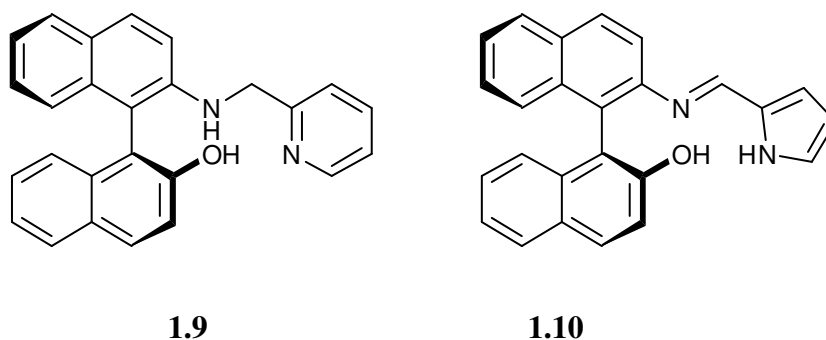
In order to improve the activity/enantioselectivity several alterations were made to the ligand skeleton.<sup>39</sup> Firstly, a methoxy group was introduced at one or both  $\text{R}_1$  positions, affording ligands with anionic N and neutral O donors. Secondly, a hydroxyl group was introduced at  $\text{R}_1$  whilst methylating the two nitrogens (**1.7** and **1.8**), affording neutral N and anionic O donors (Fig. 7).



**Fig. 7** Phenyloxy-bisarylamine complexes

The enantioselectivities obtained with **1.7** did not increase upon introducing these alterations, however **1.8**, which differs only in the methylene spacers between the amines and phenoxide groups, gave an increase in the enantioselectivity (61%). The data obtained for these complexes highlight the importance of the bonding mode and the bite angle of the supporting ligand(s) in controlling the transfer of chiral information to the catalytically active site.

Two ligands with similar coordination motifs are the 2-amino-2'-hydroxy-1,1'-binaphthyl (NOBIN) ligands.<sup>40</sup> The two ligands investigated, (S)-2-(pyridine-2-ylmethylamino)-2'-hydroxy-1,1'-binaphthyl (**1.9**) and (S)-5,5',6,6',7,7',8,8'-octahydro-2-(pyrrol-2-ylmethyleneamino)-2'-amino-2'-hydroxy-1,1'-binaphthyl (**1.10**) were coordinated to yttrium and samarium (Fig. 8).


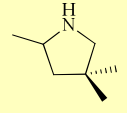
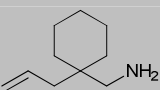
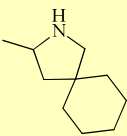
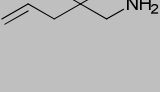
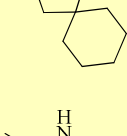
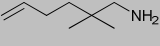
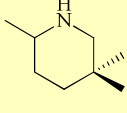

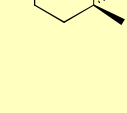

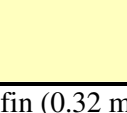


**Fig. 8** Chiral NOBIN-based ligands

Lanthanide amide complexes of **1.9** and **1.10** exist as dimeric structures. These complexes were tested in asymmetric hydroamination, and in the ring-opening polymerisation (ROP) of *rac*-lactide. The results of the hydroamination studies are shown in Table 1.

Both Y-**1.9** and Sm-**1.10** showed excellent conversions for the asymmetric hydroamination of aminoolefins, however, only moderate enantioselectivities were observed, 30-55%. When the catalysts were used in the polymerisation of *rac*-lactide, both complexes produced isotactic rich polymers. Also, the rate of reaction was found to be dependent on solvent; polymerisation with Y-**1.9** proceeded more slowly in THF than in toluene, whereas this difference was not observed when Sm-**1.10** was employed. These complexes show how solvent dependence can vary with ionic radius of the lanthanide ion, possibly as a result of varying coordination number, and must be considered when optimising a catalytic reaction.

**Table 1.** The enantioselective hydroamination of aminoolefins using NOBIN supported Ln complexes<sup>a</sup>

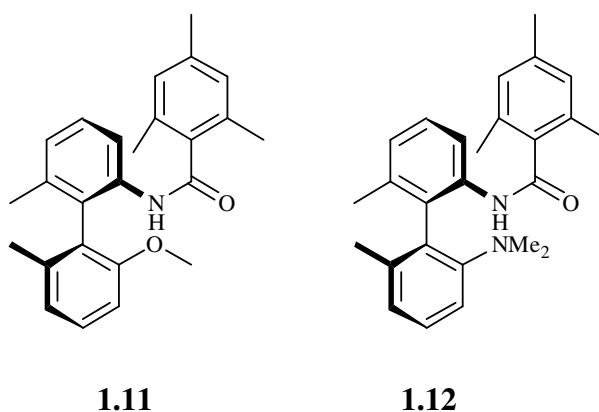
Entry	Catalyst	Substrate	Product	Temp. (°C)	Time (h)	Conv. (%) <sup>b</sup>	ee (%) <sup>c</sup>
1	Y 1.9			20	16	95	54
2	Sm1.10			20	16	98	55
3	Y 1.9			20	16	100	48
4	Sm 1.10			20	16	100	54
5	Y 1.9			120	16	92	30
6	Sm 1.10			120	16	95	34

<sup>a</sup>Conditions: C<sub>6</sub>D<sub>6</sub> (0.70 mL), aminoolefin (0.32 mmol), catalyst (0.008 mmol)

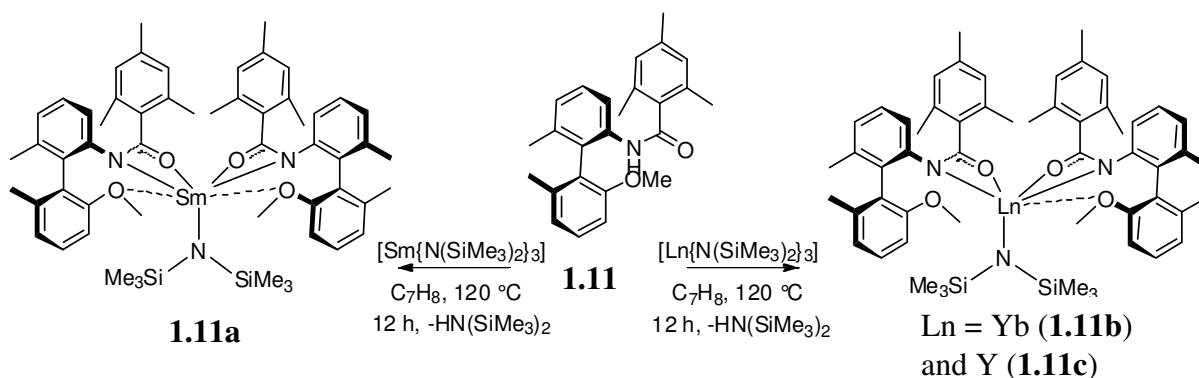
<sup>b</sup>Determined by <sup>1</sup>H NMR based on *p*-xylene as the internal standard.

<sup>c</sup>Determined by <sup>1</sup>H NMR of its diastereomeric (S)-(+)-*O*-acetylmandelic acid salt.<sup>41</sup>

The chiral amidate ligands, **1.11** and **1.12** (Fig. 9) similarly possess a same biaryl structural motif.<sup>42, 43</sup> Two equivalents of the amidate ligands were reacted with [Ln(N(SiMe<sub>3</sub>)<sub>2</sub>)<sub>3</sub>] and studied in asymmetric hydroamination and in the ROP of *rac*-lactide.<sup>44</sup>

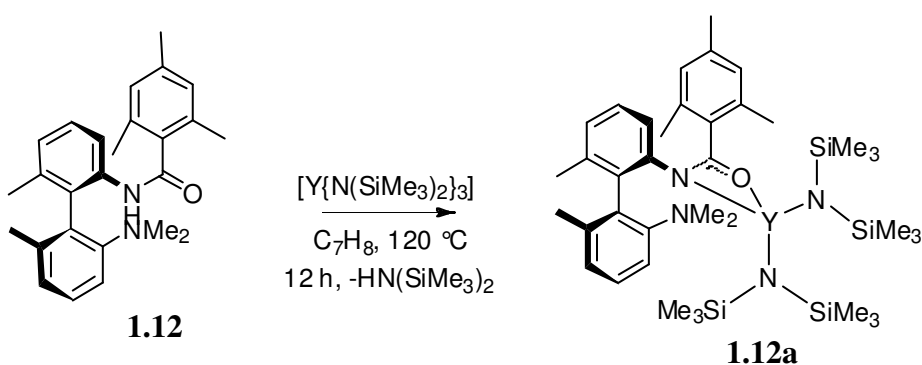
**Fig. 9** Chiral amidate ligands

When two equivalents of **1.11** were reacted with  $[\text{Sm}\{\text{N}(\text{SiMe}_3)_2\}_3]$ , a  $C_2$  symmetric complex was formed. However, when **1.11** was reacted with the analogous Y and Yb salts, a  $C_1$ -symmetric complex was formed. This differs from the Sm complex by the decoordination of one of the methoxy groups, thus affording a 6 coordinate complex for Y and Yb, and a 7 coordinate complex for Sm (Scheme 5). This difference presumably has roots in the larger ionic radius of Sm being able to more readily accommodate higher coordination numbers.



**Scheme 5** Coordination of **1.11** to Sm, Yb and Y amides

When  $[\text{Y}\{\text{N}(\text{SiMe}_3)_2\}_3]$  was reacted with **1.12**, only one ligand coordinated, even when two equivalents of ligand were added (Scheme 6). This is a result of the extra steric bulk of **1.12** compared to **1.11**.



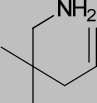
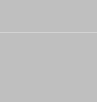

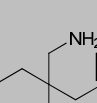
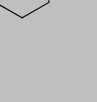
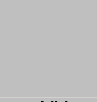
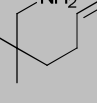

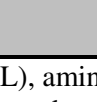
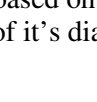
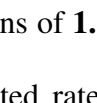
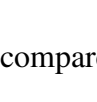

**Scheme 6** Coordination of **1.12** with  $[\text{Y}\{\text{N}(\text{SiMe}_3)_2\}_3]$

The four complexes (**1.11a-c** and **1.12a**) were used in hydroamination catalysis and the results are shown in Table 2.



It is noticeable that **1.11a** is the superior catalyst, giving higher enantiomeric excesses with comparable activity to the other catalysts at 60 °C. When the temperature was decreased to 20 °C, the enantioselectivity increased from 66 to 74% (entry 1 and 2), albeit with a decrease in conversion, from 95 to 27%.

**Table 2.** Hydroamination results for amidate complexes **1.11a-c** and **1.12a**<sup>a</sup>

Entry	Catalyst	Substrate	T (°C)	Time (h)	Conv. (%) <sup>b</sup>	ee (%) <sup>c</sup>
1	<b>1.11a</b>		60	16	95	66
2	<b>1.11a</b>		20	48	27	74
3	<b>1.11b</b>		60	16	97	54
4	<b>1.11c</b>		60	16	90	50
5	<b>1.12a</b>		60	16	100	13
6	<b>1.11a</b>		60	16	98	60
7	<b>1.11b</b>		60	16	95	48
8	<b>1.11c</b>		60	16	92	45
9	<b>1.12a</b>		60	16	100	12
10	<b>1.11a</b>		120	24	92	38
11	<b>1.11b</b>		120	24	95	34
12	<b>1.11c</b>		120	24	90	28
13	<b>1.12a</b>		120	24	100	24

<sup>a</sup> Conditions: C<sub>6</sub>D<sub>6</sub> (0.70 mL), aminoolefins (0.32 mmol), catalyst (0.016 mmol).

<sup>b</sup> Determined by <sup>1</sup>H NMR based on *p*-xylene as the internal standard.

<sup>c</sup> Determined by <sup>1</sup>H NMR of its diastereomeric (S)-(+)-*O*-acetylmandelic acid salt.<sup>41</sup>

When comparing reactions of **1.11a-c** at identical temperatures, the conversions were similar, but **1.12a** showed elevated rates. This is attributed to the reduced steric bulk around the metal, offered by **1.12** compared to **1.11**, which could also be responsible for the lower

enantioselectivities observed for **1.12a**. The range of enantioselectivities reported for all reactions (12-74%) show a clear dependence on ionic radius and ligand steric bulk.

In the ROP of *rac*-lactide, **1.11c** and **1.12a** showed a dependence on the identity of the solvent. When the reaction was carried out in THF the rate of reaction was slower, an unsurprising effect explained by the ligation of THF competing with the lactide substrate. Different behaviour was observed for Sm-**1.10**; polymerisation with Sm-**1.10** showed little dependence on solvent.<sup>40</sup> No definitive explanation was provided, but this example serves to demonstrate the subtle complexity with which solvent coordination can impact on the catalytic performance of a complex.

Similar ligand frameworks have been coordinated to lanthanides (**1.13** – **1.16**, Fig. 10), and have shown varying success in hydroamination catalysis.<sup>32</sup> When substrate **1.5** (Fig. 5) was used, enantioselectivities ranged from 8–53%. The complexes containing N(SiHMe<sub>2</sub>)<sub>2</sub> co-ligands were slow to initiate;<sup>38</sup> to overcome this issue, alkyl coligands or more basic amides were used. This dramatically increased the catalytic activity, and the rate showed the expected zero-order dependence on substrate.<sup>45</sup>

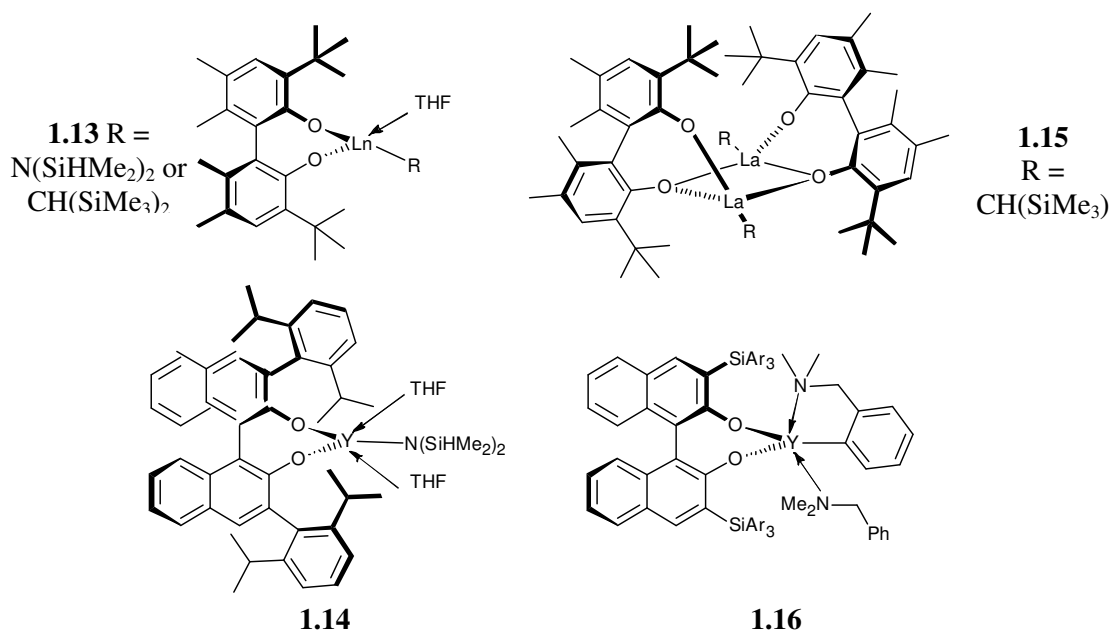
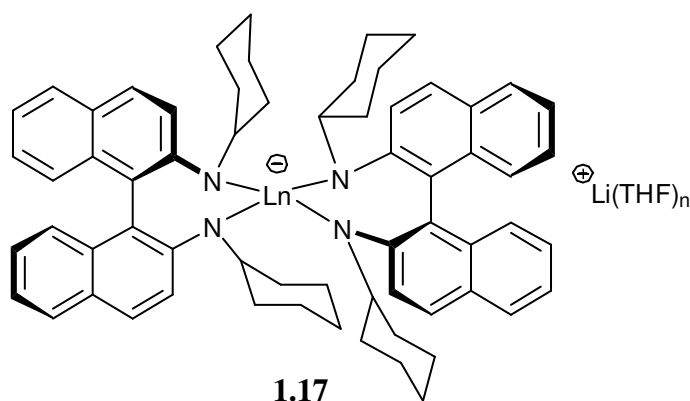


Fig. 10 Lanthanide bisphenoxy complexes

The catalyst that gave the highest enantioselectivity was the yttrium complex bearing a binaphtholate ligand containing large silyl-aryl groups (**1.16**, Fig 10).<sup>46</sup> This exhibited enantioselectivities of up to 83%.


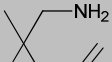
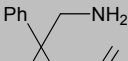

The coordination of a binap-derived ligand to several lanthanides has been investigated.<sup>34, 47</sup> Two binaphthylamine ligands coordinated to the lanthanide ion, affording an anionic “ate” complex with a  $[\text{Li}(\text{THF})_4]^+$  counterion (Fig. 11). The ytterbium and lutetium catalysts bearing cyclohexyl<sup>48</sup> (**1.17a-b**) and isopropyl groups (**1.18a-b**) were investigated in hydroamination catalysis.<sup>49</sup>



**Fig. 11** Lanthanide “ate” complexes. Ln = Yb, Sm, Nd and Lu

The catalysts showed moderate-good enantioselectivities for the small range of amino-olefins investigated; Table 3 shows the results for the ytterbium complexes. Complex **1.17a** was a more active catalyst than **1.18a**, although, on the whole there was no significant difference in enantioselectivity; the range of enantioselectivities for **1.17a** and **1.18a** was 42-78% (Table 3). Similar results were observed for **1.17b** and **1.18b**, the enantioselectivities were comparable but the activities were greater than **1.17a** and **1.18a**. The rate of conversion was twice that for the analogous ytterbium catalyst, thus allowing lower temperatures to be used. However, the enantioselectivities were only marginally increased. These complexes support the conclusions from the previously discussed complexes, that by altering the lanthanide metal, a marked difference in the catalytic behaviour can be observed.

**Table 3.** Intramolecular hydroamination reaction with  $[\text{Li}(\text{THF})_n][\text{Yb}[(\text{R})\text{-C}_{20}\text{H}_{12}\text{N}_2(\text{C}_{12}\text{H}_{22})_2]_2]$  (**1.17a** and **1.18a**)<sup>a</sup>

Entry	Catalyst	Substrate	T (°C)	Cat mol%	Time	Conv. %	ee % <sup>b</sup>
1	1.18a		25	5	48 h	67	70
2	1.18a		25	5	6 d	100	66
3	1.17a		25	6	18 h	94	65
4	1.17a		25	10	20 h	58	68
5	1.17a		0	10	4 d	88	76
6	1.18a		25	10	7 d	49	69
7	1.18a		60	10	46 h	98	42
8	1.17a		25	10	48 h	34	75
9	1.17a		25	10	7 d	77	73
10	1.18a		25	10	24 h	100	50 <sup>c</sup>
11	1.17a		25	3	21 h	100	62 <sup>c</sup>
12	1.17a		0	10	6 d	100	66 <sup>c</sup>
13	1.17a		25	10	4 d	83	69
14	1.17a		0	10	6 d	36	78
15	1.17a		0	10	16 d	74	77

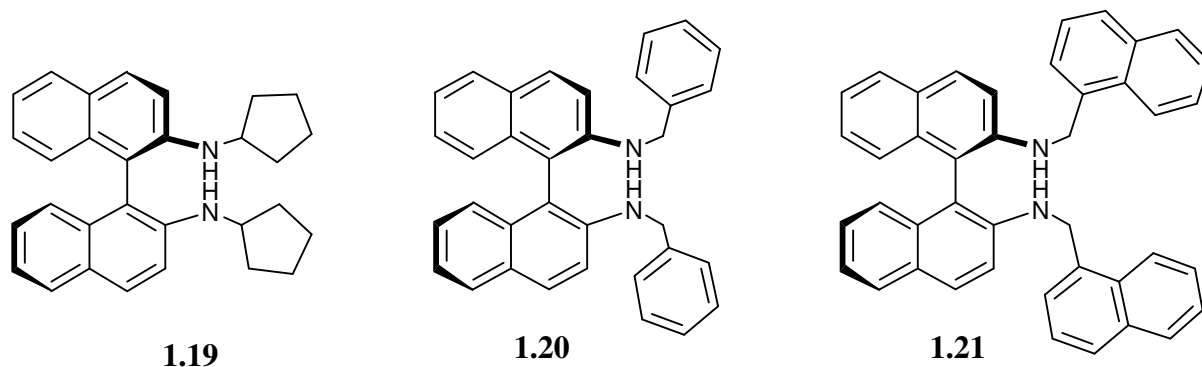
**1.18a** =  $[\text{Li}(\text{THF})_n][\text{Yb}[(\text{iPr})\text{-C}_{20}\text{H}_{12}\text{N}_2(\text{C}_{12}\text{H}_{22})_2]_2]$ , **1.17a** =  $[\text{Li}(\text{THF})_n][\text{Yb}[(\text{cyclohexyl})\text{-C}_{20}\text{H}_{12}\text{N}_2(\text{C}_{12}\text{H}_{22})_2]_2]$ .

<sup>a</sup>Reactions at 25 °C were conducted in  $\text{C}_6\text{D}_6$  and reactions at 0 °C were performed in toluene.

<sup>b</sup> Enantiomeric excesses were determined by GC analysis of Mosher amides unless otherwise indicated

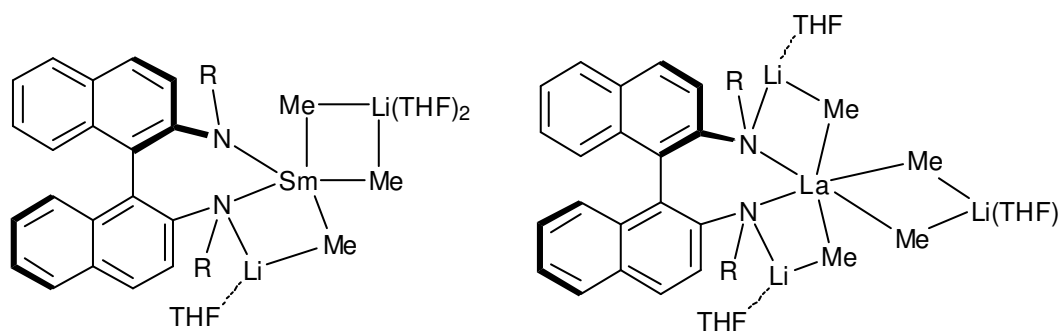
<sup>c</sup> Enantiomeric excess determined by NMR analysis in chiral liquid crystals.

A series of chiral binaphthylamido ligands were coordinated to La and Sm alkyls, and their catalytic activity investigated.<sup>50</sup> The three ligands studied (Fig. 12); are all simple binaphthyl moieties with two secondary amines at the ortho position. Thus, 2 co-ligands are eliminated by protonolysis upon coordination.



**Fig. 12** Binaphthylamido ligands coordinated to La and Sm

$[\text{Li}(\text{THF})_n]_3[\text{LnMe}_6]$  “ate” complexes were formed when the protio-ligands were reacted with  $[\text{Li}(\text{THF})_n]_3[\text{LnMe}_6]$  (Fig. 13), which were used in the asymmetric hydroamination of 1,3-amino-dienes. The previously reported yttrium complex (Y-**1.19**) was very active in hydroamination, with enantioselectivities of up to 75%. However, when it was used in the cyclisation of (4E,6)-heptadiene-1-amine, a mixture of diastereomers were isolated, all with low enantioselectivities ((E) 17-55% ee and (Z) 0 – 21% ee).

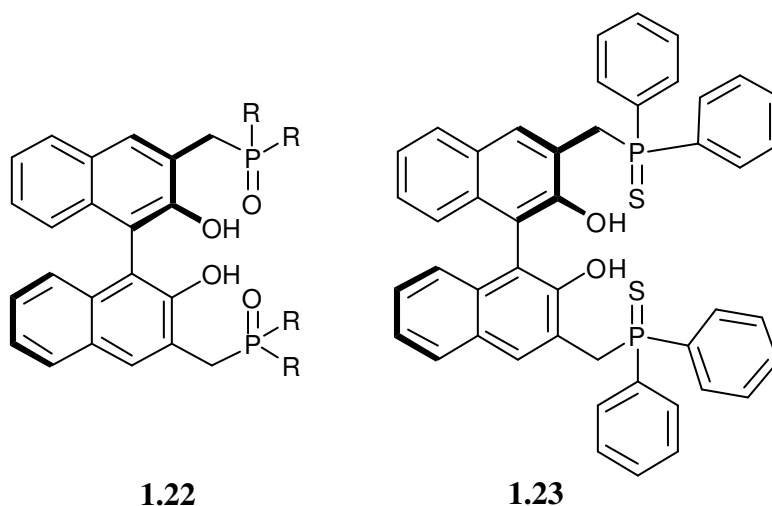


**Fig. 13** “Ate” complexes of **1.19- 1.21**,  $[\text{Li}_2\text{THF}_3][\text{Sm}(\text{R-BINAP})\text{Me}_3]$  and  $[\text{Li}_3\text{THF}_3][\text{La}(\text{R-BINAP})\text{Me}_4]$

The samarium complex (Sm-**1.19**) yielded products with a similar diastereomeric ratio, but with slightly higher enantiomeric excesses. However, the lanthanum analogue (La-**1.19**) gave products with lower selectivities.

The transformation of (5E,7)-octadien-1-amine to the corresponding piperidine was also studied. Ln-**1.19** (Ln = Sm, Y, La) was not as effective at controlling the stereochemistry of the piperidine compared to the pyrrole, although the diastereomeric ratio was excellent, (67:33, to 92:8). Therefore, even though enantioselectivities were low, these “ate” complexes were good catalysts for the more complex transformation of amino-dienes.

Organophosphine oxide (**1.22**) and sulphide (**1.23**) substituted binaphtholate ligands have also been investigated.<sup>51</sup> The ligands coordinated well to the lanthanides and showed modest to good enantioselectivities in hydroamination catalysis.



**Fig. 14** Organophosphine oxide and sulphide ligands.<sup>51-56</sup> R = Ph, Et, <sup>t</sup>Bu, 3,5-xylyl, Bn and OEt

The enantiomeric excesses were greatly dependent upon both the ligand and the metal. Ph-**1.22** was more effective when coordinated to smaller lanthanides (an increase to 61% from 26% ee), and Bn-**1.22** and Et-**1.22** with the larger lanthanides. However, complexes bearing <sup>t</sup>Bu-**1.22** and 3,5-xylyl-**1.22** showed little discrimination between metals. Complexes of **1.23** exhibited low enantioselectivities, which is an unsurprising result since two of the donor atoms are sulphurs, which are often less well matched with the hard lanthanide metals. These complexes not only highlight the symbiotic nature of ligand and metal but also show the effect of differing donor atoms.

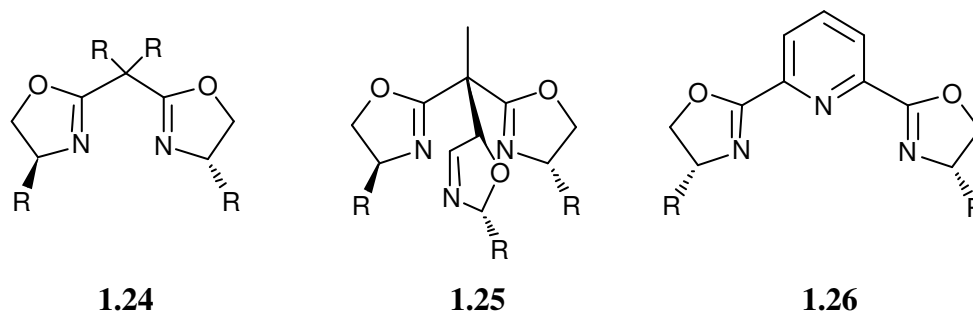
In 2004 the application of oxazoline based ligands was reported, along with their influence on asymmetric hydroamination.<sup>33, 57</sup> The applications of oxazoline-supported lanthanide complexes will now be discussed.

### 1.3 Lanthanides bearing Oxazoline ligands

Oxazoline-based ligands lend themselves well to lanthanide coordination as they are based upon imine donors, which are well-suited to the hard lanthanide ions. Also the stereodirecting group lies in the  $\alpha$  position relative to the coordinating nitrogen, placing it close to the catalytically active site.<sup>58</sup> The synthesis of chiral oxazoline ligands is readily achieved from  $\alpha$ -amino acids, thus providing a facile route to several derivatives using chiral pool materials. Given that oxazolines are forged onto nitrile or carboxylic acid precursors, an effectively limitless library of ligands is available, providing suitable supporting environments for most metals of the periodic table.

#### 1.3.1 Bis and trisoxazolines

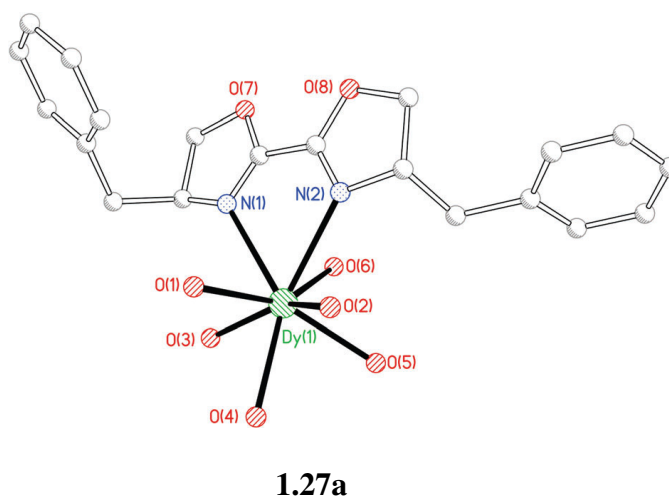
Some of the most common and successful oxazoline ligands are depicted in Fig. 15. Their denticity is a contributing factor to their success; since lanthanides tend to adopt high coordination numbers the bi/tri dentate ligands below lend themselves well to the coordination of lanthanides.



**Fig. 15** Common oxazoline ligands; bisoxazoline (BOX) **1.24**, trisoxazoline (trisox) **1.25** and pyridine bisoxazoline (pybox) **1.26**

A successful  $C_2$ -symmetric ligand is bisoxazoline (BOX) (**1.24**). The BOX ligand has received great interest, which has led to the development of many new catalytic reactions and use in various synthetic pathways; the coordination chemistry of metal complexes bearing the BOX ligand has also been studied at length.<sup>33, 57</sup>

The first ligand discussed in this series is that containing two directly bound oxazoline moieties (**1.27**), which was coordinated to several lanthanides (**a** = Dy, **b** = Sm, **c** = Eu, **d** = Gd, **e** = Tb).<sup>59</sup> This ligand is not formally recognised as a “BOX” ligand, which is reserved for the ligand in which the two oxazoline units are separated by a single carbon linker. Nevertheless, this ligand has been included for completeness.



**Fig. 16** Molecular structure of  $[Dy(Bn-BOX)(OH_2)_6]$  (**1.27a**). H atoms omitted for clarity



**1.27a-e** were not used in catalysis; however, the crystal structure displayed in Fig. 16 highlights significant features in the coordination sphere of this series. The high coordination number and the ligand geometry with its small bite angle provide little control over the coordination sites where any catalytic substrate is expected to bind. The stereodirecting groups are moreover too far away from these coordination sites to provide an efficient transfer of chiral information during catalysis.

In 2003 the application of BOX ligands and their use in hydroamination catalysis was reported.<sup>33, 57</sup> The catalysts were made *in situ*, and it was noted the ratio of ligand to metal affected the catalytic performance. A ratio of 1:1 gave the fastest rates of reaction, whilst a ratio of 1:2 retarded the reaction. However, despite the effect on reaction rates, little effect on the enantioselectivity was observed. Also, a dependence on the identity of the R group was observed; oxazoline ligands containing an aromatic group at the chiral centre generally catalysed the reaction faster and with higher selectivities, with La Ph<sub>2</sub>-BOX complexes showing the fastest rates and highest enantioselectivities (67%). However, increasing the sterics by incorporating a naphthyl group decreased the rate with no improvement in enantioselectivity.

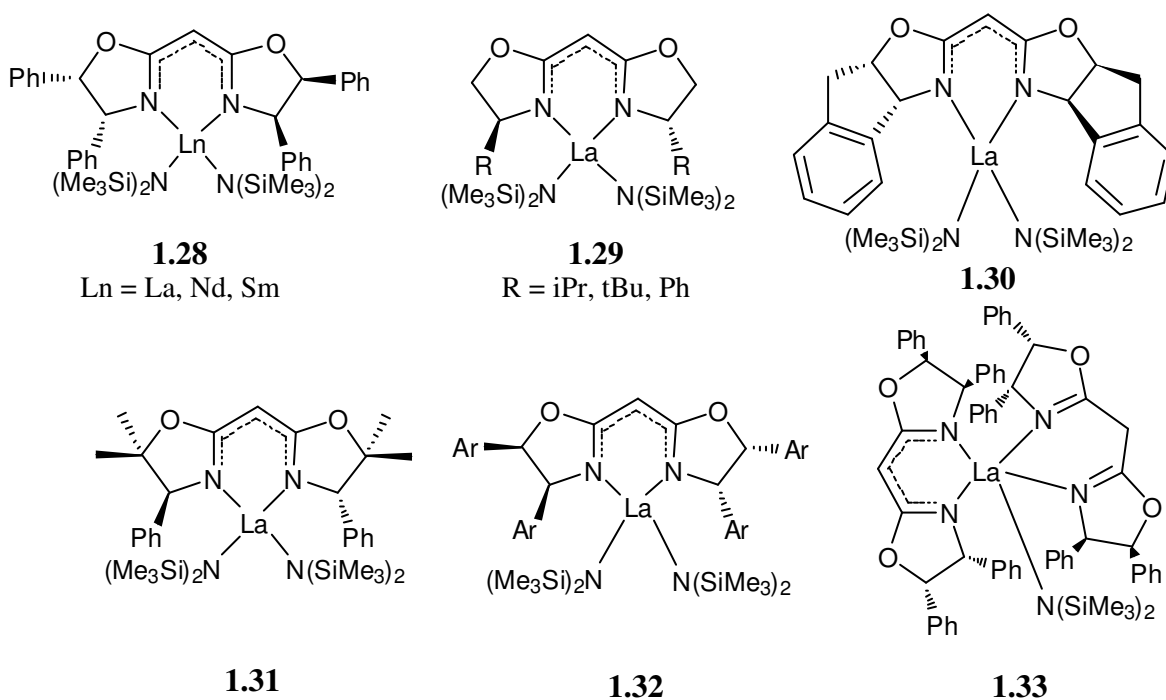
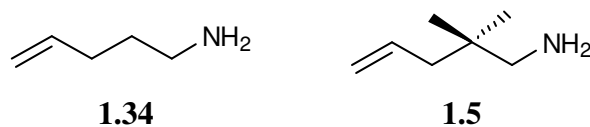


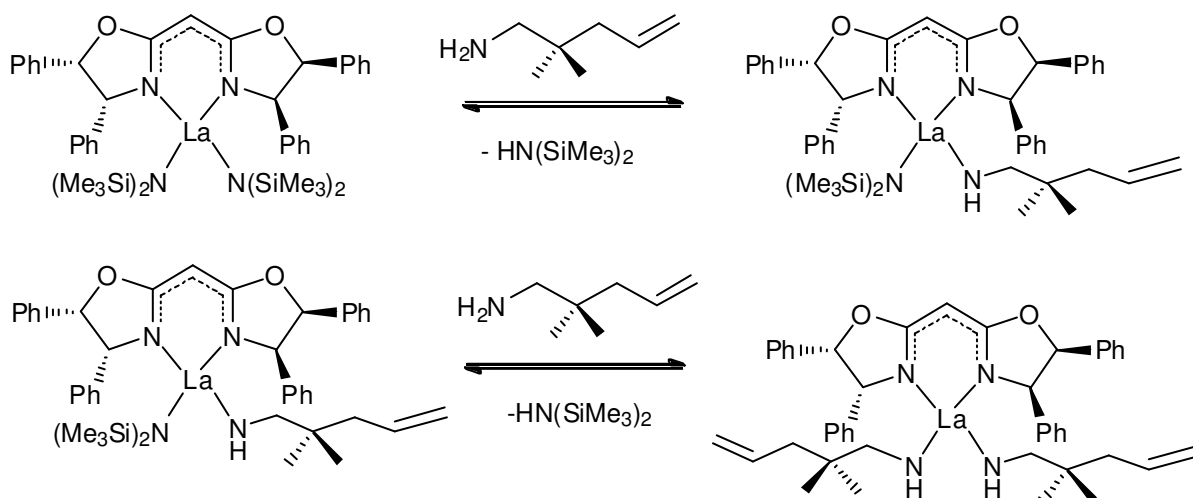
Fig. 17 Lanthanide BOX complexes

Both the substrates shown in Fig. 18 were investigated in the hydroamination reaction. Due to the Thorp-Ingold effect, rates were faster with substrate **1.5**, compared to the unsubstituted congener **1.34**.<sup>60</sup> Enantioselectivities are also higher with **1.5**.

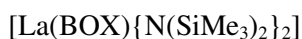


**Fig. 18** Aminoolefins used by Marks in the hydroamination reaction

Upon addition of the substrate, one equivalent of bis(trimethylsilyl)amine is liberated; in this case however, the remaining amide co-ligand was less susceptible to protonation (Scheme 7).



**Scheme 7** Protonation of  $N(\text{SiMe}_3)_2$  co-ligands upon the addition of aminoolefins to



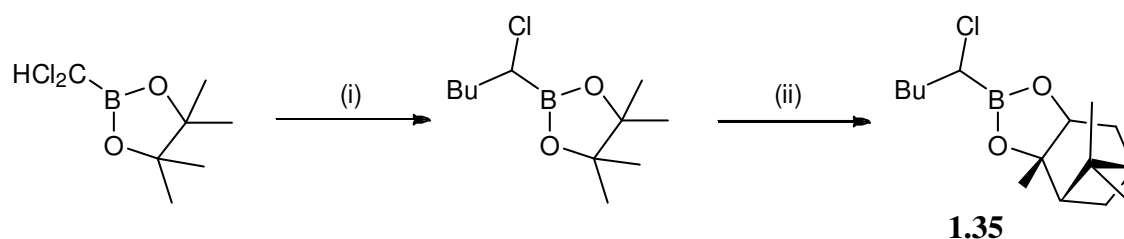
Although there were different rates of protonolysis, the rate of reaction was still zero-order with respect to substrate concentration and first order in catalyst concentration.

The BOX ligands have been extensively studied in a range of catalytic reactions, including ROP.  $[\text{Y}(\text{Me}_2\text{-BOX})_2\{\text{N}(\text{SiMe}_3)_2\}]$  was employed in the polymerisation of *rac*-

lactide and *rac*- $\beta$ -butyrolactone, resulting in an atactic polymer. The poor stereocontrol is apparently contradictory to the relative success observed in hydroamination catalysis.

Lanthanide metals are very Lewis acidic, and their triflates have been effectively used many times in Lewis acid catalysis.<sup>61</sup> Examples include the synthesis of chloroboronates,<sup>62</sup> cycloadditions, Diels-Alder reactions<sup>63</sup> and the Mukaiyama-Michael reaction,<sup>64</sup> all of which will be discussed herein. The first use of lanthanide-oxazoline complexes in catalysis involved the enantioselective synthesis of ( $\alpha$ -chloroalkyl)boronates and ( $\alpha$ -dichloro)boronates (Scheme 8).<sup>62</sup>

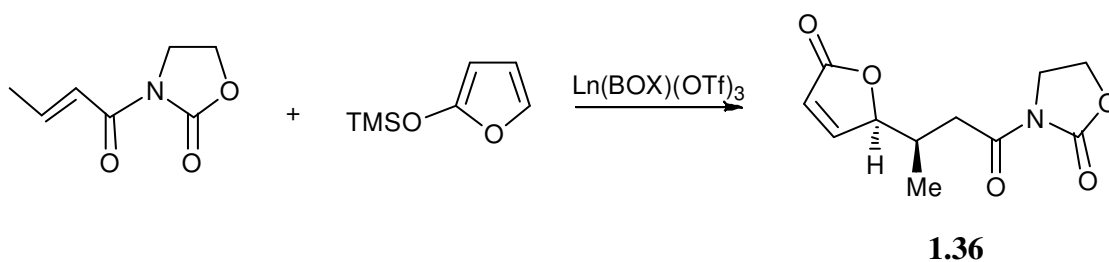
Lutetium and ytterbium BOX catalysts were the most successful catalysts for this reaction, especially when supported by Ph-BOX. Also, the lanthanide catalysts were shown to be superior to late transition metal triflates (Cu and Zn), yielding the product in 88% ee.



**Scheme 8** Synthesis of ( $\alpha$ -chloroalkyl)boronates. (i) *n*BuLi, [Ln(Ph-BOX)(OTf)<sub>3</sub>] (Ln = Yb, Lu); (ii) (s) – Pinanediol, NH<sub>4</sub>Cl

A series of catalysts supported by BOX ligands have been used in the Diels-Alder reaction and show moderate enantioselectivities.<sup>63</sup> The enantiomeric excess improved by adding two molar equivalents of the BOX ligand to Yb(OTf)<sub>3</sub>, forming [Yb(BOX)<sub>2</sub>(OTf)<sub>3</sub>]. This raised the enantiomeric excess from 17 to 46%.

As previously mentioned, lanthanide triflates have also been used in the Mukaiyama-Michael addition (Scheme 9).<sup>64</sup>

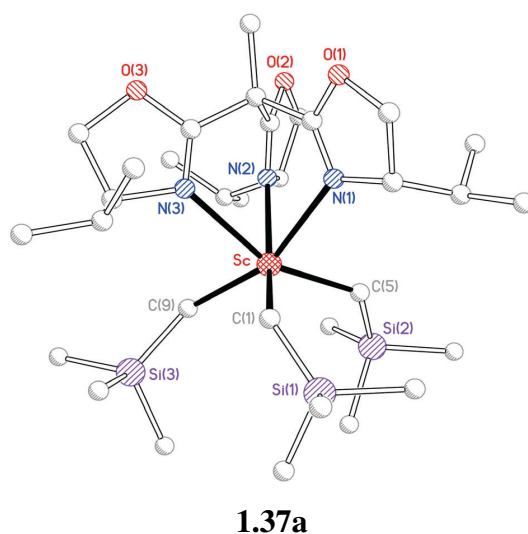


**Scheme 9** The Mukaiyama-Michael addition

The highest conversions of the Mukaiyama-Michael addition of (E)-3-crotonyl-1,3-oxazolidin-2-one and 2-trimethylsilyloxyfuran (Scheme 9) were achieved with scandium and cerium BOX triflate catalysts. Although they gave excellent control over anti/syn selectivities, the catalysts provided poor stereocontrol over the transformation.<sup>64</sup>

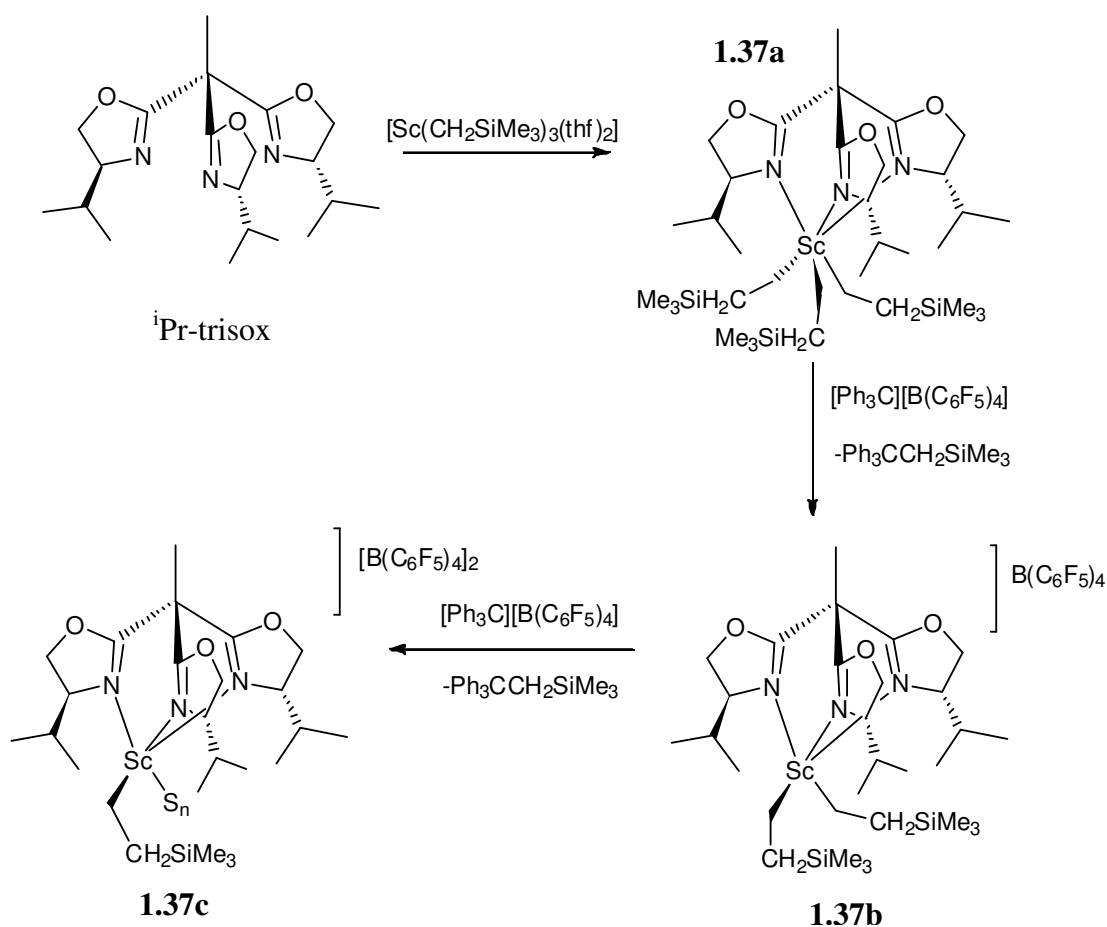
In summary, BOX supported catalysts have been applied to a variety of reactions but showed limited control over enantiomeric selectivities. This suggests that an increase in the number of donor groups and/or the inclusion of larger stereodirecting groups are required to improve the levels of selectivity provided by this class of catalyst.

A simple alteration to the BOX ligand is the incorporation of a third oxazoline moiety, this forms the tris(oxazolanyl)ethane (trisox) ligand. Trisox coordinates to lanthanides using all three nitrogens, which adopt a facial coordination mode, as shown in Fig. 19.



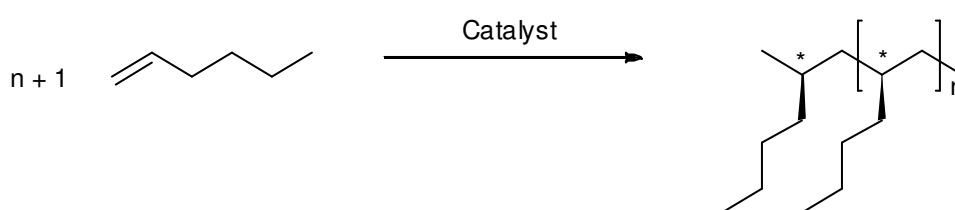
**Fig. 19** Molecular structure of  $[\text{Sc}(\text{iPr-trisox})(\text{CH}_2\text{SiMe}_3)_3]$  (**1.37a**).<sup>65</sup> H atoms omitted for clarity

The complex  $[\text{Sc}(\text{iPr-trisox})(\text{CH}_2\text{SiMe}_3)_3]$  (**1.37a**) is one of a series of lanthanide complexes synthesised ( $\text{Ln} = \text{Y}, \text{Lu}, \text{Tm}, \text{Er}, \text{Ho}$  and  $\text{Dy}$ ).<sup>65-70</sup> **1.37a** was reacted with  $[\text{Ph}_3\text{C}][\text{B}(\text{C}_6\text{F}_5)_4]$  and its activity in the polymerisation of 1-hexene probed.  $[\text{Sc}(\text{iPr-trisox})(\text{CH}_2\text{SiMe}_3)_2][\text{B}(\text{C}_6\text{F}_5)_4]$  (**1.36b**) exhibited low activity, however, upon the addition of a second equivalent of  $[\text{Ph}_3\text{C}][\text{B}(\text{C}_6\text{F}_5)_4]$ , the activity of the resulting dicationic complex  $[\text{Sc}(\text{iPr-trisox})(\text{CH}_2\text{SiMe}_3)][\text{B}(\text{C}_6\text{F}_5)_4]_2$  (**1.37c**) dramatically increased. **1.37c** polymerised 1-hexene with an activity of  $36\,000 \text{ kg (polymer) mol}^{-1} (\text{Sc}) \text{ h}^{-1}$ , which is the highest reported activity for a Group 3 or lanthanide catalyst, competitive with the most active post-metallocene Group 4 catalysts.<sup>71, 72</sup> A range of  $\alpha$ -olefins were tested and all were polymerised with high activities and isotacticities (up to 99%) at low temperatures.<sup>65-67, 70</sup> Unfortunately, the corresponding complexes of the later lanthanides showed lower activity than **1.37c**, but were still competitive in comparison to other lanthanide catalysts.



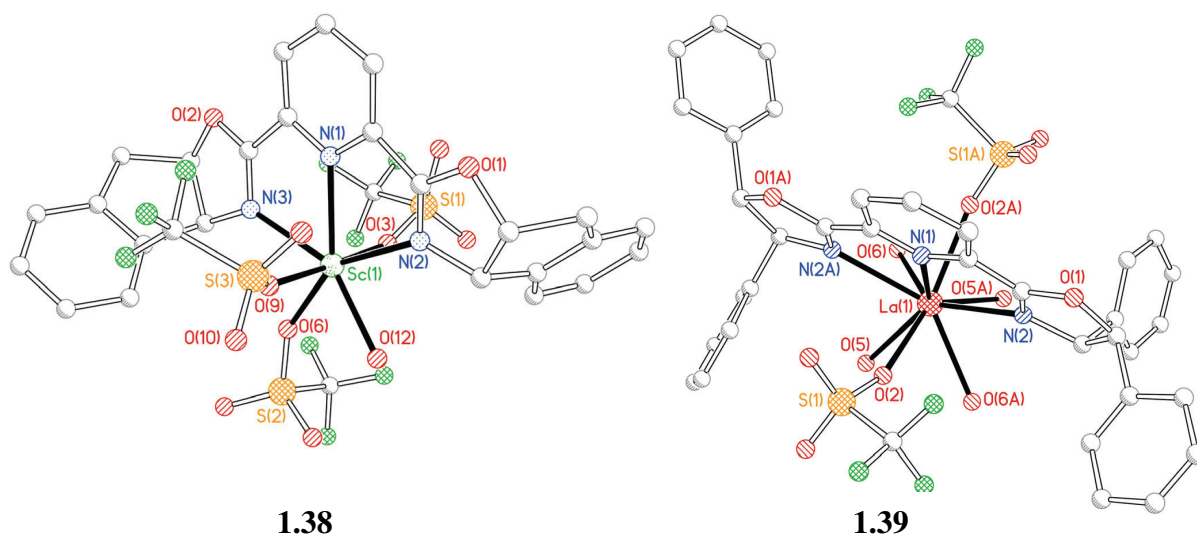
**Scheme 10** The addition of two equivalents of  $[\text{Ph}_3\text{C}][\text{B}(\text{C}_6\text{F}_5)_4]$  to form the dicationic scandium trisox complex (**1.37c**)

As expected, the polymerisation activity showed a strong dependence on the ionic radius of the lanthanide ion; for 1-hexene and 1-heptene the activity increased with increasing ionic radius of the metal. The maximum activity was obtained with thulium, after which the activity decreased with larger metals, probably owing to the reduced stability of the active species (lanthanide alkyls are known to show a reduced stability with the larger metals). Experiments were also conducted with 1-octene, the activity was constant (within experimental error) and the tacticity control was consistently high at 95%.<sup>68, 69</sup>



**Scheme 11** Polymerisation of 1-hexene

Another example of a bisoxazoline ligand possessing a third donor atom is 2,6-bis(oxazolynyl)pyridine (pybox) (**1.26**, Fig. 15). Pybox supported complexes have been used extensively in catalysis, especially with the lanthanides. Unlike the previous examples discussed, **1.26** has a different coordination mode. A *mer* arrangement is adopted where the angle subtended between the  $N_{\text{oxazoline}}-M-N_{\text{oxazoline}}$  is significantly smaller than  $180^\circ$ . This increases the space around the metal and allows for higher coordination numbers, for example  $[\text{Sc}(\text{ind-pybox})(\text{OTf})(\text{OH}_2)]$  **1.38** (Fig. 20).<sup>73</sup> Scandium tends to adopt 5 or 6 coordinate structures, whereas **1.38** has a 7 coordinate scandium centre. This is a notable complex, since it illustrates that even the smallest of the Group 3 metals can possess higher coordination numbers than expected. As a consequence, one would expect there to be little stereocontrol, however, this is not observed. The pybox ligand is highly rigid and has a sterically imposing framework that renders a well-defined chiral space, making pybox a very successful ligand for the lanthanides, both in terms of the number of reactions that these complexes have catalysed, and in the impressive levels of stereoselectivity obtained.

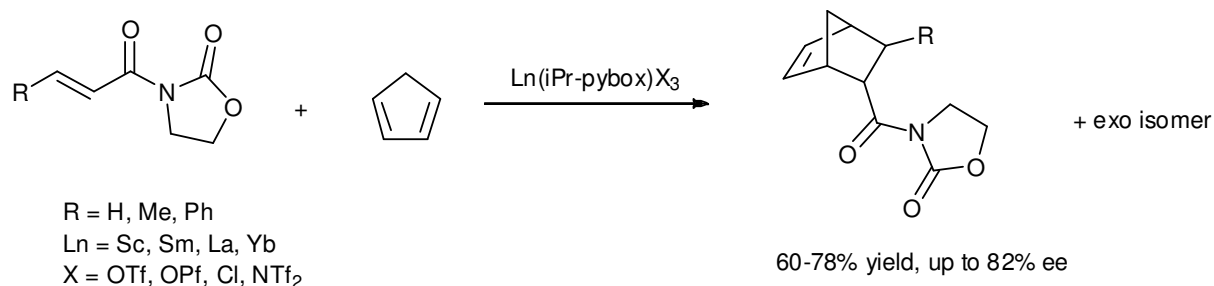


**Fig. 20** Molecular structure of: Left: [Sc(ind-pybox)(OTf)(OH<sub>2</sub>)] (**1.38**), Right: [La(Ph<sub>2</sub>-pybox)(OTf)<sub>2</sub>(OH<sub>2</sub>)<sub>4</sub>][OTf] (**1.39**). H atoms omitted for clarity

Another example of a pybox supported complex with a large coordination number is [La(Ph<sub>2</sub>-pybox)(OTf)<sub>2</sub>(OH<sub>2</sub>)<sub>4</sub>][OTf] **1.39** (Fig. 20).<sup>64</sup> This has a coordination number of 9 and reiterates how the ionic radius of the lanthanide ion dictates the coordination environment, particularly the coordination number.

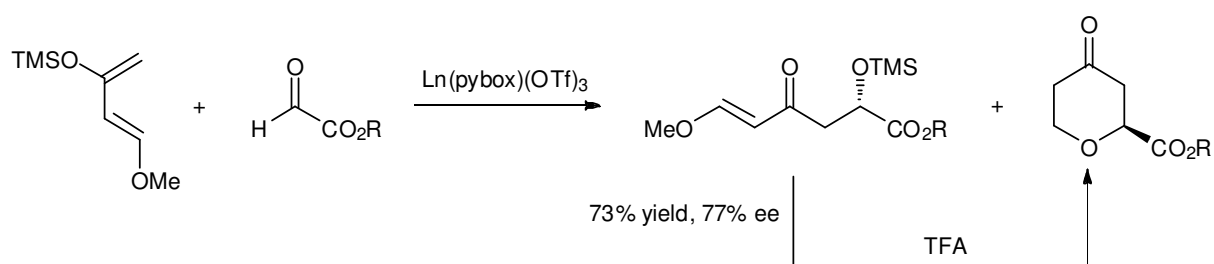
In catalysis lanthanide pybox complexes have been demonstrably superior to the corresponding BOX-supported complexes. In 1,3-dipolar cycloaddition reactions, [Ln(BOX)(OTf)<sub>3</sub>] yielded close to racemic products whereas the analogous pybox complexes yielded products with enantioselectivities of up to 73%.<sup>74</sup> Also, the ytterbium pybox complex was more active than the scandium complex. This is another example that highlights the effect of ionic radius on the properties of the catalyst.

Lanthanide pybox complexes have also been used in the asymmetric Diels-Alder reaction between acyl-1,3-oxazolinin-2-ones and 1,3-dienes, (Scheme 12).<sup>75</sup>

**Scheme 12** Asymmetric Diels-Alder reaction

All complexes showed a preference for the *endo* isomer, however, the scandium complex was the most selective. This yielded products with enantioselectivities of up to 82%, whereas the larger metals were less selective. To further enhance the enantioselectivity (up to 96%) a second Ph group was incorporated into each of the oxazoline rings.<sup>76, 77</sup> However, this caused a change in the major product to the *exo* isomer. A further facet to this investigation was the effect of the counterion. Four counterions were investigated; OTf, OPf (perfluorooctanesulphonate), NTf<sub>2</sub> and Cl. The enantioselectivities were most consistent when OTf was used. However, the highest yields were observed with Cl and NTf<sub>2</sub>.

The effects of the lanthanide ionic radius and the pybox ligand substituents on the selectivity of the hetero-Diels-Alder reaction has been studied (Scheme 13).<sup>63</sup>

**Scheme 13** The hetero-diels-alder reaction between glyoxylate esters and Danishefsky's diene

The size of the stereodirecting group as well as the chemical nature of the group has an influence on the stereinduction.<sup>78</sup> For example, *iPr*-pybox and Ph-pybox complexes



yielded products with opposite stereochemistry despite having ligands with the same stereochemistry. Also the iPr-pybox was better matched to the smaller metals (scandium), whereas Ph-pybox showed higher selectivity with lanthanum. In summary, the smaller metal ions gave good enantioselectivities and as the ionic radius increased the enantioselectivities decreased to almost racemic. Selectivities with the larger metals increased again, but show an inverse in the stereochemistry of the product.

The reactions were also conducted with and without molecular sieves being present in the reaction mixture. The smaller metals performed better in the presence of sieves whereas the larger metals performed better in their absence. The authors suggest that for the smaller metals, where a lower coordination number is preferred, the removal of competing water ligands aids in providing vacant sites for the catalytic substrate. However, for the larger metals, which prefer a higher coordination number, the presence of water provides a more rigid complex, which in turn induces better stereocontrol.<sup>78</sup>

When a second phenyl group was introduced onto the pybox oxazoline rings, there was a pronounced improvement in enantioselectivity for the hetero-Diels-Alder reaction (Scheme 13, Table 4). The best performing catalyst was [Sc(pybox)(OTf)<sub>3</sub>] giving an enantioselectivity of 99%, followed by [Y(pybox)(OTf)<sub>3</sub>] giving 95% ee, albeit yielding the opposite enantiomer. This suggests there may be a change in coordination number and geometry on changing from scandium to yttrium. For all catalysts, the enantioselectivity for the *endo* product was above 80%, apart from the lutetium catalyst, which gave 24% ee. In addition to cyclopentadiene, a second substrate was also investigated. In contrast to the previous results, when diphenylnitrone was used a significant dependence on the metal was observed; scandium gave the lowest enantioselectivity and lanthanum the highest, 54 and 85% respectively.<sup>79</sup> This reverse in selectivity highlights the significant effect that can be observed for metals with different ionic radius are used, and more importantly how the effect is not always intuitively obvious.

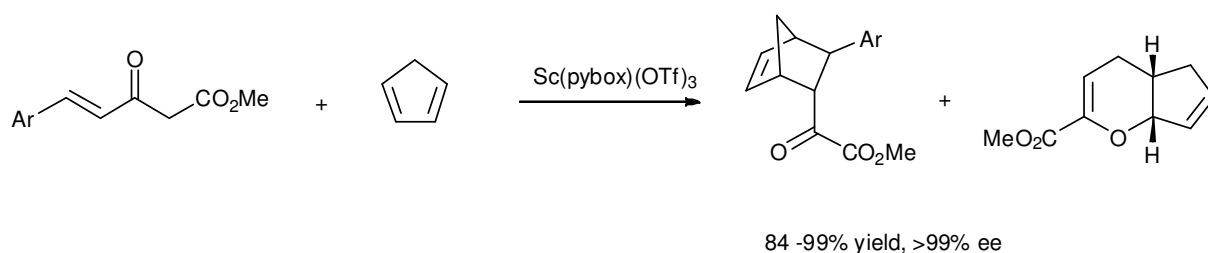
**Table 4** Asymmetric Diels-Alder reaction in Scheme 13, catalysed by [Ln(pybox)(OTf)<sub>3</sub>]

Entry	$r^a/\text{Å}$	Triflate	Time/h	<i>endo</i> : <i>exo</i> <sup>b</sup>	<i>endo</i> ee	<i>exo</i> ee
1	0.75	Sc	16	96 : 4	99	>95
2	0.86	Lu	48	90 : 10	24	Racemic
3	0.87	Yb	24	91 : 9	83	55
4	0.90	Ho	48	95 : 5	91	60
5	0.90	Y	48	90 : 10	95	67
6	0.95	Eu	48	91 : 9	90	50
7	0.99	Pr	24	93 : 7	86	24
8	1.03	La	16	94 : 6	80	racemic

$r^a$  = effective ionic radius

<sup>b</sup> = Yields were all quantitative

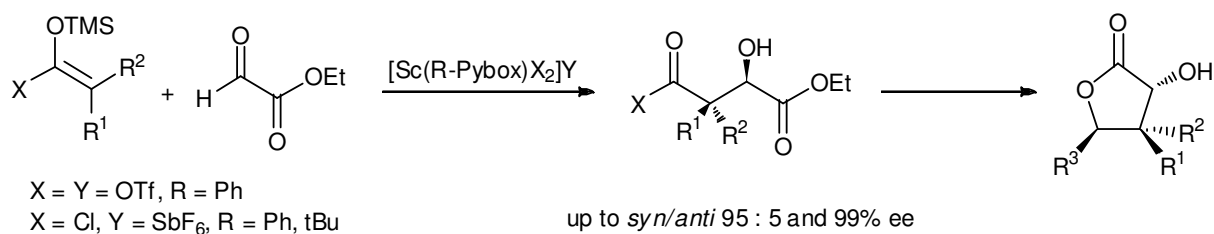
In this comprehensive analysis of the pybox ligands, a third reaction was also investigated. The Diels-Alder reaction using (*E*)-2-oxo-4-aryl-3-buteneoates was investigated but the catalysts were unreliable; two competing reactions pathways were observed, *i.e.* the Diels-Alder cyclisation and hetero-Diels-Alder reaction (Scheme 14).



**Scheme 14** Competing Diels-Alder and hetero-diels Alder reactions using Methyl (*E*)-2-oxo-4-aryl-3-buteneoates

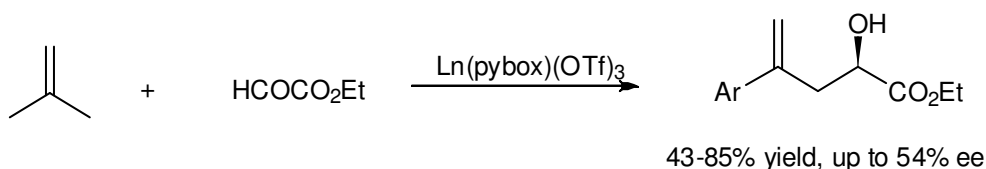
The reaction was not regioselective, giving a 1:2 mixture of Diels-Alder : hetero Diels-Alder products. However the enantioselectivities were excellent; [Sc(pybox)(OTf)<sub>3</sub>] gave products with enantioselectivities of  $\geq 99\%$ .<sup>80-82</sup>

[Sc(pybox)X<sub>3</sub>] has been successfully employed in a variety of reactions, an example being the aldol reaction. [Sc(pybox)(OTf)<sub>3</sub>] and [Sc(pybox)Cl<sub>2</sub>][SbF<sub>6</sub>] were excellent catalysts for the reaction between ethyl glyoxylate and pyruvates (Scheme 15), yielding products with enantioselectivities of up to 99%, and *syn* diastereoselectivities between 90 : 10 and 95 : 5.<sup>83</sup>



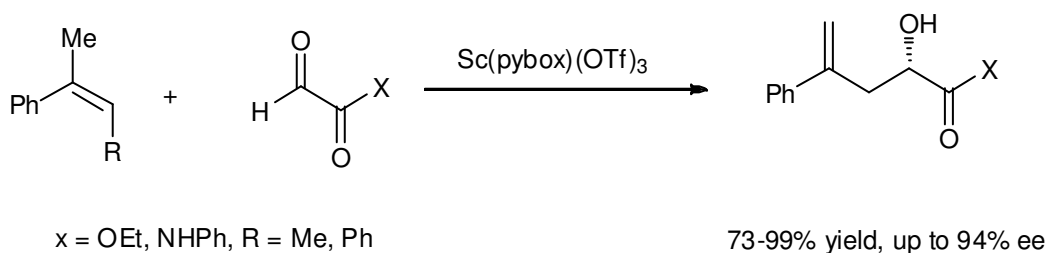
**Scheme 15** Aldol reactions of ethyl glyoxylate catalysed by [Sc(pybox)X<sub>2</sub>]Y. X = SR, Ar; R<sup>1</sup> = H, Me, iPr, <sup>t</sup>Bu, Et, OBn; R<sup>2</sup> = H; R<sup>1</sup>, R<sup>2</sup> = Me, cyclopentane, cyclohexane, Et<sub>2</sub>

The glyoxylate-ene reaction (Scheme 16) has been studied in the presence of [Ln(pybox)(OTf)<sub>3</sub>]. The ytterbium congener [Yb(pybox)(OTf)<sub>3</sub>] was the most selective catalyst, giving enantioselectivities of up to 54%,<sup>63</sup> although the activity showed a strong dependence upon solvent. When coordinating solvents were used activity was negligible.



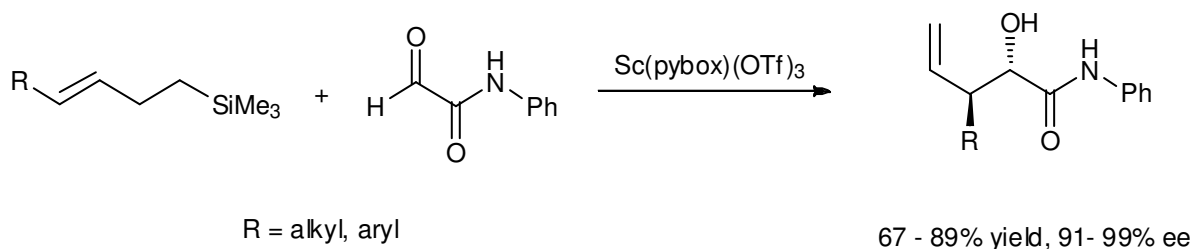
**Scheme 16** Glyoxylate-ene reaction

[Sc(Ph-pybox)(OTf)<sub>3</sub>] and [Sc(Ind-pybox)(OTf)<sub>3</sub>] (**1.38**) have been used to catalyse the reaction between disubstituted olefins and N-phenyl glyoxamide. As well as inducing good regioselectivity, products were obtained with high enantioselectivities (94%) and in good yields. When tri-substituted olefins were used, enantioselectivities increased to 99%.<sup>84</sup>



**Scheme 17** The catalysed reaction between substituted olefins and N-phenyl glyoxamide

In addition to this, [Sc(Ind-pybox)(OTf)<sub>3</sub>] (**1.38**) has been used in the Sakurai-Hosomi reaction (Scheme 18), which involves the addition of terminally substituted allylsilanes to N-phenyl glyoxamide, and yielded products with *anti*-diastereoselection, unlike the carbonyl-ene reaction where *syn*-diastereoselection was observed. When **1.38** was used as a catalyst for this reaction, the products were obtained in good yield with enantioselectivities of up to 99%.<sup>85</sup>

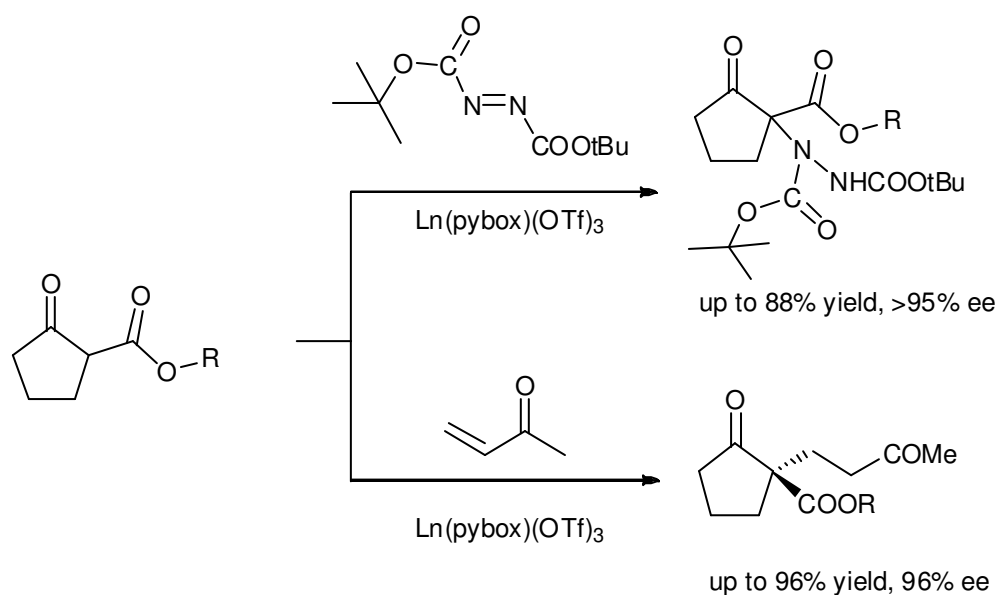


**Scheme 18** The Sakurai-Hosomi reaction

The Mukaiyama–Michael reaction is another reaction in which lanthanide pybox complexes have been successfully employed. [Ln(pybox)X<sub>3</sub>] has been used to catalyse the reaction between (E)-3-crotonyl-1,3-oxazolidin-2-one and 2-trimethylsilyloxyfuran. Unlike the BOX

supported catalysts (which have racemic products),<sup>64</sup> the pybox derivatives gave products with enantioselectivities of >99%.

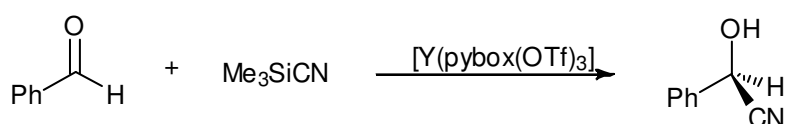
A similar reaction to the Mukaiyama–Michael reaction is the competing hydrazination and Michael addition of cyclic  $\beta$ -ketoesters (Scheme 19). The use of  $[\text{Ln}(\text{pybox})\text{X}_3]$  as a catalyst yielded products for the amination with good enantioselectivities; the highest enantioselectivities were achieved with the larger lanthanides. In particular,  $[\text{Eu}(\text{Pr-pybox})(\text{OTf})_3]$  produced products with enantiomeric excesses of >95%. However, the smaller lanthanides gave better results for the Michael addition.  $[\text{Y}(\text{pybox})\text{X}_3]$  was the best, yielding products with enantioselectivities of up to 96%, which was somewhat lower for europium (59% ee).<sup>86</sup>



**Scheme 19** The hydrazination and Michael addition of cyclic  $\beta$ -ketoesters. Ln = Yb, Eu, La and Sc

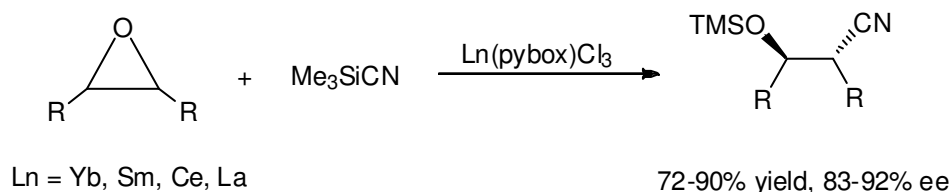
Nitrile substrates have been used to produce cyanohydrins. The lanthanide complexes  $[\text{Ln}(\text{pybox})\text{Cl}_3]$  were successfully employed as catalysts for this reaction and gave a range of selectivities with Y, Yb, Eu and La. The most successful transformation was the addition of TMS-CN to benzaldehyde which gave the product in 89% ee (Scheme 20).<sup>87, 88</sup>

Catalysts can be supported on polymers. This technique has often been employed to facilitate the separation of the catalyst from the reaction mixture. An example in lanthanide oxazoline chemistry is  $[\text{Yb}(\text{pybox})(\text{OTf})_3]$ , which was used in the reaction illustrated in Scheme 20. The polymer-supported catalyst could be isolated and reused, with selectivities remaining constant after successive runs. Only after four runs did the efficiency of the catalyst decrease; yields fell to 66-72% from 80%.<sup>89</sup> Despite this, yields and enantioselectivities were less than those reported for unsupported catalysts (80% ee). Although polymer supported catalysts have several advantages, few examples are reported that give better results than the analogous unsupported systems.



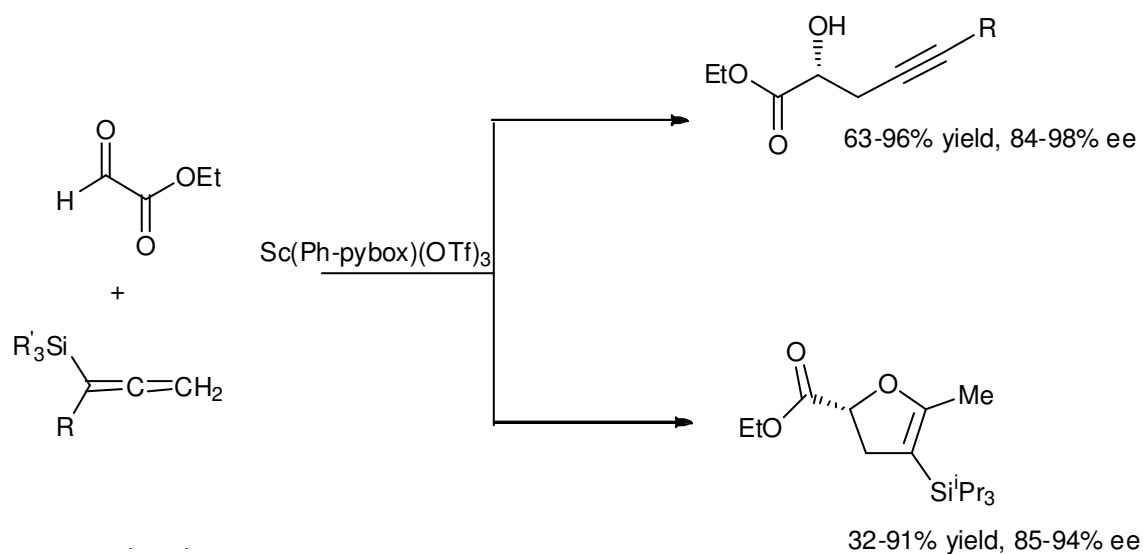
**Scheme 20** The addition of TMS-CN to benzaldehyde

The ring-opening of epoxides with TMS-CN, using  $[\text{Ln}(\text{pybox})\text{Cl}_3]$  as a catalyst, proceeded with moderate stereocontrol.<sup>90</sup> The enantioselectivities were inversely proportional to the lanthanide ionic radius; the small metals were more effective at transferring chiral information in comparison to the larger metals. Unlike the previous example in Scheme 20, the enantioselectivities decreased with successive runs: 21 and 7% on the second and third runs respectively.<sup>91</sup>



**Scheme 21** The lanthanide-catalysed ring-opening of epoxides with TMS-CN

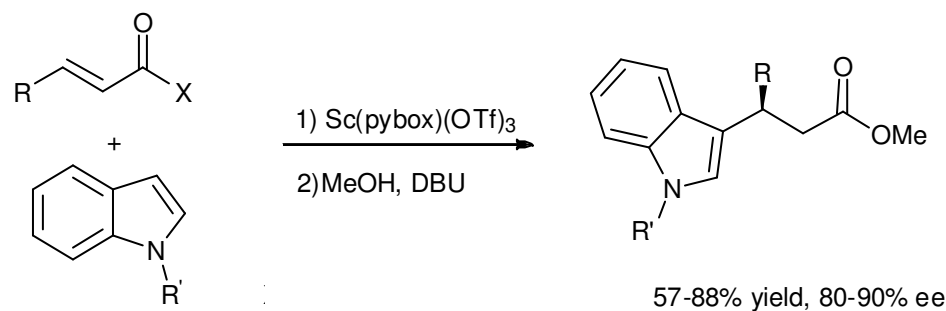
[Sc(pybox)(OTf)<sub>3</sub>] has been used as a catalyst in the synthesis of homopropargylic alcohols and dihydrofurans (Scheme 22).<sup>92</sup> These reactions were largely successful when these catalysts were employed, with enantioselectivities of up to 98 and 94% respectively. The steric bulk of the silane had an effect on the reaction pathway; when Si<sup>i</sup>Pr<sub>3</sub> was used instead of SiMe<sub>3</sub>, the dihydrofuran was produced rather than the alcohol. As with many of the systems discussed, the steric bulk of the ligand/substrate can affect the activity of the complex and even the product of the reaction.



**Scheme 22** The catalysed addition of aldehydes to allylsilanes and allenylsilanes. R = alkyl, aryl; R' = Me, <sup>i</sup>Pr

[Sc(ind-pybox)(OTf)<sub>3</sub>] **1.38** has been used in the addition of N-methylindole to  $\alpha,\beta$ -unsaturated acylphosphonates. Different substrates and catalyst loading were investigated; with 10 mol% catalyst loading, products were obtained with enantioselectivities of 99% and negligibly decreased to 95% when the catalyst loading was reduced to 3 mol%. When the steric bulk of the phosphonate was increased from methyl to isopropyl, the enantioselectivities improved to 99%. However, when an aromatic derivative was employed the enantioselectivity decreased to 80%, suggesting that the electronics of the substituent have an effect in addition to the steric bulk. The indole substituents were also altered; the effect of

changing the indole to N-benzylindole increased the enantioselectivities to 97-99% ee. The introduction of an electron withdrawing group onto the indole ring resulted in no change in stereoselectivity but decreased the yield from 85 to 60-70%.<sup>73</sup>



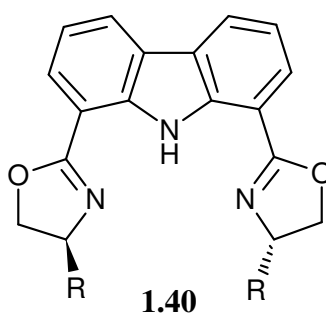
**Scheme 23** The addition of N-methylindole to  $\alpha,\beta$ -unsaturated acylphosphonates. X = P(O)(OMe)<sub>2</sub>,  
imidazole

The substitution of  $\alpha,\beta$ -unsaturated acylphosphonates with N-methylimidazoles proved successful when catalysed by [Sc(pybox)(OTf)<sub>3</sub>]. When the coupling reaction was conducted with N-methylindole at -40 °C, the product was obtained in 98% ee and 97% yield. This is comparable to the previous results with acyl phosphonates. The substitution pattern of the N-alkyl indole was also investigated. Methoxy groups were added to the indole ring which caused the reaction yield to increase (99%), without effecting the enantioselectivities.<sup>93</sup> Another variation of the indole was the substitution for pyrrole or N-methylpyrrole. The reaction still proceeded with good yields, although the enantioselectivities were reduced. The authors proposed that the effect on the enantioselectivities is caused by the sterics/electronics, where a large electronegative moiety favours high enantioselectivities. Aryl imidazole-substituents increased the stereocontrol; with N-phenylimidazole, the enantiomeric excess was 98%.<sup>94</sup> By replacing the indole with oxazolidinone, pyrazole, or Weinreb amide, only a trace amount of the product was observed, suggesting that the most suitable substrates for the reaction are acyl phosphonates and acyl N-alkylindoles.<sup>95</sup> As well as the substrates, the



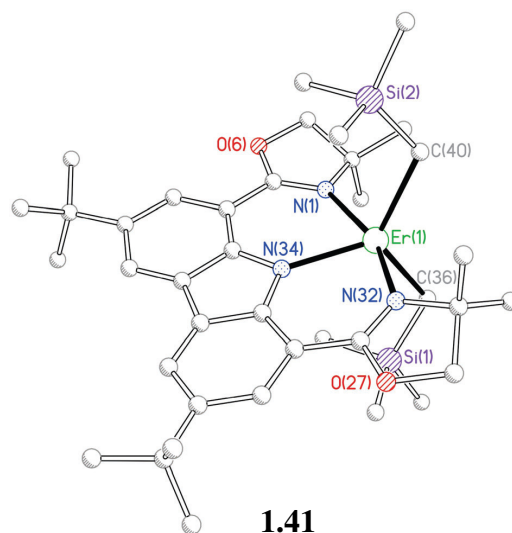
reaction conditions were also extensively investigated. The temperature effects were significant: reaction temperatures greater than  $-50\text{ }^{\circ}\text{C}$  resulted in lower enantioselectivities. Under optimised conditions, catalyst loadings of 3 mol% induced stereocontrol, and alternative oxazoline substituents (apart from *i*Pr) gave lower enantioselectivities.

Throughout this discussion it has been clear that pybox is a successful ligand, being applied to a variety of asymmetric transformations. This is probably the result of its rigidity and coordination geometry. Another ligand with an extra donor is the carbazole-bisoxazoline (Fig. 21).<sup>96</sup>



**Fig. 21** Carbazole-bisoxazoline

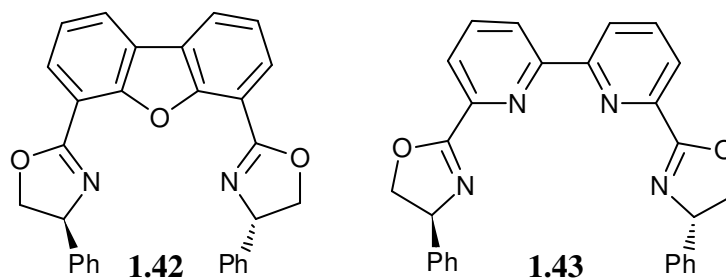
The carbazole-based ligand adopts the *mer*- $\text{N}_3$  donor environment, whilst increasing the bite angle in comparison to the pybox ligand, whilst adding an anionic donor to the ligand backbone. These features could result in a more efficient transfer of chiral information. The coordination chemistry of carbazole-bisoxazoline with the lanthanides has been investigated. A 5-coordinate erbium complex was formed when the ligand was reacted with  $[\text{Er}(\text{CH}_2\text{SiMe}_3)_3(\text{THF})_2]$  (Fig.22).<sup>97</sup> The relatively low coordination number is consistent with previously discussed organometallic systems.



**Fig. 22** Molecular structure of  $[\text{Er}(\text{Me}_2\text{-carbazole})(\text{CH}_2\text{SiMe}_3)_2]$  (**1.41**). H atoms omitted for clarity

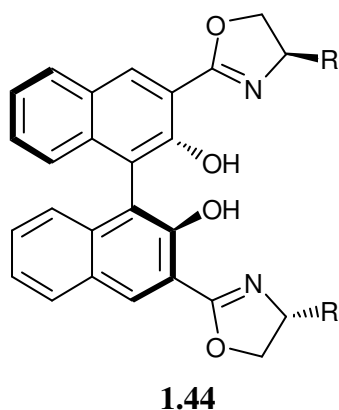
The dichloride complexes were also reported, resulting in a 6-coordinate erbium centre. Since the co-ligands (chloride) are smaller in comparison to the alkyl ligands, a THF molecule coordinated to the erbium centre. The nature of the co-ligand therefore has an effect on the ability for Lewis bases to coordinate; this could have implications in catalytic studies used with this complex (and with related systems, which form the basis of this thesis); the relative space around a metal centre available for base coordination may impact on the ability of a catalytic substrate to coordinate. Although the carbazole-bisoxazoline ligand possesses many features suited to catalysis, its application has yet to be investigated in this regard.

Similar ligands have also been synthesised containing furan and bipyridyl donors (Fig. 23). **1.42** and **1.43** have been coordinated to lanthanides and used in the glyoxylate-ene and hetero-Diels-Alder reactions.<sup>63</sup> The enantioselectivities for both reactions were lower than those observed for the pybox supported systems. A possible reason for the low enantioselectivities is that, the stereodirecting groups do not effectively cover the active site, and therefore cannot efficiently transfer any chiral information to the catalytic substrates.



**Fig. 23** Furan and bipyridyl ligands

A ligand with a similar coordination geometry to **1.43** is binaphthol-bisox (Fig. 24).<sup>98</sup> Lanthanide triflate complexes were prepared *in situ* and used in the 1,3-dipolar cycloaddition of nitrones to alkenes. The  $[\text{Ln}(\text{BINOL-bisox})(\text{OTf})_3]$  complexes were more selective than the pybox congeners;  $[\text{Sc}(\text{Ph-BINOL-bisox})(\text{OTf})_3]$  gave products with the highest enantioselectivity of 83%.



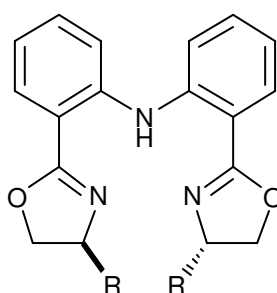
**Fig. 24** Binol(bisoxazoline)

## 1.4 Summary

The previous discussion highlights the dependence of ligand structure and the identity of the lanthanide metal (particularly the ionic radius) on the coordination chemistry of lanthanide complexes. This has been exemplified by analysing the coordination chemistry and catalytic applications of lanthanide oxazoline complexes. An appreciation of the impact of coordination chemistry on the catalytic performance is requisite, since this has a profound

effect in relation to the catalytic activity and enantioselectivity. The development of lanthanide systems, from cyclopentadienyl to post-metallocene complexes has created a wealth of knowledge, and has inspired our research into other ligands based upon oxazolines. The previous discussion also highlights the relatively few examples of oxazoline ligands being employed in *organometallic* lanthanide systems, and it is this aspect that this thesis will address, probing their reactivity with catalytic reactions appropriate to the type of complex synthesised (*e.g.* hydroamination, polymerisation).

Since lanthanide pybox complexes generally give the highest enantioselectivities, a similar ligand that will be investigated is bis(oxazolinyphenyl)amide (BOPA) (**1.45**).<sup>99</sup> This is a tridentate ligand that possesses an anionic donor. Its synthesis was first reported using long reaction times and the use of a palladium catalyst, providing the ligand in low yield.

**1.45****Fig. 25** Bis(oxazolinyphenyl)amide (BOPA)

The structure of **1.45** makes it an interesting prospect for its coordination to the lanthanides and its application in asymmetric catalysis. The research described in this thesis investigates the use of lanthanide and Group 3 complexes bearing the BOPA ligand. Investigations will focus on their fundamental organometallic / coordination chemistry and their application in the intramolecular hydroamination of aminoolefins, and in the ring opening polymerisation of *rac*-lactide. These two reactions have been chosen as

representative examples of reactions that will enable me probe to the scope and limitations of oxazoline-supported organometallic lanthanide complexes in catalysis.

## 1.5 References for Chapter 1

- 1 R. D. Shannon, *Acta Crystallogr., Sect A: Cryst. Phys., Diffraction, Theor. Gen. Crystallogr.*, 1976, **32**, 751.
- 2 P. Mountford and B. D. Ward, *Chem. Commun.*, 2003, **15**, 1797.
- 3 F. T. Edlemann, D. M. M. Freckmann, and H. Schumann, *Chem. Rev.*, 2002, **102**, 1851.
- 4 F. G. N. Cloke, *Chem. Soc. Rev.*, 1993, **22**, 17.
- 5 H. A. McManus and P. J. Guiry, *Chem. Rev.*, 2004, **104**, 4151.
- 6 J. Zhou and Y. Tang, *Chem. Soc. Rev.*, 2005, **34**, 664.
- 7 L. H. Gade and S. Bellemin-Lapponaz, *Coord. Chem. Rev.*, 2007, **251**, 713.
- 8 G. Desimoni, G. Faita, and K. A. Jørgensen, *Chem. Rev.*, 2006, **106**, 3561.
- 9 G. Desimoni, G. Faita, and P. Quadrelli, *Chem. Rev.*, 2003, **103**, 3119.
- 10 A. I. Meyers, *J. Org. Chem.*, 2005, **70**, 6137.
- 11 G. C. Hargaden and P. J. Guiry, *Chem. Rev.*, 2009, **109**, 2505.
- 12 K. C. Hultsch, *Adv. Synth. Catal.*, 2005, **347**, 367.
- 13 M. R. Gagné, C. L. Stern, and T. J. Marks, *J. Am. Chem. Soc.*, 1992, **114**, 275.
- 14 A. Motta, G. Lanza, I. L. Fragalà, and T. J. Marks, *Organometallics*, 2004, **23**, 4097.
- 15 J. -S. Ryu, G. Y. Li, and T. J. Marks, *J. Am. Chem. Soc.*, 2003, **125**, 12584.
- 16 A. L. Gott, A. J. Clarke, G. J. Clarkson, and P. Scott, *Chem. Commun.*, 2008, 1422.
- 17 A. L. Gott, A. J. Clarke, G. J. Clarkson, and P. Scott, *Organometallics*, 2007, **26**, 1729.
- 18 M. C. Wood, D. C. Leitch, C. S. Yeung, J. A. Kozak, and L. L. Schafer, *Angew. Chem., Int. Ed.*, 2007, **46**, 354.
- 19 T. E. Muller, K. C. Hultsch, M. Yus, F. Feubelo, and M. Tada, *Chem. Rev.*, 2008, **108**, 3795.

- 20 B. D. Ward, A. Maisse-Francois, P. Mountford, and L. H. Gade, *Chem. Commun.*, 2004, 704.
- 21 R. Severin and S. Doye, *Chem. Soc. Rev.*, 2007, **36**, 1407.
- 22 A. L. Odom, *Dalton Trans.*, 2005, 225.
- 23 P. Yin and T. - P. Loh, *Org. Lett.*, 2009, **11**, 3791.
- 24 Y. Li and T. J. Marks, *J. Am. Chem. Soc.*, 1998, **120**, 1757.
- 25 B. Liu, T. Roisnel, J. -F. Carpentier, and Y. Sarazin, *Angew. Chem., Int. Ed.*, 2012, **51**, 4943.
- 26 C. Brinkmann, A. G. M. Barrett, M. S. Hill, and P. A. Procopiou, *J. Am. Chem. Soc.*, 2012, **134**, 2193.
- 27 M. R. Gagné, L. Brard, V. P. Conticello, M. A. Giardello, T. J. Marks, and C. L. Stern, *Organometallics*, 1992, **11**, 2003.
- 28 M. A. Giardello, V. P. Conticello, L. Brard, M. Sabat, A. L. Rheingold, C. L. Stern, and T. J. Marks, *J. Am. Chem. Soc.*, 1994, **116**, 10212.
- 29 M. A. Giardello, V. P. Conticello, L. Brard, M. R. Gagne, and T. J. Marks, *J. Am. Chem. Soc.*, 1994, **116**, 10241.
- 30 M. R. Douglass, M. Ogasawara, S. Hong, M. V. Metz, and T. J. Marks, *Organometallics*, 2002, **21**, 283.
- 31 S. Hong, A. M. Kawaoka, and T. J. Marks, *J. Am. Chem. Soc.*, 2003, **125**, 15878.
- 32 D. V. Gribkov, K. C. Hultsch, and F. Hampel, *Chem. Eur. J.*, 2003, **9**, 4796.
- 33 S. Hong, S. Tian, M. V. Metz, and T. J. Marks, *J. Am. Chem. Soc.*, 2003, **125**, 14768.
- 34 J. Collin, J. -D. Daran, E. Schulz, and A. Trifonov, *Chem. Commun.*, 2003, 3048.
- 35 P. N. O'Shaughnessy and P. Scott, *Tetrahedron: Asymmetry*, 2003, **14**, 1979.
- 36 J. Eppinger, M. Spiegler, W. Hieringer, W. A. Herrmann, and R. Anwander, *J. Am. Chem. Soc.*, 2000, **122**, 3080.
- 37 R. R. Fraser, T. S. Mansour, and S. Savard, *J. Org. Chem.*, 1985, **50**, 3232.

- 38 K. C. Hultzsch, F. Hampel, and T. Wagner, *Organometallics*, 2004, **23**, 2601.
- 39 P. N. O'Shaughnessy, P. D. Knight, C. Morton, K. M. Gillespie, and P. Scott, *Chem. Commun.*, 2003, 1770.
- 40 Q. Wang, L. Xiang, H. Song, and G. Zi, *J. Organometallic Chem.*, 2009, **694**, 691.
- 41 J. Y. Kim and T. Livinghouse, *Org. Lett.*, 2005, **7**, 1737.
- 42 Q. Wang, H. Song, and G. Zi, *J. Organomet. Chem.*, 2010, **695**, 1583.
- 43 G. Zi, X. Liu, L. Xiang, and H. Song, *Organometallics*, 2009, **28**, 1127.
- 44 Q. Wang, F. Zhang, H. Song, and G. Zi, *J. Organometallic Chem.*, 2011, **696**, 2186.
- 45 D. V. Gribkov, F. Hampel, and K. C. Hultzsch, *Eur. J. Inorg. Chem.*, 2004, 4091.
- 46 D. V. Gribkov and K. C. Hultzsch, *Chem. Commun.*, 2004, 730.
- 47 J. Collin, J.-C. Daran, O. Jacquet, E. Schulz, and A. Trifonov, *Chem. Eur. J.*, 2005, **11**, 3455.
- 48 S. Vyskocil, S. Jaracz, M. Smrcina, M. Sticha, V. Hanus, M. Polasek, and P. Kocovsky, *J. Org. Chem.*, 1998, **63**, 7727.
- 49 D. Reigert, J. Collin, A. Meddour, E. Schulz, and A. Trifonov, *J. Org. Chem.*, 2006, **71**, 2514.
- 50 I. Aillaud, C. Olier, Y. Chapurina, J. Collin, E. Schulz, R. Guillot, J. Hannedouche, and A. Trifonov, *Organometallics*, 2011, **30**, 3378.
- 51 X. Yu and T. J. Marks, *Organometallics*, 2007, **26**, 365.
- 52 E. Ichikawa, M. Suzuki, K. Yabu, M. Albert, M. Kanai, and M. Shibasaki, *J. Am. Chem. Soc.*, 2004, **126**, 11808.
- 53 Y. Hamashima, D. Sawada, H. Nogami, M. Kanai, and M. Shibasaki, *Tetrahedron*, 2001, **57**, 805.
- 54 M. Takamura, K. Funabashi, M. Kanai, and M. Shibasaki, *J. Am. Chem. Soc.*, 2001, **123**, 6801.



- 55 M. Takamura, K. Funabashi, M. Kanai, and M. Shibasaki, *J. Am. Chem. Soc.*, 2000, **122**, 6327.
- 56 Y. Hamashima, D. Sawada, M. Kanai, and M. Shibasaki, *J. Am. Chem. Soc.*, 1999, **121**, 2641.
- 57 H. W. Görlitzer, M. Spiegler, and R. Anwender, *J. Chem. Soc. Dalton Trans.*, 1999, 4287.
- 58 B. D. Ward and L. H. Gade, *Chem. Commun.*, 2012, **48**, 10587.
- 59 D. -P. Li, T. -W. Wang, C. -H. Li, D. -S. Liu, Y. -Z. Li, and X. -Z. You, *Chem. Commun.*, 2010, **46**, 2929.
- 60 E. L. Eliel and S. H. Wilen, 'Stereochemistry of Organic Compounds', Wiley, 1994.
- 61 S. Kobayashi, 'Lanthanides: Chemistry and use in organic synthesis', Springer-Verlag, 1999.
- 62 P. K. Jadhav and H. -W. Man, *J. Am. Chem. Soc.*, 1997, **119**, 846.
- 63 C. Qian and L. Wang, *Tetrahedron: Asymmetry*, 2000, **11**, 2347.
- 64 G. Desimoni, G. Faita, S. Filippone, M. Mella, M. G. Zampori, and M. Zema, *Tetrahedron*, 2001, **57**, 10203.
- 65 L. H. Gade, G. Marconi, C. Dro, B. D. Ward, M. Poyatos, S. Bellemin-Lapponnaz, H. Wadepohl, L. Sorace, and G. Poneti, *Chem. - Eur. J.*, 2007, **13**, 3058.
- 66 B. D. Ward; S. Bellemin-lapponnez; L. H. Gade, *Angew. Chem. Int. Ed.*, 2005, **44**, 1668.
- 67 L. H. Gade and S. Bellemin-Lapponnaz, *Chem. - Eur. J.*, 2008, **14**, 4142.
- 68 L. Lukešová, B. D. Ward, S. Bellemin-Lapponnaz, H. Wadepohl, and L. H. Gade, *Dalton Trans.*, 2007, 920.
- 69 L. Lukešová, B. D. Ward, S. Bellemin-Lapponnaz, H. Wadepohl, and L. H. Gade, *Organometallics*, 2007, **26**, 4652.

- 70 B. D. Ward, L. Lukešová, H. Wadepohl, S. Bellemin-Laponnaz, and L. H. Gade, *Eur. J. Inorg. Chem.*, 2009, 866.
- 71 E. Y. Tshuva, S. Groysman, I. Goldberg, and M. Kol, *Organometallics*, 2002, **21**, 662.
- 72 S. Groysman, I. Goldberg, M. Kol, E. Genizi, and Z. Goldschmidt, *Inorg. Chim. Acta*, 2003, **345**, 137.
- 73 D. A. Evans, K. A. Scheidt, K. R. Fandrick, H. W. Lam, and J. Wu, *J. Am. Chem. Soc.*, 2003, **125**, 10780.
- 74 A. I. Sanchez-Blanco, K. V. Gothelf, and K. A. Jørgensen, *Tetrahedron Lett.*, 1997, **38**, 7923.
- 75 S. Fukuzawa, H. Matsuzawa, and K. Metoki, *Synlett*, 2001, 709.
- 76 G. Desimoni, G. Faita, M. Guala, and A. Laurenti, *Eur. J. Inorg. Chem.*, 2004, 3057.
- 77 G. Desimoni, G. Faita, M. Guala, and C. Pratelli, *Tetrahedron*, 2002, **58**, 2929.
- 78 G. Desimoni, G. Faita, M. Guala, and C. Pratelli, *J. Org. Chem.*, 2003, **68**, 7862.
- 79 G. Desimoni, G. Faita, M. Guala, A. Laurenti, and M. Mella, *Chem. - Eur. J.*, 2005, **11**, 3816.
- 80 G. Desimoni, G. Faita, M. Toscanini, and M. Boiocchi, *Chem. - Eur. J.*, 2007, **13**, 9478.
- 81 G. Desimoni, G. Faita, M. Mella, F. Piccinini, and M. Toscanini, *Eur. J. Org. Chem.*, 2007, 1529.
- 82 G. Desimoni, G. Faita, A. Livieri, M. Mella, L. Ponta, and M. Boiocchi, *Eur. J. Org. Chem.*, 2012, 2916.
- 83 D. A. Evans, C. E. Masse, and J. Wu, *Org. Lett.*, 2002, **4**, 3375.
- 84 D. A. Evans and J. Wu, *J. Am. Chem. Soc.*, 2005, **127**, 8006.
- 85 D. A. Evans, Y. Aye, and J. Wu, *Org. Lett.*, 2006, **8**, 2071.

- 86 J. Comelles, A. Pericas, M. Moreno-Manus, A. Vallribera, G. Drudis-Sole, A. Lledos, T. Parella, A. Roglans, S. Garcia-Granda, and L. Roces-Fernandez, *J. Org. Chem*, 2007, **27**, 2077.
- 87 H. C. Aspinall, N. Greeves, and P. M. Smith, *Tetrahedron Lett.*, 1999, **40**, 1763.
- 88 H. C. Aspinall, J. L. M. Dwyer, N. Greeves, P. M. Smith, and *J. Alloys Compd.*, 2000, **303-304**, 173.
- 89 S. Lundgren, S. Lutsenko, C. Jonsson, and C. Moberg, *Org. Lett.*, 2003, **5**, 3663.
- 90 S. E. Schaus and E. N. Jacobsen, *Org. Lett.*, 2000, **2**, 1001.
- 91 M. Tilliet, S. Lundgren, C. Moberg, and V. Levacher, *Adv. Synth. Catal.*, 2007, **349**, 2079.
- 92 D. A. Evans, Z. K. Sweeney, R. Tomislav, and J. S. Tedrow, *J. Am. Chem. Soc.*, 2001, **123**, 12095.
- 93 D. A. Evans, K. R. Fandrick, and H. J. Song, *J. Am. Chem. Soc.*, 2005, **127**, 8942.
- 94 D. A. Evans and K. A. Fandrick, *Org. Lett.*, 2006, **8**, 2249.
- 95 D. A. Evans, K. R. Fandrick, H. J. Song, K. A. Scheidt, and R. Xu, *J. Am. Chem. Soc.*, 2007, **129**, 10029.
- 96 M. Inoue, T. Suzuki, and M. Nakada, *J. Am. Chem. Soc.*, 2003, **125**, 1140.
- 97 J. Zou, D. J. Berg, D. Stuart, R. McDonald, and B. Twamley, *Organometallics*, 2011, **30**, 4958.
- 98 H. Kodama, J. Ito, K. Hori, T. Ohta, and I. Furakawa, *J. Organomet. Chem*, 2000, **603**, 6.
- 99 H. A. McManus and P. J. Guiry, *J. Org. Chem*, 2002, **67**, 8566.

## **CHAPTER 2**

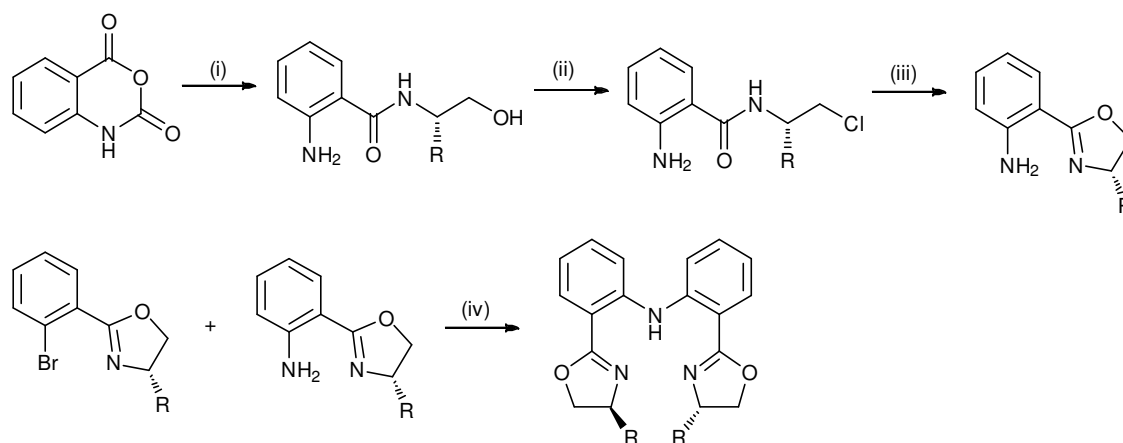
# **Coordination chemistry of BOPA supported Group 3/lanthanide complexes**

## 2.1 Introduction

Lanthanide complexes bearing chiral ligands have been shown to make highly effective catalysts for many reactions, including hydroamination,<sup>1-5</sup> hydrosilylation,<sup>6-9</sup> hydrogenation<sup>10-12</sup> and polymerisation.<sup>13-16</sup> As shown throughout Chapter 1, oxazoline ligands are privileged ligands and their complexes with lanthanide metals have found significant success in asymmetric catalysis, principally in Lewis acid catalysis. Although their success in asymmetric Lewis acid catalysis has been profound, the application of lanthanide-oxazoline complexes to organometallic and related chemistry (*i.e.* complexes bearing alkyl, amide, or hydride co-ligands), and their associated catalytic reactions has been more limited. Marks (hydroamination)<sup>4</sup> and Carpentier (ring opening polymerisation of lactide)<sup>17</sup> have provided the only examples of organometallic and related lanthanide oxazoline complexes in catalysis. Both of these reports involved the bis(oxazolinyl)methane (BOX) ligand. From an analysis of oxazoline ligands in lanthanide-catalysed reactions, it is clear that tridentate ligands, such as the pyridine-bisoxazoline (pybox) ligand have provided much greater success in terms of reactivity and stereocontrol, compared to the BOX ligand,<sup>18</sup> and it is in this context that this thesis approaches the area by discussing the coordination chemistry and catalytic performance of a tridentate bisoxazoline ligand bearing an additional donor situated between the two oxazoline donor groups. In order to reduce the number of anionic co-ligands coordinated to the lanthanide ion, a ligand bearing an anionic donor group was identified, since this would necessitate the removal of one of the co-ligands by deprotonation of the protio-ligand precursor.

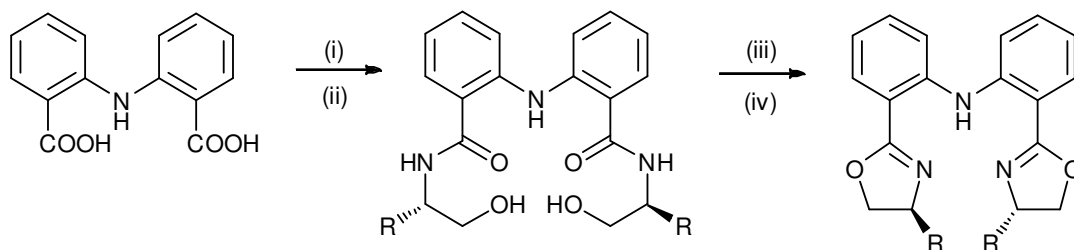
These ligand requirements are found in the bis(oxazolinylphenyl)amine (BOPA) ligand framework.<sup>19, 20</sup> The BOPA ligands have found success in asymmetric catalysis using late transition metals, but have not been extensively employed in early transition metal or lanthanide complexes.<sup>21</sup> The two oxazoline rings are bridged by an N,N-diphenylamine

moiety, thus providing a deprotonation site, rendering an anionic ligand with a central amide anchor. In addition, the highly conjugated ligand architecture provides a potential antenna for the sensitising of lanthanide ions, which could be used in the speciation of paramagnetic lanthanide catalysts and is discussed in Chapter 5.



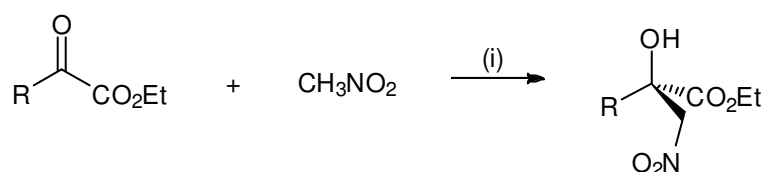
**Scheme 1** Palladium-catalysed synthesis of R-BOPA (**2.1**, R = Ph **a**, Bn **b**, iPr **c**, <sup>t</sup>Bu **d**). (i) amino alcohol, dioxane, 60 °C, 2.5h; (ii) SOCl<sub>2</sub>; (iii) NaOH, EtOH, reflux, 3 h; (iv) Pd (0)

The original literature procedure describing the synthesis of the BOPA ligands is displayed in Scheme 1. The procedure relies on forming the two oxazoline moieties separately, followed by a palladium-catalysed coupling reaction to connect the two halves of the ligand.<sup>19</sup> This synthetic route has the advantage that unsymmetrical BOPA derivatives can be prepared, but the ring-closing steps give various products, which result in a low yield (~45%). An alternative method has been reported that avoids using precious metals, and is depicted in Scheme 2. The four-step reaction involves the synthesis of the bridge structure, before formation of the bis(hydroxyamide) from the acid chloride and an amino alcohol. After appropriate activation, the bis(hydroxyamide) is cyclised using NaOH.<sup>21</sup>



**Scheme 2** Alternative synthesis of R-BOPA (**2.1**, R = Ph **a**, Bn **b**, iPr **c**, <sup>t</sup>Bu **d**). (i) SOCl<sub>2</sub>, reflux 4 hrs; (ii) amino alcohol, DCM, Et<sub>3</sub>N, RT, 24 hrs; (iii) MsCl, DCM, Et<sub>3</sub>N, 20 hrs; (iv) NaOH, MeOH/H<sub>2</sub>O, reflux 3 hrs

This study also included the catalytic performance of the R-BOPA ligands when coordinated to La(OTf)<sub>3</sub>, Zn(OTf)<sub>2</sub> and Cu(OTf)<sub>2</sub>. The complexes were screened in the asymmetric Henry reaction between ethyl pyruvate and nitromethane (Scheme 3).



**Scheme 3** The Asymmetric Henry reaction between ethyl pyruvate and nitromethane. (i) 20 mol% chiral ligand, 20 mol% Lewis acid, Et<sub>3</sub>N

The Henry reaction products were obtained with poor to good enantioselectivities (3-60%), suggesting that there is significant potential for lanthanide BOPA complexes in asymmetric catalysis.

## 2.2 Density Functional Theory (DFT)

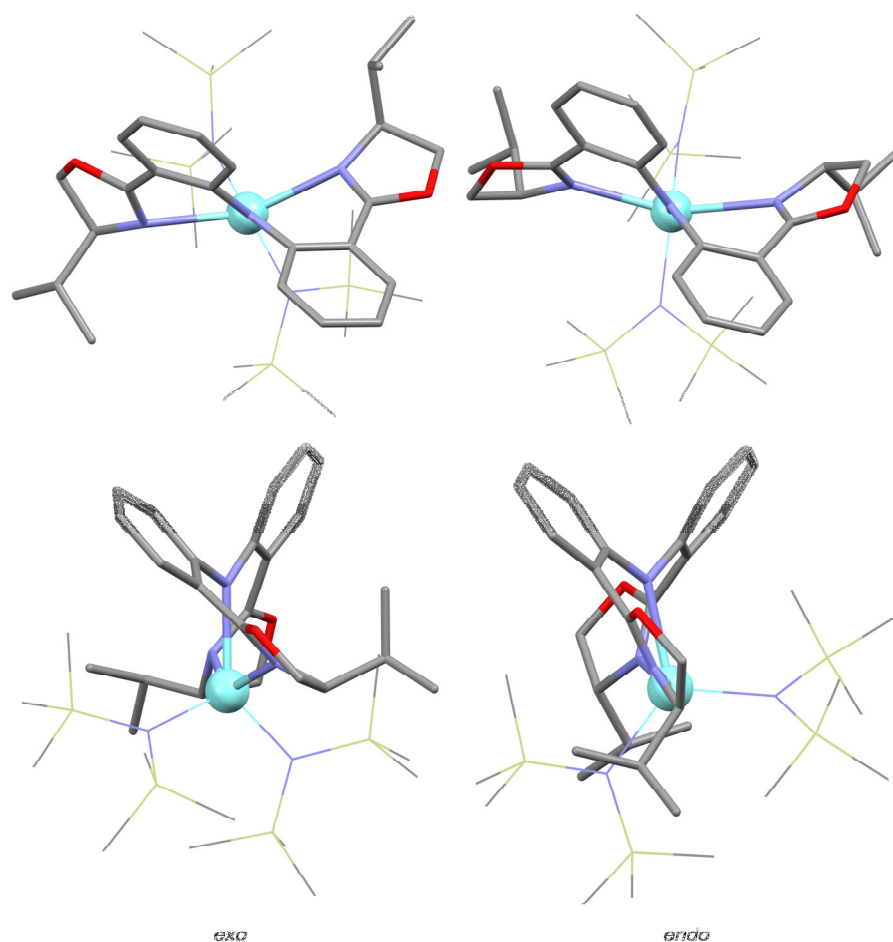
The viability of the lanthanide BOPA complexes was assessed using density functional theory (DFT) calculations, in which the structures of a selection of the proposed

complexes were calculated and evaluated. The calculations were carried out by Dr. Benjamin Ward in collaboration with the Advanced Research Computing in Cardiff (ARCCA) facility, using the Gaussian 09 software package.<sup>22</sup> All geometry optimisations were performed using the restricted hybrid B3LYP functional, employing the Stuttgart/Dresden basis set with effective core potentials for the metal ions, 6-31G(d,p) for the coordinating atoms, and 6-31G for all other centres. Geometry optimisations were performed without symmetry restraints and were followed by frequency calculations to ascertain the nature of the stationary point (minimum *vs.* saddle point).

The structures of [Sc(R-BOPA){N(SiMe<sub>3</sub>)<sub>2</sub>}Cl] (**2<sub>calc</sub>**), [Sc(R-BOPA){N(SiMe<sub>3</sub>)<sub>2</sub>}(OTf)] (**4<sub>calc</sub>**), [Ln(R-BOPA)(CH<sub>2</sub>SiMe<sub>3</sub>)<sub>2</sub>] (Ln = Sc **5<sub>calc</sub>**, Y **8<sub>calc</sub>**), [Sc(R-BOPA)(CH<sub>2</sub>SiMe<sub>3</sub>)<sub>2</sub>]<sup>+</sup> (**6<sub>calc</sub>**), [Ln(R-BOPA){N(SiMe<sub>3</sub>)<sub>2</sub>]<sub>2</sub>] (Ln = Y **7<sub>calc</sub>**, La **10<sub>calc</sub>**) bearing each of the three BOPA derivatives employed in this thesis (Ph **a**, Bn **b**, iPr **c**) were calculated in the gas phase and in a solvent continuum. Benzene was chosen since the complexes were to be analysed primarily using NMR spectroscopy in C<sub>6</sub>D<sub>6</sub>. The calculations were based on the two isomeric forms of each complex, arising from a difference in the helical twist of the diphenylamido ligand backbone. The two isomers are therefore diastereomers, and possess a significantly different orientation of the ligand substituent groups, which may be directed “*exo*”, *i.e.* away from the co-ligands, or “*endo*”, *i.e.* towards the co-ligands. The two isomeric forms are depicted in Fig. 1 for the yttrium amide complex [Y(iPr-BOPA){N(SiMe<sub>3</sub>)<sub>2</sub>]<sub>2</sub>. An analysis of the relative orientation of the stereodirecting groups suggests that the *exo* isomer is likely to provide a greater degree of control over the stereochemical outcome of a catalytic reaction, since there is greater differentiation between the two faces of the complex, with the stereodirecting groups providing a significant degree of shielding to both sides of the complex. The chirality of the ligand in the *endo* orientation is rather less well expressed in the structure and stereochemical environment of the metal.



The energies of the isomers for each of the complexes were calculated and the differences are reported in Table 1.



**Fig. 1** Calculated molecular structures of  $[Y(iPr-BOPA)\{N(SiMe_3)_2\}_2]$  **7c<sub>calc</sub>**, illustrating the *exo* and *endo* isomers. Top: view along the  $N_{amide}-Y$  bond; bottom: perpendicular view along the  $N_{oxazoline}-Y-N_{oxazoline}$  vector

In most cases, the *exo* isomer was predicted to be the most stable isomer by several  $\text{kcal.mol}^{-1}$ . The exceptions pertain solely to some of the isopropyl derivatives, which is the least sterically demanding stereodirecting group.

**Table 1** Calculated relative energies between the *exo* and *endo* isomers of [Ln(R-BOPA)<sub>n</sub>]

Entry	Complex	R	$\Delta G_{\text{calc}}$ kcal ( <i>vacuo</i> ) <sup>a</sup>	$\Delta G_{\text{calc}}$ kcal (benzene) <sup>a</sup>
1	[Sc(R-BOPA){N(SiMe <sub>3</sub> ) <sub>2</sub> }Cl] 2 <sub>calc</sub>	Ph	4.8	5.5
2		Bn	1.6	1.3
3		iPr	-1.0	-1.8
4	[Sc(R-BOPA){N(SiMe <sub>3</sub> ) <sub>2</sub> }(OTf)] 4 <sub>calc</sub>	Ph	2.4	0.9
5		Bn	3.1	3.4
6		iPr	-1.9	-0.7
7	[Sc(R-BOPA)(CH <sub>2</sub> SiMe <sub>2</sub> Ph) <sub>2</sub> ] 5 <sub>calc</sub>	Ph	11.6	11.9
8		Bn	1.9	1.1
9		iPr	7.9	7.3
10	[Sc(R-BOPA)(CH <sub>2</sub> SiMe <sub>2</sub> Ph)] <sup>+</sup> 6 <sub>calc</sub>	Ph	4.3	1.9
11		Bn	4.2	- <sup>b</sup>
12		iPr	0.0	0.0
13	[Y(R-BOPA){N(SiMe <sub>3</sub> ) <sub>2</sub> }] <sub>2</sub> 7 <sub>calc</sub>	Ph	7.0	6.8
14		Bn	3.6	1.5
15		iPr	-0.6	-0.6
16	[Y(R-BOPA)(CH <sub>2</sub> SiMe <sub>2</sub> Ph) <sub>2</sub> ] 8 <sub>calc</sub>	Ph	3.4	3.3
17		Bn	2.2	2.3
18		iPr	5.9	5.4
19	[La(R-BOPA){N(SiMe <sub>3</sub> ) <sub>2</sub> }] <sub>2</sub> 10 <sub>calc</sub>	Ph	6.1	6.5
20		Bn	2.3	1.0
21		iPr	-0.1	1.4

<sup>a</sup>  $G_{\text{endo}} - G_{\text{exo}}$ ; positive values indicate that the *exo* isomer is energetically favoured;

<sup>b</sup> calculation of optimised geometry failed to converge

For the less bulky systems,  $\Delta G_c$  is small or even negative. Increasing the steric demand tends to destabilise the *endo* system, so for example the Ph compounds, those containing a bulky coligand, and those containing a smaller metal tend to favour the *exo* isomer, where the bulky substituents are much further apart (Fig.1). Repeating the calculations in the presence of a solvent medium did not significantly change the relative

stabilities. The energies altered by up to 2 kcal.mol<sup>-1</sup>, which is within the experimental error of the calculation.

For the diamide complexes [Ln(R-BOPA){N(SiMe<sub>3</sub>)<sub>2</sub>]<sub>2</sub>] (Ln = Y **7**<sub>calc</sub>, La **10**<sub>calc</sub>) (R = Ph **a**, Bn **b**, <sup>i</sup>Pr **c**) the greatest energy differences were predicted for the Ph-BOPA supported complexes. This is presumably due to the greater steric demand of the phenyl group in comparison to the isopropyl and benzyl congeners. This suggests that when these complexes are employed in asymmetric catalysis, the ratio of *exo* to *endo* isomers will favour that of the *exo* isomer, and thereby providing higher levels of selectivity. However, the calculations clearly indicate that both isomers are energetically accessible, and therefore expected to be implicated in a detailed analysis of their coordination chemistry. Such a conclusion is entirely consistent with the experimental observations discussed *vide infra*.

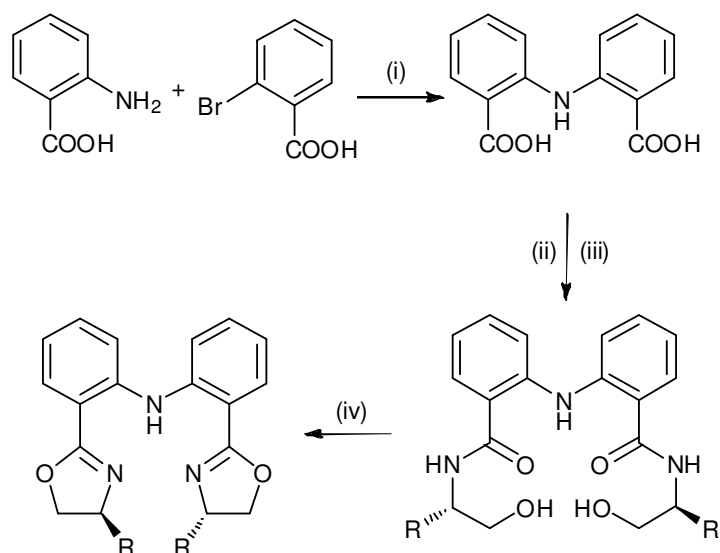
Comparing the relative stabilities of the lanthanum and yttrium amide complexes [Ln(R-BOPA){N(SiMe<sub>3</sub>)<sub>2</sub>]<sub>2</sub>], in the gas phase, the lanthanum complexes show lower energy differences than those for the corresponding yttrium congeners. Although this is a general trend in these data, the energies become less distinguishable when calculated in a solvent continuum, particularly for the phenyl derivatives (6.8 vs. 6.5 kcal.mol<sup>-1</sup> for the yttrium and lanthanum complexes respectively).

ΔG<sub>c</sub> for yttrium alkyl complexes (**8**<sub>calc</sub>) (R = Ph **a**, Bn **b**, <sup>i</sup>Pr **c**) was only 3.4 kcal mol<sup>-1</sup> compared with 7.0 kcal mol<sup>-1</sup> for the bulkier amide systems (**7**<sub>calc</sub>). This indicates that the reduction in steric strain (a result of the less sterically demanding alkyl co-ligand compared to the silylamide) gives less energetic preference between the *exo* and *endo* isomers. This situation is less clear for the benzyl and isopropyl congeners, since the energy difference for the benzyl complexes undergo a less significant change, and the energetic preference for the *exo* isomer increases for the isopropyl BOPA derivative.

The energetic preference for the *exo* isomer in the scandium alkyl complexes **5<sub>calc</sub>** increases for the phenyl and isopropyl derivatives, again reflecting the increased steric strain caused by the shorter Ln-C bonds on moving from yttrium to scandium. The benzyl derivative shows the opposite trend, and may be due to the benzyl substituents ability to rotate. The relative energies for the phenyl and isopropyl congeners was, as expected, reduced on calculating the 4-coordinate cationic complexes, although again, the benzyl derivative shows the opposite trend. An assessment of the reliability of these energies as a means of probing the experimentally determined preference for the isomers will be discussed at the end of this chapter.

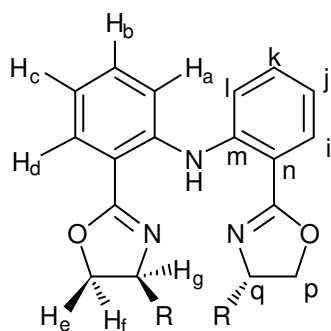
### 2.3 Ligand synthesis

A modified procedure for the synthesis of the BOPA ligand was developed, in order to increase the yields and to reduce the synthetic complexity. Instead of employing a two step cyclisation of the intermediate bis(hydroxyamide) (*i.e.* activation with methanesulphonyl chloride followed by a base-catalysed cyclisation, Scheme 2), a one-pot cyclisation route from the bis(hydroxyamide) using toluenesulphonyl chloride and N,N-dimethylaminopyridine (DMAP) was employed (Scheme 4). This method was inspired by the route employed by Gade for a series of tris(oxazolinyl)ethane (trisoX) ligands,<sup>23</sup> and was found to give improved yields of up to 80% for the BOPA ligands.



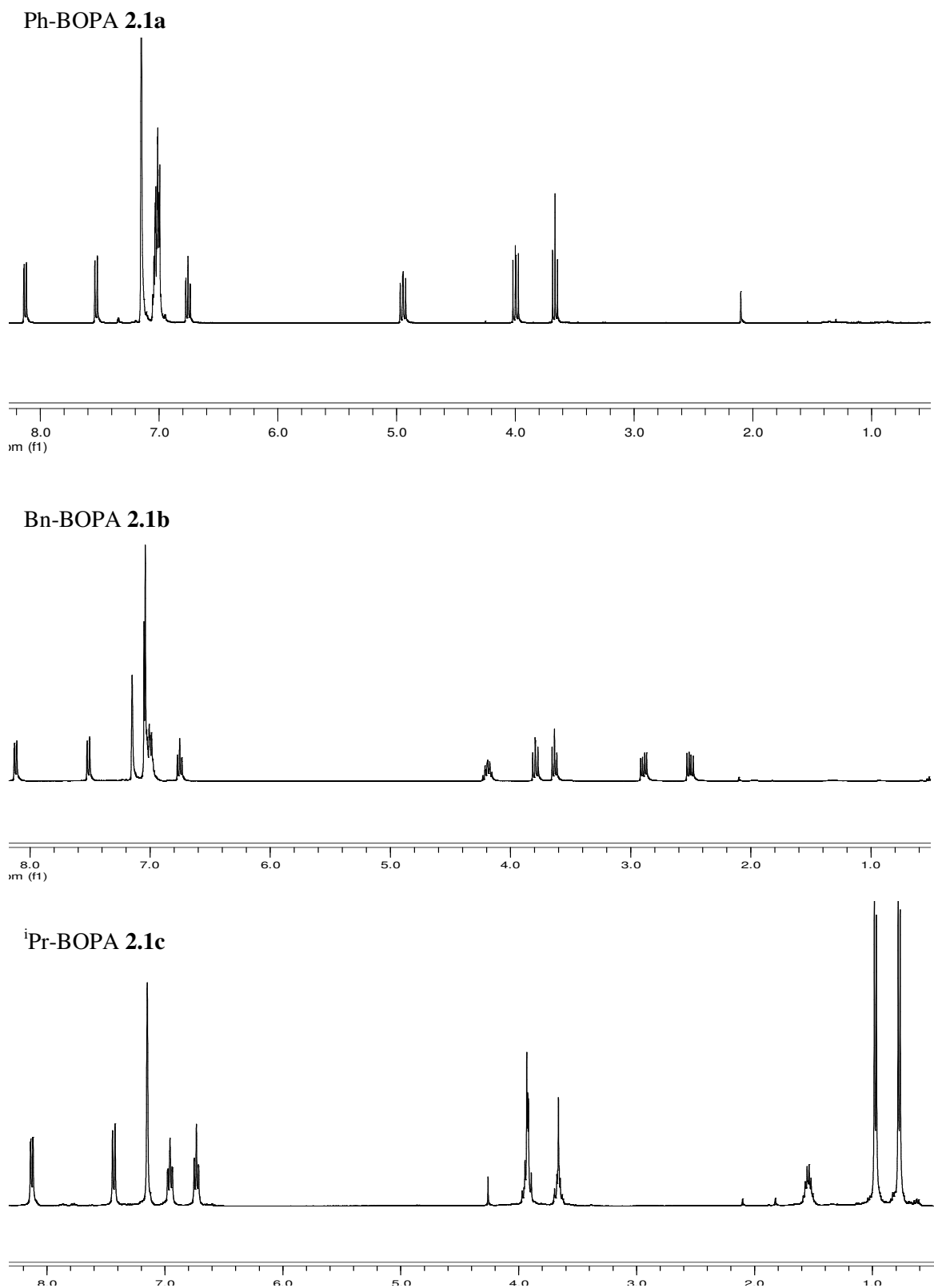
**Scheme 4** Modified procedure for the synthesis of R-BOPA (R = Ph **2.1a**, Bn **2.1b**, iPr **2.1c**). (i)  $\text{K}_2\text{CO}_3$ , DMF, CuO, Cu, reflux 4 hrs; (ii)  $\text{SOCl}_2$ , reflux 4 hrs; (iii) amino alcohol, DMAP, DCM,  $\text{Et}_3\text{N}$ , stir RT 16 hrs; (iv) TsCl, DMAP,  $\text{Et}_3\text{N}$

### 2.3.1 Spectroscopic characterisation of 2.1a-c



**Fig. 2** Labelling scheme used throughout this thesis to describe spectroscopic data pertaining to the R-BOPA ligands (**2.1**). R = Ph **a**, Bn **b** and iPr **c**

The NMR spectra of the Group 3 and lanthanide complexes described in this thesis were measured primarily in  $\text{C}_6\text{D}_6$ . In order to adequately assess and describe their spectra, the  $^1\text{H}$  NMR spectra of the three BOPA ligands were recorded in  $\text{C}_6\text{D}_6$  and are briefly discussed below.



**Fig. 3**  $^1\text{H}$  NMR (400 MHz,  $\text{C}_6\text{D}_6$ ) spectra of **2.1a-c**

The  $^1\text{H}$  NMR spectra of the three R-BOPA ligands (R = Ph **2.1a**, Bn **2.1b**,  $i\text{Pr}$  **2.1c**) are displayed in Fig. 3. Each spectrum is consistent with the expected  $C_2$  symmetry, with

both of the phenyl rings of the ligand backbone, and both of the oxazoline rings, giving equivalent signals. The spectrum of Ph-BOPA (**2.1a**) exhibits three well resolved resonances in the aromatic region at 8.13, 7.53 and 6.76 ppm, which are attributed to H<sup>d</sup>, H<sup>a</sup> and H<sup>c</sup> proton environments respectively. The multiplet at 7.07-6.96 ppm has been assigned to H<sup>b</sup> and the aromatic protons of the phenyl stereodirecting groups. The oxazoline resonances are observed at 4.95, 4.00 and 3.67 ppm, assigned to H<sup>g</sup>, H<sup>e</sup> and H<sup>f</sup> respectively.

The <sup>1</sup>H NMR spectra of Bn-BOPA (**2.1b**) and iPr-BOPA (**2.1c**) exhibit similar features to the spectrum of **2.1a**, with comparable signals being observed for the ligand backbone and the oxazoline methylene protons. The principal differences in the spectra are observed for the signals attributed to the stereodirecting groups and H<sup>g</sup>. For the benzyl derivative (**2.1b**), the signals attributed to the aromatic benzyl protons overlap with the ligand backbone signals, and are therefore indistinguishable without recourse to 2D correlation experiments. However, the benzyl methylene proton signals are observed at 2.89 and 2.51 ppm. The signal assigned to the protons attributed to H<sup>g</sup> is observed at 4.18 ppm, significantly upfield in comparison to that in the phenyl derivative (**2.1a**). In the <sup>1</sup>H NMR spectrum of iPr-BOPA (**2.1c**), the oxazoline protons give rise to multiplets at 3.93 and 3.66 ppm, H<sup>g</sup> shifting significantly upfield in comparison to **2.1a** and **2.1b**. The methine protons of the isopropyl groups were observed as a signal at 1.55 ppm, whilst the two doublets at 0.98 and 0.77 ppm correspond to the isopropyl methyl groups.

## 2.4 Preparation and Characterisation of Scandium Complexes

Studies into the coordination chemistry of the BOPA ligands with Group 3 and lanthanide metals commenced with scandium. Scandium is often chosen as a suitable starting point particularly when alkyl co-ligands are employed; since the relatively small ionic radius renders scandium complexes more thermally stable than their yttrium or lanthanide congeners. In this section, a new scandium precursor is described, along with a number of scandium complexes bearing the BOPA ligands. The scandium precursors  $[\text{Sc}(\text{CH}_2\text{SiMe}_2\text{Ph})_3(\text{THF})_2]^{24}$  (**2.2**) and  $[\text{Sc}\{\text{N}(\text{SiMe}_3)_2\}_3]^{25}$  (**2.3**) were used, and were prepared according to literature procedures.

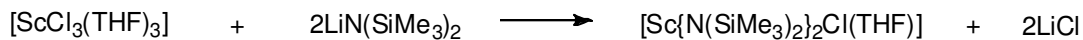
The reaction of  $[\text{Sc}\{\text{N}(\text{SiMe}_3)_2\}_3]$  (**2.3**) with R-BOPA (all derivatives) proved unsuccessful; even under forcing conditions the ligand failed to coordinate. When carried out on an NMR tube scale in  $\text{C}_6\text{D}_6$ , the  $^1\text{H}$  NMR spectrum indicated a mixture of the starting materials, although the signals attributed to the BOPA ligand were broader than those of the ligand without the scandium precursor. This suggests that there was a degree of interaction between the scandium and ligand, but without any deprotonation of the ligand, and no isolable product was obtained. Given the relatively small ionic radius of scandium, and the sterically demanding nature of the  $\text{N}(\text{SiMe}_3)_2$  co-ligands, this observation was attributed to a high activation barrier to coordination, arising from steric repulsion.

### 2.4.1 Synthesis of $[\text{Sc}\{\text{N}(\text{SiMe}_3)_2\}_2\text{Cl}(\text{THF})]$ (**1**)

In order to alleviate steric strain in the scandium complexes, the diamide monochloride precursor complex  $[\text{Sc}\{\text{N}(\text{SiMe}_3)_2\}_2\text{Cl}(\text{THF})]$  (**1**) was prepared by the reaction of  $[\text{ScCl}_3(\text{THF})_3]$  with *two* equivalents of  $\text{LiN}(\text{SiMe}_3)_2$  in cold (0 °C) THF (Scheme 5). The compound was isolated as a white, air- and moisture sensitive solid after extraction into



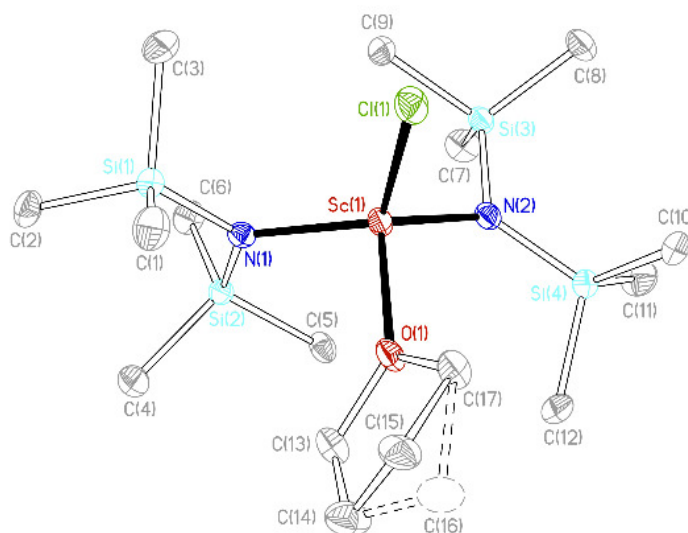
pentane, in 78% yield. Compound **1** was characterised by X-ray crystallography, NMR and IR spectroscopies.



**Scheme 5** Synthesis of  $[\text{Sc}\{\text{N}(\text{SiMe}_3)_2\}_2\text{Cl}(\text{THF})]$  (**1**)

### 2.4.1.1 X-ray crystal structure of $[\text{Sc}\{\text{N}(\text{SiMe}_3)_2\}_2\text{Cl}(\text{THF})]$ (**1**)

Single crystals of **1** suitable for X-ray diffraction were grown from a saturated pentane solution overnight at 0 °C. The X-ray data were collected by Dr. Benson Kariuki and solved by Dr. Benjamin Ward. The molecular structure of **1** is shown in Fig. 4, and selected bond lengths and angles shown in Table 2. Full listings of crystal data are provided in Appendix A.



**1**

**Fig. 4** Thermal ellipsoid plot (25%) of  $[\text{Sc}\{\text{N}(\text{SiMe}_3)_2\}_2\text{Cl}(\text{THF})]$  (**1**), H atoms emitted for clarity

**Table 2** Selected bond lengths (Å) and angles (°) for [Sc{N(SiMe<sub>3</sub>)<sub>2</sub>}<sub>2</sub>Cl(THF)] (**1**)

<b>Sc(1)-Cl(1)</b>	<b>2.381(2)</b>
<b>Sc(1)-O(1)</b>	<b>2.136(3)</b>
<b>Sc(1)-N(1)</b>	<b>2.055(3)</b>
<b>Sc(1)-N(2)</b>	<b>2.037(3)</b>
<b>Cl(1)-Sc(1)-O(1)</b>	<b>95.52(10)</b>
<b>Cl(1)-Sc(1)-N(1)</b>	<b>114.46(11)</b>
<b>O(1)-Sc(1)-N(1)</b>	<b>97.51(12)</b>
<b>Cl(1)-Sc(1)-N(2)</b>	<b>108.42(10)</b>
<b>O(1)-Sc(1)-N(2)</b>	<b>109.59(14)</b>
<b>N(1)-Sc(1)-N(2)</b>	<b>126.03(14)</b>
<b>N(1)-Si(1)-C(1)</b>	<b>110.4(2)</b>
<b>N(1)-Si(2)-C(6)</b>	<b>112.1(2)</b>
<b>N(1)-Si(1)-C(3)</b>	<b>111.4(2)</b>
<b>N(1)-Si(2)-C(4)</b>	<b>113.8(2)</b>
<b>N(1)-Si(1)-C(2)</b>	<b>114.9(2)</b>
<b>N(1)-Si(2)-C(5)</b>	<b>109.7(2)</b>
<b>N(2)-Si(3)-C(7)</b>	<b>113.2(2)</b>
<b>N(2)-Si(4)-C(11)</b>	<b>113.1(2)</b>
<b>N(2)-Si(3)-C(8)</b>	<b>113.6(2)</b>
<b>N(2)-Si(4)-C(10)</b>	<b>110.3(2)</b>
<b>N(2)-Si(3)-C(9)</b>	<b>108.4(2)</b>
<b>N(2)-Si(4)-C(12)</b>	<b>111.6(2)</b>

Complex **1** adopts a distorted tetrahedral geometry at the scandium centre. The coordinated THF ligand shows positional disorder of C(15)/C(16); one orientation is shown as a hollow ellipsoid in Fig. 4. The refined occupancy indicated the proportion of each is close to 0.5, as expected from a purely statistical distribution.

An analysis of the N-Si-C angles of Si(2) and Si(3) display a moderate degree of asymmetry. For example, the angle N(1)-Si(2)-C(5) of 109.7(2) ° is more acute than N(1)-

Si(2)-C(4) and N(1)-Si(2)-C(4) ( $113.8(2)^\circ$  and  $112.1(2)^\circ$  respectively). A similar observation was made at Si(3): The N(2)-Si(3)-C(9) angle of  $108.4(2)^\circ$  is more acute than those of N(2)-Si(3)-C(7) and N(2)-Si(3)-C(8) ( $113.2(2)^\circ$  and  $113.6(2)^\circ$  respectively). Moreover, the Sc(1)...C(5) and Sc(1)...C(9) distances of 3.380 and 3.043 Å respectively are within the sum of the Van der Waals radii of carbon (1.70 Å) and scandium (2.28 Å),<sup>26, 27</sup> which may suggest a weak  $\beta$ -Si-C interaction with the scandium. Such interactions are known for neutral Group 3 complexes bearing CH(SiMe<sub>3</sub>)<sub>2</sub> and N(SiMe<sub>3</sub>)<sub>2</sub> ligands, and have been reported for titanium complexes bearing CH<sub>2</sub>SiMe<sub>3</sub> ligands.<sup>28-30</sup> The amide ligands show approximately trigonal planar geometry (sum of angles subtended at N(1) =  $360.0(6)^\circ$ ; at N(2) =  $358.2(6)^\circ$ ) indicating that they can, in principle, act as anionic three-electron donors.

The scandium amide bond lengths (2.055(3) and 2.037(3) Å) sit within the reported range (1.900 – 2.362, average 2.097 Å for 98 compounds). The scandium chloride bond length (2.381(2) Å) sits within the reported range (2.326-2.571, average 2.423 Å) although is somewhat shorter than average. The scandium oxygen bond length (2.136(3) Å) also sits within the reported range (2.118 – 2.378, average 2.201 Å) and, as with the scandium chloride bond, shorter than average, possibly due to the low coordination number of the scandium, which tends to adopt a coordination number of 5 or 6.

#### 2.4.1.2 Spectroscopic characterisation of [Sc{N(SiMe<sub>3</sub>)<sub>2</sub>}<sub>2</sub>Cl(THF)] (1)

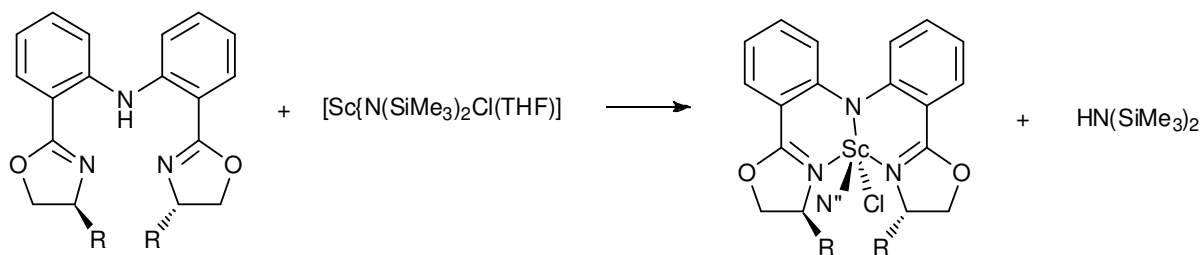
The <sup>1</sup>H and <sup>13</sup>C{<sup>1</sup>H} NMR spectra of [Sc{N(SiMe<sub>3</sub>)<sub>2</sub>}<sub>2</sub>Cl(THF)] (1) are consistent with the solid-state structure, with one resonance in the <sup>1</sup>H NMR spectrum for the SiMe<sub>3</sub> groups at 0.39 ppm (a different chemical shift in comparison to the tris amide; 0.33 ppm), and two resonances corresponding to coordinated THF at 3.82 and 1.25 ppm. The slightly downfield shift of the  $\alpha$ -THF resonance is common in related coordination complexes. Their

relative integrations are 4:4:36 ( $\alpha$ -THF:  $\beta$ -THF: SiMe<sub>3</sub>). The <sup>13</sup>C{<sup>1</sup>H} NMR spectrum exhibits resonances at 62.6, 25.5 and 4.0 ppm; the two resonances at 62.6 and 25.5 ppm arise at commonly observed shifts for coordinated THF.

The reaction of two equivalents of the lithium amide with [ScCl<sub>3</sub>(THF)<sub>3</sub>] could potentially result in a mixture of products, *i.e.* a statistical mixture of [Sc{N(SiMe<sub>3</sub>)<sub>2</sub>}]<sub>3</sub>, [Sc{N(SiMe<sub>3</sub>)<sub>2</sub>}]<sub>2</sub>Cl(THF)<sub>n</sub> and [Sc{N(SiMe<sub>3</sub>)<sub>2</sub>}]Cl<sub>2</sub>(THF)<sub>n</sub>. Although this is possible in principle, this situation was not observed and only a single species was observed in the preparation of **1**. This is readily explained by considering the high lability of ligands in *d*<sup>0</sup> metal complexes, which have no ligand field stabilisation energy. Such complexes are readily able to undergo ligand redistribution and will often favour complexes that minimise the steric repulsion in the system. In the case of **1**, facile ligand redistribution results in the amide and chloride ligands being distributed evenly, giving only a single product.

#### 2.4.2 Synthesis of [Sc(R-BOPA){N(SiMe<sub>3</sub>)<sub>2</sub>}Cl] (**2a-c**)

The scandium amide-chloride complexes [Sc(Ph-BOPA){N(SiMe<sub>3</sub>)<sub>2</sub>}Cl] (**2a**), [Sc(Bn-BOPA){N(SiMe<sub>3</sub>)<sub>2</sub>}Cl] (**2b**) and [Sc(*i*Pr-BOPA){N(SiMe<sub>3</sub>)<sub>2</sub>}Cl] (**2c**) were prepared by the reaction of the protio-ligands R-BOPA (**2.1a-c**) with **1** in cold (0 °C) THF (Scheme 6). The resulting mixture was stirred at 40 °C for 48 hours. Removal of the by-product, HN(SiMe<sub>3</sub>)<sub>2</sub>, was achieved by washing the solid with cold (-20 °C) pentane to afford **2a-c** as bright yellow solids in 75-82% yield. Compounds **2a-c** were characterised by NMR and IR spectroscopies, and by elemental analysis. Despite being spectroscopically pure, repeated attempts to obtain elemental analysis for **2a** gave unsatisfactory data.



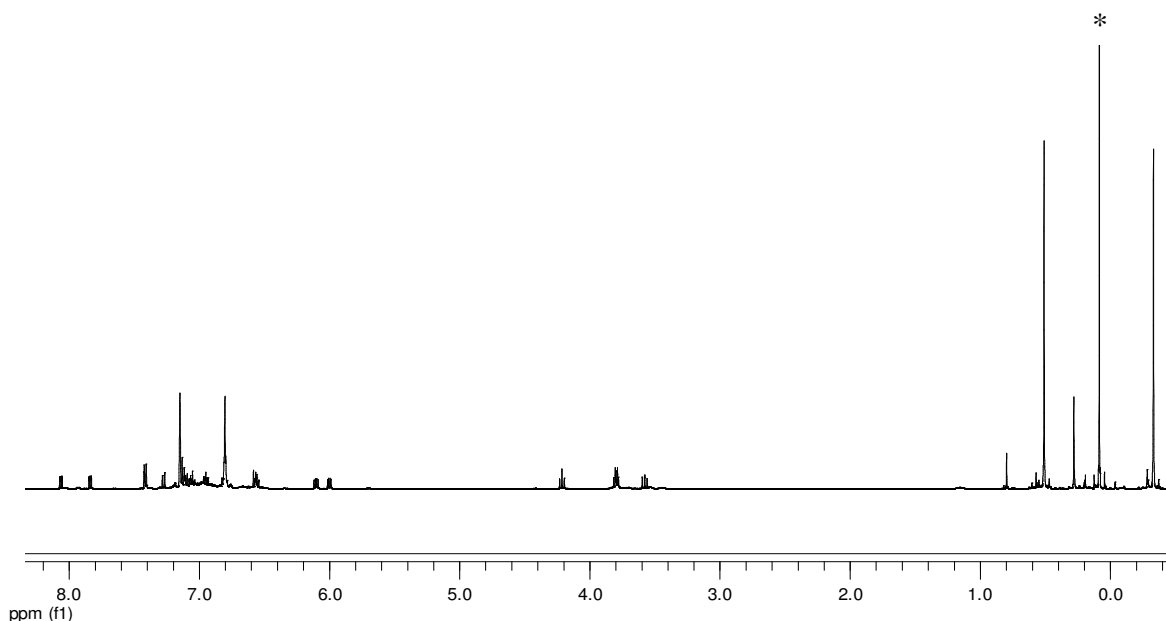
**Scheme 6** Synthesis of  $[\text{Sc}(\text{R-BOPA})\{\text{N}(\text{SiMe}_3)_2\}\text{Cl}]$  (R = Ph **2a**, Bn **2b**, iPr **2c**). N'' =  $\text{N}(\text{SiMe}_3)_2$

### 2.4.2.1 Spectroscopic Characterisation of **2a**

The  $^1\text{H}$  and  $^{13}\text{C}\{^1\text{H}\}$  NMR spectra of **2a** are consistent with  $C_1$  molecular symmetry, as expected with two different co-ligands coordinated to the scandium centre; the  $^1\text{H}$  NMR spectrum of **2a** is provided in Fig. 5. Consistent with the DFT predictions described above, two species were evident from these data and are in the ratio of 1:0.2. Based upon a comparison of the calculated energies, we attribute the major species to the *exo* isomer, and the minor species to the *endo* isomer. This assignment has been applied to all relevant complexes within this thesis. A comparison of the calculated and experimental energy differences is provided as an overarching discussion of lanthanide BOPA complexes in Section 2.9.

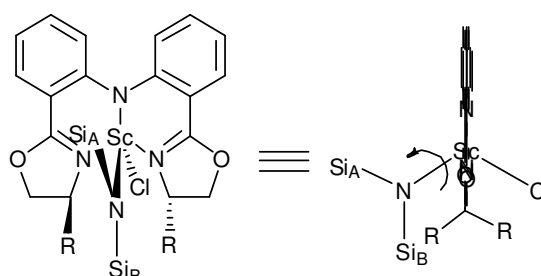
The spectra of the major (*exo*) isomer exhibit two sets of inequivalent resonances for the phenyl rings of the ligand backbone, the oxazoline protons, and the protons assigned to the stereodirecting group. However, the resonances of the minor (*endo*) isomer are more consistent with a  $C_2$  symmetric complex. Unlike the majority of reported complexes bearing  $\text{N}(\text{SiMe}_3)_2$  ligands, the NMR spectra of **2a** show inequivalent environments for the two N-bound  $\text{SiMe}_3$  groups, at 0.51 and -0.33 ppm. This is likely due to the restricted rotation about the metal-amide bond caused by the steric hindrance afforded by the BOPA ligand. This

phenomenon is described in the simplified diagram in Fig. 6, which shows the relative proximity the two SiMe<sub>3</sub> groups, arbitrarily labelled Si<sub>A</sub> and Si<sub>B</sub>.

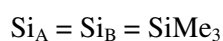


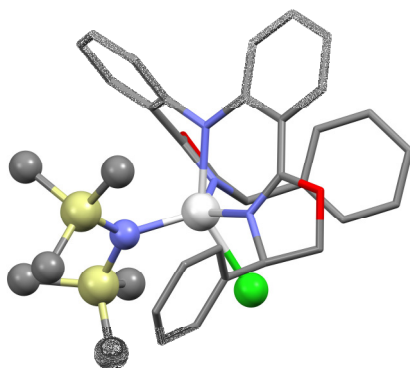
**Fig. 5** <sup>1</sup>H NMR spectrum (500 MHz) of [Sc({Ph-BOPA}){N(SiMe<sub>3</sub>)<sub>2</sub>}Cl] (**2a**) in C<sub>6</sub>D<sub>6</sub>; \* indicates impurity of silicone grease

Additionally, the restricted rotation about the Sc-N<sub>amide</sub> bond is supported by the DFT studies described above; the calculated structure of **2a<sub>calc</sub>** is displayed in Fig.7, and shows how the close proximity of one of the phenyl stereodirecting groups prevents the N(SiMe<sub>3</sub>)<sub>2</sub> ligand from undergoing free rotation, rendering one SiMe<sub>3</sub> group closer to the chloride ligand, and the other closer to the BOPA ligand backbone.



**Fig. 6** Inequivalence of SiMe<sub>3</sub> groups in [Sc(R-BOPA){N(SiMe<sub>3</sub>)<sub>2</sub>}Cl] (R = Ph **2a**, Bn **2b**, iPr **2c**).





**Fig. 7** Calculated structure of *exo*-[Sc(Ph-BOPA){N(SiMe<sub>3</sub>)<sub>2</sub>}Cl] **2a<sub>calc</sub>**

However, the remaining resonances assigned to the aromatic protons are coincident, *i.e.* not displaying the chemical shift anisotropy from the overall  $C_1$  symmetry. H<sup>d</sup> lies closest to the bridgehead nitrogen, suggesting that this proton experiences a greater anisotropy from the unsymmetrical coordination environment. H<sup>e</sup> are observed as two signals at 6.10 and 6.00 ppm (*exo*), which is significantly downfield compared to the free ligand (4.85 ppm). The diastereotopic protons, H<sup>e</sup> and H<sup>f</sup>, likewise give two sets of resonances (*i.e.* 4 in total), at 4.22, 3.82 – 3.77 and 3.58 ppm; a multiplet occurs at 3.82 – 3.77, corresponding to two coincident proton resonances. These signals exhibit less of a downfield shift in comparison to the free ligand (4.13 and 3.72 ppm).

The  $^{13}\text{C}\{^1\text{H}\}$  NMR spectrum of **2a** is consistent with the interpretation provided for the corresponding  $^1\text{H}$  NMR spectrum, above. However, the  $^{13}\text{C}\{^1\text{H}\}$  NMR could not be reported for the *endo* isomer due to the low concentration of the species. Key notable resonances are assigned to the two imine carbons (169.0 and 168.8 ppm), C<sup>m</sup> (156.0 and 151.9 ppm), C<sup>i</sup> (132.5 and 130.3 ppm), and C<sup>j</sup> (119.1 and 116.0 ppm). The remaining carbons of the BOPA bridge are coincident. Interestingly, whereas the resonances assigned to the phenyl stereodirecting groups are coincident, the *ipso*-carbons are observed as two resonances at 141.8 and 140.5 ppm, the observed inequivalence is likely due to the proximity

of the carbon to the metal centre with its unsymmetrical distribution of ligands. The oxazoline carbons are likewise observed as two sets of resonances, at 76.1 and 74.3 ppm for C<sup>p</sup>, and 70.7 and 70.5 ppm for C<sup>q</sup>. Unlike most complexes bearing the N(SiMe<sub>3</sub>)<sub>2</sub> coligand, two carbon resonances are observed at 5.8 and 5.1 ppm, which are consistent with the two resonances observed in the <sup>1</sup>H NMR spectrum and discussed above.

The N-H stretch observed at 3410 cm<sup>-1</sup> in the IR spectrum of the free ligand is not observed in the spectrum of **2a** (or in any of the complexes described in this thesis), consistent with deprotonation of the BOPA ligand. In addition, a slight change in the wavenumber of the imine stretch is observed, from 1635 cm<sup>-1</sup> in the free protio-ligand, to 1624 and 1608 cm<sup>-1</sup> in the complex. This is likewise consistent in all complexes described in this thesis.

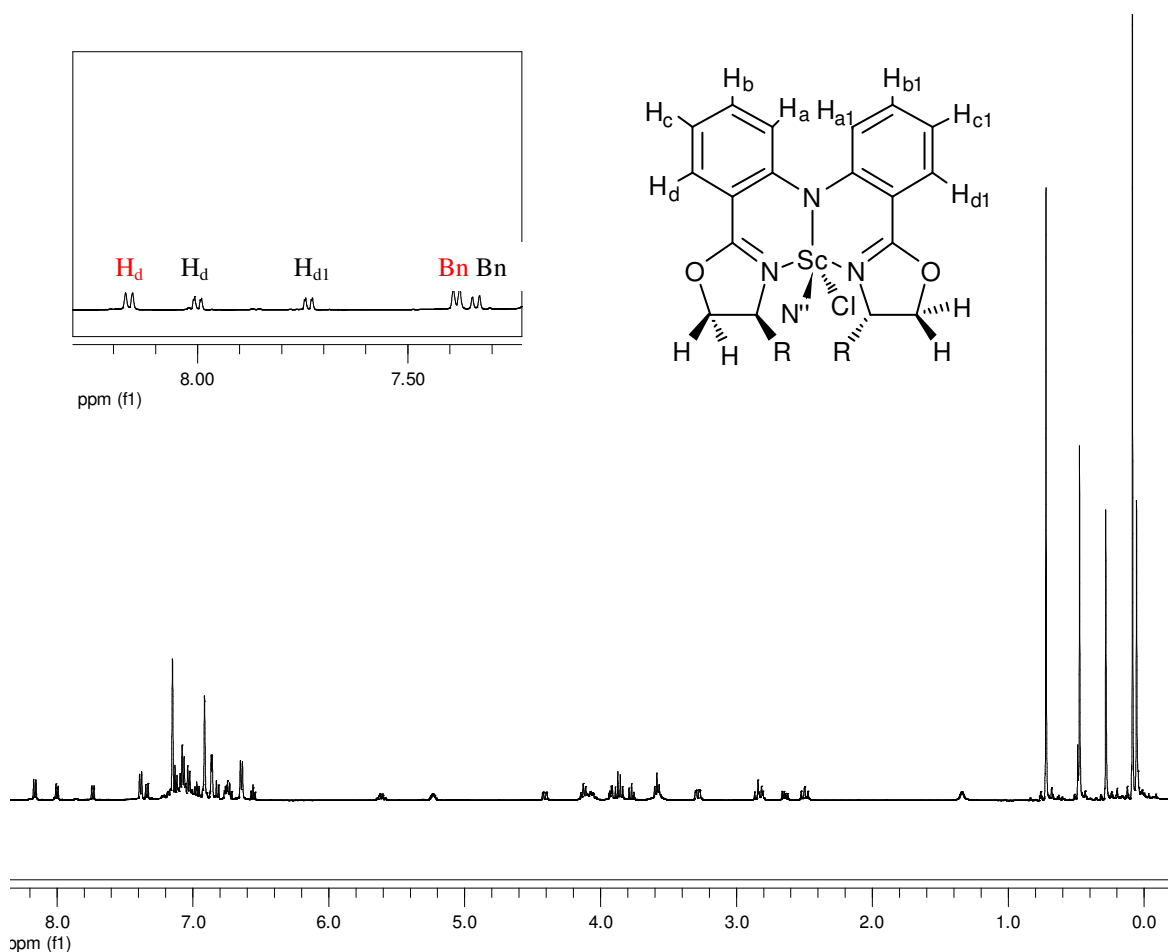
#### 2.4.2.2 Spectroscopic Characterisation of **2b-c**

Like the data for **2a**, the NMR spectra of **2b** (Fig.8) and **2c** indicate the presence of two isomers, in a 1:0.7 ratio for **2b** and a 1:0.3 ratio for **2c**. The identity of these isomers has been identified using DFT calculations and discussed above.

The <sup>1</sup>H and <sup>13</sup>C{<sup>1</sup>H} NMR spectra of the major isomers of **2b** and **2c** are consistent with C<sub>1</sub> molecular symmetry. The signals attributed to the N(SiMe<sub>3</sub>)<sub>2</sub> co-ligand are observed as two signals in the <sup>1</sup>H and <sup>13</sup>C{<sup>1</sup>H} NMR spectra, in an analogous manner to complex **2a**. The remaining resonances for the major isomers of **2b** and **2c** occur at similar shifts to those of **2a**. The <sup>13</sup>C{<sup>1</sup>H} NMR data are consistent with the conclusions drawn from the <sup>1</sup>H NMR data. The only notable anomaly is that for **2b**, only one imine resonance was observed at 168.8 ppm, rather than the expected two resonances. This is attributed to coincidental overlap, since all other signals are consistent with the afore-described C<sub>1</sub>-symmetry, and



moreover the expected two resonances were observed in the spectrum of **2c** (168.8 and 167.7 ppm).



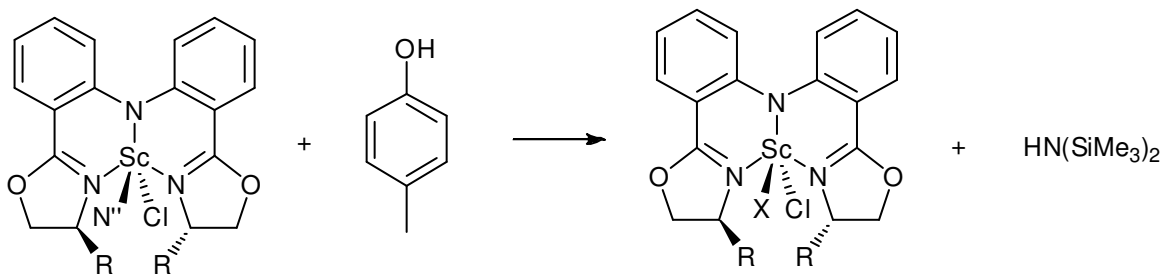
**Fig. 8** <sup>1</sup>H NMR spectrum (500 MHz) of [Sc(Bn-BOPA){N(SiMe<sub>3</sub>)<sub>2</sub>}Cl] (**2b**) in C<sub>6</sub>D<sub>6</sub>

The <sup>1</sup>H NMR signals attributed to the minor isomer of **2b** are inconsistent with a C<sub>1</sub>-symmetric complex, but rather indicate a C<sub>2</sub>-symmetric complex. In addition, only one resonance is observed for the N(SiMe<sub>3</sub>)<sub>2</sub> co-ligand at 0.72 ppm. These data suggest a rapid (hitherto unidentified) fluxional process resulting in time-averaged signals, giving NMR signals consistent with an apparently higher symmetry than expected. The data for the minor isomer of **2c** are consistent with C<sub>1</sub>-symmetry, and the N(SiMe<sub>3</sub>)<sub>2</sub> resonances are consistent with those of the major isomers (and those of **2a**), affording two signals at 0.75 and 0.49 ppm.

The IR spectra are consistent with those of **2a**, regarding the absence of an N-H stretch, consistent with the ligand being deprotonated. The imine C=N stretches are observed at 1634 and 1610  $\text{cm}^{-1}$  for **2b** (*cf.* 1639  $\text{cm}^{-1}$  for the protio-ligand), and 1617  $\text{cm}^{-1}$  for **2c** (*cf.* 1636  $\text{cm}^{-1}$  for the protio-ligand). Two imine stretches are expected for **2c**, however only one is observed, the remaining stretches may be obscured by a slight broadness of the reported imine stretch.

### 2.4.3 Synthesis of [Sc(R-BOPA)(OC<sub>6</sub>H<sub>4</sub>Me)Cl] (**3a-c**)

Complexes **2a-c** react with *p*-cresol to yield the phenoxide derivatives [Sc(Ph-BOPA)(OC<sub>6</sub>H<sub>4</sub>Me)Cl] (**3a**), [Sc(Ph-BOPA)(OC<sub>6</sub>H<sub>4</sub>Me)Cl] (**3b**) and [Sc(Ph-BOPA)(OC<sub>6</sub>H<sub>4</sub>Me)Cl] (**3c**) *via* protonolysis of the N(SiMe<sub>3</sub>)<sub>2</sub> co-ligand (Scheme 7). These reactions were subject to competing protonolysis of the BOPA ligands by the *p*-cresol, and samples were invariably contaminated with protio-ligand. Competing protonolysis of the BOPA ligand proved to be a recurring problem when Group 3 and lanthanide BOPA complexes were employed in the Ring Opening Polymerisation (ROP) of lactide, in the presence of benzyl alcohol co-initiator; these observations are discussed in their appropriate context in Chapter 4. Carrying out the reaction under kinetic control at low temperature (−78 °C) caused more of the ligand to be liberated from the scandium, suggesting that the protonation of BOPA is the kinetic product. Complexes **3a-c** were characterised using NMR spectroscopy, mass spectra showed the only signals attributed to protio-ligand.



**Scheme 7** Synthesis of  $[\text{Sc}(\text{R-BOPA})(\text{OC}_6\text{H}_4\text{Me})\text{Cl}]$  ( $\text{R} = \text{Ph}$  **3a**,  $\text{Bn}$  **3b** and  $\text{iPr}$  **3c**);  $\text{N}'' = \text{N}(\text{SiMe}_3)_2$ ;



### 2.4.3.1 Spectroscopic Characterisation of **3a–c**

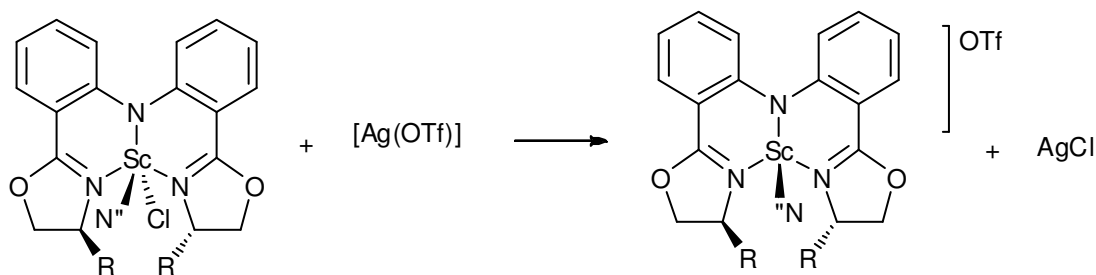
The  $^1\text{H}$  and  $^{13}\text{C}\{^1\text{H}\}$  NMR spectra of **3a** are consistent with  $C_1$  molecular symmetry, and indicate the presence of only one isomer. The  $^1\text{H}$  NMR signals assigned to the BOPA ligand are observed at a slightly different chemical shift than those for **2a**, consistent with a change of one of the co-ligands but with the resulting complex retaining a similar coordination geometry. Signals attributed to the  $\text{N}(\text{SiMe}_3)_2$  co-ligand are absent from the spectrum of **3a**. The spectrum contains two multiplets at 6.83–6.77 ppm and 7.05–6.99 ppm, assigned to the cresol aromatic protons, and a singlet is observed at 2.20 ppm, attributed to the *para*-methyl group. The assignment of this signal was confirmed by 2D NMR experiments (COSY, HMQC, HMBC); interactions between the aromatic resonances and the methyl signal are observed. Similar observations are made for the  $^{13}\text{C}\{^1\text{H}\}$  NMR spectrum, which is consistent with the proposed structure. The most upfield resonance (19.5 ppm) is attributed to the methyl group of the *p*-cresol ligand.

In an analogous manner to **2b** and **2c**, the  $^1\text{H}$  and  $^{13}\text{C}\{^1\text{H}\}$  NMR spectra of **3b** and **3c** indicate the presence of two isomers, which we attribute to the *exo* and *endo* isomers predicted using the DFT calculations. The signals of the major (*exo*) isomers are consistent with  $C_1$  molecular symmetry, with comparable signals to those discussed for **3a**, other than

the expected difference in the stereodirecting groups. The corresponding signals attributed to the minor (*endo*) isomers of **3b** and **3c** indicate an apparent  $C_2$ -symmetry, a similar characteristic to the minor isomer of **2b**. Notwithstanding the differences in apparent symmetry for the minor isomers of **3b** and **3c**, the resonances are all consistent with those discussed for **3a**, and have comparable chemical shifts. The resonances for the aromatic *p*-cresol signals are observed at 7.49 and 7.27 ppm (**3b**), and 6.97 ppm (**3c**) for the major isomer, with a multiplet at 6.58 – 6.49 ppm (**3b**) and 7.09 and 6.85 ppm (**3c**) for the minor isomer. A singlet is observed at 2.05 ppm and 2.11 ppm for the *p*-cresol methyl group of the major isomer for **3b** and **3c** respectively, whilst those of the minor isomer are observed at 2.10 ppm and 2.09 ppm. The  $^{13}\text{C}\{^1\text{H}\}$  NMR spectra are consistent with the discussion for **3a**, with additional signals being observed for the minor isomer, which indicate an apparent  $C_2$ -symmetry, as found for the  $^1\text{H}$  NMR spectra. The methyl carbon of the cresol ligand is observed at 25.3 ppm (**3b**), and 18.9 ppm (**3c**) for the major isomer, and at 20.7 ppm (**3b**) and 20.5 ppm (**3c**) for the minor isomer.

#### 2.4.4 Synthesis of $[\text{Sc}(\text{R-BOPA})\{\text{N}(\text{SiMe}_3)_2\}]\text{OTf}$ (**4a-c**)

In an effort to remove the chloride ligands from  $[\text{Sc}(\text{R-BOPA})\{\text{N}(\text{SiMe}_3)_2\}]\text{Cl}$  **2a-c**, these complexes were reacted with silver triflate to afford  $[\text{Sc}(\text{Ph-BOPA})\text{N}(\text{SiMe}_3)_2]\text{OTf}$  (**4a**),  $[\text{Sc}(\text{Ph-BOPA})\text{N}(\text{SiMe}_3)_2]\text{OTf}$  (**4b**) and  $[\text{Sc}(\text{Ph-BOPA})\text{N}(\text{SiMe}_3)_2]\text{OTf}$  (**4c**) as yellow/green, air- and moisture-sensitive solids (Scheme 8). Upon the addition of silver triflate in toluene to **2a-c** a white precipitate ( $\text{AgCl}$ ) was formed. After workup complexes **4a-c** were obtained in 68-82% yield, and were characterised using NMR and IR spectroscopies. Elemental analysis was obtained for **4a** and **4b**, however these data could not be obtained with acceptable error limits for **4c** despite repeated attempts and being spectroscopically pure.



**Scheme 8** Synthesis of  $[\text{Sc}(\text{R-BOPA})\{\text{N}(\text{SiMe}_3)_2\}]\text{OTf}$ . ( $\text{R} = \text{Ph}$  **4a**,  $\text{Bn}$  **4b** and  $\text{iPr}$  **4c**);  $\text{N}'' = \text{N}(\text{SiMe}_3)_2$

#### 2.4.4.1 Spectroscopic Characterisation of **4a–c**

The  $^1\text{H}$  and  $^{13}\text{C}\{^1\text{H}\}$  NMR spectra of **4a** show the presence of two species in solution (1:0.4), both of which are consistent with a  $C_2$ -symmetric complex, which could indicate little or no interaction of the triflate with the scandium, or else that the triflate ligand is labile. Both the major and minor isomers give rise to aromatic resonances more downfield than those observed for **2a**, whereas the oxazoline protons are observed further upfield, with  $\text{H}^g$  observed at 4.56 and 5.62 ppm for the major and minor isomer respectively (*cf.* *exo* isomer: 6.10 and 6.00 ppm for **2a**). The resonances attributed to the  $\text{N}(\text{SiMe}_3)_2$  co-ligand are observed at 0.08 and 0.04 ppm for the major and minor isomer respectively, a significant shift from 0.51 and -0.33 ppm in **2a** (*exo* isomer).

The  $^{13}\text{C}\{^1\text{H}\}$  NMR signals are comparable to those in **2a**. The most pronounced change in chemical shift is observed for the resonance of the  $\text{N}(\text{SiMe}_3)_2$  co-ligand, which are found at 7.9 and 2.6 ppm for the minor and major isomers respectively (*cf.* 5.8 and 5.1 ppm for **2a**). The remaining resonances at 114.9 and 114.3 ppm are attributed to the triflate anion for the major and minor isomer respectively.

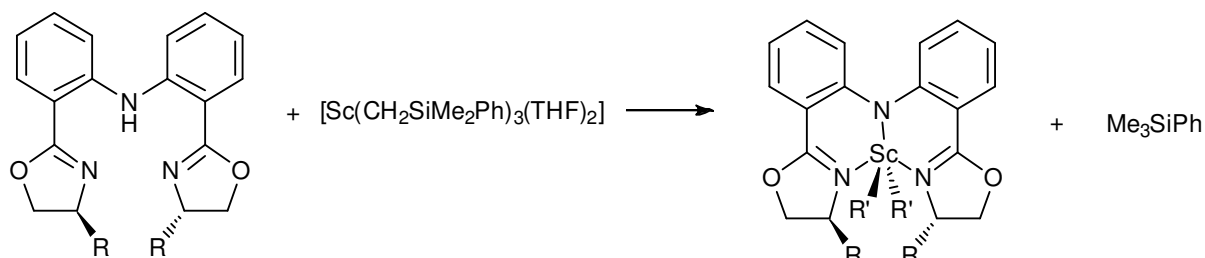
The  $^{19}\text{F}$  NMR spectrum shows two resonances, one for each of the major and minor isomers, at -77.81 ppm (major) and -78.12 ppm (minor): the chemical shift for unreacted silver triflate is -76.94 ppm. These data are consistent with a scandium-triflate interaction, since uncoordinated triflate anions would give rise to a single signal regardless of the isomeric organisation of the BOPA ligand.

In addition to the bands usually observed in the infrared spectra of these complexes, the IR spectrum of **4a** possesses signals attributed to the triflate anion, of which the  $\nu_{\text{S=O}}$  bands are distinctive. The  $\nu_{\text{S=O}}$  band for **4a** is observed at  $1161\text{ cm}^{-1}$ , which shows a modest weakening of the bond when compared to that in silver triflate ( $1181\text{ cm}^{-1}$ ),<sup>31</sup> and is therefore consistent with coordination of the triflate anion to the scandium, as predicted by the DFT calculations.

The  $^1\text{H}$  and  $^{13}\text{C}\{^1\text{H}\}$  NMR spectra of **4b** and **4c** are comparable to the spectra of **4a**, inasmuch as they indicate the presence of two species (**4b** 1:0.57, **4c** 1:0.53), and in the overall similarity of chemical shifts (with the obvious exception of the BOPA stereodirecting groups). Unlike the spectra of **4a** however, the spectra indicate  $C_1$  molecular symmetry and are therefore more consistent with a coordinated triflate anion. The  $^1\text{H}$  NMR spectra exhibit two signals for the inequivalent trimethylsilyl groups of the  $\text{N}(\text{SiMe}_3)_2$  ligands, at 0.48 and 0.06 ppm (*exo-4b*), 0.38 and -0.02 ppm (*exo-4c*), 0.37 and -0.03 ppm (*endo-4b*) and 0.56 and 0.05 ppm (*endo-4c*). This situation is significantly different from the single resonance for each isomer observed for **4a**. The  $^{13}\text{C}\{^1\text{H}\}$  and  $^{19}\text{F}$  NMR spectra are consistent with the observations and conclusions made using the  $^1\text{H}$  NMR spectra. The IR data are comparable to those of **4a**, the  $\nu_{\text{S=O}}$  bands being observed at  $1160\text{ cm}^{-1}$  (**4b**) and  $1164\text{ cm}^{-1}$  (**4c**).

### 2.4.5 Synthesis of [Sc(R-BOPA)(CH<sub>2</sub>SiMe<sub>2</sub>Ph)<sub>2</sub>] (**5a-c**)

The dialkyl complexes were synthesised by reaction of [Sc(CH<sub>2</sub>SiMe<sub>2</sub>Ph)<sub>3</sub>(THF)<sub>2</sub>] (**2.2**) with R-BOPA (**2.1a-c**) in THF at 0 °C (Scheme 9). After workup, the complexes [Sc(Ph-BOPA)(CH<sub>2</sub>SiMe<sub>2</sub>Ph)<sub>2</sub>] (**5a**), [Sc(Bn-BOPA)(CH<sub>2</sub>SiMe<sub>2</sub>Ph)<sub>2</sub>] (**5b**), and [Sc(*i*Pr-BOPA)(CH<sub>2</sub>SiMe<sub>2</sub>Ph)<sub>2</sub>] (**5c**) were obtained as bright yellow solids in 69-78% yield. Unlike the precursor **2.2**, the BOPA complexes **5a-c** are thermally stable at room temperature for several months. An increase in thermal stability is commonly observed in organoscandium chemistry when sterically demanding ligands are employed.<sup>32, 33</sup> The complexes were characterised by elemental analysis, and by NMR and IR spectroscopies. The elemental analysis of all three compounds showed a low carbon percentage. This is often observed for complexes containing scandium-carbon bonds, and is usually attributed to incomplete combustion or carbide formation.<sup>33</sup>



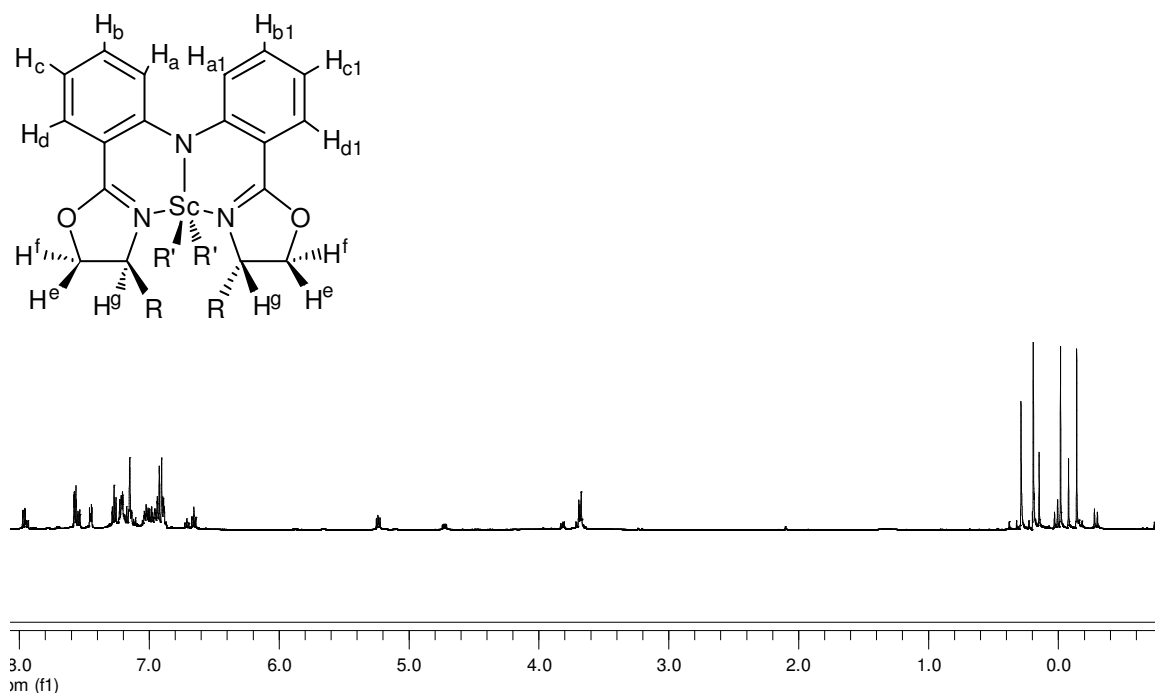
**Scheme 9** Synthesis of [Sc(R-BOPA)(CH<sub>2</sub>SiMe<sub>2</sub>Ph)<sub>2</sub>] (R = Ph **5a**, Bn **5b**, *i*Pr **5c**; R' = CH<sub>2</sub>SiMe<sub>2</sub>Ph)

#### 2.4.5.1 Spectroscopic Characterisation of **5a-c**

The <sup>1</sup>H NMR spectrum of **5a** is shown in Fig. 9. The spectrum exhibits signals attributable to the *exo* and *endo* isomers in approximately 1:0.5 ratio. The signals of both species are consistent with C<sub>2</sub> molecular symmetry. Alongside the expected silylmethyl resonances at close to 0 ppm, the resonances assigned to the phenyl group of the silyl

coligand are observed at 7.58, 7.27 and 7.15 ppm for the *exo* isomer and 7.54, 7.27 and 7.11 ppm for the *endo* isomer. The assignment was confirmed using 2D NMR experiments, which indicate that the *m*-SiC<sub>6</sub>H<sub>5</sub> protons lie most downfield.

The two silylmethyls for the major isomer give rise to two separate resonances at -0.02 and -0.14 ppm, those for the minor isomer being observed at 0.15 and -0.08 ppm. This is a significant upfield shift from the single resonance of the tris(alkyl) precursor, which appears at 0.42 ppm. The diastereotopic protons bonded to the  $\alpha$ -carbon of the CH<sub>2</sub>SiMe<sub>2</sub>Ph ligand give rise to two doublets at 0.02 and -0.29 ppm ( $^2J = 11.0$  Hz) for the *exo* isomer and at -0.17 and -0.75 ppm ( $^2J = 11.5$  Hz) for the *endo* isomer. The difference in chemical shift between the two doublets is significant, but well known for organoscandium complexes bearing either the CH<sub>2</sub>SiMe<sub>3</sub> or CH<sub>2</sub>SiMe<sub>2</sub>Ph ligands.<sup>24, 33-36</sup>



**Fig. 9** <sup>1</sup>H NMR spectrum (500 MHz, C<sub>6</sub>D<sub>6</sub>) of [Sc(Ph-BOPA)(CH<sub>2</sub>SiMe<sub>2</sub>Ph)<sub>2</sub>] (**5a**)

The <sup>13</sup>C{<sup>1</sup>H} NMR spectrum of **5a** exhibits signals that are consistent with the proposed structure in Scheme 9; chemical shifts of signals assigned to the BOPA ligand are



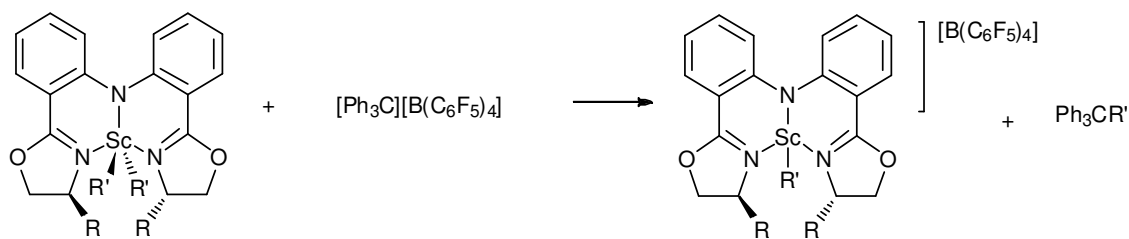
comparable to those described for the complexes already discussed in this thesis. The resonances attributed to the silyl coligands were assigned using 2D NMR spectra; the resonances at 146.5, 133.9, 128.1 and 127.6 ppm are assigned respectively to the *ipso*, *meta*, *para* and *ortho* position carbons of the *exo* (major) isomer, whilst, the resonances at 146.6, 134.0, 127.9 and 127.4 ppm are attributed to the analogous carbons of the *endo* (minor) isomer.

The  $\alpha$ -carbons of the silyl co-ligands are observed quite downfield at 38.7 and 39.1 ppm for the major and minor isomer respectively, deshielded as a result of the electron deficient metal centre. This signal is rarely observed in  $^{13}\text{C}\{^1\text{H}\}$  NMR spectra of organoscandium complexes owing to the large quadrupolar moment of scandium rendering the signal very broad.<sup>33, 34, 37</sup> Resonances attributed to the methyl carbons are observed at 2.8 and 1.0 ppm (*exo*) and at 2.3 and 1.1 ppm (*endo*). The IR spectrum shows similar features to the complexes already described in this thesis.

The  $^1\text{H}$  and  $^{13}\text{C}\{^1\text{H}\}$  NMR spectra of **5b** and **5c** indicate the presence of two species in solution, in a 1:0.6 and 1:0.5 ratio respectively. The signals attributed to both species are consistent with  $C_2$  molecular symmetry and show little variation from the spectra of **5a**, other than the expected differences in signals assigned to the BOPA stereodirecting groups. Full listings of spectroscopic data are included in Chapter 6, but are not discussed in more detail here owing to their similarity to the data already discussed for **5a**.

#### 2.4.6 Synthesis of $[\text{Sc}(\text{R-BOPA})(\text{CH}_2\text{SiMe}_2\text{Ph})][\text{B}(\text{C}_6\text{F}_5)_4]$ (**6a-c**)

Cationic complexes of early transition metal and lanthanide alkyl complexes are routinely prepared by alkyl ligand abstraction. Alkyl cations are particularly useful complexes, since they invariably exhibit a significantly higher reactivity than their neutral analogues.



**Scheme 10** Synthesis of  $[\text{Sc}(\text{R-BOPA})(\text{CH}_2\text{SiMe}_2\text{Ph})][\text{B}(\text{C}_6\text{F}_5)_4]$  ( $\text{R} = \text{Ph}$  **6a**,  $\text{Bn}$  **6b**,  $\text{iPr}$  **6c**;  $\text{R}' = \text{CH}_2\text{SiMe}_2\text{Ph}$ )

This is in part due to the increased Lewis acidity of the cationic complex, but also because the complexes have a lower coordination number, especially if the complexes are generated in the absence of a  $\sigma$ -donating solvent such as THF.<sup>35, 38-40</sup> Within the context of this thesis, this would relieve the steric strain in hydroamination catalysis, since only one substrate can bind *as an amide* during catalysis, (a second substrate has the potential to bind *as an amine*, which will be more labile). Such cationic complexes are often prepared using strong Lewis acids to abstract an alkyl ligand from the metal, or by protonation using an acid. Examples of the former are commonly based upon aryl boranes, or the trityl cation,  $\text{CPh}_3^+$ ; examples of the latter include quaternary ammonium salts such as  $\text{PhMe}_2\text{NH}^+$ . Given the strongly Lewis acidic nature of the resulting cationic complexes, they have the potential to bind coordinating solvents such as ethers. Interactions with anions are also possible, for example halide abstraction from anions such as  $\text{PF}_6^-$  and  $\text{BF}_4^-$  is well known. For this reason, weakly coordinating anions are often employed, with perfluorinated arylborates such as  $\text{B}(\text{C}_6\text{F}_5)_4^-$  being commonly used, since these anions have a lower affinity for the cationic complexes, and when employed in conjunction with a relatively weakly coordinating solvent such as bromobenzene, the “free” cationic complexes can be generated and their reactivity studied largely free from unwanted side reactions.<sup>38, 41, 42</sup> Owing to their extreme reactivity, and therefore instability, such complexes are routinely prepared, analysed, and reacted *in situ* in

relatively polar, weakly donating solvents such as dichloromethane or bromobenzene; spectroscopic analysis can be performed on these complexes when prepared in the deuterated derivatives of these solvents. To this end, the cationic scandium BOPA complexes [Sc(Ph-BOPA)(CH<sub>2</sub>SiMe<sub>2</sub>Ph)][B(C<sub>6</sub>F<sub>5</sub>)<sub>4</sub>] (**6a**), [Sc(Bn-BOPA)(CH<sub>2</sub>SiMe<sub>2</sub>Ph)][B(C<sub>6</sub>F<sub>5</sub>)<sub>4</sub>] (**6b**) and [Sc(iPr-BOPA)(CH<sub>2</sub>SiMe<sub>2</sub>Ph)][B(C<sub>6</sub>F<sub>5</sub>)<sub>4</sub>] (**6c**) were prepared by the *in situ* reaction of the dialkyl complexes **5a-c** with [Ph<sub>3</sub>C][B(C<sub>6</sub>F<sub>5</sub>)<sub>4</sub>] (**2.4**). The complexes were formed on a NMR scale in C<sub>6</sub>D<sub>5</sub>Br and yielded red solutions<sup>34</sup> that were characterised by <sup>1</sup>H, <sup>13</sup>C {<sup>1</sup>H}, <sup>11</sup>B and <sup>19</sup>F NMR spectroscopies.

#### 2.4.6.1 Spectroscopic Characterisation of **6a-c**

The <sup>1</sup>H and <sup>13</sup>C{<sup>1</sup>H} NMR spectra of **6a** and **6b** are consistent with C<sub>2</sub> molecular symmetry, whereas the spectra of **6c** are consistent with C<sub>1</sub>-symmetry. The precise chemical shifts of the resonances observed for complexes **6a-c** cannot be compared to the parent complexes **5a-c**, since they were measured in a different solvent. Nevertheless, the resonances attributed to the BOPA ligand are generally located in the expected regions and are comparable to the signals observed for complexes **2-5**. The most notable difference in each case is the reduction in the integration of resonances attributed to the alkyl ligand, and the presence of signals assigned to the Ph<sub>3</sub>CCH<sub>2</sub>SiMe<sub>2</sub>Ph by-product. The identity of by-product signals was affirmed using spectra of an independently prepared sample, synthesised from LiCH<sub>2</sub>SiMe<sub>2</sub>Ph and Ph<sub>3</sub>CCl. The two methyls of the alkyl coligand are the most distinguishable, for the phenyl derivative **6a** the signals are observed at -0.05 and -0.34 ppm, whilst two doublets are observed at -0.10 and -0.13 ppm for the protons of the CH<sub>2</sub> group. The analogous resonances for **6b** and **6c** are observed at -0.34 ppm and -0.27 ppm respectively; the diastereotopic protons attributed to the carbon directly bonded to the scandium occur at -0.31 and -0.49 ppm (**6b**) and -0.49 ppm (**6c**), shifted upfield in

comparison to **6a**. The  $^{13}\text{C}\{^1\text{H}\}$  NMR spectra are consistent with the proposed structures of **6a–c**. The  $^{11}\text{B}\{^1\text{H}\}$  NMR spectra show one resonance at -17 ppm, whilst the  $^{19}\text{F}$  NMR spectra exhibit three resonances at -131.2, -161.7 and -165.5 ppm. These data are consistent with previous reports of the  $\text{B}(\text{C}_6\text{F}_5)_4$  anion.<sup>34, 43, 44</sup>

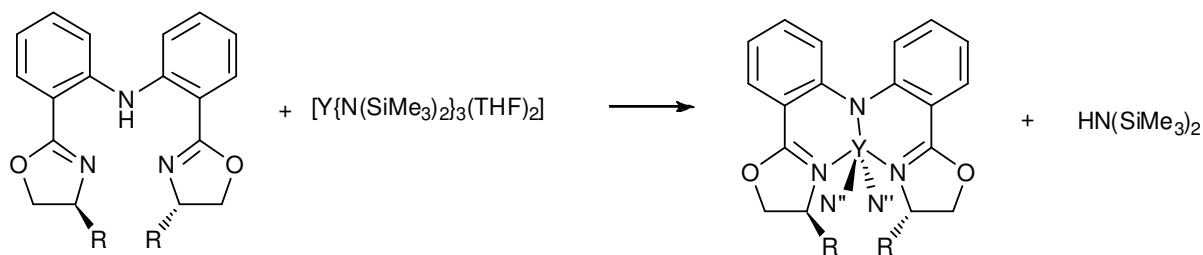
### 2.4.7 Further Reactions of $[\text{Sc}(\text{R-BOPA})(\text{CH}_2\text{SiMe}_2\text{Ph})_2]$ (**5**)

The scandium dialkyl complexes  $[\text{Sc}(\text{R-BOPA})(\text{CH}_2\text{SiMe}_2\text{Ph})_2]$  (**5a–c**) were reacted with a variety of other reagents in order to assess their reaction chemistry. Benzophenone,  $\text{Ph}_3\text{SiH}$  and  $\text{LiAlH}_4$  were all used in these analyses, but in each case no reaction was observed using NMR spectroscopy, in which signals for **5** alongside the reactant were observed (*i.e.* no evidence of any reaction). This observation was persistent even under forcing conditions. This surprising lack of reactivity may be due to the sterically encumbered ligand shielding the relatively small metal; this conclusion is supported by the catalytic studies, which are discussed in Chapters 3 and 4.

## 2.5 Preparation and Characterisation of yttrium Complexes

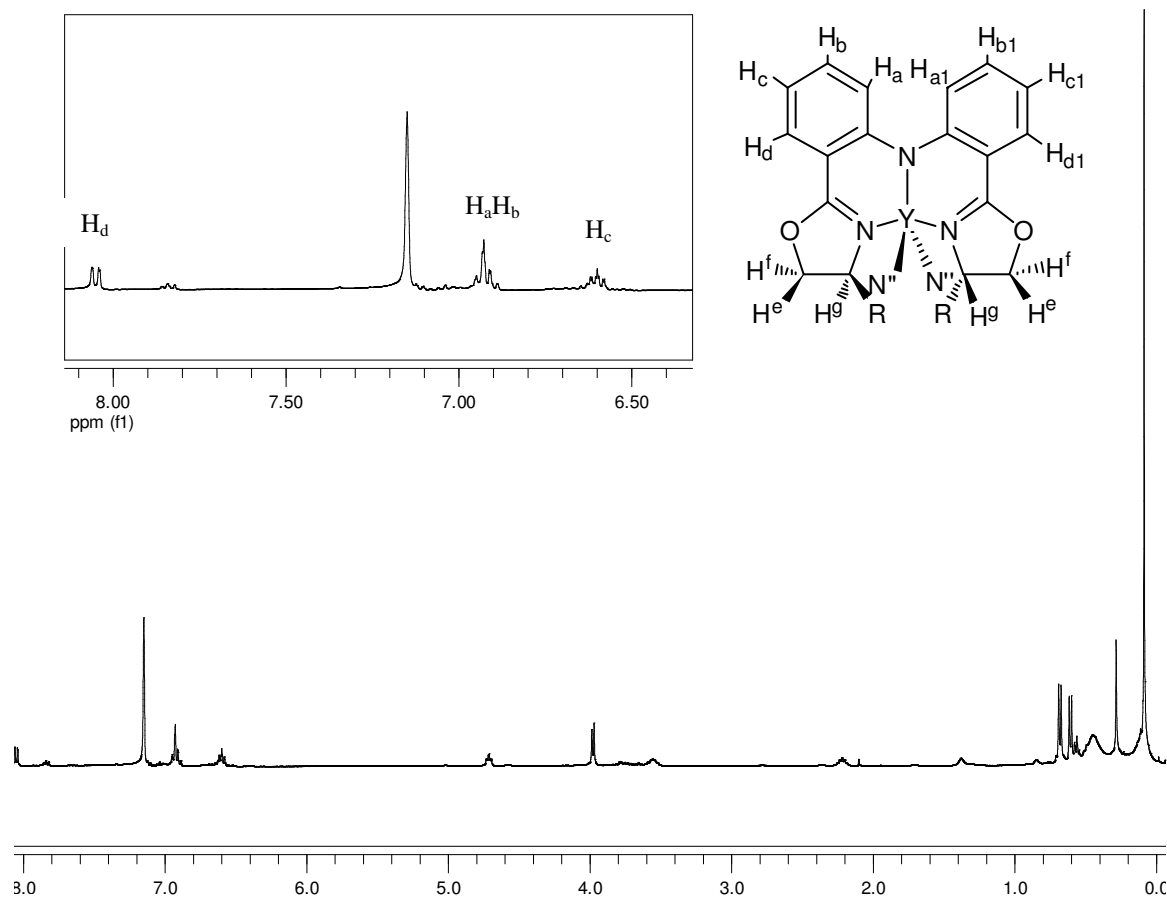
In a similar manner to the scandium complexes, the DFT calculations of the yttrium amide and alkyl BOPA complexes revealed relatively small energy differences between the two isomers. A principal objective was therefore to probe the effect of increasing the ionic radius of the metal upon the relative proportion of the two forms. The yttrium precursors  $[\text{Y}\{\text{N}(\text{SiMe}_3)_2\}_3]$  (**2.3**) and  $[\text{Y}(\text{CH}_2\text{SiMe}_2\text{Ph})_3(\text{THF})_2]$  (**2.4**) were synthesised according to literature procedures.<sup>24, 45</sup> Owing to the thermal instability of the yttrium alkyl complex, freshly prepared samples were stored in a freezer at -35 °C and used within 1 month.

## 2.5.1 Preparation of yttrium silylamide complexes



**Scheme 11** Synthesis of  $[Y(R-BOPA)\{N(SiMe_3)_2\}_2]$  (R = Ph **7a**, Bn **7b**, iPr **7c**; N'' = N(SiMe<sub>3</sub>)<sub>2</sub>)

The reaction between the BOPA protio-ligand precursors and  $[Y\{N(SiMe_3)_2\}_3]$  (**2.3**) (Scheme 11) indicated no reaction at room temperature, but complexation was achieved upon applying more forcing conditions, *i.e.* 40 °C, whereby complete consumption of the BOPA ligand was observed quickly, the  $[Y(R-BOPA)\{N(SiMe_3)_2\}_2]$  complexes being present as two isomers, as expected. However prolonged heating caused the relative proportion of the two isomers to change, reaching equilibrium after 2 days. The need for forcing conditions has been reported in cases where bulky silylamide co-ligands were employed,<sup>15</sup> and we attribute this to the sterically demanding BOPA ligand and amide co-ligands giving a high activation barrier to complexation. The complexes  $[Y(Ph-BOPA)\{N(SiMe_3)_2\}_2]$  (**7a**),  $[Y(Bn-BOPA)\{N(SiMe_3)_2\}_2]$  (**7b**) and  $[Y(iPr-BOPA)\{N(SiMe_3)_2\}_2]$  (**7c**) were obtained as bright yellow solids in 68-79% yield and were characterised by NMR and IR spectroscopies. Elemental analysis was also achieved with **7b**, however satisfactory elemental analyses were not obtained for **7a** and **7c** despite repeated attempts on spectroscopically pure samples.



**Fig. 10**  $^1\text{H}$  NMR spectrum (500 MHz,  $\text{C}_6\text{D}_6$ ) of  $[\text{Y}(\text{iPr-BOPA})\{\text{N}(\text{SiMe}_3)_2\}_2]$  (**7c**)

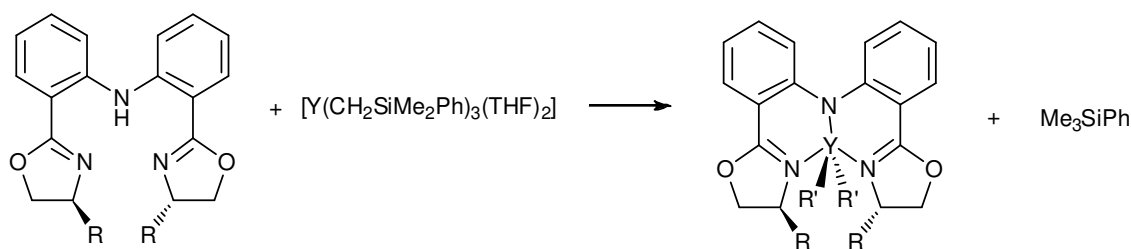
### 2.5.2 Spectroscopic Characterisation of $[\text{Y}(\text{R-BOPA})\{\text{N}(\text{SiMe}_3)_2\}_2]$ **7a–c**

The  $^1\text{H}$  and  $^{13}\text{C}\{^1\text{H}\}$  NMR spectra of **7a–b** and **c** (Fig. 10) indicate the presence of the *endo* (minor) isomer in 9%, 9%, and 10% relative abundance for **7a**, **7b**, and **7c** respectively. The signals attributed to both species are consistent with  $C_2$  molecular symmetry. In general, the chemical shifts are observed slightly upfield in comparison to the scandium complexes **2a–c**, particularly the oxazoline resonances, thus highlighting the significance of the identity of the metal and the co-ligands on the chemical shifts of the BOPA ligand signals (*i.e.* replacing a chloride for an amide). For example, the resonance attributed to  $\text{H}^g$  in **7a** arises as a multiplet at 5.65–5.60 ppm, whilst the analogous signals for **2a** are observed at 6.10 and 6.00 ppm (and 4.95 ppm for the free ligand). Signals corresponding to  $\text{H}^e$  and  $\text{H}^f$  of **7a** are

observed at 4.28 and 3.83 ppm, a slight downfield shift compared to the analogous protons of the free ligand (4.00 and 3.67 ppm). The amide co-ligand gives rise to two resonances at 0.36 and 0.09 ppm, a common observation when this co-ligand is employed; this is significantly different from that observed for **2a**, where the two resonances are observed at 0.51 and -0.33 ppm. The spectra of the benzyl and isopropyl congeners **7b** and **7c** are comparable to those of **7a**, with the exception of the different stereodirecting groups and generally with slightly different chemical shifts. The IR spectra are consistent with coordination of the ligand to the yttrium, namely in the absence of an N-H stretch indicating deprotonation of the ligand.

### 2.5.3 Synthesis of $[Y(R\text{-BOPA})(\text{CH}_2\text{SiMe}_2\text{Ph})_2]$ (**8a-c**)

In contrast to the silylamide complexes, the reaction between  $[Y(\text{CH}_2\text{SiMe}_2\text{Ph})_3(\text{THF})_2]$  (**2.4**) and the BOPA ligands (Scheme 12) proceeded at ambient temperature, and coordination occurred within minutes (when monitored by  $^1\text{H}$  NMR spectroscopy) with the concomitant liberation of one equivalent of  $\text{PhSiMe}_3$ .



**Scheme 12** Synthesis of  $[Y(R\text{-BOPA})(\text{CH}_2\text{SiMe}_2\text{Ph})_2]$  ( $R = \text{Ph}$  **8a**,  $\text{Bn}$  **8b**,  $i\text{Pr}$  **8c**;  $R' = \text{CH}_2\text{SiMe}_2\text{Ph}$ )

The observation was unsurprising, given the lower degree of steric demand of the alkyl ligand in comparison to the silylamides discussed above, as well as the more reactive nature of the Y-C bond compared to the Y-N. The alkyl complexes are stable in the solid state at room temperature for several weeks, whereas solutions of the complexes in  $\text{C}_6\text{D}_6$

slowly decompose over a period of one week. The complexes [Y(Ph-BOPA)(CH<sub>2</sub>SiMe<sub>2</sub>Ph)<sub>2</sub>] (**8a**) [Y(Bn-BOPA)(CH<sub>2</sub>SiMe<sub>2</sub>Ph)<sub>2</sub>] (**8b**) and [Y(iPr-BOPA)(CH<sub>2</sub>SiMe<sub>2</sub>Ph)<sub>2</sub>] (**8c**) were obtained as bright yellow solids in 64-77% yield, and were characterised by elemental analysis, NMR and IR spectroscopies. The elemental analysis of all three compounds showed a low carbon percentage. This is often observed for complexes containing metal-carbon bonds, owing to the formation of the metal carbide species, resulting in incomplete combustion.

#### 2.5.4 Spectroscopic characterisation of **8a-c**

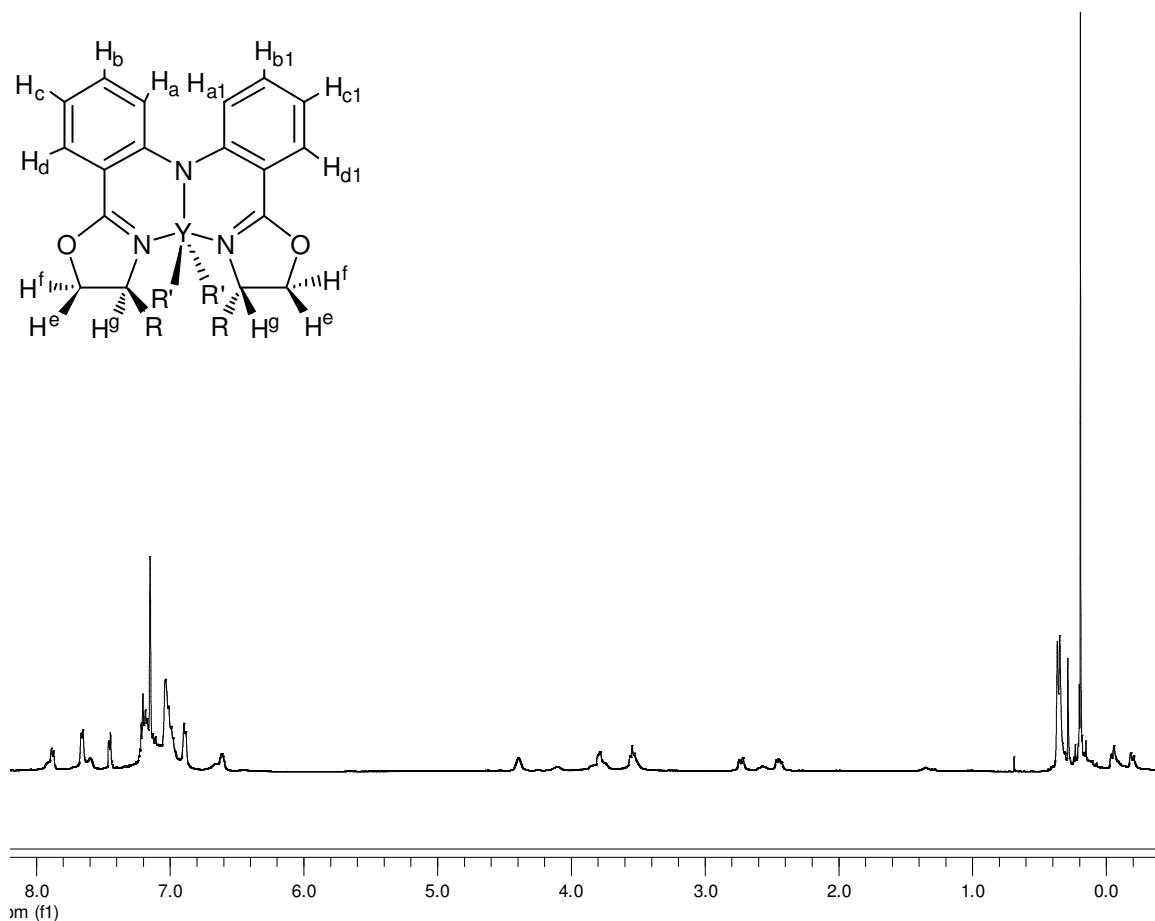
The presence of both *exo* and *endo* isomers is evident from the <sup>1</sup>H and <sup>13</sup>C{<sup>1</sup>H} NMR spectra of **8a** and the <sup>1</sup>H NMR spectrum of **8c**, which are present with ratios 1:0.6 (**8a**) and 1:0.2 (**8c**). Due to the relatively low concentration of the *endo* isomer of **8c**, the intensities of the <sup>13</sup>C{<sup>1</sup>H} NMR resonances were too low for adequate interpretation. However, the *endo* and *exo* isomers are not evident from the <sup>1</sup>H and <sup>13</sup>C{<sup>1</sup>H} NMR spectra of **8b** (Fig.11), which is likely due to the rapid conversion between the two. The signals for both isomers for each derivative are consistent with C<sub>2</sub> molecular symmetry.

The resonances are observed at similar chemical shifts to those in the analogous scandium complexes **5a-c**. The resonances attributed to the diastereotopic methylene protons of the alkyl co-ligands arise as doublets of doublets. These arise at -0.54 and -0.93 ppm for the major isomer and -0.86 and -1.17 ppm for the minor isomer for **8a** and -0.04 and -0.19 ppm for **8b**. The resonances for the major and minor isomer of **8c** are coincident and also occur as doublet of doublets at -0.13 and -0.28 ppm. The protons not only couple to each other (<sup>2</sup>J<sub>HH</sub> = 11.3 Hz for the major isomer, and 11.0 Hz for the minor isomer for **8a**) but the <sup>89</sup>Y has a spin active nucleus with I = ½ (100% abundance) and therefore the protons are observed as a doublet of doublets with <sup>2</sup>J<sub>HY</sub> giving an AMX spin system, for which <sup>2</sup>J<sub>HY</sub> =



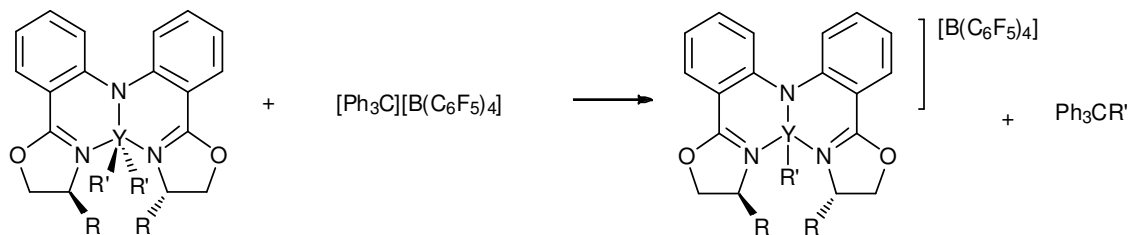
2.7 Hz for **8a** and **8c**, which lies in the range for those reported previously (2.7-3.1 Hz).<sup>46-48</sup>

The two resonances for the analogous protons of **8b** are slightly broadened which masks the fine structure, particularly the  $^2J_{HY}$ .



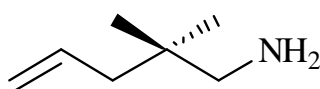
**Fig. 11**  $^1\text{H}$  NMR spectrum (500 MHz,  $\text{C}_6\text{D}_6$ ) of  $[\text{Y}(\text{Bn-BOPA})(\text{CH}_2\text{SiMe}_2\text{Ph})_2]$  (**8b**)

The  $^{13}\text{C}\{^1\text{H}\}$  NMR spectra of **8a-c** show similar characteristics to those of  $[\text{Sc}(\text{R-BOPA})(\text{CH}_2\text{SiMe}_2\text{Ph})_2]$  (**5a-c**). The carbon directly bonded to the yttrium is observed as a doublet; 35.0 ppm for the major isomer and 33.7 ppm for the minor isomer for **8a**, 34.5 ppm for **8b** and 33.5 ppm for **8c**, with  $^1J_{\text{CY}} = 38.2$  and  $37.4$  **8a**,  $39.4$  **8b**,  $37.4$  **8c** respectively. The  $\alpha$ -carbon resonances of the alkyl ligands have comparable chemical shifts and coupling constants to literature examples, which range from 25.0 – 39.0 ppm with  $^1J_{\text{CY}} = 30.3$  – 43.4 Hz.<sup>46-48</sup>

2.5.5 Synthesis of  $[Y(R\text{-BOPA})(\text{CH}_2\text{SiMe}_2\text{Ph})][\text{B}(\text{C}_6\text{F}_5)_4]$  (**9a-c**)

**Scheme 13** Synthesis of  $[Y(\text{R-BOPA})(\text{CH}_2\text{SiMe}_2\text{Ph})][\text{B}(\text{C}_6\text{F}_5)_4]$  (R = Ph **9a**, Bn **9b**, iPr **9c**; R' =  $\text{CH}_2\text{SiMe}_2\text{Ph}$ )

As mentioned previously, in the context of this thesis, one area of interest was hydroamination catalysis (discussed in Chapter 3). The dialkyl complexes were sluggish in their catalytic activity with the geminal dimethyl substrate (Fig. 12, **2.5**), and it was rationalised that by synthesising the cationic derivatives of complexes **8a-c** (*i.e.* the analogues of the scandium complexes **6a-c**) a more reactive catalyst would be synthesised. Therefore,  $[Y(\text{Ph-BOPA})(\text{CH}_2\text{SiMe}_2\text{Ph})][\text{B}(\text{C}_6\text{F}_5)_4]$  (**9a**),  $[Y(\text{Bn-BOPA})(\text{CH}_2\text{SiMe}_2\text{Ph})][\text{B}(\text{C}_6\text{F}_5)_4]$  (**9b**) and  $[Y(\text{iPr-BOPA})(\text{CH}_2\text{SiMe}_2\text{Ph})][\text{B}(\text{C}_6\text{F}_5)_4]$  (**9c**) were obtained from the corresponding alkyl complexes by reaction with  $[\text{Ph}_3\text{C}][\text{B}(\text{C}_6\text{F}_5)_4]$  (Scheme 13). The complexes were formed *in situ* on NMR tube scales in  $\text{C}_6\text{D}_5\text{Br}$ , and yielded red solutions that were characterised by  $^1\text{H}$ ,  $^{13}\text{C}\{^1\text{H}\}$ ,  $^{11}\text{B}\{^1\text{H}\}$  and  $^{19}\text{F}$  NMR spectroscopies.



**2.5**

**Fig. 12** Geminal dimethyl aminoolefin used in hydroamination catalysis

### 2.5.6 Spectroscopic characterisation of **9a-c**

The  $^1\text{H}$  and  $^{13}\text{C}\{^1\text{H}\}$  NMR spectra of **9a-c** are consistent with  $C_2$  molecular symmetry. Like the scandium alkyl cations  $[\text{Sc}(\text{R-BOPA})(\text{CH}_2\text{SiMe}_2\text{Ph})][\text{B}(\text{C}_6\text{F}_5)_4]$  (**6a-c**), only one isomer is apparent in each of the spectra and the chemical shifts of each of the resonances for **9a-c** are comparable to those of **6a-c**. Although the spectra were recorded in a different solvent, compared to the precursor complexes, a dramatic change in the chemical shifts is observed for a number of resonances, namely  $\text{H}^e$ ,  $\text{H}^f$  and  $\text{H}^g$ . The two doublets observed at 0.03 and -0.29 ppm for **9a**, -0.53 and -1.08 ppm for **9b** and -0.12 and -0.88 ppm for **9c** are attributed to the diastereotopic protons bound to the  $\alpha$ -carbon of the alkyl ligand. The fine structure arising from  $^2J_{\text{HY}}$  coupling is not observed in the case of **9a**, due to the slight broadening of the resonances obscuring the coupling to yttrium with its relatively small  $J$  value (*cf.* complexes **8a-c**). However, the coupling to the yttrium is observed for **9b-c**, with  $J$  values of 3.30 and 2.80 Hz respectively. These lie within the range of reported  $J$  couplings which are 2.1- 3.6 Hz.<sup>44, 49</sup>

The  $^{13}\text{C}\{^1\text{H}\}$  NMR spectra show similar characteristics to **6a-b** and are fully consistent with the conclusions drawn from the  $^1\text{H}$  NMR spectra. The  $\alpha$ -carbons of the alkyl ligands are observed as doublets at 33.9, 32.4 and 32.7 ppm, with  $^1J_{\text{CY}}$  coupling constants of 39.5, 40.9 and 38.2 Hz for **9a-c** respectively; the coupling constants are slightly reduced in comparison to those of the alkyl precursor complexes **8a-c**, but are comparable to reported  $^1J_{\text{CY}}$  coupling constants (37 – 54 Hz).<sup>44, 49-52</sup>

The  $^{11}\text{B}\{^1\text{H}\}$  NMR spectra show one resonance at -17.3, -16.9 and -16.8 ppm for **9a-c** respectively, whilst the  $^{19}\text{F}$  NMR spectra give three resonances at -131.3, -161.3 and -165.3 ppm, -131.4, -161.4 and -165.4 ppm, and -131.3, -161.4 and -165.3 ppm for **9a-c**. These data are comparable to those reported for cationic complexes with this anion; the  $^{11}\text{B}\{^1\text{H}\}$

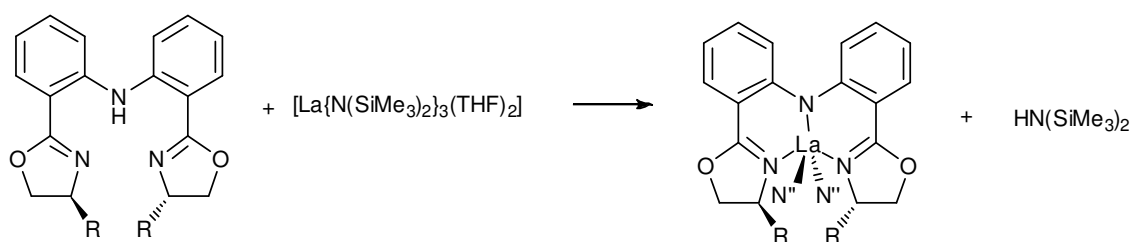
resonance is at -14.2 ppm and the three fluorine resonances occur in the ranges -130.7 - -137.7 ppm, -163.9 – 167.2 ppm and -166.4 - -171.2 ppm.<sup>44, 49-51</sup>

## 2.6 Preparation and Characterisation of Lanthanum Complexes

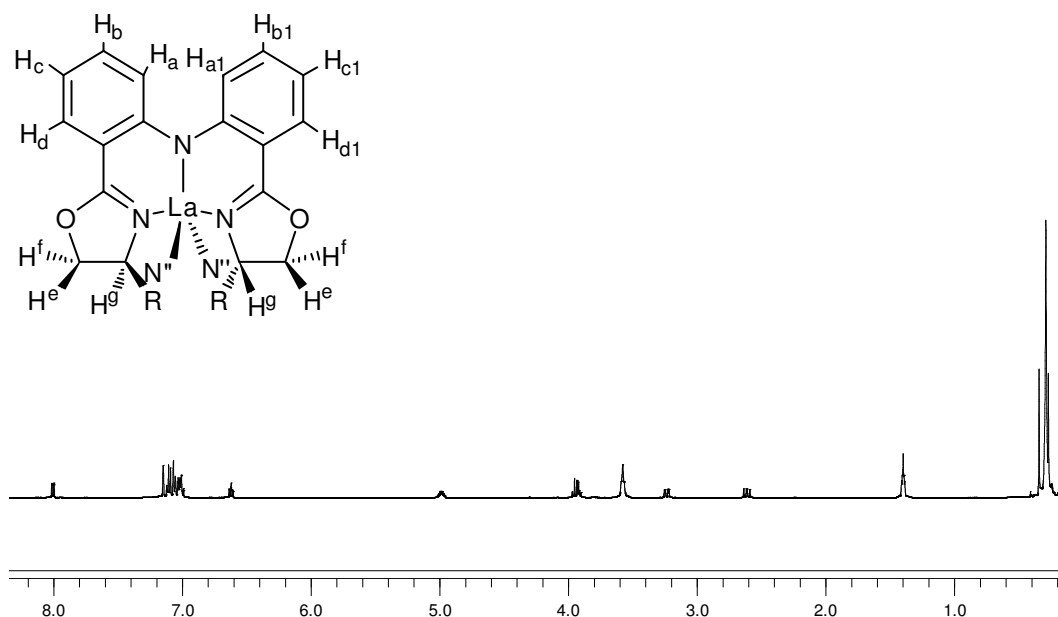
Given the relative ease of preparing the yttrium amide complexes compared to the analogous scandium congeners, it was decided to prepare the lanthanum amide complexes, in order to complete the Group 3 triad. The corresponding alkyl complexes were not prepared due to their increased thermal instability.

### 2.6.1 Synthesis of [La(R-BOPA){N(SiMe<sub>3</sub>)<sub>2</sub>}<sub>2</sub>] (**10a-c**)

The lanthanum precursor [La{N(SiMe<sub>3</sub>)<sub>2</sub>}<sub>3</sub>] (**2.6**) was prepared as reported.<sup>45</sup> Subsequent reaction with the BOPA protio-ligands at ambient temperature afforded the bis(trimethylsilyl)amide complexes [La(Ph-BOPA){N(SiMe<sub>3</sub>)<sub>2</sub>}<sub>2</sub>] (**10a**), [La(Bn-BOPA){N(SiMe<sub>3</sub>)<sub>2</sub>}<sub>2</sub>] (**10b**) and [La(iPr-BOPA){N(SiMe<sub>3</sub>)<sub>2</sub>}<sub>2</sub>] (**10c**) as bright yellow solids in 76-85% yield (Scheme 14). Compounds **10a-c** were characterised by elemental analysis, NMR and IR spectroscopies.



**Scheme 14** Synthesis of [La(R-BOPA){N(SiMe<sub>3</sub>)<sub>2</sub>}<sub>2</sub>] (R = Ph **10a**, Bn **10b**, iPr **10c**); N'' = N(SiMe<sub>3</sub>)<sub>2</sub>



**Fig. 13**  $^1\text{H}$  NMR spectrum (500 MHz,  $\text{C}_6\text{D}_6$ ) of  $[\text{La}(\text{Bn-BOPA})\{\text{N}(\text{SiMe}_3)_2\}_2]$  (**10b**)

## 2.6.2 Spectroscopic Characterisation of 10a-c

The DFT calculations suggest that two isomers of complexes **10a–c** should have similar energy differences to the yttrium amide complexes. However, the NMR data suggest the presence of only one isomer in solution, which is in contrast to the scandium and yttrium complexes. We attribute this to the larger ionic radius of lanthanum facilitating interconversion of the two isomers.  $^1\text{H}$  NMR spectra were measured at low temperature, in an attempt to decoalesce the resonances for the two isomers; however, even at low temperatures only a slight broadening of the resonances was observed. Therefore, although the energy differences between the two isomers of the yttrium and lanthanum complexes are predicted to be similar, it would appear that the activation barrier is lower for the lanthanum complexes, allowing them to interconvert more rapidly.

The  $^1\text{H}$  and  $^{13}\text{C}\{^1\text{H}\}$  NMR spectra of **10a–c** (**10b** Fig. 13) are consistent with  $C_2$  molecular symmetry, with the resonances at chemical shifts similar to those in the spectra of the yttrium complexes **7a–c**. The most notable difference between the spectra of **10a–c** and

those of **7a–c** are the  $\text{N}(\text{SiMe}_3)_2$  resonances. The spectra of the lanthanum complexes exhibit a single resonance with a relative intensity of 36 H, contrasting the spectra of the yttrium complexes which display two resonances with intensity 18 H each. This is likely to be a result of the larger ionic radius of the lanthanum (and hence longer La-N distances) allowing easier rotation about the metal-nitrogen bond. The  $^{13}\text{C}\{^1\text{H}\}$  NMR spectra show similar characteristics to **7a-b**. The amide carbon gives rise to the expected single resonances at 4.9, 5.4 and 5.1 ppm for **10a-c** respectively, and is consistent with the  $^1\text{H}$  NMR spectra.

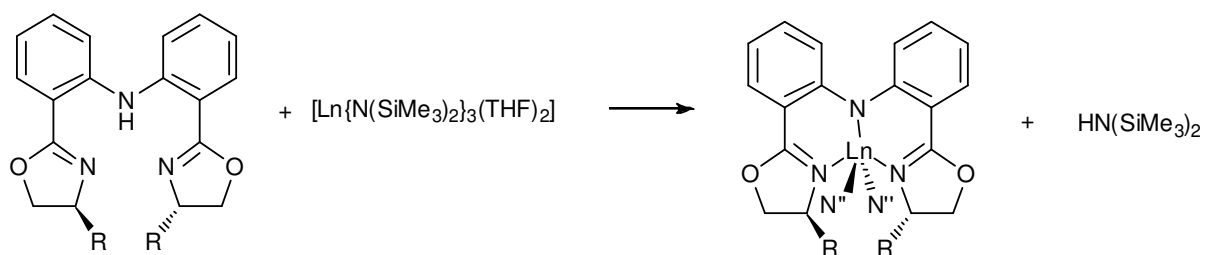
## 2.7 Preparation and Characterisation of Paramagnetic Complexes

Having established the synthesis and characterisation of lanthanide BOPA complexes using diamagnetic metals, for which high resolution NMR spectroscopy in particular has yielded a significant body of information relating to the structure of the complexes, this information was used to pursue selected paramagnetic derivatives, for which spectroscopic analyses give more ambiguous information. It is clear from the studies described thus far that the BOPA ligands are very sterically demanding. Therefore subsequent studies concentrated on earlier lanthanides, *i.e.* those with larger ionic radii. Specifically, praseodymium, neodymium and samarium complexes were prepared using the methods employed for the lanthanum complexes, from  $[\text{Ln}\{\text{N}(\text{SiMe}_3)_2\}_3]$  ( $\text{Ln} = \text{Pr}$  (**2.7**),  $\text{Nd}$  (**2.8**) and  $\text{Sm}$  (**2.9**)), which were synthesised according to literature procedures.<sup>45</sup>

### 2.7.1 Synthesis of $[\text{Ln}(\text{R-BOPA})\{\text{N}(\text{SiMe}_3)_2\}_2]$ ( $\text{Ln} = \text{Pr}$ **11**, $\text{Nd}$ **12**, $\text{Sm}$ **13**)

The reactions between the BOPA ligands and the  $[\text{Ln}\{\text{N}(\text{SiMe}_3)_2\}_3]$  precursors ( $\text{Ln} = \text{Pr}$  **2.7**,  $\text{Nd}$  **2.8**,  $\text{Sm}$  **2.9**) (Scheme 15) did not require forcing conditions; the reactions were complete after stirring overnight at room temperature. Whilst the use of NMR spectroscopy is generally less informative for the purposes of structural identification, owing to the

reduction in fine structure in the resonances, the spectra were nevertheless able to provide conclusive evidence relating to the coordination of the BOPA ligand to the lanthanide ions.



**Scheme 15** Synthesis of  $[\text{Ln}(\text{R-BOPA})\{\text{N}(\text{SiMe}_3)_2\}_2]$  ( $\text{Ln} = \text{Pr}$  **11**,  $\text{Nd}$  **12**,  $\text{Sm}$  **13**;  $\text{R} = \text{Ph}$  **a**,  $\text{Bn}$  **b**,  $i\text{Pr}$  **c**);  $\text{N}'' = \text{N}(\text{SiMe}_3)_2$ )

The resonances pertaining to the complexes were significantly shifted, and will be discussed below, but the resonances assigned to the free, uncoordinated ligand (*i.e.* impurities from an incomplete reaction) were indistinguishable from those of the free ligand in the absence of any lanthanide ion. Therefore this enabled the purity, and hence the progress of the reaction, to be monitored accurately. The complexes  $[\text{Pr}(\text{Ph-BOPA})\{\text{N}(\text{SiMe}_3)_2\}_2]$  (**11a**),  $[\text{Pr}(\text{Bn-BOPA})\{\text{N}(\text{SiMe}_3)_2\}_2]$  (**11b**),  $[\text{Pr}(i\text{Pr-BOPA})\{\text{N}(\text{SiMe}_3)_2\}_2]$  (**11c**),  $[\text{Nd}(\text{Ph-BOPA})\{\text{N}(\text{SiMe}_3)_2\}_2]$  (**12a**),  $[\text{Nd}(\text{Bn-BOPA})\{\text{N}(\text{SiMe}_3)_2\}_2]$  (**12b**),  $[\text{Nd}(i\text{Pr-BOPA})\{\text{N}(\text{SiMe}_3)_2\}_2]$  (**12c**),  $[\text{Sm}(\text{Ph-BOPA})\{\text{N}(\text{SiMe}_3)_2\}_2]$  (**13a**),  $[\text{Sm}(\text{Bn-BOPA})\{\text{N}(\text{SiMe}_3)_2\}_2]$  (**13b**) and  $[\text{Sm}(i\text{Pr-BOPA})\{\text{N}(\text{SiMe}_3)_2\}_2]$  (**13c**) were obtained as bright yellow solids in 76-87% yield. The complexes were characterised by NMR and IR spectroscopies, and elemental analysis. Despite repeated attempts on spectroscopically pure samples, elemental analysis could not be obtained for complexes **11a**, **11b**, and **13b**.

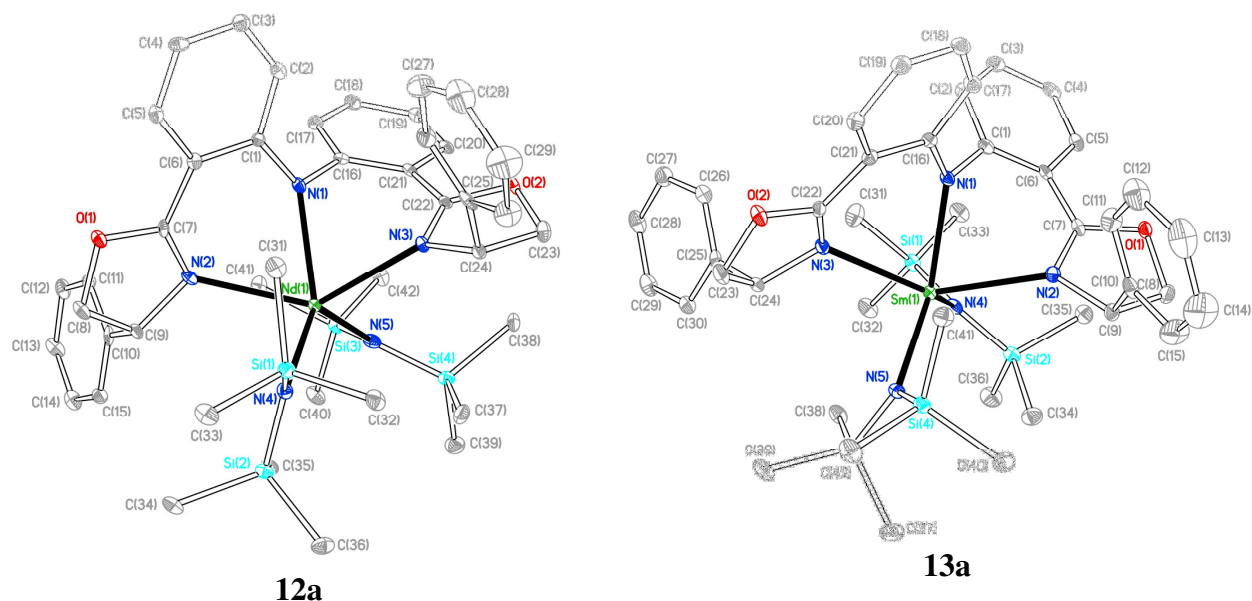
### 2.7.2 X-ray crystal structure of [Nd(Ph-BOPA){N(SiMe<sub>3</sub>)<sub>2</sub>]<sub>2</sub>] (**12a**) and [Sm(Ph-BOPA){N(SiMe<sub>3</sub>)<sub>2</sub>]<sub>2</sub>] (**13a**)

Single crystals of [Nd(Ph-BOPA){N(SiMe<sub>3</sub>)<sub>2</sub>]<sub>2</sub>] (**12a**) and [Sm(Ph-BOPA){N(SiMe<sub>3</sub>)<sub>2</sub>]<sub>2</sub>] (**13a**) suitable for X-ray diffraction were grown from saturated hexane solutions at room temperature. The X-ray data were collected by the EPSRC National Crystallography Service and solved by Dr. Benjamin Ward. The two structures are isomorphous and for the sake of conciseness, the following discussion relates primarily to the neodymium structure **12a**. The molecular structures of **12a** and **13a** are shown in Fig. 14; selected bond lengths and angles are shown in Table 3 and 4. Full listings of crystal data are provided in Appendix A.

The molecular structure of [Nd(Ph-BOPA){N(SiMe<sub>3</sub>)<sub>2</sub>]<sub>2</sub>] (**12a**) shows a distorted trigonal bipyramidal geometry at the neodymium centre, containing approximate *cis* amide co-ligands. The sum of the N<sub>amide</sub>-Ln-N<sub>amide</sub> angles = 359.92(34) °, indicating the three amides are planar in relation to each other. However, the N(2)-Ln-N(3) angle of 131.50(11) ° is significantly less than the ideal 180 °, resulting from the restrictions imposed by the relatively rigid BOPA backbone. The neodymium amide bond lengths (2.415, 2.360 and 2.332 Å) sit within the reported range (2.205 – 2.855, average 2.38 Å for 225 compounds). Whilst the neodymium imine bond lengths (2.551 and 2.535 Å) sit within the reported range (2.413 – 2.935, average 2.61 Å for 336 compounds).

An analysis of the N-Si-C angles of Si(1), Si(2), Si(3) and Si(4) suggest the presence of weak β-Si-C interactions, this is not uncommon in systems bearing alkyl co-ligands as was discussed for the scandium complex [Sc{N(SiMe<sub>3</sub>)<sub>2</sub>]<sub>2</sub>Cl] (**1**).<sup>53-56</sup> The carbons C (31), C(35), C(41) and C(37) exhibit this phenomenon, highlighted by N-Si-C bond angles of 109.66(19), 109.55(18), 107.69(19) and 109.48(18) respectively.





**Fig. 14** Thermal ellipsoid plot (25%) of  $[\text{Ln}(\text{Ph-BOPA})\{\text{N}(\text{SiMe}_3)_2\}_2]$  ( $\text{Ln} = \text{Nd}$  **12a**,  $\text{Sm}$  **13a**), H atoms emitted for clarity

**Table 3** Selected bond lengths (Å) for  $[\text{Ln}(\text{Ph-BOPA})\{\text{N}(\text{SiMe}_3)_2\}_2]$  ( $\text{Nd}$  **12a**,  $\text{Sm}$  **13a**)

Bond	$\text{Ln} = \text{Nd}$ ( <b>12a</b> ) (Å)	$\text{Ln} = \text{Sm}$ ( <b>13a</b> ) (Å)
<b>Ln-N(1)</b>	<b>2.415(3)</b>	<b>2.3874(18)</b>
<b>Ln-N(2)</b>	<b>2.535(4)</b>	<b>2.5286(19)</b>
<b>Ln-N(3)</b>	<b>2.551(3)</b>	<b>2.5062(18)</b>
<b>Ln-N(4)</b>	<b>2.360(3)</b>	<b>2.3007(19)</b>
<b>Ln-N(5)</b>	<b>2.332(3)</b>	<b>2.3430(19)</b>

These are significantly smaller than the other N-Si-C angles of the same  $\text{SiMe}_3$  group, 112.7(2) and 114.74(19) for Si(1), 114.4(2) and 115.5(2) for Si(2), 113.6(2) and 114.4(2) for Si(3), 113.14(19) and 114.1(2) for Si(4). The Van der Waals radius of carbon is reported as 1.70 Å whilst the Van der Waals radius of neodymium is not reported. Lanthanum has a Van der Waals radius of 2.51 Å and a comparable ionic radius.

**Table 4** Selected bond angles (°) for [Ln(Ph-BOPA){N(SiMe<sub>3</sub>)<sub>2</sub>]<sub>2</sub>] (Nd **12a**, Sm **13a**)

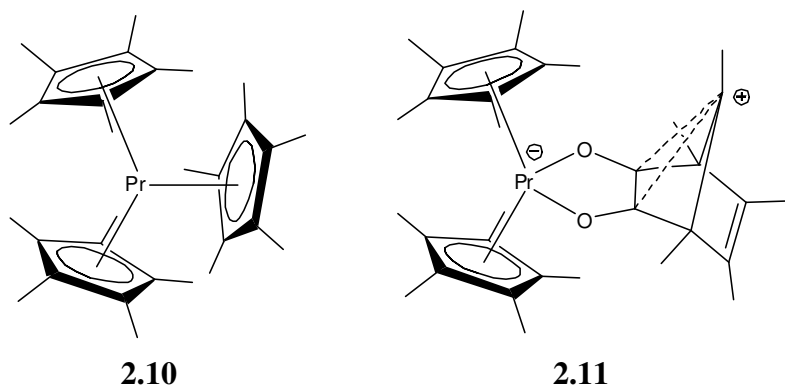
Bond angle	Ln = Nd 12a(°)	Ln = Sm 13a(°)
N(1)-Ln-N(2)	70.12(11)	70.70(6)
N(1)-Ln-N(3)	69.97(11)	71.07(6)
N(1)-Ln-N(4)	132.39(11)	109.92(7)
N(1)-Ln-N(5)	110.03(11)	134.10(6)
N(2)-Ln-N(3)	131.50(11)	133.20(6)
N(2)-Ln-N(4)	82.03(11)	89.77(6)
N(2)-Ln-N(5)	128.78(12)	106.42(6)
N(3)-Ln-N(4)	106.12(11)	128.44(7)
N(3)-Ln-N(5)	90.45(11)	82.30(6)
N(4)-Ln-N(5)	117.50(12)	115.92(6)
N(4)-Si(1)-C(31)	109.66(19)	107.83(11)
N(4)-Si(1)-C(32)	112.7(2)	114.42(11)
N(4)-Si(1)-C(33)	114.74(19)	113.62(12)
N(4)-Si(2)-C(34)	115.5(2)	109.82(11)
N(4)-Si(2)-C(35)	109.55(18)	113.43(10)
N(4)-Si(2)-C(36)	114.4(2)	114.49(12)
N(5)-Si(3)-C(37)	114.4(2)	114.35(12)
N(5)-Si(3)-C(38)	107.69(19)	109.74(11)
N(5)-Si(3)-C(39)	113.6(2)	115.26(11)
N(5)-Si(4)-C(40)	109.48(18)	112.77(11)
N(5)-Si(4)-C(41)	113.14(19)	110.27(10)
N(5)-Si(4)-C(42)	114.1(2)	114.91(11)

It is reasonable to assume that neodymium has a similar Van der Waals radius. With this in mind the distances between the carbons in question and neodymium lie within the sum of the Van der Waals radii, (Nd - C(31) 3.589, Nd - C(35) 3.473, Nd - C(37) 3.600, Nd - C(41) 3.286).

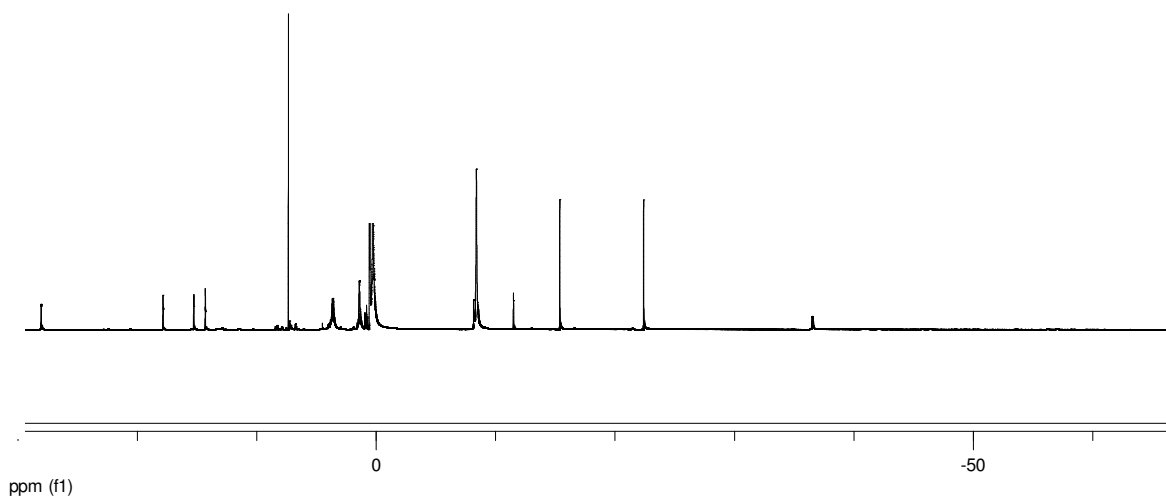
### 2.7.3 Spectroscopic Characterisation of **11–13**

Whilst the lack of fine structure renders the NMR spectra of paramagnetic complexes inherently less informative than their diamagnetic counterparts, paramagnetic complexes of the lanthanides still give relatively sharp signals; therefore the number and relative intensity can be used to infer the symmetry of the complexes. The  $^1\text{H}$  and  $^{13}\text{C}\{^1\text{H}\}$  NMR spectra of **11–13** are consistent with  $C_2$  molecular symmetry, and the resonances exhibit relative intensities that are consistent with the proposed structure deduced from the X-ray analyses, and inferred from the data of the diamagnetic complexes. The  $^1\text{H}$  NMR spectrum of  $[\text{Pr}(\text{iPr-BOPA})\{\text{N}(\text{SiMe}_3)_2\}_2]$  (**11c**) is displayed in Fig. 15. As expected, the spectra showed a significant reduction in fine structure, and the  $^1\text{H}$  NMR spectra gave resonances over a significantly expanded spectral width, 35 – -66 ppm (**11a–c**), 20 – -40 ppm (**12a–c**), and 10 – -2 ppm (**12a–c**).

There are relatively few examples of NMR data for praseodymium complexes, characterisation consisting mainly of infrared and UV-vis data. Complexes bearing cyclopentadienyl and alkoxide ligands have been characterised by  $^1\text{H}$  NMR spectroscopy (Fig. 15), which exhibited resonances between 14.7 and -12.7 ppm, a somewhat smaller range than in the praseodymium BOPA complexes **11** (Fig. 16).



**Fig. 15**  $[\text{Pr}(\text{C}_5\text{Me}_5)_3]$  and  $[\text{Pr}(\text{C}_5\text{Me}_5)_2(\text{O}_2\text{C}_7\text{Me}_5)]$



**Fig. 16**  $^1\text{H}$  NMR spectrum (400 MHz,  $\text{C}_6\text{D}_6$ ) of  $[\text{Pr}(\text{iPr-BOPA})\{\text{N}(\text{SiMe}_3)_2\}_2]$  (**11c**)

In these complexes, the greatest degree of paramagnetic shifting came from the alkoxide, rather than the cyclopentadienyl supporting ligand.<sup>57</sup>  $[\text{Pr}\{\text{N}(\text{SiMe}_3)_2\}_3]$  (**2.10**) shows a single resonance at -8.64 ppm,<sup>45</sup> a very similar chemical shift to the amide co-ligand of **11a-c**, for which The  $\text{N}(\text{SiMe}_3)_2$  groups are observed as a singlet at -8.68 ppm (**11a**), with similar chemical shifts found for **11b** and **11c**. Tentative assignments can be suggested on the basis of integration, and on comparing similar resonances in the spectra of **11a-c**. For example, the two resonances in the  $^1\text{H}$  NMR spectrum of **11a** integrating to 4 H, observed at -4.32 and

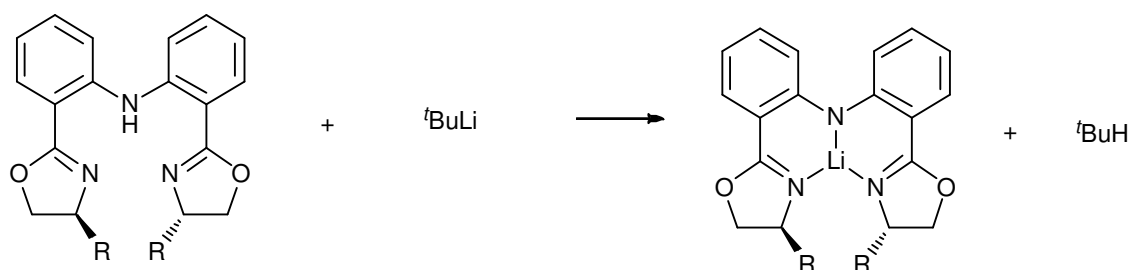
-17.12 ppm, may be assigned as one of the three environments for the phenyl group at the stereocentre (i.e. *ortho* or *meta*), whilst the two resonances in the spectrum of **11b** at 2.07 and -7.93 ppm, integrating to 4 H, can also be assigned as one of the three environments for the benzyl group (i.e. *ortho* or *meta*). The two resonances at -15.58 and -22.60 ppm, integrating to 6 H each, observed in the spectrum of **11c** can be assigned to the two isopropyl methyl environments. Although there is little fine structure in the spectra, broad but identifiable doublets and triplets are observed for some resonances, which are consistent with the spectra for similar complexes discussed above.

The  $^1\text{H}$  NMR spectra of **12a-c** exhibit a wide range of chemical shifts, from 20 to -39 ppm. The  $\text{N}(\text{SiMe}_3)_2$  groups are observed at -5.95 ppm (**12a**), -5.93 ppm (**12b**) and -5.96 ppm (**12c**), comparable to -5.60 ppm for  $[\text{Nd}\{\text{N}(\text{SiMe}_3)_2\}_3]$ .<sup>45</sup> Whilst few other resonances can be assigned, two resonances at -0.96 and -3.60 ppm (**12a**) and 4.40 and -1.08 ppm (**12b**), integrating to 4 H, can be assigned to one of the three environments for the phenyl and benzyl groups at the stereocentre respectively. Also, two resonances at -9.17 and -12.83 ppm (**12c**), integrating to 6 H each, can be assigned the two isopropyl methyl environments.

The  $^1\text{H}$  NMR spectra of **13a-c** exhibit signals over a comparatively narrow chemical shift range, 10 – -2 ppm. The chemical shift range for the samarium complexes is similar to that of diamagnetic systems; this is a common feature of samarium complexes in the literature.<sup>45, 58</sup> The most prominent resonance is assigned to the  $\text{N}(\text{SiMe}_3)_2$  ligand, and is observed at 0.09 ppm (**13a-b**) and -1.58 ppm (**13c**). Two resonances are observed at 5.39 and 4.16 ppm, integrating to 4 H, can be assigned the one of the three environments for the phenyl group at the stereocentre (**13a**). The spectrum of **13b** exhibits two multiplets at 6.75 – 6.71 and 5.96 – 5.92 ppm, integrating to 4 H and 8 H respectively, which can be similarly assigned. The spectrum of **13c** possesses two resonances at -1.09 and -1.83 ppm (6 H integration) which are assigned the two isopropyl methyl environments.

The  $^{13}\text{C}\{^1\text{H}\}$  NMR spectra of **11–13** show similar features to those previously discussed and with relatively little paramagnetic shifting. Although the resonances could not be unambiguously assigned with the aid of 2D NMR experiments, some resonances are essentially identical to those of the diamagnetic complexes and assignment has been made on that basis. For example, the imine carbons are observed at 168.5 for **11a**, a similar chemical shift to all previous complexes. All  $^{13}\text{C}\{^1\text{H}\}$  NMR spectra are consistent with  $C_2$ -symmetric complexes. The ranges of carbon data could not be compared to literature compounds, given the relative void of such information in the chemical literature.

## 2.8 Synthesis and characterisation of Li(R-BOPA) (**14a-c**)



**Scheme 16** Synthesis of Li(R-BOPA) (R = Ph **a**, Bn **b**, iPr **c**)

Metal complexes are often prepared by reacting a metal halide with a ligand lithium salt. Whilst the complexes prepared in this thesis were prepared by protonolysis reactions with metal alkyl and amide precursor complexes, the lithium BOPA complexes were prepared as they may be useful in future avenues not covered by the research reported herein. To this end, the BOPA protio-ligands **2.1a-c** were reacted with  $t$ butyllithium (Scheme 16) to form the lithium complexes Li(Ph-BOPA) (**14a**), Li(Bn-BOPA) (**14b**) and Li(iPr-BOPA) (**14c**) as bright yellow solids in 75-80% yield.  $t$ Butyllithium was employed since it is significantly less nucleophilic than  $n$ BuLi, and therefore less likely to cause ring-opening side-reactions of

the oxazoline rings. Compounds **14a-c** were characterised by elemental analysis, NMR and IR spectroscopies.

### 2.8.1 Spectroscopic Characterisation of **14a-c**

The  $^1\text{H}$  and  $^{13}\text{C}\{^1\text{H}\}$  NMR spectra of  $\text{Li}(\text{R-BOPA})$  **14a-c** indicate the presence of two species in solution, both of which are consistent with  $C_2$  molecular symmetry. The resonances attributed to the ligand arise at similar  $\delta$  to that of **2.1a**, with a small shift of the resonance chemical shifts, which is greatest for the oxazoline protons.  $\text{H}^{\text{s}}$  of  $\text{Li}(\text{Ph-BOPA})$  **14a** occurs at 4.32 and 3.89 ppm for the major and minor isomer respectively, which is a significant shift from the same resonance in the protio-ligand (4.95 ppm).  $\text{H}^{\text{e}}$  and  $\text{H}^{\text{f}}$  protons give rise to two multiplets at 4.03 and 3.67-3.60 ppm for the major and minor isomer respectively, again a significant shift compared to the resonances of the protio-ligand (4.32 and 4.03 ppm). Similar observations were made regarding the benzyl and isopropyl congeners **14b** and **c**. An interesting observation made for the isopropyl derivative **14c** is that upon coordination to lithium, the oxazoline proton resonances become more resolved. The  $^{13}\text{C}\{^1\text{H}\}$  NMR spectra are consistent with the conclusions drawn from the  $^1\text{H}$  NMR spectra. The IR spectra show no N-H stretch at  $3410\text{ cm}^{-1}$ , which is consistent with the deprotonation of the ligand.

### 2.9 Relative proportion of isomers

The relative proportions of the *exo* and *endo* isomers of the complexes  $[\text{Sc}(\text{R-BOPA})\{\text{N}(\text{SiMe}_3)_2\}\text{Cl}]$  (**2a-c**),  $[\text{Sc}(\text{R-BOPA})\{\text{N}(\text{SiMe}_3)_2\}(\text{OTf})]$  (**4a-c**),  $[\text{Ln}(\text{R-BOPA})(\text{CH}_2\text{SiMe}_3)_2]$  ( $\text{Ln} = \text{Sc}$  **5a-c**,  $\text{Y}$  **8a-c**),  $[\text{Ln}(\text{R-BOPA})\{\text{N}(\text{SiMe}_3)_2\}_2]$  ( $\text{Ln} = \text{Y}$  **7a-c**,  $\text{La}$  **10a-c**) and  $\text{Li}(\text{R-BOPA})$  (**14a-c**) were determined from the relative integration of their  $^1\text{H}$

NMR signals measured at 293 K. The relative proportions are provided in Table 5; the calculated energies already discussed are provided for reference. The exceptions to this are the neodymium complexes  $[\text{Nd}(\text{R-BOPA})\{\text{N}(\text{SiMe}_3)_2\}_2]$  (**12a-c**). The relative proportion of the isomers for these complexes were determined using NIR photophysics, and are discussed in Chapter 5. These data are included here to provide a fuller appreciation of the relative energies of these isomers.

It is clear from these data that the predicted energy differences between the *exo* and *endo* isomers are largely of the same order of magnitude as the experimentally measured ones. Given the generally accepted error of DFT energies (1-2 kcal.mol<sup>-1</sup>; 4-8 kJ.mol<sup>-1</sup>), detailed comparisons of energies of this magnitude are inappropriate, however an analysis of general trends can be more informative. The DFT-calculated energies indicate a slight trend towards larger energy differences with metals having larger ionic radii (*i.e.* a general increasing of the energies on progressing down the table); this trend is, to a degree, reproduced experimentally, since the scandium complexes have  $\Delta G$  values of typically 0.7 – 1.7 kJ.mol<sup>-1</sup>, whereas the yttrium, lanthanum, and neodymium complexes often exhibit  $\Delta G$  values of > 4 kJ.mol<sup>-1</sup>. It is impossible (and inappropriate) to speculate the precise effect that this may have on their catalytic behaviour without further experimental data, but the remainder of this thesis will attempt to answer this question by examining these complexes in the catalytic hydroamination/cyclisation of aminoolefins, and in the ring opening polymerisation of *rac*-lactide.



**Table 5** Calculated vs. experimental  $\Delta G$  values for the *exo* and *endo* isomers of complexes described in this chapter.

Entry	Complex	R	Ratio (experimental) <sup>a</sup>	$\Delta G$ (experimental) kJmol <sup>-1</sup>	$\Delta G$ (theoretical) kJmol <sup>-1</sup>
1	[Sc(R-BOPA){N(SiMe <sub>3</sub> ) <sub>2</sub> }Cl] (2)	Ph	1:0.2	3.99	1.61
2		Bn	1:0.7	0.75	0.43
3		iPr	1:0.4	2.53	0.26
4	[Sc(R-BOPA){N(SiMe <sub>3</sub> ) <sub>2</sub> }OTf] (4)	Ph	1:0.4	2.15	0.68
5		Bn	1:0.6	1.39	0.93
6		iPr	1:0.5	1.57	0.52
7	[Sc(R-BOPA)(CH <sub>2</sub> SiMe <sub>3</sub> Ph) <sub>2</sub> ] (5)	Ph	1:0.5	1.67	2.20
8		Bn	1:0.6	1.35	0.53
9		iPr	1:0.5	1.67	3.81
10	[Y(R-BOPA){N(SiMe <sub>3</sub> ) <sub>2</sub> } <sub>2</sub> ] (7)	Ph	1:0.2	3.99	2.82
11		Bn	1:0.2	3.99	3.64
12		iPr	1:0.4	2.27	2.46
13	[Y(R-BOPA)(CH <sub>2</sub> SiMe <sub>3</sub> Ph) <sub>2</sub> ] (8)	Ph	1:0.6	1.48	1.95
14		Bn	-	-	2.12
15		iPr	1:0.2	4.54	1.91
16	[La(R-BOPA){N(SiMe <sub>3</sub> ) <sub>2</sub> } <sub>2</sub> ] (10)	Ph	-	-	2.60
17		Bn	-	-	3.64
18		iPr	-	-	3.11
19	[Nd(R-BOPA){N(SiMe <sub>3</sub> ) <sub>2</sub> } <sub>2</sub> ] (13)	Ph	1:0.1 <sup>b</sup>	5.47	-
20		Bn	1:0.3 <sup>b</sup>	3.43	-
21		iPr	1:0.4 <sup>b</sup>	2.09	-

<sup>a</sup> Calculated from the <sup>1</sup>H NMR spectra unless otherwise stated<sup>b</sup> Calculated from the luminescence data discussed in Chapter 5.

## 2.10 Summary

This chapter describes the synthesis and characterisation of a series of lanthanide complexes supported by the BOPA series of ligands. These complexes have been analysed by DFT to assess the suitability of the BOPA ligand for coordination with these metals. The calculations revealed the possibility of isomers when the ligand is coordinated, arising from the relative 'twist' of the ligand backbone, giving rise to two diastereomeric forms, *exo* and *endo*, referring to the relative orientation of the stereodirecting group. The metal centre in the *exo* isomer is more shielded than in the *endo* isomer, which may have an effect when the complexes are used in catalysis.

Experimentally, the bis(amide) complexes of scandium,  $[\text{Sc}(\text{R-BOPA})\{\text{N}(\text{SiMe}_3)_2\}_2]$  could not be synthesised. However, the synthesis of a new scandium-amide/chloride precursor allowed the synthesis of a mixed amide/chloride complex  $[\text{Sc}(\text{R-BOPA})\{\text{N}(\text{SiMe}_3)_2\}\text{Cl}]$  (**2a-c**). These complexes were used in reactivity studies, but in their reactions with protonating reagents the BOPA was found to undergo competing protonolysis, alongside the amide co-ligand.

The preparation of yttrium amide complexes  $[\text{Y}(\text{R-BOPA})\{\text{N}(\text{SiMe}_3)_2\}_2]$  (**7a-c**) was successful, but required forcing conditions. Conversely the reaction of the BOPA ligands with  $[\text{Y}(\text{CH}_2\text{SiMe}_2\text{Ph})_3(\text{THF})_2]$  proceeded easily at room temperature. The lanthanum congeners  $[\text{La}(\text{R-BOPA})\{\text{N}(\text{SiMe}_3)_2\}_2]$  (**10a-c**) were synthesised much more readily than for yttrium; No heating was required in this case, and this enabled the paramagnetic praseodymium, neodymium, and samarium derivatives to be prepared under identical conditions. The DFT calculations provided estimates of the relative energies of the *exo* and *endo* isomers, which were compared to those obtained experimentally. The energies were found to show a general trend of increasing energy with increasing ionic radius of the metal, which probably reflects the reduction in steric strain of the *exo* isomer as the Ln-N and/or Ln-

C bond lengths increase. All of the complexes synthesised and discussed throughout this thesis are luminescent and a selection of the complexes were analysed for their photophysical properties (Chapter 5).

## 2.11 References for Chapter 2

- 1 S. Hong and T. J. Marks, *Acc. Chem. Res.*, 2004, **37**, 673.
- 2 H. F. Yuen and T. J. Marks, *Organometallics*, 2007, **27**, 155.
- 3 M. Rastatter, A. Zulys, and P. W. Roesky, *Chem. Commun.*, 2006, 874
- 4 S. Hong, S. Tian, M. V. Metz, and T. J. Marks, *J. Am. Chem. Soc.*, 2003, **125**, 14768.
- 5 E. Lu, W. Gan, and Y. Chen, *Organometallics*, 2009, **28**, 2318.
- 6 S. P. Nolan, M. Porchia, and T. J. Marks, *Organometallics*, 1991, **10**, 1450.
- 7 T. K. Panda A. G. Trambitas, J. Jenter, P. W. Roesky, C. Daniliuc, C. G. Hrib, P. G. Jones, M. Tamm., *Inorg. Chem.*, 2010, **49**, 2435.
- 8 M. Konkol, M. Kondracka, P. Voth, T. P. Spaniol, and J. Okuda, *Organometallics*, 2008, **27**, 3774.
- 9 B. R. Elvidge, S. Arndt, T. P. Spaniol, and J. Okuda, *Dalton Trans*, 2006, 890.
- 10 W. J. Evans, L. Bloom, W. E. Hunter, and J. A. Atwood, *J. Am. Chem. Soc.*, 1983, **105**, 1401.
- 11 M. A. Giardello, V. P. Conticello, L. Brard, M. R. Gagne, and T. J. Marks, *J. Am. Chem. Soc.*, 1994, **116**, 10241.
- 12 M. A. Giardello, V. P. Conticello, L. Brard, M. Sabat, A. L. Rheingold, C. L. Stern, and T. J. Marks, *J. Am. Chem. Soc.*, 1994, **116**, 10212.
- 13 M. A. Giardello, Y. Yamamoto, L. Brard, and T. J. Marks, *J. Am. Chem. Soc.*, 1995, **117**, 3276.
- 14 X. Xu, Y. Chen, G. Zou, and J. Sun, *Dalton Trans.*, 2010, **39**, 3952.
- 15 A. Alaaeddine, A. Amgoune, C. M. Thomas, S. Dagorne, S. Bellemin-Laponnaz, and J.-F. Carpentier, *Eur. J. Inorg. Chem.*, 2006, 3652.
- 16 D. Robert, E. Abinet, T. P. Spaniol, and J. Okuda, *Chem. Eur. J.*, 2009, **15**, 11937.

- 17 A. Alaaeddine, A. Amgoune, S. Bellemin-Lapponnaz, J. -F. Carpentier, S. Dagorne, and C. M. Thomas, *Eur. J. Inorg. Chem.*, 2006, 3652.
- 18 B. D. Ward and L. H. Gade, *Chem. Commun.*, 2012, **48**, 10587.
- 19 H. A. McManus and P. J. Guiry, *J. Org. Chem.*, 2002, **67**, 8566.
- 20 H. A. McManus and P. J. Guiry, *Abstr. Pap. Am. Chem. S.*, 2001, **222**, 392.
- 21 S. Lu, D. Du, S. Zhang, and J. Xu, *Tet. Asymm.*, 2004, **15**, 3433.
- 22 M. J. Frisch, G. W. Trucks, H. B. Schlegel, G. E. Scuseria, M. A. Robb, J. R. Cheeseman, G. Scalmani, V. Barone, B. Mennucci, G. A. Petersson, H. Nakatsuji, M. Caricato, X. Li, H. P. Hratchian, A. F. Izmaylov, J. Bloino, G. Zheng, J. L. Sonnenberg, M. Hada, M. Ehara, K. Toyota, R. Fukuda, J. Hasegawa, M. Ishida, T. Nakajima, Y. Honda, O. Kitao, H. Nakai, T. Vreven, J. A. Montgomery Jr, J. E. Peralta, F. Ogliaro, M. Bearpark, J. J. Heyd, E. Brothers, K. N. Kudin, V. N. Staroverov, T. Keith, R. Kobayashi, J. Normand, K. Raghavachari, A. Rendell, J. C. Burant, S. S. Iyengar, J. Tomasi, M. Cossi, N. Rega, J. M. Millam, M. Klene, J. E. Knox, J. B. Cross, V. Bakken, C. Adamo, J. Jaramillo, R. Gomperts, R. E. Stratmann, O. Yazyev, A. J. Austin, R. Cammi, C. Pomelli, J. W. Ochterski, R. L. Martin, K. Morokuma, V. G. Zakrzewski, G. A. Voth, P. Salvador, J. J. Dannenberg, S. Dapprich, A. D. Daniels, O. Farkas, J. B. Foresman, J. V. Ortiz, J. Cioslowski, and D. J. Fox, in 'Gaussian 09, Revision C.01', Gaussian Inc. Wallingford CT, 2010.
- 23 C. Foltz, M. Enders, S. Bellemin-Lapponnaz, H. Wadepohl, and L. H. Gade, *Chem. Eur. J.*, 2007, **13**, 5994.
- 24 D. J. H. Emslie, W. E. Piers, M. Parvez, and R. McDonald, *Organometallics*, 2002, **21**, 4226.
- 25 E. C. Alyea, D. C. Bradley, and R. G. Copperthwaite, *J. Chem. Soc. Dalt*, 1972, 1580.
- 26 A. Bondi, *J. Phys. Chem.*, 1964, **68**, 441.

- 27 S. S. Batsanov, *Inorg. Mat.*, 2001, **37**, 871.
- 28 P. Bolton, A. R. Cowley, and P. Mountford, *Chem. Commun.*, 2005, 3313.
- 29 G. I. Nikonov, *J. Oranomet. Chem.*, 2001, **635**, 24.
- 30 W. T. Klooster, L. Brammer, C. J. Schaverien, and P. H. M. Budzelaar, *J. Am. Chem. Soc.*, 1999, **121**, 1381.
- 31 W. Grochala, M. K. Cyranski, M. Derzsi, T. Michalowski, P. J. Malinowski, Z. Mazej, D. Kurzydowski, W. Kozminski, A. Budzianowski, and P. J. Leszczynski, *Dalton Trans.*, 2012, **41**, 2034.
- 32 P. Mountford and B. D. Ward, *Chem. Commun.*, 2003, **15**, 1797.
- 33 B. D. Ward, S. R. Dubberley, A. Maisse-Francois, L. H. Gade, and P. Mountford, *Dalton Trans.*, 2002, **24**, 4649
- 34 B. D. Ward; S. Bellemin-laponnez; L. H. Gade, *Angew. Chem. Int. Ed.*, 2005, **44**, 1668.
- 35 S. Arndt, T. P. Spaniol, and J. Okuda, *Organometallics*, 2003, **22**, 775.
- 36 P. Voth, T. P. Spaniol, and J. Okuda, *Organometallics*, 2003, **22**, 3921.
- 37 B. D. Ward, L. Lukešová, H. Wadepohl, S. Bellemin-Laponnaz, and L. H. Gade, *Eur. J. Inorg. Chem.*, 2009, 866.
- 38 P. M. Zeimentz, S. Arndt, B. R. Elvidge, and J. Okuda, *Chem. Rev.*, 2006, **106**, 2404
- 39 W. J. Evans, C. A. Seibel, and J. W. Ziller, *J. Am. Chem. Soc.*, 1998, **120**, 6745.
- 40 L. Zhang, Y. Luo, and Z. Hou, *J. Am. Chem. Soc.*, 2005, **127**, 14562.
- 41 F. Focante, P. Mercandelli, A. Sironi, and L. Resconi, *Coord. Chem. Rev.*, 2006, **250**, 170.
- 42 E. Y.-X. Chen and T. J. Marks, *Chem. Rev.*, 2000, **100**, 1391.
- 43 X. Song, M. Thornton-Pett, and M. Bochmann, *Organometallics*, 1998, **17**, 1004.

- 44 S. Bambirra, D. Van Leusen, A. Meetsma, B. Hessen, and J. H. Teuben, *Chem. Commun.*, 2001, 637.
- 45 D. C. Bradley, J. S. Ghotra, and F. A. Hart, *J. C. S. Dalton*, 1973, 1021.
- 46 S. Ge, S. Bombirra, A. Meetsma, and B. Hessen, *Chem. Commun.*, 2006, 3320
- 47 Y. Chapurina, R. Guillot, D. Lyubov, A. Trifnov, J. Hannedouche, and E. Schulz, *Dalton Trans.*, 2013, **42**, 507
- 48 A. V. Karpov, A. S. Sharyrin, A. V. Cherkasov, G. K. Fukin, and A. A. Trifonov, *Organometallics*, 2012, **31**, 5349.
- 49 P. G. Hayes, G. C. Welch, D. J. H. Emslie, C. L. Noack, W. E. Piers, and M. Parvez, *Organometallics*, 2003, **22**, 1577.
- 50 L. Lee, D. J. Berg, F. W. Einstein, and R. J. Batchelor, *Organometallics*, 1997, **16**, 1819.
- 51 S. Bambirra, D. Van Leusen, A. Meetsma, B. Hessen, and J. H. Teuben, *Chem. Commun.*, 2003, 522.
- 52 S. Bambirra, M. W. Bouwkamp, A. Meetsma, and B. Hessen, *J. Am. Chem. Soc.*, 2004, **126**, 9182.
- 53 P. D. Bolton, E. Clot, N. Adams, S. R. Dubberley, A. R. Cowley, and P. Mountford, *Organometallics*, 2006, **25**, 2806.
- 54 A. D. Horton and A. G. Orpen, *Organometallics*, 1991, **10**.
- 55 L. Perrin, L. Maron, O. Eisenstein, and M. F. Lappert, *New J. Chem.*, 2003, **27**, 121.
- 56 C. S. Tredget, E. Clot, and P. Mountford, *Organometallics*, 2008, **27**, 3458
- 57 W. J. Evans, J. M. Perotti, S. A. Kozimor, T. M. Champagne, B. L. Davies, G. W. Nyce, C. H. Fujimoto, R. D. Clark, M. A. Johnston, and J. W. Ziller, *Organometallics*, 2005, **24**, 3916.

- 58 H. E. Dyer, S. Huijser, N. Susperregui, F. Bonnet, A. D. Schwarz, R. Duchateau, L. Maron, and P. Mountford, *Organometallics*, 2010, **29**, 3602.

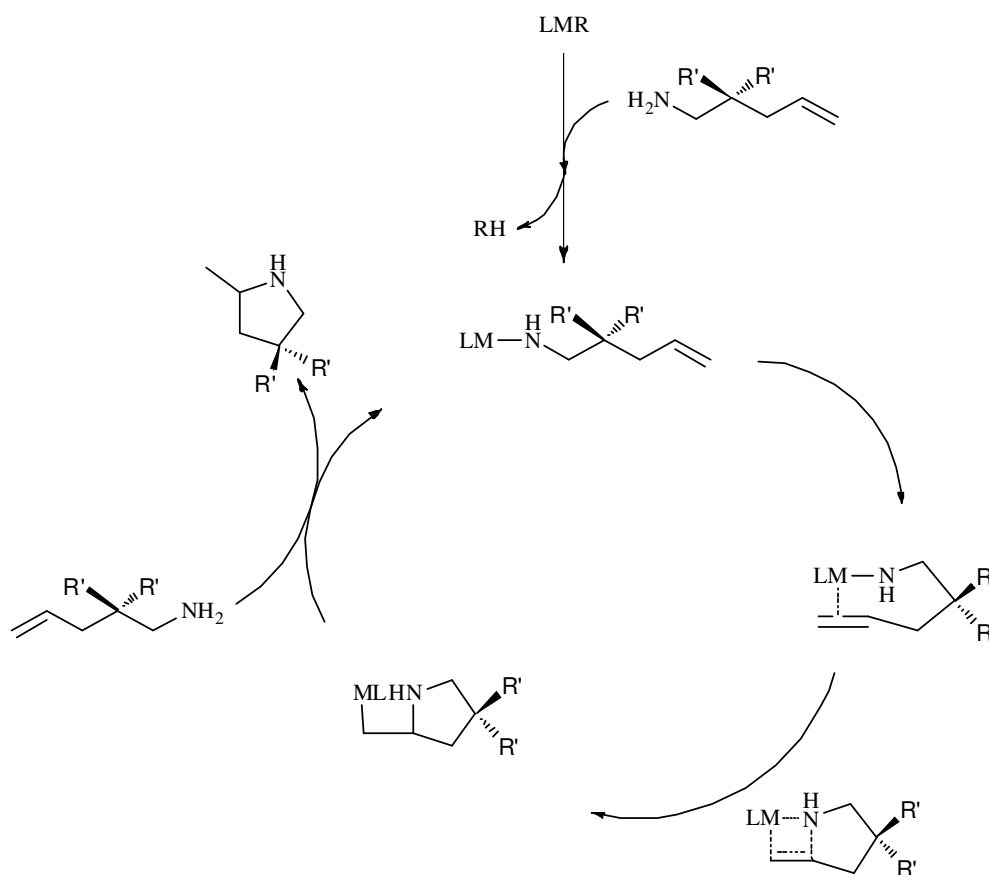


## **CHAPTER 3**

# **Intramolecular Hydroamination Reaction with BOPA Supported Catalysts**

### 3.1 Introduction

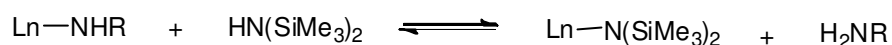
Many catalytic reactions involve the coordination of a *deprotonated* substrate, which subsequently undergoes a metal-mediated transformation. An example of this is the intramolecular hydroamination/cyclisation of aminoolefins catalysed by lanthanides (Scheme 1); for a discussion of the mechanism of this reaction see Chapter 1.



**Scheme 1** The widely accepted mechanism for Ln/group 3 metal-catalysed intramolecular hydroamination

Since the reaction involves the deprotonation of an amine, the metal complex must contain a basic co-ligand that is more basic than the substrate. Common examples are  $\text{N}(\text{SiMe}_3)_2$  and  $\text{CH}_2\text{SiMe}_3$ , both of which have been commonly employed in this manner.<sup>1-7</sup>

Although both of these co-ligands have been widely reported for lanthanide complexes, each have advantages and disadvantages associated with their use in coordination chemistry and catalysis. The alkyl co-ligand is often the preferred co-ligand for use in hydroamination catalysis, since the conjugate acid formed from the deprotonation of the substrate is  $\text{SiMe}_4$ , which is inert and cannot subsequently interact with the metal-substrate complex (*i.e.* it cannot re-protonate the substrate amide ligand). However lanthanide alkyl complexes are known for their thermal instability, which may sometimes involve side reactions with the support ligand(s) and becomes increasingly problematic with the earlier lanthanides (possessing larger ionic radii). This phenomenon is exemplified by the fact that  $\text{Sc}(\text{CH}_2\text{SiMe}_3)_3(\text{THF})_2$  is easily isolable at 0 °C,  $\text{Y}(\text{CH}_2\text{SiMe}_3)_3(\text{THF})_2$  is more challenging to isolate under comparable conditions, and the La congener is often prepared and reacted *in situ*. Lanthanide complexes bearing amide co-ligands are not generally thermally unstable (unless it involves a reaction with the supporting ligand) and therefore can be employed more widely for the earlier lanthanides. However this can cause additional complexity in any subsequent catalytic reaction. To use the hydroamination reaction as a representative example, the liberated amine  $\text{HN}(\text{SiMe}_3)_2$  can, in principle, re-protonate the metal-bound substrate resulting in an additional equilibrium between the initial co-ligand and the substrate being bound to the metal, Scheme 2.

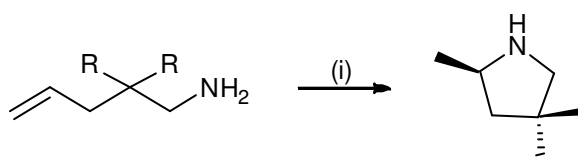


**Scheme 2.** The exchange of ligands between the liberated amine and metal-bound substrate

Notwithstanding these considerations, amide co-ligands have been largely employed in the studies described within this thesis. Yttrium alkyl complexes have been studied, however in these cases the larger  $\text{CH}_2\text{SiMe}_2\text{Ph}$  co-ligand has been employed since this is

known to exhibit similar behaviour to the  $\text{CH}_2\text{SiMe}_3$  ligand, but possesses sufficient steric bulk to reduce the thermal instability of the complexes.

In Chapter 2, the synthesis of a series of Group 3 and lanthanide complexes bearing the bis(oxazolinyphenyl)amine (BOPA) ligand was described. In particular, it was noted that the BOPA ligand can adopt two conformations, differing in the relative ‘twist’ in the diphenylamide backbone. This differing twist causes the stereodirecting groups of the oxazoline moieties to lie *exo* or *endo* relative to each other. The relative proportion of the two isomeric forms was investigated using NMR spectroscopy, and was determined for all three stereodirecting groups (phenyl, isopropyl, benzyl) and for a number of metals and co-ligands. The relative energies of the two isomers were additionally investigated from a computational standpoint, and the calculated energies largely correlate with the experimental data. Having ascertained the intricate properties of the ligand conformation, these data can be used to interpret the behaviour of these complexes in the intramolecular hydroamination/cyclisation of amino olefins, (Scheme 3). The effect of the relative proportion of isomers, and of the ionic radius of the metal, on the enantioselectivities are described below.



**Scheme 3** Hydroamination reaction. R = Me (**A**) or Ph (**B**). (i) 10% mol. Cat

## 3.2 Asymmetric hydroamination/cyclisation catalysis using Group 3 and lanthanide complexes

### 3.2.1 Hydroamination catalysis with scandium complexes

A solution of an aminoolefin substrate (**A** or **B**, synthesised according to literature procedures)<sup>8</sup> was added to a solution of [Sc(R-BOPA)(CH<sub>2</sub>SiMe<sub>2</sub>Ph)<sub>2</sub>] (R = Ph **5a**, Bn **5b**, iPr **5c**), and the progress of the cyclisation reaction monitored using NMR spectroscopy; the results are provided in Table 1. Where appropriate, enantiomeric excesses were determined by adding an excess of *R*-(-)-*O*-acetylmandelic acid to the reaction mixture.<sup>9</sup> The signal assigned to the pyrrolidine methyl substituent was observed as two distinct doublets due to the formation of diastereomeric ion pairs, and could be subsequently integrated using the line fitting utility of the iNMR software package.

When employing the dimethyl substrate **A**, no conversion was observed for any of the three complexes at room temperature after several weeks (entries 1–3), as well as at 80 °C (entries 4–6). This was not the case with substrate **B**, but the cyclisation was nevertheless extremely slow, with a good conversion being obtained only after 6 weeks at ambient temperature (entries 7–9). Additionally, the enantioselectivities obtained were low (5-13%), the highest selectivity (13% ee, entry 9) was obtained for the iPr derivative, but given a typical error margin of 2-3% on enantiomeric excess determinations, these results are not significantly different. Given the slow rate of reaction at room temperature, the reaction temperature was increased to 40 °C to affect an increase in reaction rate. Under these conditions the aminoolefin was completely cyclised in 3 weeks, representing a significant increase in reaction rate from that observed at room temperature, but still very slow for this reaction, in comparison to many other catalyst systems.<sup>10-13</sup> The effect of increasing the

temperature on the enantioselectivities was to reduce the enantiomeric excesses to 5–7 % ee (entries 10–12), a common observation when the reaction temperature is increased.

**Table 1** Intramolecular Hydroamination reaction (Scheme 3) with [Sc(R-BOPA)(CH<sub>2</sub>SiMe<sub>2</sub>Ph)<sub>2</sub>] (**5a-c**). R = Ph **5a**, Bn **5b**, iPr **5c**; solvent = C<sub>6</sub>D<sub>6</sub>

Entry	Catalyst <sup>a</sup>	Substrate	Temp. °C	Time weeks	Conv. <sup>b</sup> %	e.e. <sup>c</sup> %
1	<b>5a</b>	A	22	3	0	-
2	<b>5b</b>	A	22	3	0	-
3	<b>5c</b>	A	22	3	0	-
4	<b>5a</b>	A	80	1	0	-
5	<b>5b</b>	A	80	1	0	-
6	<b>5c</b>	A	80	1	0	-
7	<b>5a</b>	B	22	6	90	10
8	<b>5b</b>	B	22	6	90	12
9	<b>5c</b>	B	22	6	85	13
10	<b>5a</b>	B	40	3	>99	6
11	<b>5b</b>	B	40	3	>99	5
12	<b>5c</b>	B	40	3	>99	7

<sup>a</sup>10 % mol. cat.

<sup>b</sup>Determined from <sup>1</sup>H NMR spectra when no further conversion observed.

<sup>c</sup>Determined by <sup>1</sup>H NMR using R-(-)-*O*-acetylmandelic acid.<sup>9</sup>

The lower activity found for the cyclisation of substrate **A** compared to substrate **B** is common, and is a recurring observation throughout this thesis. As a representative example, the cyclisation of these two substrates using the calcium complex [Ca{N(SiMe<sub>3</sub>)<sub>2</sub>}(THF)<sub>2</sub>] gives complete conversion in 23 h for **A** and in 20 min. for **B**;<sup>14</sup> the relative activities found for the two substrates are therefore unsurprising, although the rates are extremely low compared to other lanthanide based catalysts. Given the discussion in Chapter 2, relating the apparent incompatibility of this sterically demanding ligand with the small ionic radius of scandium, it seems likely that these low activities are probably the result of the steric

demands of the BOPA ligand, when coordinated to scandium, giving a sufficiently high activation barrier to almost entirely suppress the catalytic reaction. The low enantioselectivities may be partially attributed to the complexes existing as two interchanging isomers, in which one isomer may be less selective than the other and giving lower enantioselectivities than expected. This interpretation is discussed later in greater depth.

Owing to the low activities observed with the dialkyl complexes (**5a–c**), the catalytic reactions were repeated with the cationic complexes  $[\text{Sc}(\text{R-BOPA})(\text{CH}_2\text{SiMe}_2\text{Ph})][\text{B}(\text{C}_6\text{F}_5)_4]$  ( $\text{R} = \text{Ph}$  **6a**,  $\text{Bn}$  **6b**,  $\text{iPr}$  **6c**). Removing one of the alkyl ligands leaves only one basic co-ligand available to deprotonate a substrate molecule, and therefore limits the number of bound deprotonated substrates to one per scandium. Whilst a second (or more) substrate or solvent molecule may also bind to the metal centre, these will be only neutral donors that may be more easily displaced than an amide ligand, providing additional space at the metal centre for the catalytic reaction to proceed. The catalytic results are provided in Table 2.

**Table 2.** Intramolecular Hydroamination reaction (Scheme 3) with  $[\text{Sc}(\text{R-BOPA})(\text{CH}_2\text{SiMe}_2\text{Ph})][\text{B}(\text{C}_6\text{F}_5)_4]$  (**6a–c**).  $\text{R} = \text{Ph}$  **6a**,  $\text{Bn}$  **6b**,  $\text{iPr}$  **6c**; solvent =  $\text{C}_6\text{D}_5\text{Br}$

Entry	Catalyst <sup>a</sup>	Substrate	Temp. °C	Time Weeks	Conv. <sup>b</sup> %	e.e. <sup>c</sup> %
1	<b>6a</b>	A	22	3	0	0
2	<b>6b</b>	A	22	3	0	0
3	<b>6c</b>	A	22	3	0	0
4	<b>6a</b>	B	22	3	90	7
5	<b>6b</b>	B	22	3	90	8
6	<b>6c</b>	B	22	3	90	10

<sup>a</sup>10 % mol. cat.

<sup>b</sup>Determined from  $^1\text{H}$  NMR spectra when no further conversion observed.

<sup>c</sup>Determined by  $^1\text{H}$  NMR using R-(-)-*O*-acetylmandelic acid.<sup>9</sup>

The cationic complexes **6a-c** cyclised substrate **B** faster than the neutral analogues [Sc(R-BOPA)(CH<sub>2</sub>SiMe<sub>2</sub>Ph)<sub>2</sub>] (**5a-c**) (Table 1, entries 7-9 and Table 2 entries 4-6), with the reaction time being reduced from 6 weeks to 3 weeks at room temperature (Table 1, entries 7-12). The increase in rate of reaction is a common observation made with cationic complexes,<sup>15</sup> however, the rate was still too slow to allow investigations into decreasing the temperature to influence enantioselectivities.

Although this is a significant increase in reaction rate, it is still nevertheless very slow and is indicative that scandium complexes bearing BOPA ligands are unlikely to excel in this reaction. Attempting to conduct the catalysis using [Sc(R-BOPA){N(SiMe<sub>3</sub>)<sub>2</sub>}Cl] (**2a-c**) and [Sc(R-BOPA)N(SiMe<sub>3</sub>)<sub>2</sub>]OTf (**4a-c**) reinforced this conclusion, since these complexes were completely unreactive under the conditions employed.

### 3.2.2 Hydroamination catalysis with yttrium complexes

Since it is possible that the scandium BOPA complexes are inactive in hydroamination catalysis owing to the small ionic radius of the scandium, the catalytic studies were repeated using yttrium. Yttrium has a significantly larger ionic radius than scandium and therefore may be more compatible with the steric demands of the BOPA ligand architecture. Therefore the complexes [Y(R-BOPA){N(SiMe<sub>3</sub>)<sub>2</sub>}<sub>2</sub>] (**7a-c**), [Y(R-BOPA)(CH<sub>2</sub>SiMe<sub>2</sub>Ph)<sub>2</sub>] (**8a-c**) and [Y(R-BOPA)(CH<sub>2</sub>SiMe<sub>2</sub>Ph)][B(C<sub>6</sub>F<sub>5</sub>)<sub>4</sub>] (**9a-c**) were all investigated in the intramolecular hydroamination/cyclisation of the two substrates **A** and **B** discussed previously. The yttrium amide complexes [Y(R-BOPA){N(SiMe<sub>3</sub>)<sub>2</sub>}<sub>2</sub>] (R = Ph **7a**, Bn **7b**, iPr **7c**) were unreactive towards both substrates. Although the yttrium has a larger ionic radius than scandium, the complexes bear the bulky bis(trimethylsilyl)amide co-ligands, significantly increasing the steric demand around the metal centre and shielding the metal centre from attack by the substrate NH<sub>2</sub> group. This is consistent with the forcing



conditions required for the coordination of the BOPA ligand to  $[Y\{N(SiMe_3)_2\}_3]$  (Chapter 2). In addition, analysis of the reaction mixtures using NMR spectroscopy indicated that the  $[Y(R-BOPA)\{N(SiMe_3)_2\}_2]$  complexes were unaffected by the addition of substrate, and it may be concluded that the bis(trimethylsilyl)amide co-ligands are too sterically demanding and that there is insufficient space around the coordination sphere for the substrate to displace the co-ligands.

Yttrium complexes bearing  $CH_2SiMe_2Ph$  were employed to reduce the steric demand imposed by the co-ligands, and the catalysis results are provided in Table 3. The complexes  $[Y(R-BOPA)(CH_2SiMe_2Ph)_2]$  (**8a-c**) were again found to be completely inactive towards the dimethyl substrate **A** (entries 1-3), long rates of conversion have been observed with other yttrium systems and **A**,<sup>16</sup> for example, 14 days at 60 °C yielded a product of 50% e.e.<sup>7</sup> Conversely,  $[Y(R-BOPA)(CH_2SiMe_2Ph)_2]$  (**8a-c**) were much more reactive towards the diphenyl substrate **B** (Scheme 3). Forcing conditions were not required and relatively fast rates were observed, which allowed the reaction to be studied at reduced temperature (entries 7-9 and 13-15). These data support the conclusions discussed for the amide complexes  $[Y(R-BOPA)\{N(SiMe_3)_2\}_2]$  (**7a-c**) (*vide supra*), since once these two classes of complex enter the catalytic cycle, the active species is likely to be identical in both cases since the co-ligand is displaced. The reaction times were determined using <sup>1</sup>H NMR spectroscopy by integration of the resonances attributed to the substrate and product.

The highest enantioselectivities were observed for the phenyl and isopropyl congeners **8a** and **8c**, 44% and 43% respectively (entries 4 and 6), these are average compared to the majority of complexes which lie within the reported range of 9 - 77%.<sup>17-22</sup>

However, one scandium complex does stand out, whereby the substrate is yielded in 95% e.e.,<sup>23</sup> as illustrated previously, this is unusually high and is by no means routine

**Table 3.** Intramolecular Hydroamination reaction (Scheme 3) with [Y(R-BOPA)(CH<sub>2</sub>SiMe<sub>2</sub>Ph)<sub>2</sub>] (**9a-c**). R = Ph **8a**, Bn **8b**, iPr **8c**

Entry	Catalyst <sup>a</sup>	Solvent	Substrate	Temp. °C	Time	Conv. <sup>b</sup> %	e.e. <sup>c</sup> %
1	<b>8a</b>	C <sub>6</sub> D <sub>6</sub>	A	50	1 wk	0	-
2	<b>8b</b>	C <sub>6</sub> D <sub>6</sub>	A	50	1 wk	0	-
3	<b>8c</b>	C <sub>6</sub> D <sub>6</sub>	A	50	1 wk	0	-
4	<b>8a</b>	C <sub>6</sub> D <sub>6</sub>	B	22	0.25 hrs	>99	44
5	<b>8b</b>	C <sub>6</sub> D <sub>6</sub>	B	22	0.25 hrs	>99	30
6	<b>8c</b>	C <sub>6</sub> D <sub>6</sub>	B	22	0.25 hrs	>99	43
7	<b>8a</b>	C <sub>6</sub> D <sub>6</sub>	B	10	12 hrs	>99	41
8	<b>8b</b>	C <sub>6</sub> D <sub>6</sub>	B	10	12 hrs	>99	28
9	<b>8c</b>	C <sub>6</sub> D <sub>6</sub>	B	10	12 hrs	>99	42
10	<b>8a</b>	C <sub>7</sub> D <sub>8</sub>	B	22	12 hrs	>99	42
11	<b>8b</b>	C <sub>7</sub> D <sub>8</sub>	B	22	12 hrs	>99	26
12	<b>8c</b>	C <sub>7</sub> D <sub>8</sub>	B	22	12 hrs	>99	40
13	<b>8a</b>	C <sub>7</sub> D <sub>8</sub>	B	10	18 hrs	>99	40
14	<b>8b</b>	C <sub>7</sub> D <sub>8</sub>	B	10	18 hrs	>99	26
15	<b>8c</b>	C <sub>7</sub> D <sub>8</sub>	B	10	18 hrs	>99	30
16	<b>8a</b>	C <sub>7</sub> D <sub>8</sub>	B	0	24 hrs	>99	40
17	<b>8b</b>	C <sub>7</sub> D <sub>8</sub>	B	0	24 hrs	>99	26
18	<b>8c</b>	C <sub>7</sub> D <sub>8</sub>	B	0	24 hrs	>99	36

<sup>a</sup>10 % mol. cat.<sup>b</sup> Determined from <sup>1</sup>H NMR spectra when no further conversion observed.<sup>c</sup> Determined by <sup>1</sup>H NMR using R-(-)-*O*-acetylmandelic acid.<sup>9</sup>

The benzyl group of **8b** has the ability to rotate away from the catalytic site, thus decreasing the influence on the reaction and thus explaining the lower enantiomeric excesses. When the cyclisation studies were carried out at a lower temperature (10 °C) the reaction rates were understandably reduced, and there was a slight decrease in enantioselectivity (entries 4-9).

An interesting observation was made when changing the solvent for the catalysis reaction. In general, the polarity and/or donor ability of the solvent can have a significant effect on the activity or selectivity of a catalyst, arising from differences in transition state energies in different reaction media, or involving complexes with different coordination numbers.<sup>24, 25</sup> Although C<sub>6</sub>D<sub>6</sub> and C<sub>7</sub>D<sub>8</sub> have similar polarities (dielectric constants of 2.28 and 2.38 respectively)<sup>26</sup> and neither contains a  $\sigma$ -donor group, the cyclisation reaction rates were significantly different in these two solvents. In C<sub>6</sub>D<sub>6</sub>, the cyclisation reaction gave quantitative conversion within *ca.* 15 minutes (*i.e.* the time taken to record the initial <sup>1</sup>H NMR spectrum) (entries 4-6), whereas in C<sub>7</sub>D<sub>8</sub> (but otherwise identical conditions) the same conversion was only achieved after 12 hours (entries 10-12). There were no significant differences in the enantiomeric excesses. It is known that coordinating solvents (*i.e.* THF, ether) are known to suppress the reaction *via* competing coordination to the hard, Lewis acidic metal centres like yttrium,<sup>24, 25</sup> but an investigation into other weakly donating solvents such as CH<sub>2</sub>Cl<sub>2</sub> and CHCl<sub>3</sub> were not attempted because of the probability of halide abstraction by the precatalyst complexes.

In an analogous manner to the scandium complexes discussed above, the cationic complexes [Y(R-BOPA)(CH<sub>2</sub>SiMe<sub>2</sub>Ph)][B(C<sub>6</sub>F<sub>5</sub>)<sub>4</sub>] (R = Ph **9a**, Bn **9b**, iPr **9c**) were also investigated in the hydroamination reaction; the catalytic performances are summarised in Table 4.

The rationale behind using the cationic complexes was to alleviate some of the steric strain around the metal centre and to therefore increase the rate of cyclisation, particularly for the geminal dimethyl substrate **A**. Disappointingly however, complexes **9a–c** exhibited no activity in the cyclisation of this substrate at room temperature (entries 1-3), as previously discussed, the cyclisation of **A** has been shown to be slow.<sup>7, 16</sup>

**Table 4.** Intramolecular Hydroamination reaction (Scheme 3) with [Y(R-BOPA)(CH<sub>2</sub>SiMe<sub>2</sub>Ph)][B(C<sub>6</sub>F<sub>5</sub>)<sub>4</sub>] (**9a-c**). R = Ph **9a**, Bn **9b**, iPr **9c**

Entry	Catalyst <sup>a</sup>	Solvent	Substrate	Temp. °C	Time	Conv. <sup>b</sup> %	e.e. <sup>c</sup> %
1	<b>9a</b>	C <sub>6</sub> D <sub>5</sub> Br	A	22	1 wk	0	-
2	<b>9b</b>	C <sub>6</sub> D <sub>5</sub> Br	A	22	1 wk	0	-
3	<b>9c</b>	C <sub>6</sub> D <sub>5</sub> Br	A	22	1 wk	0	-
4	<b>9a</b>	C <sub>6</sub> D <sub>5</sub> Br	B	22	0.25 hrs	>99	36
5	<b>9b</b>	C <sub>6</sub> D <sub>5</sub> Br	B	22	0.25 hrs	>99	32
6	<b>9c</b>	C <sub>6</sub> D <sub>5</sub> Br	B	22	0.25 hrs	>99	38

<sup>a</sup>10 % mol. cat.<sup>b</sup>Determined from <sup>1</sup>H NMR spectra when no further conversion observed.<sup>c</sup>Determined by <sup>1</sup>H NMR using R-(-)-*O*-acetylmandelic acid.<sup>9</sup>

Owing to the reactive nature of organolanthanide cations,<sup>27</sup> the catalytic reactions could not be heated, moreover and their limited solubility limited the solvents that could be used. The activities for substrate **B** were analogous to those obtained for the neutral complexes **8a-c** in C<sub>6</sub>D<sub>6</sub> (Table 2 entries 4-6 and Table 3 entries 4-6). Interestingly, the enantioselectivities obtained with **9a** and **9c** (entries 4 and 6) were lower than with **8a** and **8c** (Table 3 entries 4 and 6), but the selectivity obtained for **9b** (entry 5) was higher than for **8b** (Table 3 entry 5). The precise origin of this observation is unclear, but it stands to illustrate how subtle differences to the catalyst structure can make a significant difference to the catalytic performance.

### 3.2.3 Hydroamination catalysis with lanthanum complexes

Since the yttrium BOPA complexes showed a marked improvement in rate and enantioselectivity in the hydroamination/cyclisation of substrate **B** (Scheme 3), compared to the analogous scandium complexes, these studies were extended to lanthanum. Since lanthanum alkyls are known to be thermally unstable, these studies were confined to the amide derivatives. The complexes [La(R-BOPA){N(SiMe<sub>3</sub>)<sub>2</sub>]<sub>2</sub>] (R = Ph **10a**, Bn **10b**, iPr

**10c**) were therefore employed in the hydroamination/cyclisation of both the dimethyl and diphenyl substrates **A** and **B** respectively under a variety of reaction conditions (Table 5).

The most noteworthy results were obtained with the dimethyl substrate **A**, which was not cyclised for any of the scandium or yttrium complexes, but were cyclised at 30 °C with the lanthanum congeners (entries 4-6). The highest enantioselectivity was obtained with [La(Ph-BOPA){N(SiMe<sub>3</sub>)<sub>2</sub>]<sub>2</sub>] (**10a**) (entry 4) (28% e.e), which is within the reported range (6-67%) for lanthanum supported catalysts.<sup>1, 3, 5, 7, 16, 28</sup> The phenyl group (Ph-BOPA) is more sterically demanding than an iPr group, and commonly gives higher levels of selectivity.<sup>5</sup> The relative flexibility of a benzyl group, exemplified by its ability to rotate around the methylene group may be a contributing factor towards the low enantioselectivity found for [La(Bn-BOPA){N(SiMe<sub>3</sub>)<sub>2</sub>]<sub>2</sub>] (**10b**) (entries 2 and 5).

The enantioselectivities obtained for substrate **B** when cyclised by [La(R-BOPA){N(SiMe<sub>3</sub>)<sub>2</sub>]<sub>2</sub>] (**10a-c**) (entries 8-10) were generally lower than those obtained with the yttrium complexes [Y(R-BOPA)(CH<sub>2</sub>SiMe<sub>2</sub>Ph)<sub>2</sub>] (**8a-c**) and [Y(R-BOPA)(CH<sub>2</sub>SiMe<sub>2</sub>Ph)][B(C<sub>6</sub>F<sub>5</sub>)<sub>4</sub>] (**10a-c**), but were slightly higher than those of substrate **A**.

The highest enantioselectivities were obtained with [La(Ph-BOPA){N(SiMe<sub>3</sub>)<sub>2</sub>]<sub>2</sub>] (**10a**) (entry 8), consistent with the reasoning above. It is common for the enantioselectivities to be lower with lanthanum supported catalysts in comparison to yttrium congeners, owing to the larger ionic radius of lanthanum reducing the level of overall control over the chiral active space by the supporting ligand.<sup>7, 16</sup> Unexpected results were obtained when the catalysis was carried out in C<sub>7</sub>D<sub>8</sub>. As with the yttrium complexes, the reactions were all significantly slower than in C<sub>6</sub>D<sub>6</sub>. Substrate **A** showed no conversion in 1 week at 30 °C (entries 15-17) (*c.f.* >99% conv. 72 hours in benzene), and **B** in 12 hours at room temperature (entries 18-20) (*c.f.* 15 minutes in benzene).

**Table 5.** Intramolecular hydroamination reaction (Scheme 3) with [La(R-BOPA){N(SiMe<sub>3</sub>)<sub>2</sub>]<sub>2</sub>] (**10a-c**). R = Ph **10a**, Bn **10b**, iPr **10c**

Entry	Catalyst <sup>a</sup>	Solvent	Substrate	Temp. °C	Time	Conv. <sup>b</sup> %	e.e. <sup>c</sup> %
1	10a	C <sub>6</sub> D <sub>6</sub>	A	50	18 hrs	>99	15
2	10b	C <sub>6</sub> D <sub>6</sub>	A	50	18 hrs	>99	6
3	10c	C <sub>6</sub> D <sub>6</sub>	A	50	18 hrs	>99	7
4	10a	C <sub>6</sub> D <sub>6</sub>	A	30	72 hrs	>99	28
5	10b	C <sub>6</sub> D <sub>6</sub>	A	30	72 hrs	>99	6
6	10c	C <sub>6</sub> D <sub>6</sub>	A	30	72 hrs	>99	7
7	10a	C <sub>6</sub> D <sub>6</sub>	A	22	-	0	-
8	10a	C <sub>6</sub> D <sub>6</sub>	B	22	0.25 hrs	>99	25
9	10b	C <sub>6</sub> D <sub>6</sub>	B	22	0.25 hrs	>99	6
10	10c	C <sub>6</sub> D <sub>6</sub>	B	22	0.25 hrs	>99	5
11	10a	C <sub>6</sub> D <sub>6</sub>	B	10	36 hrs	>99	6
12	10a	C <sub>7</sub> D <sub>8</sub>	A	50	36 hrs	90	14
13	10b	C <sub>7</sub> D <sub>8</sub>	A	50	36 hrs	90	7
14	10c	C <sub>7</sub> D <sub>8</sub>	A	50	36 hrs	90	7
15	10a	C <sub>7</sub> D <sub>8</sub>	A	30	1 wk	0	-
16	10b	C <sub>7</sub> D <sub>8</sub>	A	30	1 wk	0	-
17	10c	C <sub>7</sub> D <sub>8</sub>	A	30	1 wk	0	-
18	10a	C <sub>7</sub> D <sub>8</sub>	B	22	12 hrs	>99	45
19	10b	C <sub>7</sub> D <sub>8</sub>	B	22	12 hrs	>99	6
20	10c	C <sub>7</sub> D <sub>8</sub>	B	22	12 hrs	>99	6
21	10a	C <sub>7</sub> D <sub>8</sub>	B	10	48 hrs	>99	22
22	10b	C <sub>7</sub> D <sub>8</sub>	B	10	48 hrs	>99	6
23	10c	C <sub>7</sub> D <sub>8</sub>	B	10	48 hrs	>99	7
24	10a	C <sub>7</sub> D <sub>8</sub>	B	0	1 wk	0	-
25	10a	C <sub>6</sub> D <sub>5</sub> Br	B	22	0.25 hrs	>99	26
26	10a	CD <sub>3</sub> Cl	B	22	48 hrs	30	22

<sup>a</sup>10 % mol. cat.<sup>b</sup>Determined from <sup>1</sup>H NMR spectra when no further conversion observed.<sup>c</sup>Determined by <sup>1</sup>H NMR using R-(-)-*O*-acetylmandelic acid.<sup>9</sup>

Less expected observations were made regarding the effect of the solvent on the enantiomeric excesses in this reaction. In  $C_7D_8$ , the phenyl derivative **10a** gave an enantiomeric excess of 45% (entry 18), an increase from 25% in benzene (entry 8). This behaviour was not observed for the benzyl and isopropyl complexes **10b-c**, suggesting that whilst benzene and toluene may act as similar solvents, discrete catalyst-solvent interactions may be responsible for the phenomenon, in which a  $C_7D_8$  molecule may be able to interact in a manner that  $C_6D_6$  cannot (or *vice versa*).

Another explanation could be that the different solvents are able to affect the relative proportions of the *exo* and *endo* isomers of the catalyst complexes during the catalytic reactions. Whilst this is plausible, more support for this hypothesis was sought by conducting the catalytic reaction with substrate **B** and the affected complex **10a**, but using two other solvents:  $C_6D_5Br$  and  $CD_2Cl_2$  (dielectric constants of 5.17 and 8.93 respectively).<sup>26</sup> The enantioselectivities in both cases were similar to those obtained in  $C_6D_6$  (entries 25 and 26), albeit with a lower conversion in dichloromethane, possibly arising as a result of catalyst poisoning or decomposition.

### 3.2.4 Hydroamination catalysis with paramagnetic lanthanide complexes

Having established the catalytic performance of the diamagnetic Group 3 complexes, the paramagnetic lanthanide congeners were investigated for their activity in the asymmetric hydroamination/cyclisation of substrates **A** and **B**. Since the highest activities were found for the largest of the Group 3 series (*i.e.* lanthanum), these studies focused on the earlier lanthanides, as the ionic radii of these elements is likely to be more compatible with the steric demands of the BOPA ligand framework.

Complexes  $[Pr(R-BOPA)\{N(SiMe_3)_2\}_2]$  (R = Ph **11a**, Bn **11b**, iPr **11c**) cyclised both substrates **A** and **B** (Table 6). Forcing conditions were not required and fast rates were

observed for the phenyl substrate **B** (entries 4-6 and 10-12); due to the lack of reported Pr supported catalysts the enantioselectivities cannot be compared. As with the lanthanum complexes **10a–c**, these observations support the conclusion that the low activities found for  $[\text{Y}(\text{R-BOPA})\{\text{N}(\text{SiMe}_3)_2\}_2]$  (**7a–c**) were caused by the amide coligand being too sterically demanding, and therefore preventing the coordination of the substrate. The catalysis data for  $[\text{Pr}(\text{R-BOPA})\{\text{N}(\text{SiMe}_3)_2\}_2]$  (**11a–c**) are displayed in Table 6.

**Table 6.** Intramolecular Hydroamination reaction (Scheme 3) with  $[\text{Pr}(\text{R-BOPA})\{\text{N}(\text{SiMe}_3)_2\}_2]$  (**11a–c**). R = Ph **11a**, Bn **11b**, iPr **11c**

Entry	Catalyst <sup>a</sup>	Solvent	Substrate	Temp. °C	Time	Conv. <sup>b</sup> %	e.e. <sup>c</sup> %
1	11a	C <sub>6</sub> D <sub>6</sub>	A	22	12 hr	>99	16
2	11b	C <sub>6</sub> D <sub>6</sub>	A	22	12 hr	>99	10
3	11c	C <sub>6</sub> D <sub>6</sub>	A	22	12 hr	>99	14
4	11a	C <sub>6</sub> D <sub>6</sub>	B	22	1 hr	>99	18
5	11b	C <sub>6</sub> D <sub>6</sub>	B	22	1 hr	>99	42
6	11c	C <sub>6</sub> D <sub>6</sub>	B	22	1 hr	>99	16
7	11a	C <sub>7</sub> D <sub>8</sub>	A	22	48 hr	>99	8
8	11b	C <sub>7</sub> D <sub>8</sub>	A	22	48 hr	>99	2
9	11c	C <sub>7</sub> D <sub>8</sub>	A	22	48 hr	>99	20
10	11a	C <sub>7</sub> D <sub>8</sub>	B	22	12 hr	>99	26
11	11b	C <sub>7</sub> D <sub>8</sub>	B	22	12 hr	>99	4
12	11c	C <sub>7</sub> D <sub>8</sub>	B	22	12 hr	>99	18

<sup>a</sup>10 % mol. cat.

<sup>b</sup> Determined from <sup>1</sup>H NMR spectra when no further conversion observed.

<sup>c</sup> Determined by <sup>1</sup>H NMR using R-(-)-*O*-acetylmandelic acid.<sup>9</sup>

The cyclisation of the dimethyl substrate **A** gave low enantioselectivities (entries 1-3 and 7-9). As expected, the phenyl complex  $[\text{Pr}(\text{Ph-BOPA})\{\text{N}(\text{SiMe}_3)_2\}_2]$  (**11a**) gave the



highest enantioselectivity for praseodymium (16% ee in benzene, entries 1 and 6), which is lower than that obtained with the lanthanum complex  $[\text{La}(\text{Ph-BOPA})\{\text{N}(\text{SiMe}_3)_2\}_2]$  (**10a**) under comparable conditions (28% ee). Conversely, the benzyl and isopropyl derivatives **11b** and **11c** gave the dimethyl-substituted pyrrolidine with higher enantioselectivities than with the lanthanum complexes (10% and 14% with **11b** and **11c** in benzene respectively (entries 2 and 3), compared to 6% and 7% with **10b** and **10c**).

Interestingly, whereas a slight elevation in temperature was required to initiate this reaction for  $[\text{La}(\text{R-BOPA})\{\text{N}(\text{SiMe}_3)_2\}_2]$  (**10a-c**), this was not required for  $[\text{Pr}(\text{R-BOPA})\{\text{N}(\text{SiMe}_3)_2\}_2]$  (**11a-c**), which proceeded at room temperature. This was an unexpected observation, since the ionic radius of praseodymium is smaller than that of lanthanum and might be expected to show the opposite trend, as exemplified in the difference between yttrium and lanthanum.

When the cyclisation of substrate **A** was carried out in  $\text{C}_7\text{D}_8$  instead of  $\text{C}_6\text{D}_6$ , the reaction times were significantly increased (entries 7-12), as observed for the yttrium and lanthanum complexes. The enantioselectivity obtained with  $[\text{Pr}(\text{iPr-BOPA})\{\text{N}(\text{SiMe}_3)_2\}_2]$  (**11c**) increased from 14% to 20% (entries 3 and 9), whereas the enantioselectivities obtained with the phenyl and benzyl congeners **11a** and **11b** decreased from 16% and 10% to 8% and 2% respectively (entries 1,2 7 and 8). This contrasts the observations made for  $[\text{La}(\text{R-BOPA})\{\text{N}(\text{SiMe}_3)_2\}_2]$  (**10a-c**) in  $\text{C}_7\text{D}_8$ , which was inactive in the cyclisation of **A**.

As expected, the cyclisation of the diphenyl substrate **B** using  $[\text{Pr}(\text{R-BOPA})\{\text{N}(\text{SiMe}_3)_2\}_2]$  (**11a-c**) proceeded at a faster rate in comparison to **A**. When the reaction was performed in  $\text{C}_6\text{D}_6$ , the enantioselectivity obtained with  $[\text{Pr}(\text{Ph-BOPA})\{\text{N}(\text{SiMe}_3)_2\}_2]$  (**11a**) was lower than that obtained with  $[\text{La}(\text{Ph-BOPA})\{\text{N}(\text{SiMe}_3)_2\}_2]$  (**10a**), 18% and 25% respectively (entry 4). However, the enantioselectivities obtained with **11b** and **11c** were higher, 42 and 16% (entries 5 and 6) (compared to 6% and 5% for **10b** and

**10c** respectively). These selectivities are comparable to the enantioselectivities obtained with  $[Y(R\text{-BOPA})(\text{CH}_2\text{SiMe}_2\text{Ph})_2]$  (**8a-c**) (despite a significant difference in ionic radii), 44, 30 and 43% respectively.

When the solvent was changed to  $\text{C}_7\text{D}_8$ , the reaction times increased from 1 hour to 12 hours (entries 4-6 and 10-12). The effect on the enantioselectivities was most pronounced for the aromatic substituted BOPA complexes **11a** and **11b**: The enantioselectivity of  $[\text{Pr}(\text{Ph-BOPA})\{\text{N}(\text{SiMe}_3)_2\}_2]$  (**11a**) in  $\text{C}_6\text{D}_6$  was 18% ee (entry 4), whereas in  $\text{C}_7\text{D}_8$ , the enantioselectivity increased to 26% ee (entry 10).

This trend mirrors that for the lanthanum complex  $[\text{La}(\text{Ph-BOPA})\{\text{N}(\text{SiMe}_3)_2\}_2]$  (**10a**), although it is much less pronounced for praseodymium (18% to 26% ee for praseodymium and 25% to 45% ee for lanthanum). The opposite trend was observed when  $[\text{Pr}(\text{Bn-BOPA})\{\text{N}(\text{SiMe}_3)_2\}_2]$  (**11b**) was employed. In  $\text{C}_6\text{D}_6$  the enantioselectivity was 42% ee (entry 5), compared to 4% ee in  $\text{C}_7\text{D}_8$  (entry 11). The isopropyl congener  $[\text{Pr}(\text{iPr-BOPA})\{\text{N}(\text{SiMe}_3)_2\}_2]$  (**11c**) exhibited a negligible change in enantioselectivity when changing the solvent from  $\text{C}_6\text{D}_6$  to  $\text{C}_7\text{D}_8$  (16% to 18% ee, entries 6 and 12). This is a similar observation to that made for the lanthanum complexes; substrate **B** was cyclised with enantioselectivities of 5% and 6% ee in  $\text{C}_6\text{D}_6$  and  $\text{C}_7\text{D}_8$  respectively.

The corresponding catalysis data obtained for the complexes  $[\text{Nd}(R\text{-BOPA})\{\text{N}(\text{SiMe}_3)_2\}_2]$  (**12a-c**) are provided in Table 7. In contrast to the observations made with the praseodymium complexes, only the isopropyl derivative **12a** was found to cyclise the dimethyl substrate **A** (entry 1), albeit with <10% conversion and with 14% ee. This is much lower than a similar system that has been reported, whereby an enantioselectivity of 61% was achieved.<sup>5</sup>

**Table 7.** Intramolecular Hydroamination reaction (Scheme 3) with  $[\text{Nd}(\text{R-BOPA})\{\text{N}(\text{SiMe}_3)_2\}_2]$  (**12a-c**). R = **12a**, Bn **12b**, iPr **12c**

Entry	Catalyst <sup>a</sup>	Solvent	Substrate	Temp. °C	Time	Conv. <sup>b</sup> %	e.e. <sup>c</sup> %
1	<b>12a</b>	$\text{C}_6\text{D}_6$	A	22	1 week	<10	14
2	<b>12b</b>	$\text{C}_6\text{D}_6$	A	22	1 week	-	-
3	<b>12c</b>	$\text{C}_6\text{D}_6$	A	22	1 week	-	-
4	<b>12a</b>	$\text{C}_6\text{D}_6$	B	22	<15 mins	>99	24
5	<b>12b</b>	$\text{C}_6\text{D}_6$	B	22	<15 mins	>99	10
6	<b>12c</b>	$\text{C}_6\text{D}_6$	B	22	<15 mins	>99	12
7	<b>12a</b>	$\text{C}_7\text{D}_8$	B	22	12 hrs	>99	44
8	<b>12b</b>	$\text{C}_7\text{D}_8$	B	22	12 hrs	>99	46
9	<b>12c</b>	$\text{C}_7\text{D}_8$	B	22	12 hrs	>99	36

<sup>a</sup>10 % mol. cat.<sup>b</sup>Determined from  $^1\text{H}$  NMR spectra when no further conversion observed.<sup>c</sup>Determined by  $^1\text{H}$  NMR using R-(-)-*O*-acetylmandelic acid.<sup>9</sup>

The phenyl and benzyl derivatives **12b** and **12c** gave no conversion, even at elevated temperatures. These results are somewhat surprising, although if sterics are the overriding influence, decreasing the ionic radius of the metal is expected to reduce the activity (and it is duly noted that the only active catalyst is the isopropyl derivative, which possesses the least sterically demanding stereodirecting group), the difference in ionic radius of praseodymium vs. that of neodymium is rather small to effect such a large change in catalysis performance. Moreover, the samarium complexes are all active in this catalytic reaction; and samarium has a smaller ionic radius (*vide infra*).

The hydroamination/cyclisation of the diphenyl substrate **B** in  $\text{C}_6\text{D}_6$  proceeded with >99 conversion within 15 minutes (entries 4-6), and gave enantiomeric excesses of 24%, 10%, and 12% when catalysed by  $[\text{Nd}(\text{R-BOPA})\{\text{N}(\text{SiMe}_3)_2\}_2]$  **12a**, **12b**, and **12c**, respectively. These are below average, where the majority of Group 3/lanthanide complexes

yield products with an enantioselectivity in the reported range of 9 - 77%.<sup>17-22</sup> As of yet, no direct comparisons can be made to Nd supported catalysts and substrate **B** in the literature. The phenyl complex [Nd(Ph-BOPA){N(SiMe<sub>3</sub>)<sub>2</sub>}<sub>2</sub>] (**12a**) gave a higher enantiomeric excess (entry 4) than the analogous praseodymium complex **11a** (18% ee), whereas the benzyl complex [Nd(Bn-BOPA){N(SiMe<sub>3</sub>)<sub>2</sub>}<sub>2</sub>] (**12b**) gave a lower enantiomeric excess (entry 5) than [Pr(Bn-BOPA){N(SiMe<sub>3</sub>)<sub>2</sub>}<sub>2</sub>] (**11b**, 42% ee). The isopropyl complex [Nd(iPr-BOPA){N(SiMe<sub>3</sub>)<sub>2</sub>}<sub>2</sub>] (**12c**) gave the cyclised product with a similar enantioselectivity to **11c**, (12% and 16% respectively), and is consistent with the previously discussed amide complexes, where the phenyl and benzyl BOPA complexes provide the greatest enantioselectivities. By changing the solvent from C<sub>6</sub>D<sub>6</sub> to C<sub>7</sub>D<sub>8</sub> the enantioselectivities increase significantly, from 24%, 10%, and 12%, to 36%, 44%, and 46% with **12a**, **12b**, and **12c** respectively (entries 4-9), these enantioselectivities a more representative of the average range (9 - 77%).<sup>17-22</sup>

The catalytic data obtained for the samarium complexes [Sm(R-BOPA){N(SiMe<sub>3</sub>)<sub>2</sub>}<sub>2</sub>] (R = Ph **13a**, Bn **13b**, iPr **13c**) are provided in Table 8. All of the samarium catalysts were found to cyclise the dimethyl substrate **A** (entries 1-3 and 7-9). This is in contrast to the neodymium congeners, where only the isopropyl derivative was active. In C<sub>6</sub>D<sub>6</sub> the enantioselectivities were 16%, 12%, and 14% respectively (entries 1-3) which are lower than average for reported Sm supported catalysts and substrate **A** (27-74%),<sup>1, 3, 5, 7, 28, 29</sup> but are comparable to those of [Pr(R-BOPA){N(SiMe<sub>3</sub>)<sub>2</sub>}<sub>2</sub>] (**11a-c**) which were 16%, 10%, and 14%. The enantioselectivities for **13b** and **13c** are also higher than those obtained with [La(R-BOPA){N(SiMe<sub>3</sub>)<sub>2</sub>}<sub>2</sub>] (**10b** and **10c**, 6% and 7% respectively).

When the same reaction was carried out in C<sub>7</sub>D<sub>8</sub>, the enantioselectivity of the product did not change for the benzyl and isopropyl catalysts **13b** and **13c** (entries 8 and 9), but increased from 16% to 24% with [Sm(Ph-BOPA){N(SiMe<sub>3</sub>)<sub>2</sub>}<sub>2</sub>] (**13a**) (entries 1 and 7).

**Table 8.** Intramolecular Hydroamination reaction (Scheme 3) with [Sm(R-BOPA){N(SiMe<sub>3</sub>)<sub>2</sub>]<sub>2</sub>] (**13a-c**). R = Ph **13a**, Bn **13b**, iPr **13c**

Entry	Catalyst <sup>a</sup>	Solvent	Substrate	Temp. °C	Time	Conv. <sup>b</sup> %	e.e. <sup>c</sup> %
1	13a	C <sub>6</sub> D <sub>6</sub>	A	22	12 hr	>99	16
2	13b	C <sub>6</sub> D <sub>6</sub>	A	22	12 hr	>99	12
3	13c	C <sub>6</sub> D <sub>6</sub>	A	22	12 hr	>99	14
4	13a	C <sub>6</sub> D <sub>6</sub>	B	22	1 hr	>99	16
5	13b	C <sub>6</sub> D <sub>6</sub>	B	22	1 hr	>99	28
6	13c	C <sub>6</sub> D <sub>6</sub>	B	22	1 hr	>99	20
7	13a	C <sub>7</sub> D <sub>8</sub>	A	22	48 hr	>99	24
8	13b	C <sub>7</sub> D <sub>8</sub>	A	22	48 hr	>99	12
9	13c	C <sub>7</sub> D <sub>8</sub>	A	22	48 hr	>99	14
10	13a	C <sub>7</sub> D <sub>8</sub>	B	22	12 hr	>99	28
11	13b	C <sub>7</sub> D <sub>8</sub>	B	22	12 hr	>99	30
12	13c	C <sub>7</sub> D <sub>8</sub>	B	22	12 hr	>99	30

<sup>a</sup>10 % mol. cat.<sup>b</sup> Determined from <sup>1</sup>H NMR spectra when no further conversion observed.<sup>c</sup> Determined by <sup>1</sup>H NMR using R-(-)-*O*-acetylmandelic acid.<sup>9</sup>

These data show a subtle dependence on the identity of the metal ion, since when [La(R-BOPA){N(SiMe<sub>3</sub>)<sub>2</sub>]<sub>2</sub>] (**10a-c**) were used the enantioselectivities were unaffected upon changing the solvent from C<sub>6</sub>D<sub>6</sub> to C<sub>7</sub>D<sub>8</sub>, but with [Pr(R-BOPA){N(SiMe<sub>3</sub>)<sub>2</sub>]<sub>2</sub>] (**11a-c**) the enantioselectivity of the aromatic derived BOPA complexes **11a** and **11b** decreased, whilst the enantioselectivity of [Pr(iPr-BOPA){N(SiMe<sub>3</sub>)<sub>2</sub>]<sub>2</sub>] (**11c**) increased.

Cyclisation of the diphenyl substrate **B** in C<sub>6</sub>D<sub>6</sub> proceeded with similar success to that already observed with the previously discussed lanthanide complexes. The enantioselectivities obtained for the complexes [Sm(R-BOPA){N(SiMe<sub>3</sub>)<sub>2</sub>]<sub>2</sub>] (**13a-c**) were 16%, 28% and 20% for the phenyl, benzyl, and isopropyl derivatives respectively (entries 4-6) (lower than enantioselectivities reported for Group 3/lanthanide complexes and substrate

**B**, 9 - 77%),<sup>17-22</sup> and mirror the trend observed for [Pr(R-BOPA){N(SiMe<sub>3</sub>)<sub>2</sub>]<sub>2</sub>] (**11a-c**), *i.e.* 18%, 42% and 16%. The enantioselectivities are higher than those obtained for [La(R-BOPA){N(SiMe<sub>3</sub>)<sub>2</sub>]<sub>2</sub>] (**10a-c**), as for the praseodymium and neodymium complexes. These data are consistent with the hypothesis that a lanthanide BOPA complex containing a metal with a smaller ionic radius imposes more stereocontrol over the catalysis product. When the analogous reaction was carried out in C<sub>7</sub>D<sub>8</sub> with [Sm(R-BOPA){N(SiMe<sub>3</sub>)<sub>2</sub>]<sub>2</sub>] (**13a-c**), the enantioselectivities increased to 28, 30 and 30%, (entries 10-12) in the same manner observed for [Nd(R-BOPA){N(SiMe<sub>3</sub>)<sub>2</sub>]<sub>2</sub>] (**12a-c**), where all three complexes give higher enantioselectivities upon changing the solvent.

### 3.3 Summary and Conclusions

Both [Sc(R-BOPA)(CH<sub>2</sub>SiMe<sub>2</sub>Ph)<sub>2</sub>] (**5a-c**) and [Sc(R-BOPA)CH<sub>2</sub>SiMe<sub>2</sub>Ph][B(C<sub>6</sub>F<sub>5</sub>)<sub>4</sub>] (**6a-c**) were found to be active in the hydroamination/cyclisation of the aminoolefin **B**, but not substrate **A**. Moreover, these catalytic reactions were very slow, with reactions typically taking weeks to give acceptable conversions. The enantioselectivities for both **5a-c** and **6a-c** were low (<13%).

The yttrium complexes were more reactive than the scandium complexes in the cyclisation of **B**, but again showed no reactivity towards substrate **A**. [Y(Ph-BOPA)(CH<sub>2</sub>SiMe<sub>2</sub>Ph)<sub>2</sub>] (**8a**) and [Y(*i*Pr-BOPA)(CH<sub>2</sub>SiMe<sub>2</sub>Ph)<sub>2</sub>] (**8c**) gave the highest enantioselectivities, which were unaffected by changing the solvent from benzene to toluene, although the reaction rates were significantly reduced.

The catalysts containing the earlier lanthanides (*i.e.* with larger ionic radii) catalysed the cyclisation of both aminoolefins (**A** and **B**) in most cases, although when [La(R-BOPA){N(SiMe<sub>3</sub>)<sub>2</sub>]<sub>2</sub>] was used, a slightly elevated temperature was required to effect the cyclisation of the dimethyl substrate. A change in reaction rate and enantioselectivity was

observed for most complexes upon changing the solvent to toluene. The highest enantioselectivities in toluene were obtained with [La(Ph-BOPA){N(SiMe<sub>3</sub>)<sub>2</sub>}<sub>2</sub>] (**10a**) and [Nd(R-BOPA){N(SiMe<sub>3</sub>)<sub>2</sub>}<sub>2</sub>] (**12a-c**).

Typical enantiomeric excesses for this reaction vary considerably, both within the confines of this thesis and also in the wider chemical literature. This is mainly owing to the fact that there are no general catalysts for this cyclisation reaction that perform equally across a wide range of substrates. Most catalysts give high selectivities for one or two substrates, but low selectivities for others. To place the selectivities obtained in this Chapter into a wider context, it is important to compare only the data reported for these specific substrates. The selectivities reported here are lower than the highest reported enantioselectivities for substrate **B**. The highest reported example is for a scandium catalyst, which cyclised the substrate with an enantioselectivity of 95%.<sup>23</sup> This extremely high enantioselectivity has not been universally reported for all stereoselective hydroamination catalysts however, the reported range of enantiomeric excesses for this substrate ranges across from 0-95%, with most enantioselectivities lying between 25-75%.<sup>18, 19, 21, 22, 30-33</sup>

The data discussed so far suggest that as the ionic radius of the coordinated metal decreases, higher enantiomeric excesses are achievable, and in these cases the change in solvent from benzene-d<sub>6</sub> to toluene-d<sub>8</sub> causes a greater difference in the enantioselectivities. For the lanthanum and praseodymium complexes, changing the solvent increases the enantiomeric excess only with the phenyl BOPA derivatives [La(Ph-BOPA){N(SiMe<sub>3</sub>)<sub>2</sub>}<sub>2</sub>] (**10a**) and [Pr(Ph-BOPA){N(SiMe<sub>3</sub>)<sub>2</sub>}<sub>2</sub>] (**11a**), whereas an increase in enantioselectivity was found with all three derivatives of [Nd(R-BOPA){N(SiMe<sub>3</sub>)<sub>2</sub>}<sub>2</sub>] (**12a-c**). These data are far from being completely conclusive, but suggest that a discrete solvent molecule-catalyst interaction may be responsible for the observed activity and selectivity trends, and that this interaction is more pronounced with metals having smaller ionic radii.

### 3.4 References for Chapter 3

- 1 M. R. Gagné, L. Brard, V. P. Conticello, M. A. Giardello, T. J. Marks, and C. L. Stern, *Organometallics*, 1992, **11**, 2003.
- 2 M. A. Giardello, V. P. Conticello, L. Brard, M. Sabat, A. L. Rheingold, C. L. Stern, and T. J. Marks, *J. Am. Chem. Soc.*, 1994, **116**, 10212.
- 3 M. A. Giardello, V. P. Conticello, L. Brard, M. R. Gagne, and T. J. Marks, *J. Am. Chem. Soc.*, 1994, **116**, 10241.
- 4 D. V. Gribkov, K. C. Hultsch, and F. Hampel, *Chem. Eur. J.*, 2003, **9**, 4796.
- 5 S. Hong, S. Tian, M. V. Metz, and T. J. Marks, *J. Am. Chem. Soc.*, 2003, **125**, 14768.
- 6 J. Collin, J. -D. Daran, E. Schulz, and A. Trifonov, *Chem. Commun.*, 2003, 3048.
- 7 P. N. O'Shaughnessy and P. Scott, *Tetrahedron: Asymmetry*, 2003, **14**, 1979.
- 8 M. R. Gagné, C. L. Stern, and T. J. Marks, *J. Am. Chem. Soc.*, 1992, **114**, 275.
- 9 G. Zi, F. Zhang, L. Xiang, Y. Chen, W. Fang, and H. Song, *Dalton Trans.*, 2010, **39**, 4048.
- 10 K. Manna, M. L. Kruse, and A. D. Sadow, *ACS Catal.*, 2011, **1**, 1637
- 11 T. D. Nixon and B. D. Ward, *Chem. Commun.*, 2012, 11790
- 12 Y. Zhang, W. Yao, H. Li, and Y. Mu, *Organometallics*, 2012, **31**, 4670
- 13 A. L. Reznichenko and K. C. Hultsch, *Organometallics*, 2013, **32**, 1394
- 14 J. S. Wixey and B. D. Ward, *Dalton Trans.*, 2011, **40**, 7693.
- 15 B. D. Ward; S. Bellemin-laponnez; L. H. Gade, *Angew. Chem. Int. Ed.*, 2005, **44**, 1668.
- 16 P. N. O'Shaughnessy, K. M. Gillespie, P. D. Knight, I. Munslow, and P. Scott, *J. Chem. Soc. Dalton Trans.*, 2004, 2251.
- 17 N. Meyer, A. Zulys, and P.W. Roesky, *Organometallics*, 2006, **25**, 4179.



- 18 J. Hannedouche, I. Aillaud, J. Collin, E. Schulz, and A. Trifnov, *Chem. Commun.*, 2008, **30**, 3552.
- 19 I. Aillaud, D. Lyubov, J. Collin, R. Guillot, J. Hannedouche, E. Schulz, and A. Trifnov, *Organometallics*, 2008, **22**, 5929.
- 20 D. Reigert, J. Collin, A. Meddour, E. Schulz, and A. Trifonov, *J. Org. Chem*, 2006, **71**, 2514.
- 21 P. Benndorf, J. Jeneter, L. Zielke, and P. W. Roesky, *Chem. Commun.*, 2011, **9**, 2574.
- 22 D. V. vitanova, F. Hampel, and K. C. Hultzs, *J. Org. Chem*, 2010, **1**, 321.
- 23 D. V. Gribkov, K. C. Hultzs, and F. Hampel, *J. Am. Chem. Soc.*, 2006, **11**, 3748.
- 24 Q. Wang, L. Xiang, H. Song, and G. Zi, *J. Organometallic Chem.*, 2009, **694**, 691.
- 25 Q. Wang, F. Zhang, H. Song, and G. Zi, *J. Organometallic Chem.*, 2011, **696**, 2186.
- 26 'CRC Handbook of Chemistry and Physics', ed. D. R. Lide, CRC Press, 2005.
- 27 P. M. Zeimentz, S. Arndt, B. R. Elvidge, and J. Okuda, *Chem. Rev.*, 2006, **106**, 2404
- 28 P. N. O'Shaughnessy, P. D. Knight, C. Morton, K. M. Gillespie, and P. Scott, *Chem. Commun.*, 2003, 1770.
- 29 M. R. Douglass, M. Ogasawara, S. Hong, M. V. Metz, and T. J. Marks, *Organometallics*, 2002, **21**, 283.
- 30 J. S. Wixey and B. D. Ward, *Chem. Commun.*, 2011, **47**, 5449
- 31 Y. Zhang, W. Yao, H. Li, and Y. Mu, *Organometallics*, 2012, **13**, 4670.
- 32 P. R. Payne, J. A. Bexrud, D. C. Leitch, and L. L. Schafer, *Canadian J. Chem.*, 2011, **10**, 1222.
- 33 J. Deschamp, J. Collin, J. Hannedouche, and E. Schulz, *Eur. J. Inorg. Chem*, 2011, **18**, 3329.

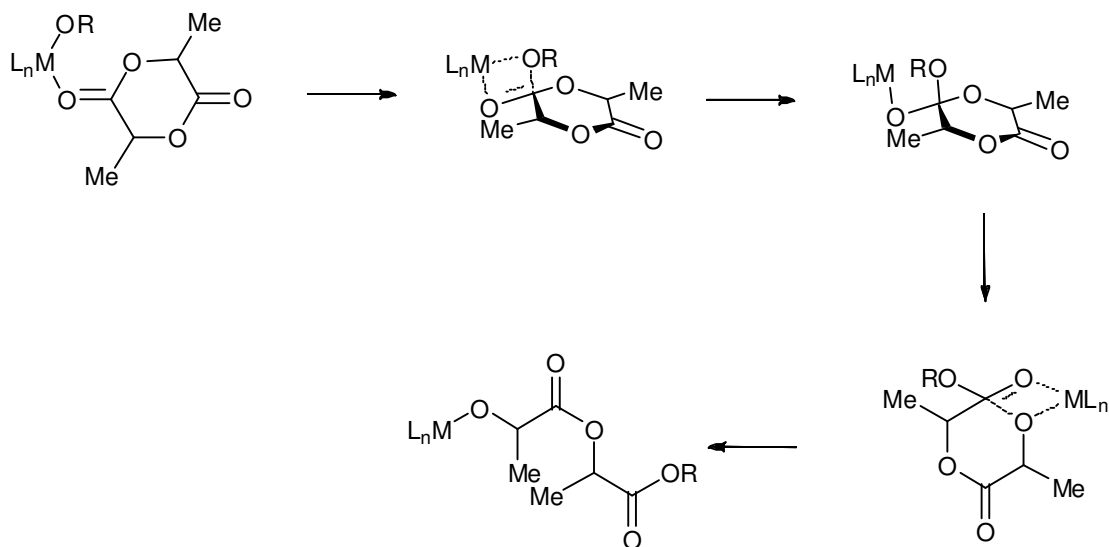
## CHAPTER 4

# Ring Opening Polymerisation of *rac*-lactide with BOPA supported catalysts

## 4.1 Introduction

There is an ever-increasing need to develop and use sustainable chemical processes. This includes cleaner manufacturing processes that are less reliant on fossil fuel feedstocks, as well as generating less persistent waste from consumer products. An area in which this movement is having a large impact is the plastics industry: plastics permeate almost every aspect of society, being used in everything from packaging to consumer goods. The development of biodegradable polymers therefore has clear advantages.<sup>1-5</sup> The polymerisation of cyclic esters is a rapidly growing area of chemical research at the present time, and this chapter particularly focuses on the catalytic polymerisation of lactide *via* the ring opening polymerisation (ROP) of lactide monomers. Lactide is obtained from renewable resources such as corn, and is a dimeric ester consisting of two lactic acid units. Lactic acid is a chiral molecule and lactide consequently exists as three stereoisomers, *meso*, L and D. Therefore, the polymerisation of pure samples of these dimeric esters will have a significant effect on the properties of the resulting polymer, but ROP studies are often (as exemplified in this thesis) performed on samples of *rac*-lactide, containing equal amounts of L- and D-lactide, the *meso* isomer having been removed.

Catalysts based upon the lanthanide and Alkaline Earth metals have been shown to be excellent catalysts for ROP.<sup>6, 7</sup> Lanthanide complexes offer the ability to fine-tune the catalyst by varying the ionic radius of the metal. This has the potential to significantly affect the catalyst activity and stability, resulting in differences in the properties of the polymer produced (*e.g.* molecular weight, molecular weight distribution, and tacticity).



**Scheme 1** The coordination-insertion mechanism for the polymerisation of lactide.  $ML_n$  = Group 2, 3 or 4 metal complex

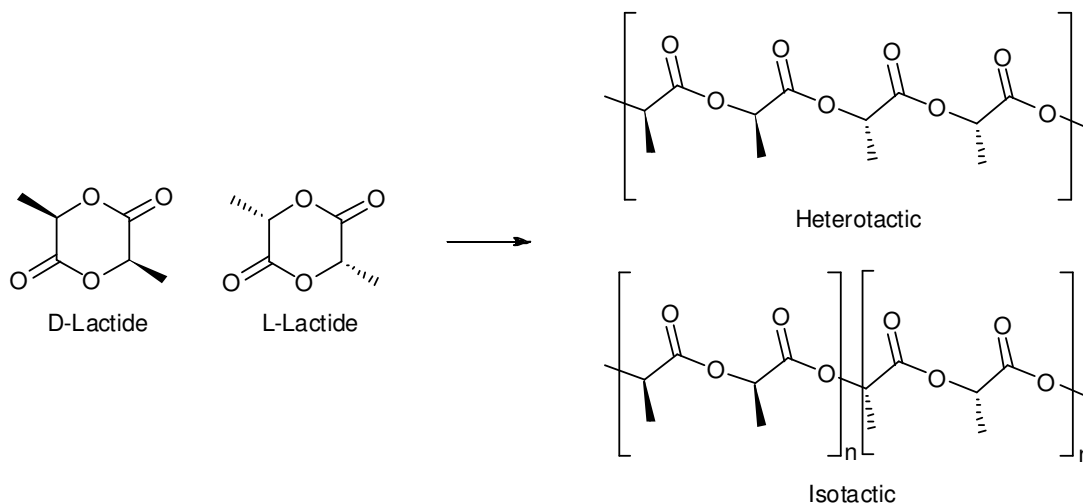
There are several mechanisms by which lactide can be polymerised. The one that usually operates in metal catalysed ROP is the coordination-insertion mechanism (Scheme 1). In this mechanism, a lactide monomer inserts into an anionic co-ligand (which becomes the chain-end group) before undergoing ring-opening, affording an alkoxide-ligated polymer chain. This alkoxide is subsequently able to act as an initiator for the following insertion of lactide, and so on. This process continues until the substrate is consumed or the polymerisation is terminated by a proton source.

Metal alkoxides have been shown to be amongst the best initiators for this reaction, with alcohol co-catalysts acting as chain transfer agents during the polymerisation reaction. Homoleptic aryloxides were some of the first lanthanide catalysts employed for the ring opening polymerisation of lactide.<sup>8,9</sup> ROP catalysis using  $[Ln(OAr(^tBu)_2)_3]$  resulted in non-identifiable end groups and large  $M_n$  values (number average molecular weight) compared to the weight expected for one chain growth per  $Ln-OAr$  initiator group. However, the catalyst performed much better upon the addition of alcohols, resulting in identifiable end groups and

molecular weights that were closer to the predicted values. The authors suggested that the addition of an alcohol ROH afforded the *in situ* generated complex  $[Ln(OR)_3]$ . A similar observation has also been reported, whereby the use of less bulky aryloxides lead to greater control over the molecular weight of the polymer, although the polydispersity indices remained large.<sup>10</sup>

Alternative initiators include metal amides,  $M(NR_2)$ . It has been reported that these tend to have little control over polymer molecular weight and can form cyclic polyesters as an undesired byproduct.<sup>11, 12</sup> The relative lack of control over the polymer microstructure offered by metal amide initiators means that there are few routes to amine-terminated poly(lactic acid) (PLA). Amine-terminated PLA has been identified as a potentially useful scaffold for block/graft polymers.<sup>13</sup>

An important parameter in many polymers (including PLA) is its tacticity, or the relative stereochemistry of the monomer units along the polymer chain. Differences in tacticity affect the physical bulk properties of polymers to a significant extent, e.g. melting point and crystallinity. The most common forms of tacticity obtained by the polymerisation of *rac*-lactide are shown in Scheme 2. There are two mechanisms by which the tacticity of a polymer is dictated during the polymerisation reaction, *enantiomorphic site control* and *chain end control*. Enantiomorphic site control operates by transferring chiral information from a chiral catalyst, and usually (although not always) involves a complex bearing a chiral ligand. Conversely, chain end control involves the transfer of chirality from the stereochemistry of the previous insertion step in the polymerisation reaction, and is independent of the chirality of the supporting ligand set. Therefore, depending on which of these two mechanisms operates for a particular catalyst, the application of a chiral ligand in polymerisation is not always necessary or effective, and one goal of this research area is to determine to what extent the use of chiral complexes can influence the microstructure of poly(lactic acid).



**Scheme 2** Poly(lactic acid) tacticities obtained from the polymerisation of *rac*-lactide

The chiral BOPA ligand has been applied to a wide variety of asymmetric transformations using late transition metals, including asymmetric Friedel-Crafts alkylation,<sup>14-17</sup> asymmetric hydrosilylation<sup>18</sup> and asymmetric enantioselective allylation of aldehydes.<sup>19</sup> Herein, the first instance of the application of rare earth chiral BOPA complexes in the ROP of *rac*-lactide will be discussed.

## 4.2 Results and Discussion

### 4.2.1 Ring-opening polymerisation of lactide using lanthanide BOPA complexes

The complexes described in Chapter 2 make ideal catalysts to investigate the ROP of *rac*-lactide with chiral amide initiators. A selection of catalysts have been investigated; [Y(R-BOPA){N(SiMe<sub>3</sub>)<sub>2</sub>]<sub>2</sub> (**7a-c**), [Y(R-BOPA)(CH<sub>2</sub>SiMe<sub>2</sub>Ph)<sub>2</sub>] (**8a-c**), [La(R-BOPA){N(SiMe<sub>3</sub>)<sub>2</sub>]<sub>2</sub> (**10a-c**) and [Sm(R-BOPA){N(SiMe<sub>3</sub>)<sub>2</sub>]<sub>2</sub> (**13a-c**) were used so as to provide a representative cross-section of catalysts containing Group 3 / lanthanide metals

with a various ionic radii. The studies were carried out in collaboration with Professor Philip Mountford and co-workers (University of Oxford). Some of the data were measured myself during a visit to the laboratory of Prof. Mountford, whilst some of the data were collected by Bryony Core and Matt Blake in the Mountford group.

Samples of *rac*-lactide were polymerised by adding 100 equivalents of lactide to a solution of the chosen precatalyst in THF solution. All experiments were performed in a glovebox. Aliquots were removed periodically in order to ascertain the conversion, molecular weight of the polymers and PDIs ( $M_w/M_n$ ). Conversion was monitored using  $^1\text{H}$  NMR spectroscopy, and molecular weights were determined using gel permeation chromatography (GPC) using the appropriate Mark-Houwink corrections for PLA.<sup>20-22</sup> The catalytic data obtained from the polymerisation reactions are summarised in Table 1.

Graphs showing the conversion of lactide to PLA using  $[\text{Y}(\text{R-BOPA})\{\text{N}(\text{SiMe}_3)_2\}_2]$  (**7a-c**) (R = Ph **a**, Bn **b**, iPr **c**) as the precatalysts are presented in Fig. 1. These conversion curves were used to calculate the rates of reaction, by analysing the percentage conversion over a given time. The reaction rates of **7a-c** (entries 1, 3 and 4) lie in the order **7b** >> **7a** > **7c**, corresponding to Bn >> Ph > iPr.

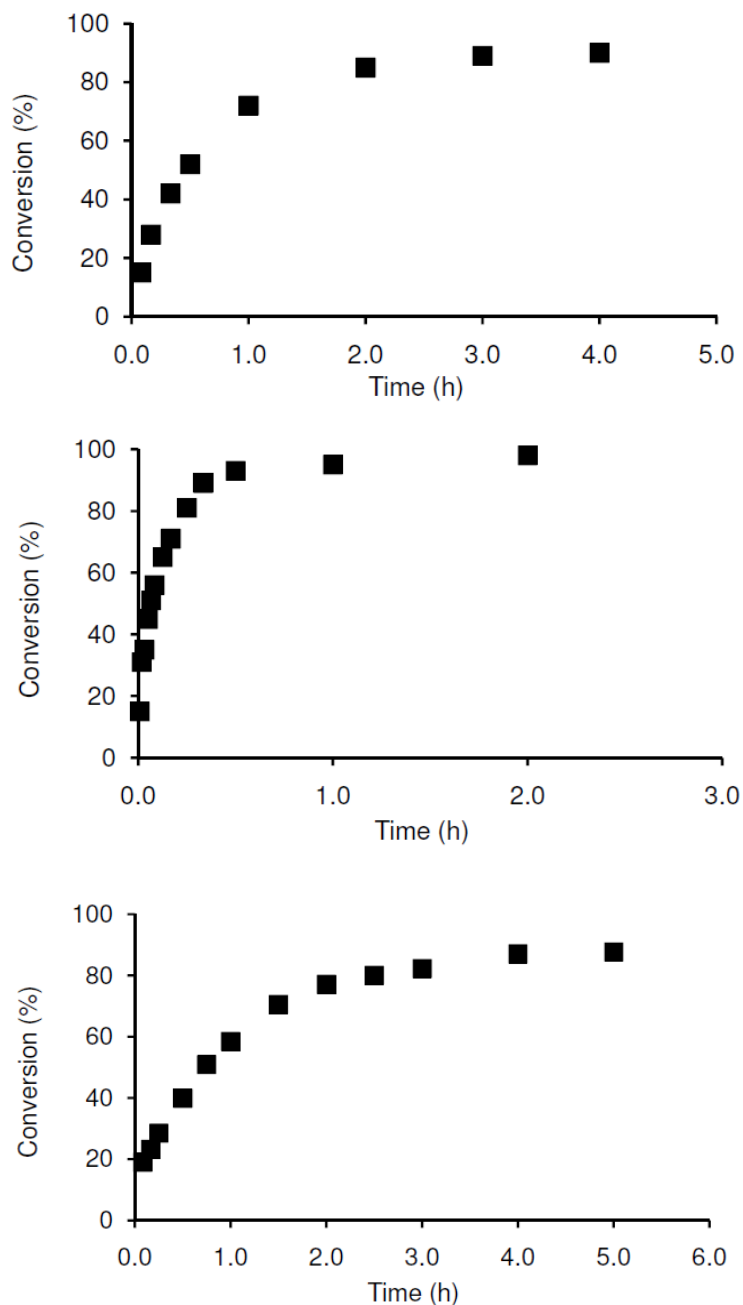
**Table 1** ROP of *rac*-LA in solution with [Ln(R-BOPA){N(SiMe<sub>3</sub>)<sub>2</sub>]<sub>2</sub>] (Ln = Y (**7**), La (**10**) or Sm (**13**); and [Y(R-BOPA)(CH<sub>2</sub>SiMe<sub>2</sub>Ph)<sub>2</sub>] (**8**); R = Ph (**a**) Bn (**b**) iPr (**c**)

Entry	Cat.	Conv. % <sup>b</sup>	Time (mins)	$k_{app}$ <sup>c</sup>	$M_n$ <sup>d</sup> (GPC)	$M_n$ <sup>e</sup> (calcd)	$M_w/M_n$	$P_r$ <sup>g</sup>
1	7a	90	240	2.88(9) M <sup>-1</sup> h <sup>-1</sup>	19 590	13 133	1.36	0.71
2	7b	81	15	16.1(7) M <sup>-1</sup> h <sup>-1</sup>	15 720	11 840	1.54	0.81
3	7b	98	120	16.1(7) M <sup>-1</sup> h <sup>-1</sup>	22 290	14 286	1.44	0.73
4	7c	88	300	1.52(5) M <sup>-1</sup> h <sup>-1</sup>	17 880	12 791	1.55	0.70
5	8a	73	0.5	<sup>f</sup>	30 740	10 726	1.24	0.78
6	8a	95	1.5	<sup>f</sup>	35 450	13 881	1.38	0.76
7	8b	78	0.5	<sup>f</sup>	23 780	11 376	1.24	0.71
8	8b	95	1.5	<sup>f</sup>	31 070	13 484	1.23	0.69
9	8c	95	0.5	<sup>f</sup>	32 000	13 805	1.18	0.72
10	8c	99	1.5	<sup>f</sup>	30 080	14 357	1.24	0.73
11	10a	90	120	6.7(7) M <sup>-1</sup> h <sup>-1</sup>	12 570	13 076	2.29	0.68
12	10b	92	150	5.6(4) M <sup>-1</sup> h <sup>-1</sup>	20 690	13 259	1.43	0.72
13	10c	88	10	13.4(2) h <sup>-1</sup>	22 750	12 844	2.15	0.68
14	10c	98	60	13.4(2) h <sup>-1</sup>	9 770	14 290	4.44	0.68
15	13a	87	255	1.56(2) M <sup>-1</sup> h <sup>-1</sup>	13 540	12 631	1.84	0.68
16	13b	38	30	2.1(1) M <sup>-1</sup> h <sup>-1</sup>	35 890	5 586	1.95	0.81
17	13b	88	210	2.1(1) M <sup>-1</sup> h <sup>-1</sup>	21 400	12 779	1.54	0.77
18	13c	90	300	1.90(3) M <sup>-1</sup> h <sup>-1</sup>	13 220	13 199	1.92	0.66

<sup>a</sup> Conditions: [*rac*-LA]<sub>0</sub>: [cat] = 100:1, 4.0 mL THF at 25 °C, [*rac*-LA]<sub>0</sub> = 1.00 M. See Experimental section for other details. <sup>b</sup> NMR conversion. <sup>c</sup> Apparent rate constant with units h<sup>-1</sup> or M<sup>-1</sup> h<sup>-1</sup> derived from the first- or second-order log plots over first 3 half-lives, respectively (all systems were second-order with respect to *rac*-LA except for entries 11-12. <sup>d</sup> Molecular weights (g mol<sup>-1</sup>) determined by GPC in THF at 30 °C using the appropriate Mark-Houwink corrections. <sup>e</sup> Expected  $M_n$  (g mol<sup>-1</sup>) for 1 chain growing per metal centre at the stated % conversions assuming CH<sub>2</sub>SiMe<sub>2</sub>Ph (entries 1-4) or N(SiMe<sub>3</sub>)<sub>2</sub> (entries 5-12) initiating groups. <sup>f</sup>  $k_{app}$  not measured. <sup>g</sup>  $P_r$  measured at between 73%-90% conversion except for entry 16.

A possible explanation of the relative reaction rates lies in the fact that isopropyl and phenyl groups are generally more rigid than a benzyl group, which possesses the extra flexibility at the methylene linker.





**Fig. 1** Conversion vs. time graphs for  $[Y(R\text{-BOPA})\{N(\text{SiMe}_3)_2\}_2]$  (**7a-c**) ( $R = \text{Ph}$  **a** (top),  $\text{Bn}$  **b** (middle),  $\text{iPr}$  **c** (bottom)). Conditions:  $[\text{rac-LA}]_0 : [\text{cat}] = 100:1$ , 4.0 mL THF at 25 °C,  $[\text{rac-LA}]_0 = 1.00\text{M}$

This extra flexibility of the benzyl group could potentially allow more space at the metal, and hence facilitate an increase in reaction rate by providing less hindrance to monomer coordination and/or insertion. Complexes **7a** and **7c** proceeded according to second order kinetics with respect to  $[\text{LA}]$ , with  $k_{\text{app}}$  of 2.88(9) and 1.52(5)  $\text{M}^{-1} \text{h}^{-1}$  respectively. **7b** was

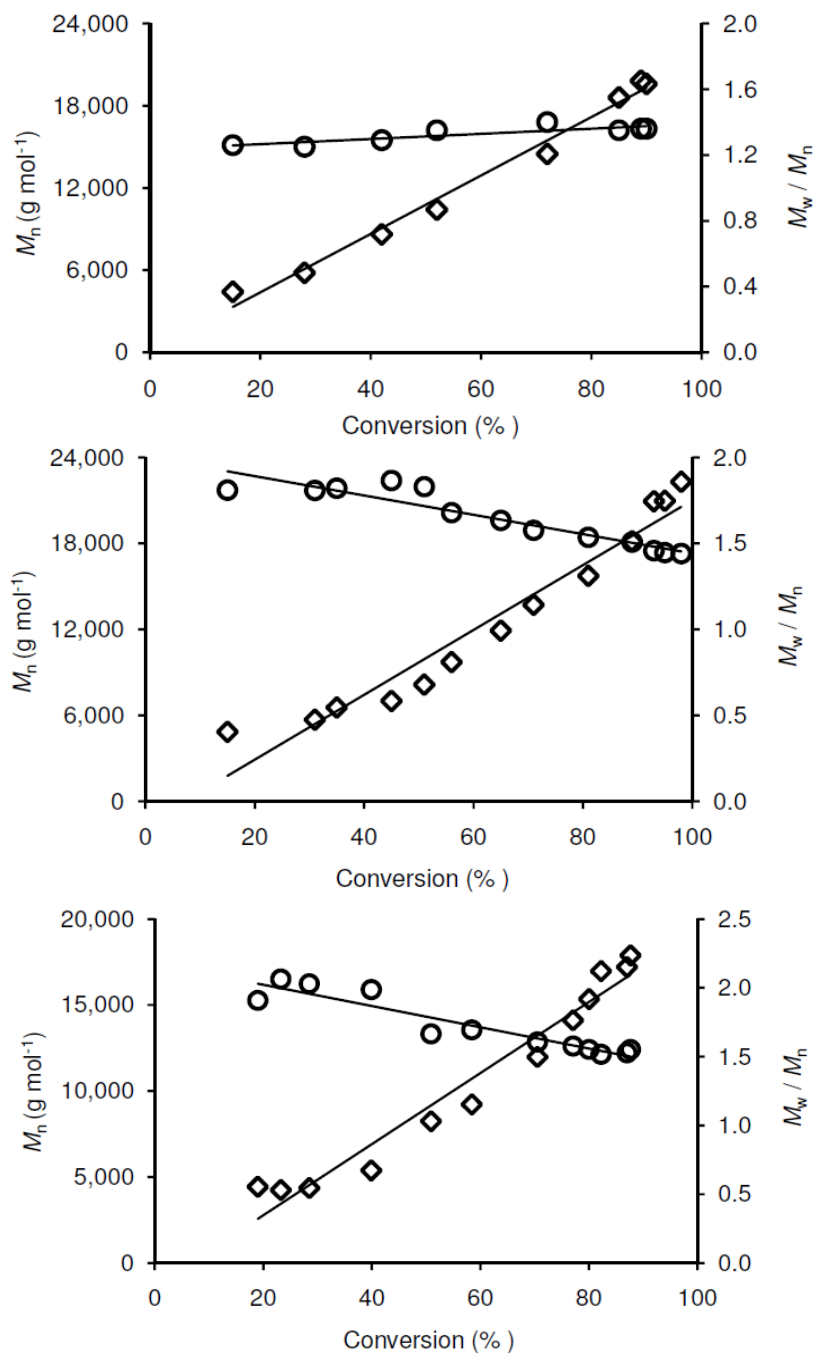
also second order, but was an order of magnitude faster than either **7a** or **7c** at  $16.1(7) \text{ M}^{-1} \text{ h}^{-1}$ . Despite the fact that *i*Pr and Ph groups are smaller than Bn, the presence of the methylene groups may confer additional rotational flexibility, allowing the substituents on the oxazoline rings to twist away from the active site, which may account for the faster rate observed in **7b**.

The graphs displayed within Fig. 2 depict the  $M_n$  vs percentage conversion. The number of chains growing per metal centre can be extracted from the gradient of the trend line according to the following equation:

$$\text{Number of chains per metal} = \text{gradient}/144.12$$

Where  $144.12 \text{ g mol}^{-1} (\% \text{ conversion})^{-1}$  corresponds to the molecular weight of the lactide monomer. Values that are greater than one suggest that some of the complex added to the reaction does not actually take part in the catalysis, leaving more lactide available per metal centre and resulting in a polymer with a higher  $M_n$  than predicted using stoichiometry calculations.

The  $M_n$  vs percentage conversion graphs of  $[\text{Y}(\text{Bn-BOPA})\{\text{N}(\text{SiMe}_3)_2\}_2]$  and  $[\text{Y}(\text{iPr-BOPA})\{\text{N}(\text{SiMe}_3)_2\}_2]$  (**7b-c**) have gradients of 152.09 and  $162.77 \text{ g mol}^{-1} (\% \text{ conversion})^{-1}$  respectively, suggesting that the majority of the catalyst was taking part in the reaction, yielding a polymer close to the expected molecular weight. However, the graph of  $[\text{Y}(\text{Ph-BOPA})\{\text{N}(\text{SiMe}_3)_2\}_2]$  (**7a**) has a much higher gradient ( $207.26 \text{ g mol}^{-1} (\% \text{ conversion})^{-1}$ ), indicating that ~25% of the catalyst was inactive, this results in poor agreement between the  $M_n$  obtained experimentally and that calculated stoichiometrically, as is typical for metal-amide systems.<sup>11</sup> Interestingly, in all of the graphs in Fig 2, all three intercepts are much greater than 0.



**Fig. 2**  $M_n$  vs % conversion graphs for  $[Y(R\text{-BOPA})\{N(\text{SiMe}_3)_2\}_2]$  (**7a-c**) ( $R = \text{Ph a, Bn b, iPr c}$ ).

(Top) **7a**  $M_n$  (diamonds) and  $M_w/M_n$  (circles) vs % conversion: the gradient of  $M_n$  vs conversion plot is  $214(10) \text{ g mol}^{-1} (\% \text{ conversion})^{-1}$  ( $R^2 = 0.986$ ). (Middle) **7b**  $M_n$  (diamonds) and  $M_w/M_n$  (circles) vs % conversion: the gradient of  $M_n$  vs conversion plot is  $226(17) \text{ g mol}^{-1} (\% \text{ conversion})^{-1}$  ( $R^2 = 0.945$ ). (Bottom) **7c**  $M_n$  (diamonds) and  $M_w/M_n$  (circles) vs % conversion: the gradient of  $M_n$  vs conversion plot is  $202(14) \text{ g mol}^{-1} (\% \text{ conversion})^{-1}$  ( $R^2 = 0.950$ ). Conditions:  $[\text{rac-LA}]_0 : [\text{cat}] = 100:1$ , 4.0 mL

THF at 25 °C,  $[\text{rac-LA}]_0 = 1.00\text{M}$ .

This indicates that the polymer rapidly attains a high molecular weight (*i.e.* fast propagation), before the rate of polymerisation decreases (*i.e.* slow initiation); this is consistent with the use of amide initiators which generally exhibit poorly controlled polymerisation, particularly with respect to the relative rates of initiation vs propagation.<sup>4, 23</sup>

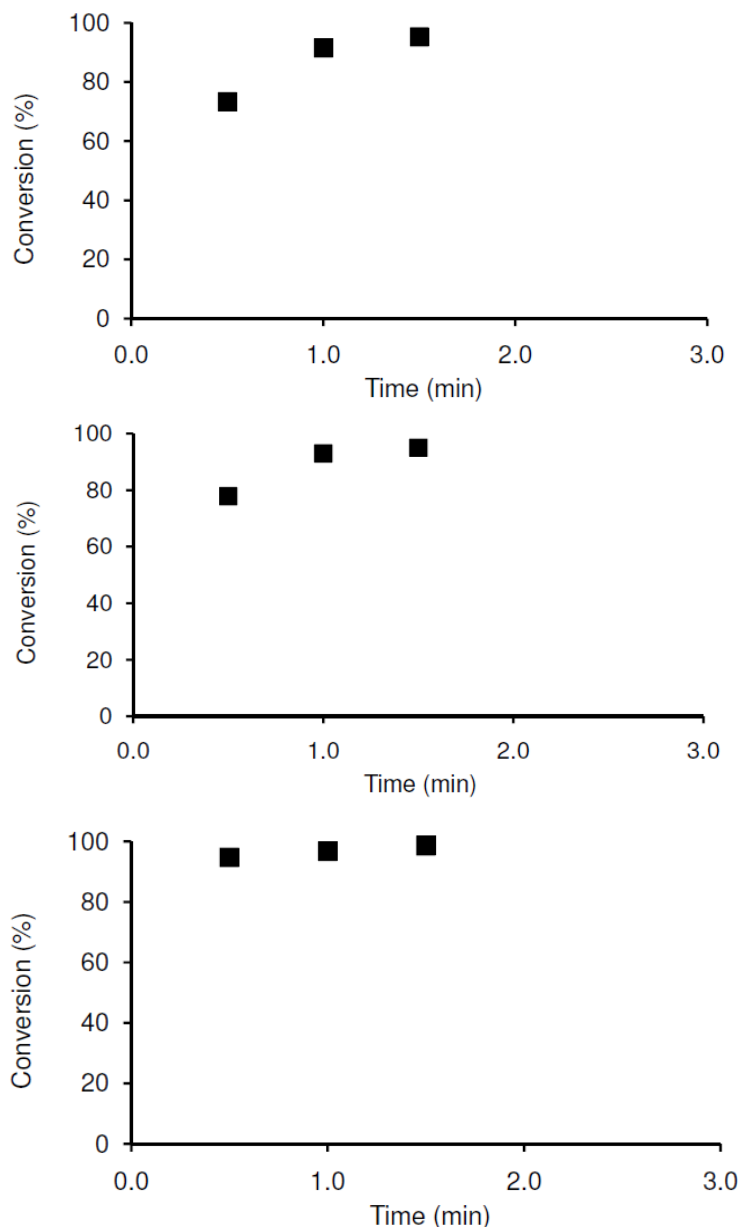
The kinetics of these reactions were also investigated, and  $k(\text{obs})$  determined from the line of best fit for the most suitable rate equation. For example, the data were fitted to both first and second order rate equations, and the reaction order obtained from the best fit; these graphs have been included in the appendix. The data for  $[\text{Y}(\text{Ph-BOPA})\{\text{N}(\text{SiMe}_3)_2\}_2]$  (**7a**),  $[\text{Y}(\text{Bn-BOPA})\{\text{N}(\text{SiMe}_3)_2\}_2]$  (**7b**) and  $[\text{Y}(\text{iPr-BOPA})\{\text{N}(\text{SiMe}_3)_2\}_2]$  (**7c**) indicate second order kinetics with respect to lactide, where plots of  $1/[\text{LA}]$  vs time give a linear fit of the data. The value of  $k(\text{obs})$  for **7b** is an order of magnitude faster than for **7a** and **7c**, consistent with the empirical rates of reaction discussed above.

The heterotactic enrichment of the polymer samples were determined using NMR spectroscopy. The phenyl and isopropyl catalysts  $[\text{Y}(\text{Ph-BOPA})\{\text{N}(\text{SiMe}_3)_2\}_2]$  (**7a**) and  $[\text{Y}(\text{iPr-BOPA})\{\text{N}(\text{SiMe}_3)_2\}_2]$  (**7c**) gave moderate levels of heterotactic enrichment ( $P_r = 0.71$  and  $0.70$  respectively) (entries 1 and 4). The benzyl catalyst  $[\text{Y}(\text{Bn-BOPA})\{\text{N}(\text{SiMe}_3)_2\}_2]$  (**7b**) produced a polymer with the highest heterotactic enrichment,  $P_r = 0.81$  at 81% conversion (entry 2), which dropped to  $0.73$  at 98% conversion (entry 3). Both **7a** and **7b** exhibited heterotacticity scrambling, but no conclusions can be drawn with the data currently available on these systems. Analysis of PLA produced by complex **7a** by MALDI-ToF mass spectrometry showed the polymer to be terminated with hydroxyl groups, suggesting the amide co-initiator was hydrolysed upon quenching. Complexes **7b** and **7c** produced cyclic polymer, and all complexes confirmed the incidence of transesterification, with a peak separation of  $m/z$  72. The PDIs for all complexes generally exhibited a slight downwards trend to reach completion with moderate results of 1.35-1.55. This can also be attributed to

the poor rate of initiation of the complexes whereby fewer active metal centres produce polymer chains of varying length, however as the reaction proceeds and transesterification side reactions feature more prominently, the length of chains redistribute closely around an average.

The polymerisation data for the analogous yttrium alkyl complexes [Y(R-BOPA)(CH<sub>2</sub>SiMe<sub>2</sub>Ph)<sub>2</sub>] (**8a-c**) (R = Ph **a**, Bn **b**, iPr **c**) are provided in Fig. 3, and indicate that the reaction rates were significantly faster than for [Y(R-BOPA){N(SiMe<sub>3</sub>)<sub>2</sub>]<sub>2</sub>] (**7a-c**) (entries 1-10). All reactions were complete in a matter of minutes, rather than hours, which necessarily reduced the amount of data that could be collected. Consequently, the kinetics of the reactions were not analysed due to the lack of data points and end group analysis by MALDI-ToF could not be performed due to the high  $M_n$  of the samples. However, these complexes had a reasonably narrow  $M_w/M_n$  of 1.18-1.38, which either remained constant or marginally increased during the polymerisation reaction, suggesting that once polymerisation was underway, there was little transesterification or back-biting side reactions. Based upon the conversion curves, empirically it appears that all three catalysts exhibited rates of a similar order of magnitude, although more precise interpretation is neither possible nor appropriate. These results are consistent with previously established metal-amide and -alkyl systems in which the rate of propagation (insertion of lactide into the M-O bond) exceeds the rate of initiation (insertion of lactide into the M-R bond).<sup>11, 24-26</sup>

The heterotactic enrichment ( $P_r$ ) values for the polymers obtained with **8a-c** were 0.78, 0.71 and 0.73 respectively (entries 5, 7 and 10). Catalyst **8a** gave a marginally higher heterotactic enrichment, suggesting that the phenyl ring has more influence over the catalysis. This contrasts with the amide congeners, for which the benzyl derivative gave the highest level of heterotactic enrichment.

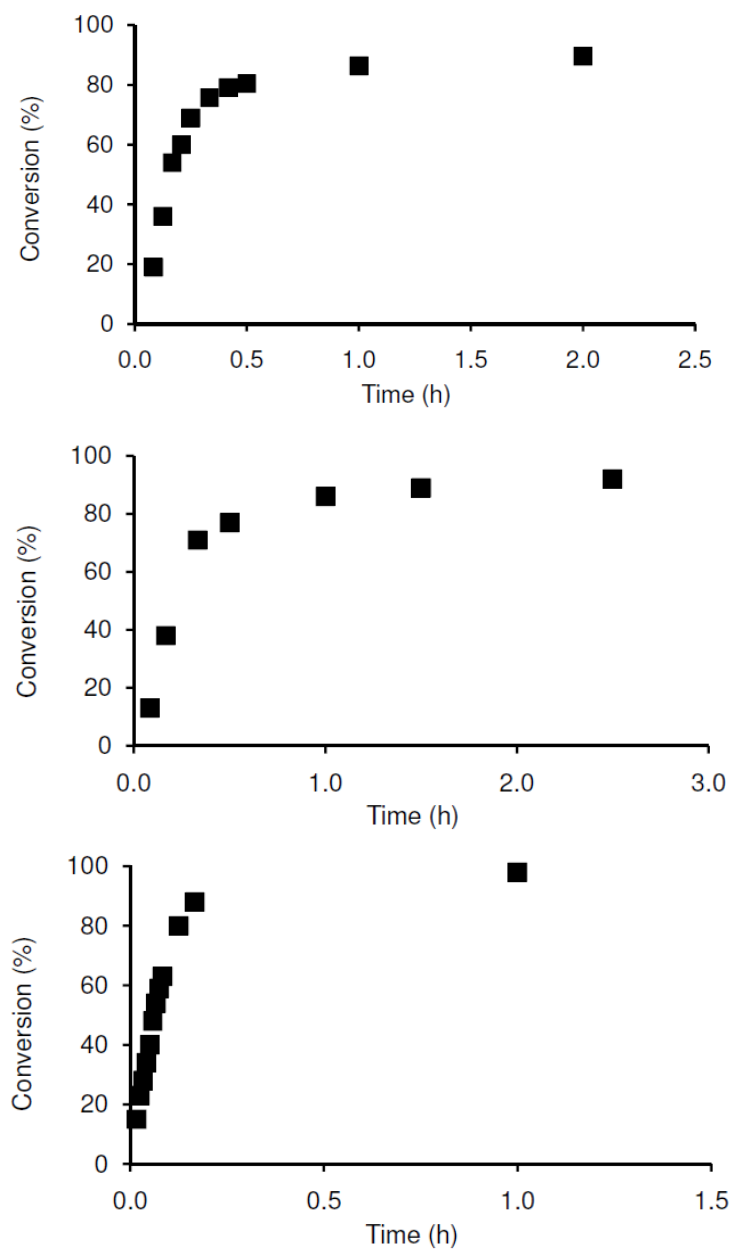


**Fig. 3** Conversion vs. time graphs of lactide to PLA for  $[\text{Y}(\text{R-BOPA})(\text{CH}_2\text{SiMe}_2\text{Ph})_2]$  (**8a-c**) (R = Ph **a** (top), Bn **b** (middle), iPr **c** (bottom)). Conditions:  $[\text{rac-LA}]_0:[\text{cat}] = 100:1$ , 4.0 mL THF at 25 °C,  $[\text{rac-LA}]_0 = 1.00\text{M}$

The polymerisation studies using lanthanide amide precatalysts were extended to lanthanum, in order to compare the effect of varying the ionic radius of the metal ion on the catalytic performance. The graphs depicted in Fig. 4 display conversion vs time for  $[\text{La}(\text{R-BOPA})\{\text{N}(\text{SiMe}_3)_2\}_2]$  (**10a-c**) (R = Ph **a**, Bn **b**, iPr **c**). The isopropyl derivative **10c** gave the

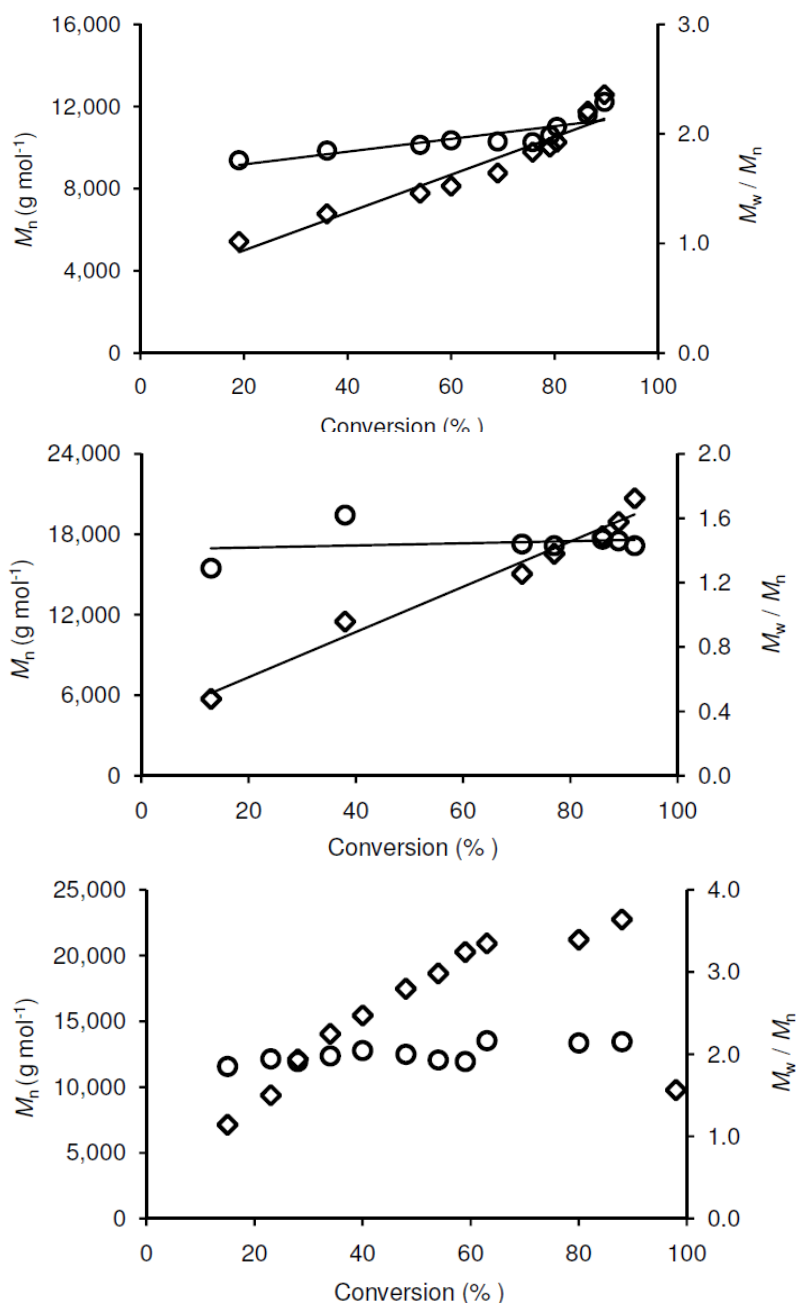
fastest rate ( $13.4(2) \text{ h}^{-1}$ ) (entry 13), where ~90% conversion was achieved after 15 minutes. When catalysts  $[\text{La}(\text{Ph-BOPA})\{\text{N}(\text{SiMe}_3)_2\}_2]$  (**10a**) and  $[\text{La}(\text{Bn-BOPA})\{\text{N}(\text{SiMe}_3)_2\}_2]$  (**10b**) were employed, the same conversion was achieved in ~1 hour (entries 11 and 12). This contrasts the observed order for  $[\text{Y}(\text{R-BOPA})\{\text{N}(\text{SiMe}_3)_2\}_2]$  (**7a-c**), where the fastest rate was observed for the benzyl derivative  $[\text{Y}(\text{Bn-BOPA})\{\text{N}(\text{SiMe}_3)_2\}_2]$  (**7b**) (entries 2 and 3).

These results highlight the strong dependence of the catalytic performance on the relative size of the metal; lanthanum has a considerably larger ionic radius compared to yttrium. The relative rates are consistent with the isopropyl group having a smaller steric footprint in comparison to the phenyl and benzyl groups, thereby providing a greater degree of space around the metal for the coordination of lactide, and consequently giving a faster reaction rate. The number of polymer chains produced per metal centre was determined for each of the lanthanum catalysts by an analysis of graphs showing  $M_n$  vs percentage conversion (Fig. 5). The gradients were close to  $144.12 \text{ g mol}^{-1} (\% \text{ conversion})^{-1}$  for both  $[\text{La}(\text{Ph-BOPA})\{\text{N}(\text{SiMe}_3)_2\}_2]$  (**10a**) and  $[\text{La}(\text{Bn-BOPA})\{\text{N}(\text{SiMe}_3)_2\}_2]$  (**10b**), 187.55 and  $135.05 \text{ g mol}^{-1} (\% \text{ conversion})^{-1}$  respectively, indicating that in each case one polymer chain was produced per metal. The gradient obtained for **10a** indicates that the majority of the catalyst was taking part in the reaction, whereas for **10b** the gradient is slightly lower than the expected value of  $144.12 \text{ g mol}^{-1} (\% \text{ conversion})^{-1}$ , suggesting that more than one chain was obtained per metal centre, yielding a lower molecular weight polymer. Conversely, the gradient for  $[\text{La}(\text{iPr-BOPA})\{\text{N}(\text{SiMe}_3)_2\}_2]$  (**10c**) was  $291.24 \text{ g mol}^{-1} (\% \text{ conversion})^{-1}$ , approximately double  $144.12 \text{ g mol}^{-1} (\% \text{ conversion})^{-1}$ . This suggests that half of the metal centres are not entering into the catalytic cycle, thereby yielding a polymer of approximately double the expected molecular weight. As with the yttrium amide complexes **7a-c**, each of the graphs in Fig. 5 have an intercept that is greater than 0, as is often observed with amide initiators and discussed previously.



**Fig. 4** Conversion vs. time graphs of lactide to PLA for  $[\text{La}(\text{R-BOPA})\{\text{N}(\text{SiMe}_3)_2\}_2]$  (**10a-c**) (R = Ph **a** (top), Bn **b** (middle), iPr **c** (bottom)). Conditions:  $[\text{rac-LA}]_0:[\text{cat}] = 100:1$ , 4.0 mL THF at 25 °C,  $[\text{rac-LA}]_0 = 1.00\text{M}$



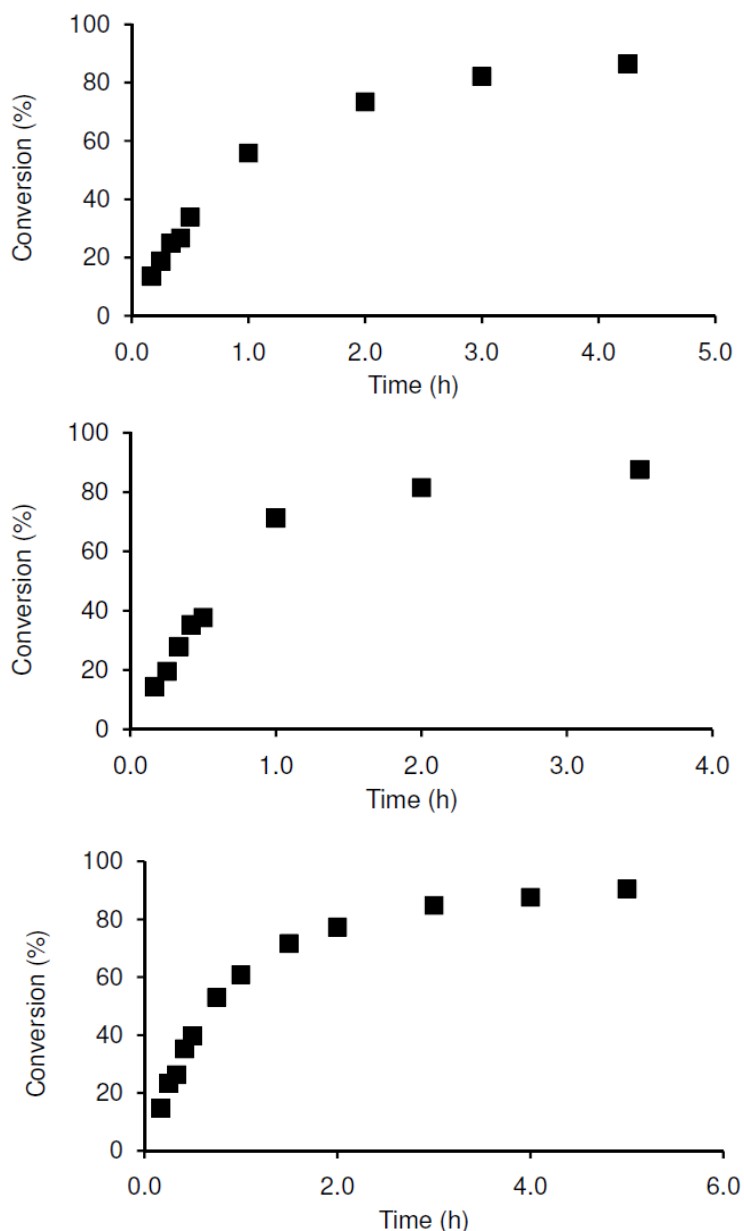


**Fig. 5**  $M_n$  vs % conversion graphs for  $[\text{La}(\text{R-BOPA})\{\text{N}(\text{SiMe}_3)_2\}_2]$  (**10a-c**) ( $\text{R} = \text{Ph}$  **a**,  $\text{Bn}$  **b**,  $\text{iPr}$  **c**). (Top) **10a**  $M_n$  (diamonds) and  $M_w/M_n$  (circles) vs % conversion: the gradient of  $M_n$  vs conversion plot is  $92(10) \text{ g mol}^{-1} (\% \text{ conversion})^{-1}$  ( $R^2 = 0.919$ ). (Middle) **10b**  $M_n$  (diamonds) and  $M_w/M_n$  (circles) vs % conversion: the gradient of  $M_n$  vs conversion plot is  $168(8) \text{ g mol}^{-1} (\% \text{ conversion})^{-1}$  ( $R^2 = 0.973$ ). (Bottom) **10c**  $M_n$  (diamonds) and  $M_w/M_n$  (circles) vs % conversion. Conditions:  $[\text{rac-LA}]_0 : [\text{cat}] = 100:1$ , 4.0 mL THF at 25 °C,  $[\text{rac-LA}]_0 = 1.00\text{M}$

The kinetics of the reactions were investigated, which indicated that the isopropyl congener [La(iPr-BOPA){N(SiMe<sub>3</sub>)<sub>2</sub>]<sub>2</sub> (**10c**) polymerised lactide with first order kinetics in lactide, whereas [La(Ph-BOPA){N(SiMe<sub>3</sub>)<sub>2</sub>]<sub>2</sub> (**10a**) and [La(Bn-BOPA){N(SiMe<sub>3</sub>)<sub>2</sub>]<sub>2</sub> (**10b**) gave poorly defined kinetics, for which it was not possible to reliably determine the order of the reaction. The well-behaved isopropyl complex exhibited a fast rate, where the lactide was consumed within ~15 minutes, despite the fact that only half of the catalyst was active in the reaction. The presence of transesterification side reactions is confirmed by MALDI-ToF which shows peak separation of  $m/z$  72 g mol<sup>-1</sup>. However, a decrease in  $P_r$  was not observed, despite the presence of significant transesterification reactions.

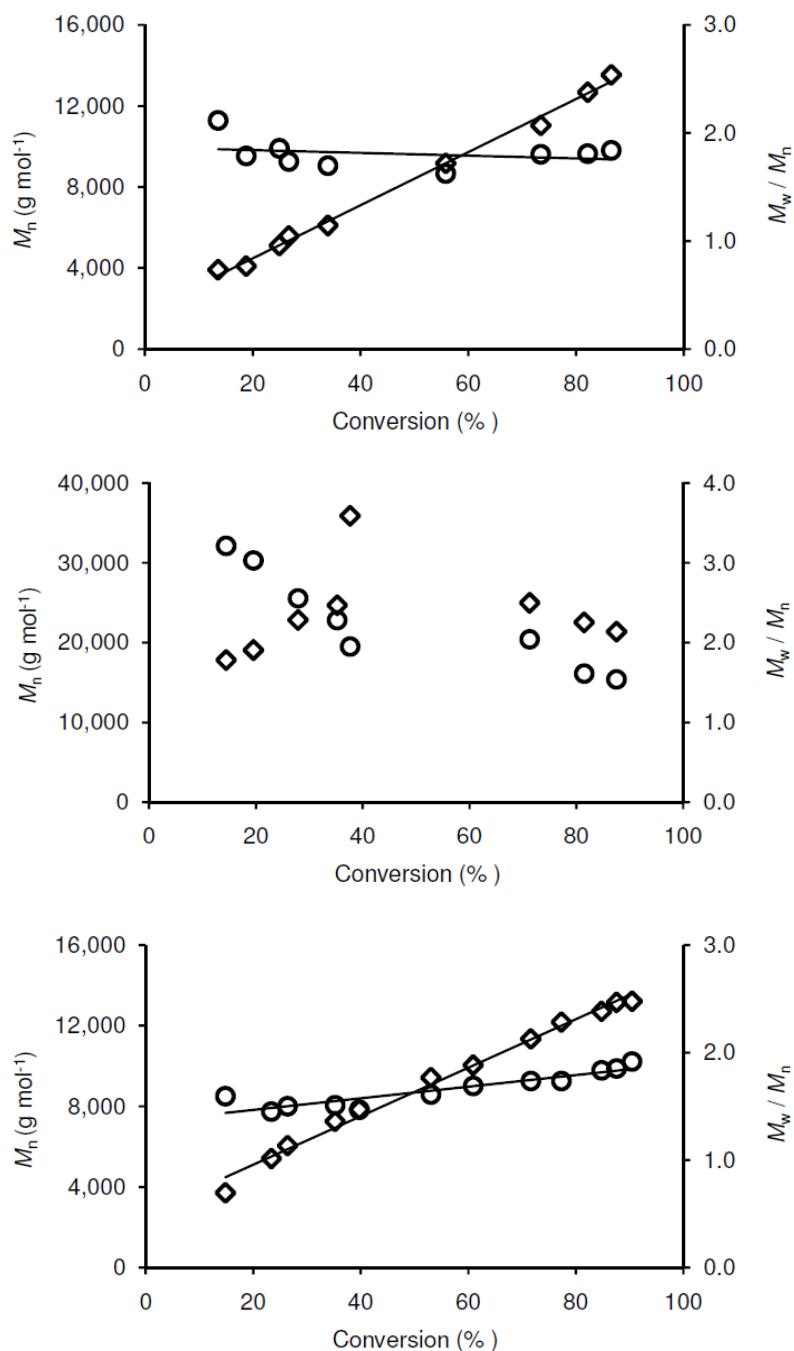
The heterotactic enrichment ( $P_r$ ) for [La(Bn-BOPA){N(SiMe<sub>3</sub>)<sub>2</sub>]<sub>2</sub> (**10b**) was 0.72 (entry 12), and marginally the highest of the triad, whereas the phenyl and isopropyl derivatives **10a** and **10c** each gave identical heterotactic enrichment of  $P_r = 0.68$  (entries 11 and 13). These tacticities are noticeably lower than those for [Y(R-BOPA){N(SiMe<sub>3</sub>)<sub>2</sub>]<sub>2</sub> (**7a-c**) (entries 1-4), which were much closer to 0.80, and suggesting that for catalysts bearing the BOPA ligand, higher levels of control are observed for metals having smaller ionic radii. Both complexes showed a gradual linear increase of PDI as the reaction continued. This is consistent with the data obtained from the MALDI-ToF, which confirm the presence of transesterification in all complexes observed.

On progressing these studies with the samarium complexes [Sm(R-BOPA){N(SiMe<sub>3</sub>)<sub>2</sub>]<sub>2</sub> (**13a-c**), the rates were found to be similar to those of [Y(Ph-BOPA){N(SiMe<sub>3</sub>)<sub>2</sub>]<sub>2</sub> (**7a**) and [Y(iPr-BOPA){N(SiMe<sub>3</sub>)<sub>2</sub>]<sub>2</sub> (**7c**). The conversion curves are provided in Fig. 6. For these precatalysts, there was a negligible difference between the rates of each of the derivatives, which contrasts the data obtained for the yttrium and lanthanum complexes, where the rates varied with the specific identity of the BOPA ligand.



**Fig. 6** Conversion vs. time graphs of lactide to PLA for  $[\text{Sm}(\text{R-BOPA})\{\text{N}(\text{SiMe}_3)_2\}_2]$  (**13a-c**) (R = Ph **a** (top), Bn **b** (middle), iPr **c** (bottom)). Conditions:  $[\text{rac-LA}]_0:[\text{cat}] = 100:1$ , 4.0 mL THF at 25 °C,  $[\text{rac-LA}]_0 = 1.00\text{M}$

Graphs of  $M_n$  vs percentage conversion are displayed in Fig. 7, and indicate that  $[\text{Sm}(\text{Ph-BOPA})\{\text{N}(\text{SiMe}_3)_2\}_2]$  (**13a**) and  $[\text{Sm}(\text{iPr-BOPA})\{\text{N}(\text{SiMe}_3)_2\}_2]$  (**13c**) gave better defined catalytic behaviour.



**Fig. 7**  $M_n$  vs % conversion graphs for  $[\text{Sm}(\text{R-BOPA})\{\text{N}(\text{SiMe}_3)_2\}_2]$  (**13a-c**) ( $\text{R} = \text{Ph}$  **a**,  $\text{Bn}$  **b**,  $\text{iPr}$  **c**). (Top) **13a**  $M_n$  (diamonds) and  $M_w/M_n$  (circles) vs % conversion: the gradient of  $M_n$  vs conversion plot is  $131(3) \text{ g mol}^{-1} (\% \text{ conversion})^{-1}$  ( $R^2 = 0.995$ ). (Middle) **13b**  $M_n$  (diamonds) and  $M_w/M_n$  (circles) vs % conversion. (Bottom) **13c**  $M_n$  (diamonds) and  $M_w/M_n$  (circles) vs % conversion: the gradient of  $M_n$  vs conversion plot is  $120(4) \text{ g mol}^{-1} (\% \text{ conversion})^{-1}$  ( $R^2 = 0.990$ ). Conditions:  $[\text{rac-LA}]_0 : [\text{cat}] = 100:1$ , 4.0 mL THF at 25 °C,  $[\text{rac-LA}]_0 = 1.00\text{M}$

Conversely, few conclusions can be drawn for [Sm(Bn-BOPA){N(SiMe<sub>3</sub>)<sub>2</sub>]<sub>2</sub>] (**13b**), partly due to poor GPC trace signals, where the signal was significantly broadened into the baseline causing significant uncertainty in the molecular weight measurements.

The gradient obtained for the catalytic performance of the phenyl derivative was 150.17 g mol<sup>-1</sup> (% conversion)<sup>-1</sup>, close to 144.12 g mol<sup>-1</sup> (% conversion)<sup>-1</sup> and indicating that the majority of catalyst used in the reaction was active. Conversely, the gradient obtained for [Sm(iPr-BOPA){N(SiMe<sub>3</sub>)<sub>2</sub>]<sub>2</sub>] (**13c**) was 110.57 g mol<sup>-1</sup> (% conversion)<sup>-1</sup> and is consistent with more than one polymer chain per metal centre, yielding a lower molecular weight polymer. As discussed previously, the two graphs have an intercept that is greater than 0.

The kinetics of the polymerisation reactions were investigated, and all three were found to be first order in lactide, albeit with relatively slow values of *k*(obs): 1.56(2), 2.1(1), and 1.90(3) M<sup>-1</sup>h<sup>-1</sup> respectively (entries 15-18). The heterotactic enrichment for each of the samarium-derived polymers were similar to those found for the previous complexes. The benzyl complex [Sm(Bn-BOPA){N(SiMe<sub>3</sub>)<sub>2</sub>]<sub>2</sub>] (**13b**) produced a polymer with the highest heterotactic enrichment (*P<sub>r</sub>* = 0.81 after 38% conversion; 0.77 after 88% conversion) (entries 16 and 17), whilst [Sm(Ph-BOPA){N(SiMe<sub>3</sub>)<sub>2</sub>]<sub>2</sub>] (**13a**) and [Sm(iPr-BOPA){N(SiMe<sub>3</sub>)<sub>2</sub>]<sub>2</sub>] (**13c**) result in polymers with heterotactic enrichments of *P<sub>r</sub>* = 0.68 and 0.66 respectively (entries 15 and 18). Analysis of polymers produced by **13a** and **c** show PDIs increased throughout the polymerisation to 1.84 and 1.92 respectively, indicating the presence of transesterification side reactions at the end of the reaction. This was confirmed by MALDI-ToF and all complexes were found to produce cyclic polymers with no evidence of the amide initiating group.

All amide complexes tested gave generally poor control over *M<sub>n</sub>*, forming macrocyclic polymers consistent with previously reported initiators.<sup>11, 27</sup> Metal alkoxides (M-OR) are generally considered to be superior initiators exerting good control over *M<sub>n</sub>*, and it is

possible to generate these species *in situ* through the addition of an alcohol co-initiator to the metal amide.<sup>28</sup> Addition of 2 eq BnOH to complex **7a** failed to generate the desired [Y(Ph-BOPA)(OBn)<sub>2</sub>] complex, instead resulting in the formation of the protio-ligand, consistent with stoichiometric reactions performed on isolated amido complexes bearing the BOPA ligand. As such, no further attempts were made to improve the catalytic activity of the amide complexes through the addition of alcohol as a coinitiator.

### 4.3 Summary and conclusions

The yttrium amide complexes [Y(R-BOPA){N(SiMe<sub>3</sub>)<sub>2</sub>]<sub>2</sub> (**7a-c**) are active in the ring-opening polymerisation of *rac*-lactide and result in conversion times between one and five hours, with a clear distinction in reaction rates depending on the identity of the BOPA stereodirecting group. The graphs of *M<sub>n</sub>* vs conversion indicated that the benzyl and isopropyl derivatives polymerise the lactide with one chain growing per metal centre, whereas the phenyl derivative produces polymers that have larger than expected molecular weights, since *ca.* 25% of the catalyst was inactive. The reactions catalysed by the yttrium amide complexes possess second order kinetics. [Y(Bn-BOPA){N(SiMe<sub>3</sub>)<sub>2</sub>]<sub>2</sub> (**7b**) produces a polymer with the highest heterotactic enrichment, whilst **7a** and **7c** produce polymers with lower enrichment. The heterotacticity enrichment was found to decrease over time for whilst the heterotacticity decreased over time for the benzyl derivative **7b**.

[Y(R-BOPA)(CH<sub>2</sub>SiMe<sub>2</sub>Ph)<sub>2</sub>] (**8a-c**), were much more reactive than their amide counterparts, possibly as a result of lower steric crowding at the metal centre and consistent with the ease of which the alkyl complexes were synthesised in comparison to the corresponding amide complexes. The polymerisation rates were extremely fast, therefore limiting the amount of data available for a detailed analysis of the reaction kinetics. The highest level of heterotactic enrichment was obtained with [Y(Ph-BOPA)(CH<sub>2</sub>SiMe<sub>2</sub>Ph)<sub>2</sub>]

(**8a**), which produced a polymer with a heterotactic enrichment of 0.78, whereas **8b-c** produced polymers with  $P_r$  values closer to 0.70.

The polymerisation data for the lanthanum complexes  $[\text{La}(\text{R-BOPA})\{\text{N}(\text{SiMe}_3)_2\}_2]$  (**10a-c**) indicate less well-defined behaviour in comparison to the yttrium complexes. The conversion rates reached a maximum after 1 hour, a much shorter timeframe than for **7a-c** and **8a-c**. The heterotactic control was noticeably less, with heterotacticities  $\sim 0.70$ . In comparison to  $[\text{Y}(\text{R-BOPA})\{\text{N}(\text{SiMe}_3)_2\}_2]$  (**7a-c**), the lanthanum systems are much less predictable, where most of the metal centres of  $[\text{Y}(\text{R-BOPA})\{\text{N}(\text{SiMe}_3)_2\}_2]$  (**7a-c**) were taking part in the reaction with only one chain growing per metal centre. The data for both  $[\text{La}(\text{Ph-BOPA})\{\text{N}(\text{SiMe}_3)_2\}_2]$  (**10a**) and  $[\text{La}(\text{Bn-BOPA})\{\text{N}(\text{SiMe}_3)_2\}_2]$  (**10b**) indicate that one polymer chain was obtained per metal, whereas  $[\text{La}(\text{iPr-BOPA})\{\text{N}(\text{SiMe}_3)_2\}_2]$  (**10c**) produced polymers with approximately double the theoretical weight, indicating that only half of the catalyst was active. All three complexes exhibited poorly defined kinetics.

The polymerisation reactions catalysed by  $[\text{Sm}(\text{R-BOPA})\{\text{N}(\text{SiMe}_3)_2\}_2]$  (**13a-c**) were found to take approximately 4-5 hours to complete, much longer than for  $[\text{La}(\text{R-BOPA})\{\text{N}(\text{SiMe}_3)_2\}_2]$  (**10a-c**). The heterotacticities range from 0.68-0.80, similar to the previously discussed BOPA complexes. The benzyl complex  $[\text{Sm}(\text{Bn-BOPA})\{\text{N}(\text{SiMe}_3)_2\}_2]$  (**13b**) exhibited poorly controlled behaviour, and limited the information from the data. The data indicate that the polymerisation using  $[\text{Sm}(\text{Ph-BOPA})\{\text{N}(\text{SiMe}_3)_2\}_2]$  (**13a**) gave one chain per metal, whereas more than one chain was obtained per metal when  $[\text{Sm}(\text{iPr-BOPA})\{\text{N}(\text{SiMe}_3)_2\}_2]$  (**13c**) was used, suggesting that some of the catalyst was not active in the reaction. The kinetics also indicated that the reactions were first order in lactide.

#### 4.4 References for Chapter 4

- 1 C. Emo and S. Roberto, *Adv. Mater.*, 1996, **8**, 305.
- 2 R. E. Drumright, P. R. Gruber, and D. E. Henton, *Adv. Mater.*, 2000, **12**, 1841.
- 3 M. Stefan, *Angew. Chem., Int. Ed.*, 2004, **43**, 1078.
- 4 O. Dechy-Cabaret, B. Martin-Vaca, and D. Bourissou, *Chem. Rev.*, 2004, **104**, 6147.
- 5 N. E. Kamber, W. Jeong, R. M. Weymouth, R. C. Pratt, B. G. G. Lohmeijer, and J. L. Hendrick, *Chem. Rev.*, 2007, **107**, 5813.
- 6 S. Agarwal, C. Mast, K. Dehnicke, and A. Greiner, *Macromol. Rapid Commun.*, 2000, **21**, 195.
- 7 I. Palard, M. Schappacher, A. Soum, and S. M. Guillaume, *Polym. Int.*, 2006, **55**, 1132.
- 8 W. M. Stevels, M. J. K. Ankoné, P. J. Dijkstra, and J. Feijen, *Macromolecules*, 1996, **29**, 3332.
- 9 W. M. Stevels, M. J. K. Ankoné, P. J. Dijkstra, and J. Feijen, *Macromolecules*, 1996, **29**, 6132.
- 10 C. Yu, L. Zhang, X. Ni, Z. Shen, and K. Tu, *J. Polym. Sci., Part A: Polym. Chem.*, 2004, **42**, 6209.
- 11 H. Y. Ma and J. Okuda, *Macromolecules*, 2005, **38**, 2665.
- 12 M. H. Chisholm and E. E. Delbridge, *New. J. Chem.*, 2003, **27**, 1167.
- 13 L. Clark, M. G. Cushion, H. E. Dyer, A. D. Schwarz, R. Duchateau, and P. Mountford, *Chem. Commun.*, 2010, **46**, 273.
- 14 D. -M. Du, S. -F. Lu, and J. Xu, *Org. Lett.*, 2006, **8**, 2115.
- 15 D. -M. Du, H. Liu, and J. Xu, *Org. Lett.*, 2007, **9**, 4725.
- 16 D. -M. Du, H. Liu, S. -F. Lu, and J. Xu, *Chem. Asian J.*, 2008, **3**, 1111.
- 17 D. -M. Du, Y. Jia, and W. Yang, *Org. Biomol. Chem.*, 2012, **10**, 4739.



- 18 A. Furuta, T. Inagaki, J. -I. Ito, H. Nishiyama, and L. T. Phong, *Chem. Eur. J.*, 2010, **16**, 3090.
- 19 P. G. Cozzi, P. J. Guiry, and H. A. McManus, *Adv. Synth. Catal.*, 2006, **348**, 551.
- 20 H. L. W. Hoegy and A. Rudin, *J. Polym. Sci., Part A: Polym. Chem.*, 1972, **10**, 217.
- 21 I. Barakat, P. Dubois, R. Jérôme, and P. Teyssié, *J. Polym. Sci., Part A: Polym. Chem.*, 1993, **31**, 505.
- 22 J. R. Dorgan, S. B. Hait, M. H. Hutchinson, J. Janzen, D. M. Knauss, and B. R. Limoges, *J. Polym. Sci., Part B: Polym. Phys.*, 2005, **43**, 3100.
- 23 C. A. Wheaton, P. G. Hayes, and B. J. Ireland, *Dalton Trans.*, 2009, **25**, 4832
- 24 M. H. Chisholm, J. C. Gallucci, and K. Phomphrai, *Inorg. Chem.*, 2002, **41**, 2785.
- 25 M. H. Chisholm, J. C. Gallucci, and K. Phomphrai, *Inorg. Chem.*, 2005, **44**, 8004.
- 26 F. Bonnet, R. Duchateau, H. E. Dyer, S. Huijser, L. Maron, P. Mountford, A. D. Schwarz, and N. Susperregui, *Organometallics*, 2010, **29**, 3602.
- 27 M. H. Chisholm, J. Gallucci, and K. Phomphrai, *Chem. Commun.*, 2003, 48.
- 28 A. Amgoune, J. -F. Carpentier, and C. M. Thomas, *Macromol. Rapid Commun.*, 2007, **28**, 693.

## **CHAPTER 5**

# **Photophysical properties of trivalent Group 3 and lanthanide BOPA complexes**

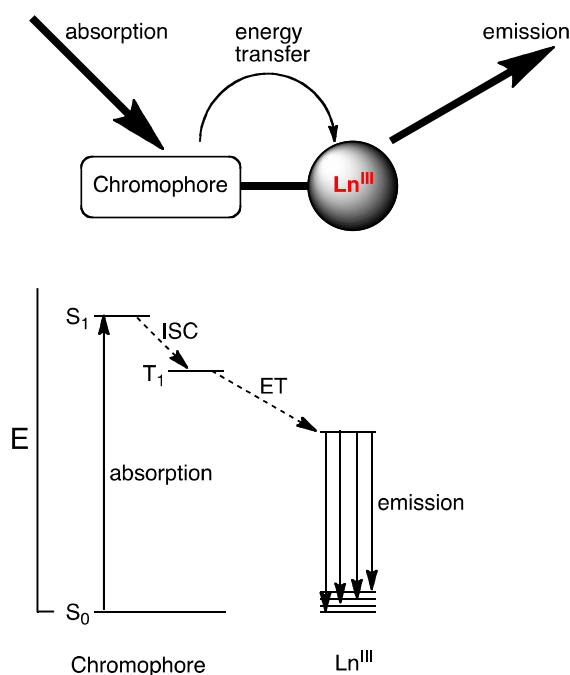
## 5.1 Introduction

The majority of the trivalent lanthanide ions possess low-lying, often partially occupied  $4f$  orbitals. These give the lanthanide ions unique spectroscopic properties that has led to many industrial applications, for example in light devices,<sup>1</sup> optical fibres,<sup>2</sup> display screens and lasers, as well as their medical applications in cell imaging and biomedical stains.<sup>3-5</sup>

The lanthanide ions are inefficient in absorbing energy for direct excitation due to the formally forbidden  $f-f$  transitions. Therefore an indirect transfer of energy is required, achieved by incorporating a sensitising chromophore (often referred to as an antenna) (Fig. 1). The chromophore transfers the energy to the lanthanide ion, usually *via* an intermediate triplet excited state localised on the ligand.<sup>6, 7</sup> The emission bands are typically sharp in appearance, and are therefore characteristic of each specific ion. Due to the sensitisation process the apparent Stokes shifts can therefore be large. Since the  $f-f$  relaxation is a forbidden process, the lifetimes of the emissions can be very long (micro-millisecond), and for many of the lanthanide ions are formally assigned to phosphorescence. More importantly, the spectroscopic fingerprint of a luminescent lanthanide ion (spectral profile and lifetime of  $f$ -centred emission) is uniquely sensitive to the environment around the lanthanide ion, and can provide information relating to the coordination environment and the relative proximity of quenchers (*e.g.* O-H, C-H, N-H oscillators).

Many chromophores have been investigated for the sensitisation of lanthanides. The antenna can be introduced in several ways: by being part of the ligand architecture, by being directly bonded to the lanthanide, or both. It must absorb light very effectively, but also possess a triplet state that is of sufficient energy (*i.e.*  $>2000\text{ cm}^{-1}$ ) above the accepting  $\text{Ln}^{\text{III}}$  state to allow sensitisation and prevent back energy transfer. If the triplet state is close in

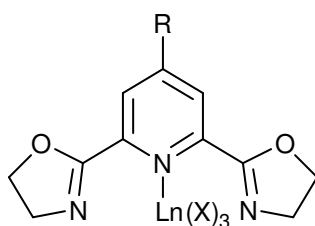
energy to the accepting lanthanide state, back energy transfer occurs, resulting in an emission of low intensity.



**Fig. 1** Top: simplified model for sensitised lanthanide luminescence. Bottom: typical energy level diagram for an emissive chromophore-appended lanthanide complex sensitised *via* a ligand-centred triplet excited state

The quantum yields of emissive Ln(III) complexes vary due to the sensitive nature of the 4*f*-centred excited states to O-H, N-H and C-H oscillators. These provide efficient, non-radiative deactivation pathways; the efficiency of energy transfer between the antenna and lanthanide ion also determines overall quantum yields. A well-documented approach to maximising the emissivity of Ln(III) complexes is to inhibit the approach of solvent to the inner coordination sphere using sterically demanding peripheral groups on the supporting ligand(s). This can be counterproductive, as by surrounding the lanthanide with a large organic ligand can also provide deactivation pathways through the C-H oscillators incorporated into the ligand structure.

There are several possible ways that the energy can be transferred from the ligand to the metal. The most likely mechanism for the transfer of energy from the ligand to the metal is the Förster (dipole-dipole) mechanism, the efficiency of which decreases exponentially with distance. This is where the dipole of the  $T_1$  state of the ligand couples with the dipole moment of the  $4f$  orbitals, allowing the transfer of energy. There are two other means for transferring energy to lanthanide ions, one is the use of ligand to metal transfer states (as previously discussed) and the second is the transfer of energy from a  $d$ -transition metal ion.



**Fig. 2** Lanthanide pybox complexes. Ln = Eu, Tb; R = H, OMe, Br; X = NO<sub>3</sub>, CF<sub>3</sub>SO<sub>3</sub>

The BOPA complexes discussed throughout Chapter 2 were found to be luminescent. Oxazoline based ligands, when part of a conjugated ligand framework, have been found to sensitise lanthanide ions. For example, Eu(III) and Tb(III) complexes bearing the pyridine-bisoxazoline (pybox) ligand (Fig. 2) have been investigated for their photophysical properties.<sup>8, 9</sup> The *para* substituent of the pyridine ring was altered to enable tuning of the energy levels of the ligand. Thiophen-3-yl, methoxy and bromide groups were used in this study, and the singlet and triplet states were found to be at appropriate energies to successfully sensitise the lanthanide ions. Three equivalents of the ligand were also coordinated to the lanthanide to prevent quenching *via* solvent interactions. This report concentrated on the synthesis of the complexes, and the photophysical measurements; however there was no investigation to determine if the luminescence spectroscopy could be

used as a probe for functional metal complexes. The focus of this chapter is to establish whether these spectroscopic properties can afford any insight into the nature of the complexes, and thereby providing information that cannot be obtained using other spectroscopic methods.

The paramagnetic complexes  $[\text{Ln}(\text{R-BOPA})\{\text{N}(\text{SiMe}_3)_2\}_2]$  ( $\text{Ln} = \text{Pr}$ , **11**  $\text{Nd}$  **12**,  $\text{Sm}$  **13**) described in Chapter 2 are ideal candidates for this study, although there is one significant limitation. These complexes were employed as pre-catalysts, as described in Chapter 3, but they are not representative of any of the species present in the catalytic reaction. By definition, a catalytic intermediate cannot be prepared for an *intramolecular* reaction, and so a *pseudo* substrate was prepared, which is identical to the hydroamination substrate **B** except that the unsaturated chain end has been replaced by the saturated equivalent (Fig. 3). This allows the substrate to coordinate in the same way as the ‘real’ substrate, but prevents the cyclisation step. Complexes bearing this substrate (*i.e.*  $[\text{Ln}(\text{R-BOPA})(\text{NHCH}_2\text{C}(\text{Ph})_2\text{C}_3\text{H}_7)_2]$  ( $\text{Ln} = \text{La}$  **15**,  $\text{Pr}$  **16**,  $\text{Nd}$  **17a-c**)) are therefore the closest to a catalytic intermediate that can be reasonably prepared.



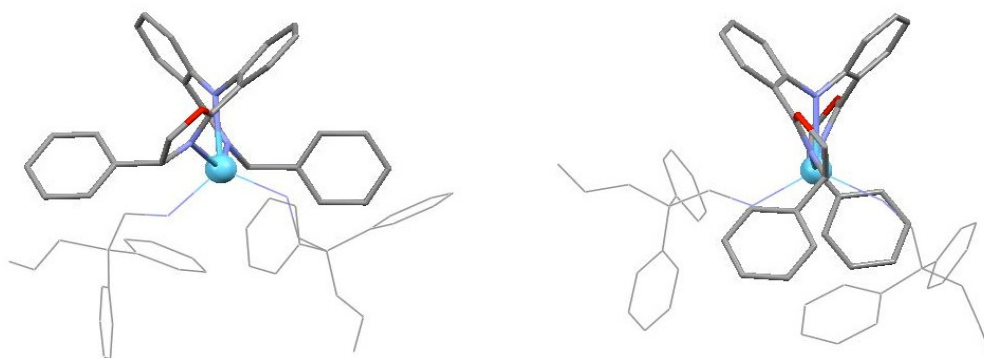
**Fig.3** *Pseudo* substrate (**5.1**) and aminoolefin hydroamination substrate **B**

## 5.2 Density Functional Theory (DFT) Calculations

The complexes  $[\text{Ln}(\text{R-BOPA})(\text{NHCH}_2\text{C}(\text{Ph})_2\text{C}_3\text{H}_7)_2]$  ( $\text{Ln} = \text{La}$  **15**,  $\text{Pr}$  **16**,  $\text{Nd}$  **17a-c**), were evaluated by calculating the structures of the lanthanum congeners (as representative examples) using density functional theory calculations. The calculations were carried out by

Dr. B. Ward in collaboration with the Advanced Research Computing in Cardiff (ARCCA) facility, using the Gaussian 09 software package.<sup>10</sup> All geometry optimisations were performed using the restricted hybrid B3LYP functional, employing the Stuttgart/Dresden basis set with effective core potentials for the metal ions, 6-31G(d,p) for the coordinating atoms, and 6-31G for all other centres. Geometry optimisations were performed without symmetry restraints and were followed by frequency calculations to ascertain the nature of the stationary point (minimum *vs.* saddle point).

Lanthanum BOPA complexes bearing the *pseudo* substrate were calculated *in vacuo* and in the presence of a solvent continuum (benzene and toluene). Although the calculations in benzene and toluene are not expected to show significant differences, these calculations were prompted by the interesting and unexplained differences in the BOPA complexes' catalytic behaviour in the hydroamination/cyclisation of aminoolefins. Based upon the calculations described in Chapter 2, two isomeric forms, *exo* and *endo*, were expected; this assumption was ratified by the calculations (Fig. 4), and their relative energies are provided in Table 1.



**Fig. 4** Calculated isomeric structures of  $[\text{La}(\text{R-BOPA})(\text{C}_3\text{H}_7\text{CHPh}_2\text{CH}_2\text{NH})_2]$  ( $15\text{a}_{\text{calc}}$ )

The two isomers, depicted in Fig. 4 suggest that the metal centre in the *endo* isomer is significantly less shielded (more exposed to solvent) than the *exo* isomer. This could have a

significant impact on the observed luminescence lifetimes of the two species. Moreover, an examination of the two isomers suggests that the *exo* isomer is likely to be more efficient at controlling the chiral space at the metal. The *endo* isomer, by virtue of placing the stereodirecting groups on the same face of the coordination sphere, leaves a significant amount of achiral space and is therefore less likely to provide adequate stereocontrol in catalysis. This suggests that the relative proportion of these two isomers *during a catalytic reaction* may be a significant contributor to the complexes' ability to evoke enantiocontrol in catalytic reactions.

**Table 1** Calculated relative energies between the *exo* and *endo* isomers of  $[\text{La}(\text{R-BOPA})\text{N}''']_2$  (**15a-c<sub>calc</sub>**);  $\text{N}''' = \text{C}_3\text{H}_7\text{CHPh}_2\text{CH}_2\text{NH}$ ; R = Ph **a**, Bn **b**, <sup>i</sup>Pr **c**

Entry	Complex	R	$\Delta G_{\text{calc}}$ kcal	$\Delta G_{\text{calc}}$ kcal	$\Delta G_{\text{calc}}$ kcal
			( <i>vacuo</i> ) <sup>a</sup>	(benzene) <sup>a</sup>	(toluene) <sup>a</sup>
1	[La(R-BOPA)N'''] <b>15<sub>calc</sub></b>	Ph	7.72	5.94	5.87
2		Bn	2.67	4.35	2.08
3		<sup>i</sup> Pr	2.62	4.42	4.42

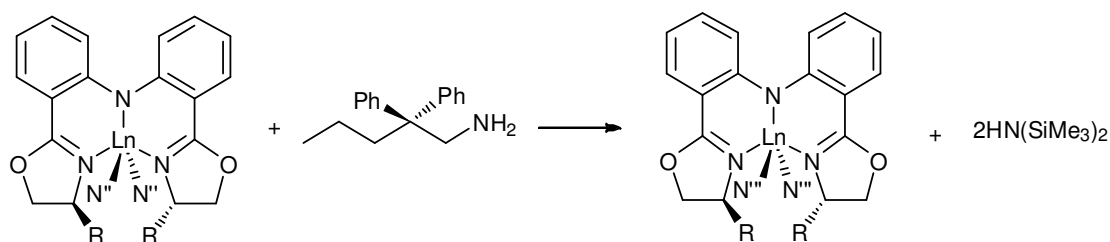
<sup>a</sup>  $G_{\text{endo}} - G_{\text{exo}}$ ; positive values indicate that the *exo* isomer is energetically favoured

As expected, the *exo* isomers are favoured over the *endo* isomers. The energy differences lie in the order Ph > Bn  $\approx$  <sup>i</sup>Pr. When the calculations include a solvent continuum, the energetic preference for the phenyl derivative is reduced slightly whereas that of the isopropyl congener increases. The relative energies for the phenyl and isopropyl congeners were within error in benzene and toluene, whilst those of the benzyl derivative showed more deviation upon changing the solvent continuum. Interestingly, the calculated relative energy of the benzyl derivative was seen to increase in benzene and decrease in toluene. This may highlight an inherent inaccuracy in calculations of this type: with relatively flexible co-ligands the potential energy surface is likely to contain multiple minima



of similar energy, and we cannot guarantee that the calculated structure represents the global minimum. Additionally, these calculations do not consider that experimentally, the coordinated *pseudo* substrate is likely to exist in many interchanging conformations in solution. Nevertheless, these calculations do suggest that a difference in the relative proportions of *exo* and *endo* isomers is to be expected under catalytic conditions, and that this should show a dependence on the nature of the stereodirecting group. The lack of significant solvent effects for the phenyl derivative (for which large differences in catalytic performance were observed experimentally) may suggest that the experimental effects are likely owing to discrete solvent-complex interactions, which are not considered in calculations of this type.

### 5.3 Preparation and Characterisation of $[\text{Ln}(\text{R-BOPA})\{\text{NHCH}_2\text{C}(\text{Ph})_2\text{C}_3\text{H}_7\}_2]$ ( $\text{Ln} = \text{La } \mathbf{15}, \text{Pr } \mathbf{16}, \text{Nd } \mathbf{17}$ )



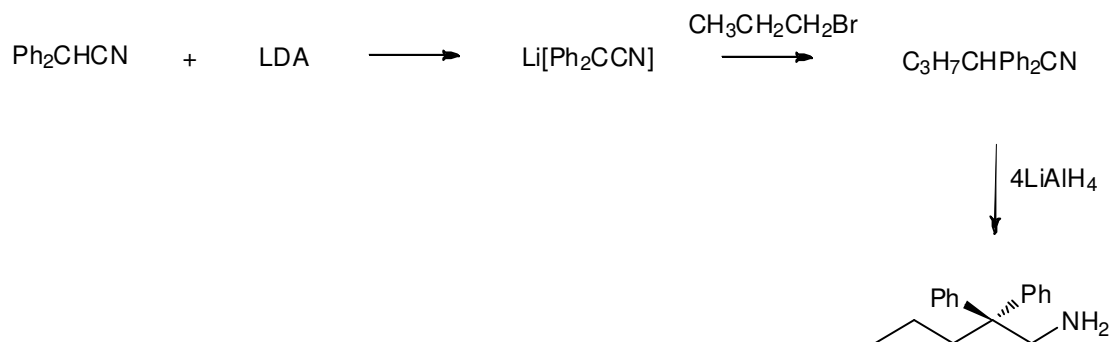
**Scheme 1** Synthesis of  $[\text{Ln}(\text{R-BOPA})\{\text{NHCH}_2\text{C}(\text{Ph})_2\text{C}_3\text{H}_7\}_2]$  ( $\text{Ln} = \text{La } \mathbf{15}, \text{Pr } \mathbf{16}, \text{Nd } \mathbf{17}$ )  $\text{R} = \text{Ph } \mathbf{a}$ ,

$\text{Bn } \mathbf{b}$ ,  $\text{iPr } \mathbf{c}$ ;  $\text{N}'' = \text{N}(\text{SiMe}_3)_2$ ;  $\text{N}''' = \text{HN}\{\text{CH}_2\text{C}(\text{Ph})_2\text{C}_3\text{H}_7\}$

The complexes bearing the *pseudo* substrate,  $[\text{La}(\text{iPr-BOPA})\{\text{NHCH}_2\text{C}(\text{Ph})_2\text{C}_3\text{H}_7\}_2]$  (**15**),  $[\text{Pr}(\text{Bn-BOPA})\{\text{NHCH}_2\text{C}(\text{Ph})_2\text{C}_3\text{H}_7\}_2]$  (**16**) and  $[\text{Nd}(\text{Ph-BOPA})\{\text{NHCH}_2\text{C}(\text{Ph})_2\text{C}_3\text{H}_7\}_2]$  (**17a**),  $[\text{Nd}(\text{Bn-BOPA})\{\text{NHCH}_2\text{C}(\text{Ph})_2\text{C}_3\text{H}_7\}_2]$  (**17b**),  $[\text{Nd}(\text{iPr-BOPA})\{\text{NHCH}_2\text{C}(\text{Ph})_2\text{C}_3\text{H}_7\}_2]$  (**17c**) were prepared by the reaction of the parent silyl amide complex  $[\text{Ln}(\text{R-BOPA})\{\text{N}(\text{SiMe}_3)_2\}_2]$  **10a**, **11b** or **12a-c** with the *pseudo* substrate (**5.1**) in

hexanes (Scheme 1). Compounds **15**, **16** and **17a-c** were obtained as bright yellow solids in 55-71% yield, and were characterised by elemental analysis, NMR and IR spectroscopies.

### 5.3.1 Synthesis of the *pseudo* substrate **5.1**



**Scheme 2** Synthesis of the *pseudo* substrate (**5.1**)

The *pseudo* substrate (**5.1**) was synthesised *via* a modified literature procedure (Scheme 2).<sup>11</sup>  $\text{Ph}_2\text{CHCN}$  was deprotonated (LDA) and coupled with  $\text{CH}_3\text{CH}_2\text{CH}_2\text{Br}$ . The resulting nitrile was reduced with  $\text{LiAlH}_4$  to yield **5.1** as a pale yellow oil in 87% yield. NMR spectra obtained for this compound are comparable to those reported previously.

### 5.3.2 Spectroscopic Characterisation of $[\text{La}(\text{iPr-BOPA})\{\text{NHCH}_2\text{C}(\text{Ph})_2\text{C}_3\text{H}_7\}_2]$ (**15**)

The lanthanum complex was prepared primarily to assist in characterisation, by providing a diamagnetic complex that could be more accurately characterised by NMR spectroscopy, and to provide greater confidence for the identity of the paramagnetic derivatives. Despite the computational predictions of two isomers, only one isomer was observed in the  $^1\text{H}$  and  $^{13}\text{C}\{^1\text{H}\}$  NMR spectra of  $[\text{La}(\text{iPr-BOPA})\{\text{NHCH}_2\text{C}(\text{Ph})_2\text{C}_3\text{H}_7\}_2]$  (**15**), the resonances of which are consistent with a  $C_2$ -symmetric molecule. The principal differences between the spectra of **15** and those of  $[\text{La}(\text{iPr-BOPA})\{\text{N}(\text{SiMe}_3)_2\}_2]$  (**10c**) are

the absence of the silyl resonance (0.23 ppm in **11c**), and the presence of additional signals attributed to the coordinated *pseudo* substrate. The resonances attributed to the BOPA ligand are shifted slightly from those of the free ligand and **10c**, but nevertheless remain consistent with the general structure discussed in Chapter 2 and depicted in Scheme 1. This indicates the *pseudo* substrate has replaced the silyl amide ligand, and that no competitive protonation of the BOPA ligand has occurred.

The  $^{13}\text{C}\{^1\text{H}\}$  NMR spectrum exhibits a resonance at 165.7 ppm, assigned to the C=N carbon, and is slightly different from the equivalent signal in **10c** (168.4 ppm). The remaining carbons of the BOPA ligand are consistent with the conclusions drawn from the  $^1\text{H}$  NMR spectrum. The resonance attributed to the silyl amide ligand is not observed (5.1 ppm in **10c**), and additional signals are observed for the *pseudo* substrate.

### 5.3.3 Spectroscopic Characterisation of $[\text{Ln}(\text{R-BOPA})\{\text{NHCH}_2\text{C}(\text{Ph})_2\text{C}_3\text{H}_7\}_2]$ ( $\text{Ln} = \text{Pr } \mathbf{16}, \text{Nd } \mathbf{17}$ )

Having established the structure of  $[\text{La}(\text{iPr-BOPA})\{\text{NHCH}_2\text{C}(\text{Ph})_2\text{C}_3\text{H}_7\}_2]$ , the data were used to supplement the data acquired for the paramagnetic complexes. As discussed in Chapter 2, the reduction of fine structure, and the paramagnetic shifting of the resonances, renders the reliable assignment of the signals inaccurate. Nevertheless, the overall symmetry, number of signals, and relative integration are sufficient to provide a detailed comparison with the diamagnetic derivatives. The  $^1\text{H}$  and  $^{13}\text{C}\{^1\text{H}\}$  NMR spectra of  $[\text{Pr}(\text{Bn-BOPA})\{\text{NHCH}_2\text{C}(\text{Ph})_2\text{C}_3\text{H}_7\}_2]$  (**16**) and  $[\text{Nd}(\text{R-BOPA})\{\text{NHCH}_2\text{C}(\text{Ph})_2\text{C}_3\text{H}_7\}_2]$  ( $\text{R} = \text{Ph } \mathbf{17a}, \text{Bn } \mathbf{17b}, \text{iPr } \mathbf{17c}$ ) indicate the presence of one isomer, and are consistent with  $C_2$  molecular symmetry. In each case, the large signals assigned to the silyl resonances are not observed, with additional signals being found for the *pseudo* substrate. There are no resonances attributed to the free ligands, indicating that no competitive protonation of the BOPA ligands

has taken place, as found for the lanthanum complex. The resonance at 3.14 ppm is attributed to the CH<sub>3</sub> of the *pseudo* substrate in **16**, whereas the equivalent resonance for **17a–c** are observed at 7.01, 0.25, and 5.64 ppm respectively. The <sup>13</sup>C{<sup>1</sup>H} NMR spectra show little difference in comparison to those of the N(SiMe<sub>3</sub>)<sub>2</sub>-ligated precursors, and are fully consistent with the conclusions drawn from the <sup>1</sup>H NMR spectra.

## 5.4 Photophysical Measurements

### 5.4.1 Diamagnetic complexes **2a-c**, **5a-c** and **10a-c**

The photophysical properties of a representative selection of complexes discussed throughout this thesis have been investigated. All of the complexes give rise to ligand-centred luminescence, whereas only the paramagnetic complexes show lanthanide sensitisation. Solutions of [Sc(R-BOPA){N(SiMe<sub>3</sub>)<sub>2</sub>}Cl] (**2a-c**), [Sc(R-BOPA)(CH<sub>2</sub>SiMe<sub>2</sub>Ph)<sub>2</sub>] (**5a-c**) and [La(R-BOPA){N(SiMe<sub>3</sub>)<sub>2</sub>}<sub>2</sub>] (**10a-c**) (in dry benzene, 10<sup>-4</sup> M under N<sub>2</sub> atmosphere) and [Pr(R-BOPA){N(SiMe<sub>3</sub>)<sub>2</sub>}] (**11a-c**), [Nd(R-BOPA){N(SiMe<sub>3</sub>)<sub>2</sub>}] (**12a-c**), [Sm(R-BOPA){N(SiMe<sub>3</sub>)<sub>2</sub>}] (**13a-c**), [Pr(Bn-BOPA){NHCH<sub>2</sub>C(Ph)<sub>2</sub>C<sub>3</sub>H<sub>7</sub>}<sub>2</sub>] (**16**) and [Nd(R-BOPA){NHCH<sub>2</sub>C(Ph)<sub>2</sub>C<sub>3</sub>H<sub>7</sub>}<sub>2</sub>] (**17a-c**) (in dry toluene, 10<sup>-4</sup> M under N<sub>2</sub> atmosphere) were investigated in collaboration with Dr. Simon Pope (Cardiff University).

The excitation profiles of [Sc(R-BOPA){N(SiMe<sub>3</sub>)<sub>2</sub>}Cl] (**2a-c**), [Sc(R-BOPA)(CH<sub>2</sub>SiMe<sub>2</sub>Ph)<sub>2</sub>] (**5a-c**) and [La(R-BOPA){N(SiMe<sub>3</sub>)<sub>2</sub>}<sub>2</sub>] (**10a-c**) are provided in Fig. 5. These profiles are typical of the excitation profiles obtained for all of the diamagnetic complexes. Also, the complexes show a single emission between (500-510 nm) with a small associated Stokes' shift (*ca.* 1000 cm<sup>-1</sup>), the precise positioning showed a small dependence on the identity of the BOPA ligand. The diphenylamine anion is known to be non emissive,<sup>12</sup> and therefore the fluorescence is attributed to a ligand centred excited state with a charge

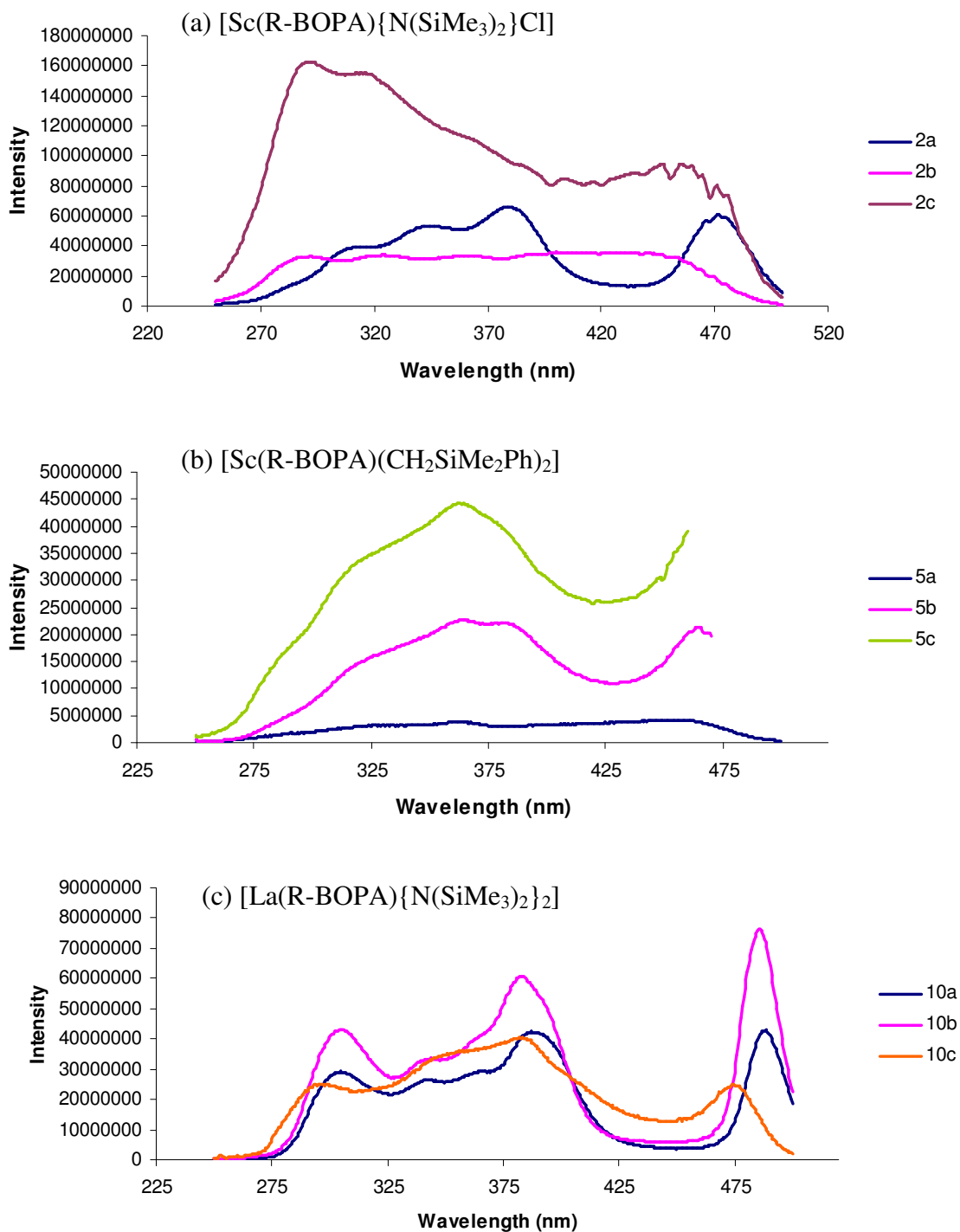
transfer ( $N \rightarrow \pi^*$ ) component originating from the deprotonated/coordinated amide bridge-head.

The excitation profiles of  $[\text{La}(\text{R-BOPA})\{\text{N}(\text{SiMe}_3)_2\}_2]$  (**10a-c**) are most defined, whereas those for  $[\text{Sc}(\text{R-BOPA})\{\text{N}(\text{SiMe}_3)_2\}\text{Cl}]$  (**2a-c**) and  $[\text{Sc}(\text{R-BOPA})(\text{CH}_2\text{SiMe}_2\text{Ph})_2]$  (**5a-c**) show much broader profiles and are therefore less well-defined. The lifetimes of spectral emissions for the diamagnetic complexes are tabulated below (Table 2). The lifetimes are short, indicative of a ligand-centred fluorescence, with small Stokes' shifts. Interestingly, for the scandium complexes the spectral profiles indicate the presence of two components. These are attributed to the *exo* and *endo* isomers, since the relative intensities obtained from the emission lifetime spectra are in approximately the same ratio observed in the  $^1\text{H}$  NMR spectra (Chapter 2) (Table 2).

**Table 2** Lifetimes of  $[\text{Sc}(\text{R-BOPA})\{\text{N}(\text{SiMe}_3)_2\}\text{Cl}]$  (**2a-c**),  $[\text{Sc}(\text{R-BOPA})(\text{CH}_2\text{SiMe}_2\text{Ph})_2]$  (**5a-c**) and  $[\text{La}(\text{R-BOPA})\{\text{N}(\text{SiMe}_3)_2\}_2]$  (**10a-c**) (benzene,  $\text{N}_2$ ;  $\lambda_{\text{ex}} = 487$  nm;  $\lambda_{\text{em}} = 515$  nm). R = Ph (**a**), Bn (**b**) and iPr (**c**)

Entry	Compound	Lifetime, $\tau$ (ns)	Experimental ratio <sup>a</sup>
1	2a	3.6	1:0.25
2	2b	2.8, 4.5	1:0.7
3	2c	2.3, 3.7	1:0.4
4	5a	0.8, 3.2	1:0.5
5	5b	1.3, 3.3	1:0.6
6	5c	1.5, 3.6	1:0.5
7	11a	4.6	-
8	11b	4.5	-
9	11c	5.0	-

<sup>a</sup> Calculated from the  $^1\text{H}$  NMR spectra unless otherwise stated



**Fig. 5** Steady state excitation profiles ( $\lambda_{\text{ex}}$  485 nm) of (a)  $[\text{Sc}(\text{R-BOPA})\{\text{N}(\text{SiMe}_3)_2\}\text{Cl}]$  (**2a-c**), (b)  $[\text{Sc}(\text{R-BOPA})(\text{CH}_2\text{SiMe}_2\text{Ph})_2]$  (**5a-c**), (c)  $[\text{La}(\text{R-BOPA})\{\text{N}(\text{SiMe}_3)_2\}_2]$  (**10a-c**); R = Ph (**a**), Bn (**b**) and *i*Pr (**c**)

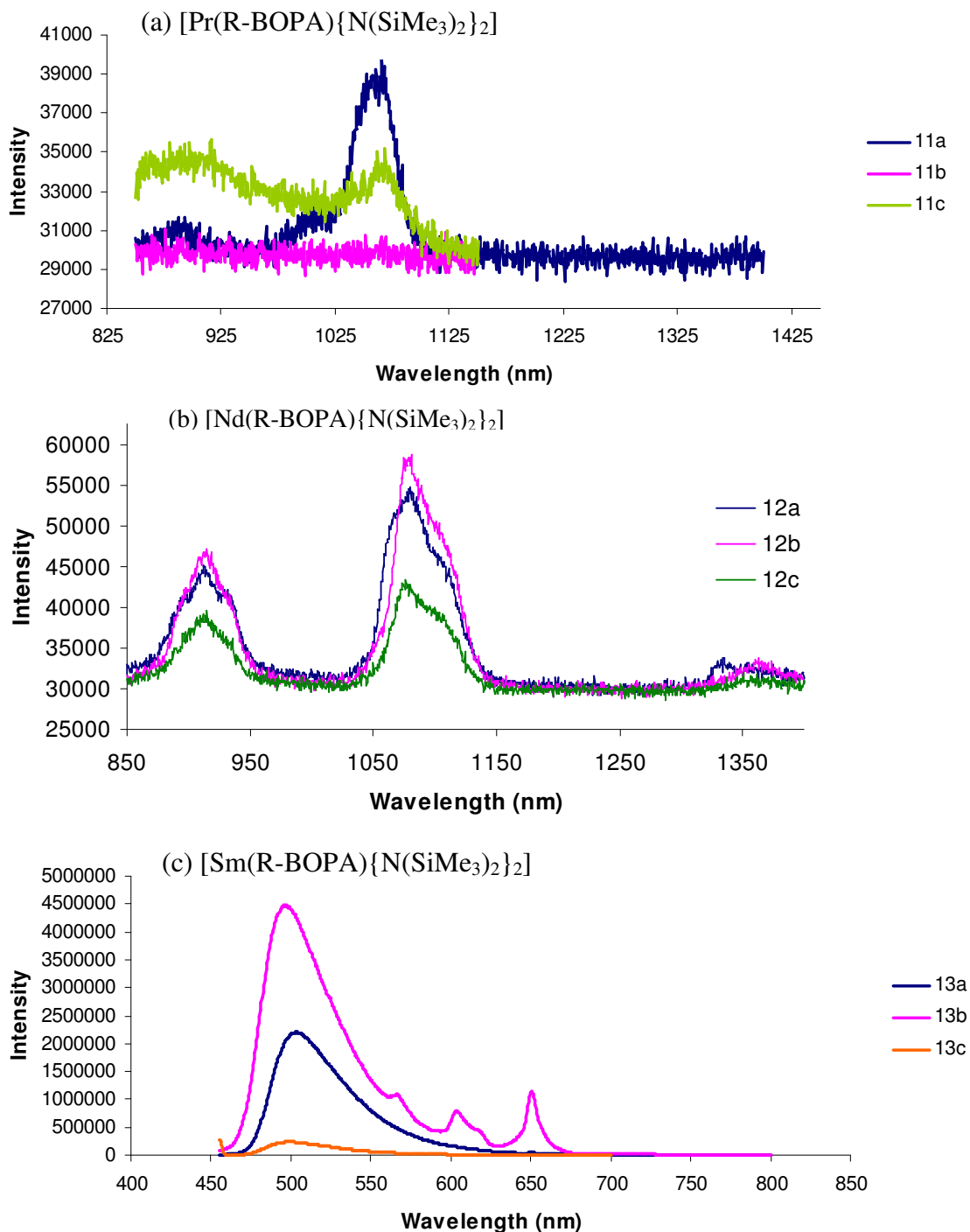
### 5.4.2 Paramagnetic complexes **11a-c**, **12a-c** and **13a-c**

The photophysical properties of the paramagnetic complexes proved more interesting than their diamagnetic counterparts. The graphs below (Fig. 6) depict the emission profiles from the paramagnetic complexes [Pr(R-BOPA){N(SiMe<sub>3</sub>)<sub>2</sub>}<sub>2</sub>] (**11a-c**), [Nd(R-BOPA){N(SiMe<sub>3</sub>)<sub>2</sub>}<sub>2</sub>] (**12a-c**) and [Sm(R-BOPA){N(SiMe<sub>3</sub>)<sub>2</sub>}<sub>2</sub>] (**13a-c**).

The emission profiles of the paramagnetic complexes vary in their quality. The spectra of [Pr(R-BOPA){N(SiMe<sub>3</sub>)<sub>2</sub>}<sub>2</sub>] (**11a-c**) can exhibit six bands, for the following *f-f* transitions; <sup>1</sup>D<sub>2</sub> → <sup>3</sup>H<sub>6</sub> (608 nm), <sup>1</sup>D<sub>2</sub> → <sup>3</sup>F<sub>2</sub> (890 nm), <sup>1</sup>D<sub>2</sub> → <sup>3</sup>F<sub>3</sub> (1015 nm), <sup>1</sup>D<sub>2</sub> → <sup>3</sup>F<sub>4</sub> (1065 nm), <sup>1</sup>G<sub>4</sub> → <sup>3</sup>H<sub>3</sub> (1320 nm) and <sup>1</sup>D<sub>2</sub> → <sup>1</sup>G<sub>4</sub> (1550 nm).<sup>13</sup> The emission profile of [Pr(Ph-BOPA){N(SiMe<sub>3</sub>)<sub>2</sub>}<sub>2</sub>] (**11a**) is the most informative with three broad transitions visible; <sup>1</sup>D<sub>2</sub> → <sup>3</sup>F<sub>2</sub> (890 nm), <sup>1</sup>D<sub>2</sub> → <sup>3</sup>F<sub>3</sub> (1015 nm) and <sup>1</sup>D<sub>2</sub> → <sup>3</sup>F<sub>4</sub> (1065 nm). This is unlike the profiles for **11b** and **11c**, whereby no transitions are observed (**11b**) and one transition at 1065 nm (<sup>1</sup>D<sub>2</sub> → <sup>3</sup>F<sub>4</sub>) visible for **11c**. The energy of the <sup>1</sup>G<sub>4</sub> and <sup>1</sup>D<sub>2</sub> states are 10000 and 17500 cm<sup>-1</sup> respectively, and must lie at a similar energy or below that of the ligand excited state. The observation of the emission signal at 1065 nm indicates that the <sup>1</sup>D<sub>2</sub> is populated by the transfer of energy from the ligand, however, the lack of signals in the emission profiles for the three praseodymium complexes indicate that this energy state must be quenched by non-radiative processes.

The emission profiles of [Nd(R-BOPA){N(SiMe<sub>3</sub>)<sub>2</sub>}<sub>2</sub>] (**12a-c**) are more indicative of literature examples of neodymium emission spectra. The transitions at 880 nm (<sup>4</sup>F<sub>3/2</sub> → <sup>4</sup>I<sub>9/2</sub>), 1058 nm (<sup>4</sup>F<sub>3/2</sub> → <sup>4</sup>I<sub>11/2</sub>) and 1340 nm (<sup>4</sup>F<sub>3/2</sub> → <sup>4</sup>I<sub>13/2</sub>) are all observed. The energy transfer from the ligand excited state to the Nd(III) quartet state is more efficient than for [Pr(R-BOPA){N(SiMe<sub>3</sub>)<sub>2</sub>}<sub>2</sub>] (**11a-c**). This is probably due to the energy of the <sup>4</sup>F<sub>3/2</sub> state (~12000 cm<sup>-1</sup>), lying far lower than that of Pr(III). As the sensitisation of [Nd(R-

BOPA) $\{N(SiMe_3)_2\}_2$ ] (**12a-c**) was successful, these systems make ideal candidates for probing the complexes' during catalysis.



**Fig. 6** (a) Emission profile of [Pr(R-BOPA) $\{N(SiMe_3)_2\}_2$ ] (**11a-c**); (b) Emission profile of [Nd(R-BOPA) $\{N(SiMe_3)_2\}_2$ ] (**12a-c**); (c) Emission profile of [Sm(R-BOPA) $\{N(SiMe_3)_2\}_2$ ] (**13a-c**). R = Ph

(a), Bn (b) and iPr (c). ( $\lambda_{ex}$  445 nm)



Unfortunately, when investigating the photophysical properties of  $[\text{Sm}(\text{R-BOPA})\{\text{N}(\text{SiMe}_3)_2\}_2]$  (**13a-c**), little information could be obtained. A strong ligand-based residual emission was superimposed over the expected Sm(III) emission bands, perhaps indicating that an inefficient transfer of energy from the ligand's excited state to the  $^4\text{G}_{5/2}$  level of the samarium ( $\sim 18000\text{ cm}^{-1}$ ) occurs.

The lifetimes of the *f*-centred emission of  $[\text{Pr}(\text{R-BOPA})\{\text{N}(\text{SiMe}_3)_2\}_2]$  (**11a-c**) provide little information (Table 3). The lifetimes are short and consistent with the literature on other Pr(III) complexes.<sup>14</sup>

**Table 3** Lifetime measurements of  $[\text{Pr}(\text{R-BOPA})\{\text{N}(\text{SiMe}_3)_2\}_2]$  (**11a-c**) (toluene,  $\text{N}_2$ ;  $\lambda_{\text{ex}} = 445\text{ nm}$ ;  $\lambda_{\text{em}} = 1080\text{ nm}$ ), and  $[\text{Nd}(\text{R-BOPA})\{\text{N}(\text{SiMe}_3)_2\}_2]$  (**12a-c**) (toluene,  $\text{N}_2$ ;  $\lambda_{\text{ex}} = 445\text{ nm}$ ;  $\lambda_{\text{em}} = 1055\text{ nm}$ ). R = Ph (**a**), Bn (**b**) and iPr (**c**)

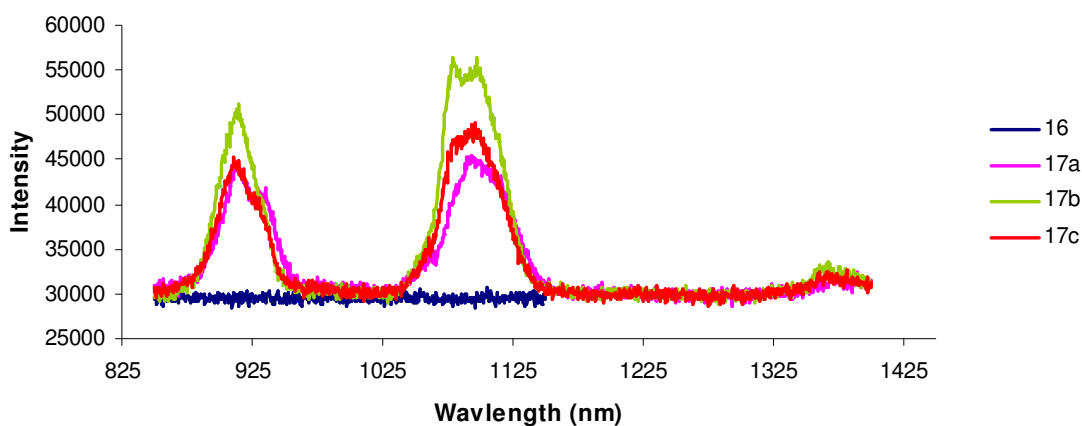
Entry	Metal	Compound	Lifetime, $\tau$ (ns)
1	Pr	11a	30
2	Pr	11b	47
3	Pr	11c	34
4	Nd	12a	129, 677 (90%)
5	Nd	12b	41, 308 (80%)
6	Nd	12c	148, 621 (70%)

Deconvolution of the emission profiles  $[\text{Nd}(\text{R-BOPA})\{\text{N}(\text{SiMe}_3)_2\}_2]$  (**12a-c**), however, indicate the presence of two species, with two distinct lifetimes (Table 3). This is inconsistent with the NMR data, which suggested only one species in solution. However, this is more consistent with the DFT predictions and the observations made for the scandium complexes described in Chapter 2. The observation of two species for the neodymium complexes therefore suggests that the two species may correspond to the *exo* and *endo*

isomers undergoing fast interconversion on the NMR timescale. One isomer possesses a significantly longer lifetime than the other, indicating that the neodymium in one isomer is more shielded from proximate quenchers than in the other. It is probable that the *exo* isomer is more shielded, and therefore possesses the longer emission lifetime, based upon an analysis of the DFT-calculated structures.

### 5.4.3 Photophysical properties of complexes **16** and **17a-c**

The graph in Fig. 7 depicts the emission profiles of [Pr(Bn-BOPA){NHCH<sub>2</sub>C(Ph)<sub>2</sub>C<sub>3</sub>H<sub>7</sub>}<sub>2</sub>] (**16**) and [Nd(R-BOPA){NHCH<sub>2</sub>C(Ph)<sub>2</sub>C<sub>3</sub>H<sub>7</sub>}<sub>2</sub>] (**17a-c**). R = Ph (a), Bn (b) and *i*Pr(c).



**Fig. 7** Emission profiles of [Pr(Bn-BOPA){NHCH<sub>2</sub>C(Ph)<sub>2</sub>C<sub>3</sub>H<sub>7</sub>}<sub>2</sub>] (**16**) and [Nd(R-BOPA){NHCH<sub>2</sub>C(Ph)<sub>2</sub>C<sub>3</sub>H<sub>7</sub>}<sub>2</sub>] (**17a-c**). R = Ph (a), Bn (b) and *i*Pr(c). ( $\lambda_{\text{ex}}$  445 nm)

The luminescence studies of [Pr(Bn-BOPA){NHCH<sub>2</sub>C(Ph)<sub>2</sub>C<sub>3</sub>H<sub>7</sub>}<sub>2</sub>] (**16**) provided no useful data for the purposes of this study; the data indicate the luminescence may be quenched by nearby oscillators. By coordinating a co-ligand with an N-H donor, an oscillator is brought into close proximity of the metal and is likely to cause the quenching of the excited state to be more efficient.

More information can be obtained from the emission spectra of [Nd(R-BOPA){NHCH<sub>2</sub>C(Ph)<sub>2</sub>C<sub>3</sub>H<sub>7</sub>}<sub>2</sub>] (**17a-c**). **17a-c** provide good emission profiles with measurable changes in peak position and intensity in comparison to that of [Nd(R-BOPA){N(SiMe<sub>3</sub>)<sub>2</sub>}<sub>2</sub>] (**12a-c**). This is indicative of a significant change in coordination environment, consistent with the exchange of the bis(trimethyl)silylamide ligand for the *pseudo* substrate (Scheme 1).

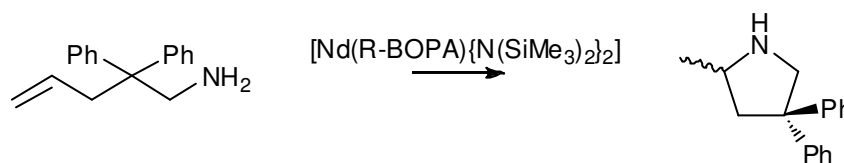
**Table 4** The lifetimes measurements of [Pr(Bn-BOPA){NHCH<sub>2</sub>C(Ph)<sub>2</sub>C<sub>3</sub>H<sub>7</sub>}<sub>2</sub>] (**16**) and [Nd(R-BOPA){NHCH<sub>2</sub>C(Ph)<sub>2</sub>C<sub>3</sub>H<sub>7</sub>}<sub>2</sub>] (**17a-c**) (toluene, N<sub>2</sub>; λ<sub>ex</sub> = 445 nm; λ<sub>em</sub> = 1055 nm). R = Ph (**a**), Bn (**b**) and iPr (**c**)

Entry	Compound	Lifetime, τ (ns)
1	16	32
2	17a	71, 165 (90%)
3	17b	41, 182 (93%)
4	17c	111, 267 (59%)

The lifetimes of the four complexes [Pr(Bn-BOPA){NHCH<sub>2</sub>C(Ph)<sub>2</sub>C<sub>3</sub>H<sub>7</sub>}<sub>2</sub>] (**16**) and [Nd(R-BOPA){NHCH<sub>2</sub>C(Ph)<sub>2</sub>C<sub>3</sub>H<sub>7</sub>}<sub>2</sub>] (**17a-c**) were measured and are shown in Table 4. For the Nd(III) complexes, there are two lifetimes for each complex, similar to [Nd(R-BOPA){N(SiMe<sub>3</sub>)<sub>2</sub>}<sub>2</sub>] (**12a-c**), indicating that there are still two isomers in solution. The lifetimes of the two species are remarkably different, and suggest that the main component (60-95%) represents a well shielded Nd(III) centre. The second component (10-30%), has a significantly shorter lifetime and suggests a species that is more readily quenched by proximate C-H oscillators. This is consistent with the DFT calculated structures of the lanthanum complexes discussed previously, in which one isomer has a more shielded metal centre than the other. In comparison to [Nd(R-BOPA){N(SiMe<sub>3</sub>)<sub>2</sub>}<sub>2</sub>] (**12a-c**) the lifetimes of

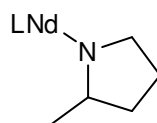
$[\text{Nd}(\text{R-BOPA})\{\text{NHCH}_2\text{C}(\text{Ph})_2\text{C}_3\text{H}_7\}_2]$  have decreased. This is due to the change in coordination sphere, where the neodymium centres in **17a-b** are less shielded from X-H quenchers (*i.e.* the presence of additional N-H groups in close proximity to the metal centre). The differences observed for these complexes are likely owing to a combination of the proximity of the stereodirecting group of the BOPA ligand to the metal (*i.e.* the proximity of the stereodirecting group's C-H groups), and its efficiency at shielding the metal from solvent molecules (*i.e.* relating to the steric footprint of the group).

The lifetime of  $[\text{Nd}(\text{Bn-BOPA})\{\text{N}(\text{SiMe}_3)_2\}_2]$  (**12b**) during catalysis was also measured (Scheme 3). For ease of comparison the lifetimes of all the neodymium complexes  $[\text{Nd}(\text{R-BOPA})\{\text{N}(\text{SiMe}_3)_2\}_2]$  (**12a-c**),  $[\text{Nd}(\text{R-BOPA})\{\text{NHCH}_2\text{C}(\text{Ph})_2\text{C}_3\text{H}_7\}_2]$  (**17a-c**) have been collated in Table 5.



**Scheme 3** Catalysis reaction used to measure lifetime of the catalyst resting state. R = Bn

Upon adding substrate **B** to  $[\text{Nd}(\text{Bn-BOPA})\{\text{N}(\text{SiMe}_3)_2\}_2]$  (**12b**) the emission lifetime decreased from 308 to 252 ns. It is likely that the species measured at this point was the cyclised N-bound pyrrolidine product, since the substrate will spontaneously undergo hydroamination/cyclisation under these conditions (Fig. 8).



**Fig. 8** Cyclised N-bound pyrrolidine species

An increase in the emission lifetime compared to the *pseudo* substrate complex (182 ns) suggests that there is a removal or reduction in the proximity of X-H oscillators, which is consistent with the removal of a coordinated NH group (*i.e.* substrate coordinated before cyclisation), in favour of the N-bound pyrrolidine (*i.e.* after cyclisation).

**Table 5** Lifetime measurements of  $[\text{Nd}(\text{R-BOPA})\{\text{N}(\text{SiMe}_3)_2\}_2]$  (**12a-c**),  $[\text{Nd}(\text{R-BOPA})\{\text{NHCH}_2\text{C}(\text{Ph})_2\text{C}_3\text{H}_7\}_2]$  (**17a-c**) and  $[\text{Nd}(\text{Bn-BOPA})\{\text{N}(\text{SiMe}_3)_2\}_2]$  (**12b**) during catalysis (toluene,  $\text{N}_2$ ;  $\lambda_{\text{ex}} = 445 \text{ nm}$ ;  $\lambda_{\text{em}} = 1055 \text{ nm}$ ). R = Ph (**a**), Bn (**b**) and *i*Pr (**c**)

Entry	Compound	Lifetime, $\tau$ (ns)
1	12a	129, 677 (90%)
2	12b	41, 308 (80%)
3	12c	148, 621 (70%)
4	17a	71, 165 (90%)
5	17b	41, 182 (93%)
6	17c	111, 267 (59%)
7	12b + B	81, 252 (85%)

Interestingly, the photophysical measurements allow us to analyse the relative proportions of the isomers present when bearing the *pseudo* substrate. This is a significant breakthrough, since this information was unavailable using NMR spectroscopy, which indicated the presence of only one isomer (presumably interconverting, as discussed above). Since the structures of  $[\text{Nd}(\text{R-BOPA})\{\text{NHCH}_2\text{C}(\text{Ph})_2\text{C}_3\text{H}_7\}_2]$  (**17a-c**) are comparable to the proposed catalytic intermediate during the hydroamination cycle,<sup>15, 16</sup> it is appropriate to compare the enantioselectivities obtained from the precatalysts  $[\text{Nd}(\text{R-BOPA})\{\text{N}(\text{SiMe}_3)_2\}_2]$  (**12a-c**), with speciation information obtained for  $[\text{Nd}(\text{R-BOPA})\{\text{NHCH}_2\text{C}(\text{Ph})_2\text{C}_3\text{H}_7\}_2]$  (**17a-c**). It has already been suggested that the *exo* isomer is likely to exert the greatest degree

of stereocontrol in catalysis, and it is noteworthy that the relative proportion of the two species of  $[\text{Nd}(\text{R-BOPA})\{\text{NHCH}_2\text{C}(\text{Ph})_2\text{C}_3\text{H}_7\}_2]$  (**17a-c**) reflect the enantioselectivities obtained when  $[\text{Nd}(\text{R-BOPA})\{\text{N}(\text{SiMe}_3)_2\}_2]$  (**12a-c**) are employed in the hydroamination reaction, Table 6. The phenyl and benzyl derivatives contain 90% and 93% *exo* respectively (essentially identical within experimental error), and give the highest enantiomeric excesses, whereas the isopropyl derivative contains less (59%) of the *exo* isomer and give a lower enantiomeric excess.<sup>17</sup>

**Table 6** Lifetime measurements of precatalysts  $[\text{Nd}(\text{R-BOPA})\{\text{N}(\text{SiMe}_3)_2\}_2]$  (**12a-c**),  $[\text{Nd}(\text{R-BOPA})\{\text{NHCH}_2\text{C}(\text{Ph})_2\text{C}_3\text{H}_7\}_2]$  (**17a-c**) and enantioselectivities obtained in the hydroamination reaction using substrate **B** in toluene, (toluene,  $\text{N}_2$ ;  $\lambda_{\text{ex}} = 445 \text{ nm}$ ;  $\lambda_{\text{em}} = 1055 \text{ nm}$ ). R = Ph (**a**), Bn (**b**) and iPr (**c**).

Entry	Precatalyst	R	13 lifetime, $\tau$ (ns)	17 lifetime, $\tau$ (ns)	ee <sup>a</sup>
1	12a	Ph	129, 677 (90%)	71, 165 (90%)	44
2	12b	Bn	41, 308 (80%)	41, 182 (93%)	46
3	12c	iPr	148, 621 (70%)	111, 267 (59%)	36

<sup>a</sup> Determined by  $^1\text{H}$  NMR using R-(-)-*O*-acetylmandelic acid.

These observations therefore suggest that luminescence spectroscopy, until now an untried and unproven method for probing catalytically active lanthanide complexes could be used to elucidate detailed information about complexes involved in catalytic reactions. This may involve the detection of multiple species, but also can provide crucial information pertaining to the coordination sphere and the degree of ‘shielding’ offered by the supporting ligand (*via* the emission lifetime).

## 5.5 Summary

Density functional theory (DFT) was used to calculate the structures of complexes bearing a *pseudo* substrate that is representative of the intermediate present during the catalytic hydroamination of aminoolefins. These calculations gave insight into the relative space at the lanthanide metals for the two isomers. These isomers could not be detected by NMR spectroscopy, but were detected using luminescence spectroscopy. The emission lifetimes of each isomer were considerably different, consistent with a visual analysis of the calculated structures.

This area of research represents the first such use of luminescence spectroscopy, and its continued development is likely to prove useful in providing information regarding the encapsulation of a metal during catalytic reactions.

## 5.6 References for Chapter 6

- 1 S. Shionoya and W. M. Yen, 'Phosphor Handbook', CRC Press Inc., 1999.
- 2 J. Kido and Y. Okamoto, *Chem. Rev.*, 2002, **102**, 2357.
- 3 A. de Bettencourt-Dias, *Dalton Trans.*, 2007, **2229**, 2241.
- 4 K. Matsumoto and J. G. Yuan, 'Metal Ions in Biological Systems', Marcel Dekker Inc., 2003.
- 5 S. Faulkner, S. J. A. Pope, and B. P. Burton-Pye, *Appl. Spectrosc. Rev.*, 2005, **40**, 1.
- 6 J. -C. G. Bunzli, 'Spectroscopic Properties of Rare Earth in Optical Materials', Springer, 2005.
- 7 A. de Bettencourt-Dias, *Curr. Org. Chem*, 2007, **11**, 1460.
- 8 A. De Bettencourt-Dias, P. S. Barber, S. Viswanathan, D. T. de Lill, A. Rollett, G. Ling, and S. Altun, *Inorg. Chem.*, 2010, **49**, 8848.
- 9 A. de Bettencourt-Dias, S. Viswanathan, and A. Rollett, *J. Am. Chem. Soc.*, 2007, **129**, 15436.
- 10 M. J. Frisch, G. W. Trucks, H. B. Schlegel, G. E. Scuseria, M. A. Robb, J. R. Cheeseman, G. Scalmani, V. Barone, B. Mennucci, G. A. Petersson, H. Nakatsuji, M. Caricato, X. Li, H. P. Hratchian, A. F. Izmaylov, J. Bloino, G. Zheng, J. L. Sonnenberg, M. Hada, M. Ehara, K. Toyota, R. Fukuda, J. Hasegawa, M. Ishida, T. Nakajima, Y. Honda, O. Kitao, H. Nakai, T. Vreven, J. A. Montgomery Jr, J. E. Peralta, F. Ogliaro, M. Bearpark, J. J. Heyd, E. Brothers, K. N. Kudin, V. N. Staroverov, T. Keith, R. Kobayashi, J. Normand, K. Raghavachari, A. Rendell, J. C. Burant, S. S. Iyengar, J. Tomasi, M. Cossi, N. Rega, J. M. Millam, M. Klene, J. E. Knox, J. B. Cross, V. Bakken, C. Adamo, J. Jaramillo, R. Gomperts, R. E. Stratmann, O. Yazyev, A. J. Austin, R. Cammi, C. Pomelli, J. W. Ochterski, R. L. Martin, K. Morokuma, V. G. Zakrzewski, G. A. Voth, P. Salvador, J. J. Dannenberg, S.



- Dapprich, A. D. Daniels, O. Farkas, J. B. Foresman, J. V. Ortiz, J. Cioslowski, and D. J. Fox, in 'Gaussian 09, Revision C.01', Gaussian Inc. Wallingford CT, 2010.
- 11 E. M. Schultz, C. M. Robb, and J. M. Spague, *J. Am. Chem. Soc.*, 1947, **69**, 2454
- 12 N. Chattopadhyay, A. Samanta, T. Kundu, and M. Chowdhury, *J. Photochem. Photobiol.*, 1989, **48**, 61.
- 13 Z. Hong, C. Liang, R. Li, F. Zang, D. Fan, and W. Li, *Appl. Phys. Lett.*, 2001, **79**, 1942.
- 14 G. M. Davies, S. J. A. Pope, H. Adams, S. Faulkner, and M. D. Ward, *Inorg. Chem.*, 2005, **44**, 4656.
- 15 M. R. Gagné, C. L. Stern, and T. J. Marks, *J. Am. Chem. Soc.*, 1992, **114**, 275.
- 16 A. Motta, G. Lanza, I. L. Fragalà, and T. J. Marks, *Organometallics*, 2004, **23**, 4097.
- 17 S. D. Bennett, S. J. A. Pope, and B. D. Ward, *Chem. Commun.*, 2013, **49**, 6072.

## **CHAPTER 6**

### **Experimental and characterising data**

## 6.1 General Methods and Instrumentation

All manipulations of air and moisture sensitive species were performed under an atmosphere of argon or dinitrogen using standard Schlenk line or glove box techniques. Solvents were dried by passing through an alumina drying column incorporated into an MBraun SPS800 solvent purification system, except in the case of tetrahydrofuran (THF), which was dried over potassium and distilled under argon. All solvents were degassed and stored under argon in Teflon valve ampoules. Deuterated chloroform was passed through a column of basic alumina before being stored over 4 Å molecular sieves prior to use. Deuterated solvents were dried over potassium ( $C_6D_6$ ,  $C_7D_8$ ) or calcium hydride ( $C_6D_5Br$ ,  $CD_2Cl_2$ ), distilled under reduced pressure and stored under dinitrogen in Teflon valve ampoules. Air sensitive NMR samples were prepared under dinitrogen in 5 mm Nolan tubes fitted with J. Young Teflon valves, all other samples were prepared in Wilmad 5 mm NMR tubes. All other reagents were purchased from commercial suppliers and used as received unless otherwise stated.

$^1H$  and  $^{13}C\{^1H\}$  NMR spectra were recorded on Bruker Avance DPX 400, 500, 600 spectrometers,  $^{19}F$  and  $^{11}B\{^1H\}$  NMR spectra were recorded on a Jeol Eclipse 300 MHz spectrometer. NMR spectra were referenced internally relative to the residual protio-solvent ( $^1H$ ) or solvent ( $^{13}C$ ) resonances, and are reported relative to tetramethylsilane ( $\delta = 0$  ppm). Chemical shifts are quoted in  $\delta$  (ppm) and coupling constants in Hertz. In all cases, NMR assignments were confirmed by the use of two-dimensional  $^1H$ - $^1H$  or  $^1H$ - $^{13}C$  correlation experiments (HSQC and HMBC).

Infrared spectra were prepared as KBr pellets and were recorded on a Jasco 660-Plus FT/IR spectrometer. Infrared data are quoted in wavenumbers ( $cm^{-1}$ ). All photophysical data were obtained on a Jobin Yvon-Horiba Fluorolog-3 spectrometer fitted with a JY TBX picosecond photodetection module. A Hamamatsu R5509-73 detector (cooled to  $-80$  °C using

a C9940 housing) was used for near-IR luminescence measurements. For the near-IR lifetimes the pulsed laser source was a Continuum Minilite Nd:YAG configured for 355 nm output, whilst for fluorescence lifetimes a 459 nm NanoLEDs (operating at 1 MHz) was utilised. All lifetime data were collected using the JY-Horiba FluoroHub single photon counting module in multi-channel scalar mode. Lifetimes were obtained using the provided software, DAS6.

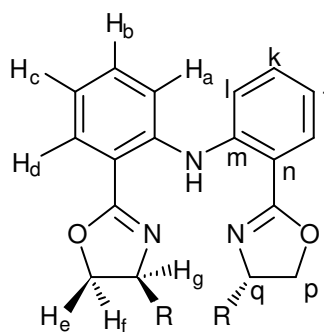
MALDI-ToF-MS analysis was performed on a Waters MALDI micro equipped with a 337 nm nitrogen laser. An accelerating voltage of 25kV was applied. The polymer samples were dissolved in THF at a concentration of 1 mg mL<sup>-1</sup>. The cationisation agent used was potassium trifluoroacetate (Fluka, > 99%) dissolved in THF at a concentration of 5 mg mL<sup>-1</sup>. The matrix used was *trans*-2-[3-(4-*tert*-butylphenyl)-2-methy-2-propenylidene]malononitrile (DCTB) (Fluka) and was dissolved in THF at a concentration of 40 mg mL<sup>-1</sup>. Solutions of matrix, salt and polymer were mixed in a volume ratio of 4:1:4, respectively. The mixed solution was hand-spotted on a stainless steel MALDI target and left to dry. The spectra were recorded in reflectron mode.

Polymer molecular weights ( $M_n$ ,  $M_w$ ) were determined by GPC using a Polymer Laboratories Plgel Mixed-D column (300 mm length, 7.5 mm diameter) and a Polymer Laboratories PL-GPC50 Plus instrument equipped with a refractive index detector. THF (HPLC grade) was used as an eluent at 30 °C with a flow rate of 1 mL<sup>-1</sup> min. Linear polystyrenes were used as primary calibration standards, and Mark –Houwink corrections for poly(*rac*-LA) in THF were applied for the experimental samples.<sup>1-3</sup>

Microanalysis were obtained by the elemental analysis service at London Metropolitan University. Crystallography was conducted by Cardiff University or the National Crystallography service at Southampton University.

### 6.1.1 Literature preparations

The compounds  $[\text{LiN}(\text{SiMe}_3)_2]$ ,<sup>4</sup>  $[\text{LiCH}_2\text{SiMe}_2\text{Ph}]$ ,<sup>5</sup>  $[\text{Sc}\{\text{N}(\text{SiMe}_3)_2\}_3]$ ,<sup>4</sup>  $[\text{Sc}(\text{CH}_2\text{SiMe}_2\text{Ph})_3(\text{THF})_2]$ ,<sup>5</sup>  $[\text{Y}(\text{CH}_2\text{SiMe}_2\text{Ph})_3(\text{THF})_2]$ ,<sup>5</sup>  $[\text{Y}\{\text{N}(\text{SiMe}_3)_2\}_3]$ ,<sup>6</sup>  $[\text{Sm}\{\text{N}(\text{SiMe}_3)_2\}_3]$ ,<sup>6</sup>  $[\text{Nd}\{\text{N}(\text{SiMe}_3)_2\}_3]$ ,<sup>6</sup>  $[\text{Pr}\{\text{N}(\text{SiMe}_3)_2\}_3]$ ,<sup>6</sup>  $[\text{La}\{\text{N}(\text{SiMe}_3)_2\}_3]$ <sup>6</sup> and 1-amino-2-diphenylpent-4-ene<sup>7</sup> were synthesised according to literature procedures.  $[\text{Ph}_3\text{C}][\text{B}(\text{C}_6\text{F}_5)_4]$  was kindly provided by Dr B. D. Ward and 1-amino-2-dimethylpent-4-ene was kindly provided by Dr James S. Wixey. *P* – cresol was distilled prior to use and stored under dinitrogen in a dry-box. All other compounds and reagents were purchased from chemical suppliers and used without further purification.



**Fig.1** Labelling scheme used throughout this thesis to denote specific carbons and protons of the BOPA ligand.

The assignment of NMR spectra for all complexes will refer to the number schemes for the identification of the carbon and protons of the BOPA ligand as shown within fig. 1.

## 6.2 Chapter 2

### 6.2.1 General procedure for the synthesis of R-BOPA

Thionyl chloride (10 mL) was added to a flask containing 2,2'-diaminobenzoic acid (1.4 g) and refluxed for 4 hours. The reaction mixture was allowed to cool and the thionyl

chloride removed under reduced pressure to yield a yellow/brown solid. The solid was stirred in pentane overnight at room temperature (15 mL), and the suspension was filtered the next day to yield the acyl halide as a yellow solid. Without further purification the acyl halide was used in the next step.

A DCM solution of the acyl halide (80 mL) was added dropwise to a DCM solution (20 mL) of amino alcohol (2 eqs.), Et<sub>3</sub>N (5 eqs.) and DMAP (10 mg) over a period of 3 hours at -10 °C. The resulting solution was allowed to warm to room temperature and left to stir for 16 hours. The reaction mixture was then washed with a saturated solution of NH<sub>4</sub>Cl (2 x 50 mL), 2M HCl (2 x 50 mL), 2M NaCO<sub>3</sub> (2 x 50 ml) and brine (2 x 50 mL), and subsequent removal of solvent under reduced pressure yielded a yellow/brown solid. The bishydroxyamide was purified by column chromatography (ethyl acetate) to yield a pale yellow solid. Spectroscopy data consistent to that reported.

To a DCM solution (20 mL) of the bishydroxyamide, Et<sub>3</sub>N (8 eqs.) and DMAP (10 mg), a DCM solution (50 mL) of TsCl (2 eqs.) was added at 0 °C. The reaction mixture was allowed to stir at room temperature for 3 days, after which, the mixture was washed with a saturated solution of NH<sub>4</sub>Cl (2 x 50 mL) and brine (2 x 50 mL). Solvent was then removed under reduced pressure to yield a yellow/brown solid. The BOPA ligand was purified by column chromatography (DCM) to yield the BOPA ligand as a pale yellow solid. Spectroscopy data were consistent with that reported.

### 6.2.1.1 Ph-BOPA (2.1a)

<sup>1</sup>H NMR (400.1 MHz, CDCl<sub>3</sub>, 293 K) δ<sub>H</sub> 7.88 (dd, <sup>4</sup>J<sub>HH</sub> = 1.40 Hz, <sup>3</sup>J<sub>HH</sub> = 8.00 Hz, NArH<sup>d</sup>, 2 H), 7.53 (d, <sup>3</sup>J<sub>HH</sub> = 8.20 Hz, NArH<sup>a</sup>, 2 H), 7.37 - 7.12 (m, 12 H), 6.96 - 6.87 (m, NArH<sup>c</sup>, 2 H), 5.17 (dd, <sup>3</sup>J<sub>HH</sub> = 10.20 Hz, <sup>3</sup>J<sub>HH</sub> = 8.20 Hz, H<sup>e</sup>, 2 H), 4.46 (dd, <sup>3</sup>J<sub>HH</sub> = 10.20 Hz, <sup>2</sup>J<sub>HH</sub> = 8.20 Hz, H<sup>e</sup>, 2 H), 3.98 (app. t, <sup>2</sup>J<sub>HH</sub> = 8.20 Hz, H<sup>f</sup>, 2 H).

$^1\text{H}$  NMR (400.1 MHz,  $\text{C}_6\text{D}_6$ , 293 K)  $\delta_{\text{H}}$  8.13 (dd,  $^4J_{\text{HH}} = 1.61$  Hz,  $^3J_{\text{HH}} = 7.89$  Hz, NArH<sup>d</sup>, 2 H), 7.53 (dd,  $^4J_{\text{HH}} = 1.02$  Hz,  $^3J_{\text{HH}} = 8.48$  Hz, NArH<sup>a</sup>, 2 H), 7.07-6.96 (m, 12 H), 6.76 (app. t,  $^3J_{\text{HH}} = 7.60$  Hz, NArH<sup>c</sup>, 2 H), 4.95 (dd,  $^3J_{\text{HH}} = 8.04$  Hz,  $^3J_{\text{HH}} = 9.2$  Hz, H<sup>g</sup>, 2 H), 4.00 (dd,  $^3J_{\text{HH}} = 8.04$  Hz,  $^2J_{\text{HH}} = 10.23$  Hz, H<sup>e</sup>, 2 H), 3.67 (app. t,  $^2J_{\text{HH}} = 8.19$  Hz, H<sup>f</sup>, 2 H).

### 6.2.1.2 Bn-BOPA (2.1b)

$^1\text{H}$  NMR (400.1 MHz,  $\text{CDCl}_3$ , 293 K)  $\delta_{\text{H}}$  7.81 (dd,  $^4J_{\text{HH}} = 1.8$  Hz,  $^3J_{\text{HH}} = 7.8$  Hz, NArH<sup>d</sup>, 2 H), 7.47 (d,  $^3J_{\text{HH}} = 8.2$  Hz, NArH<sup>a</sup>, 2 H), 7.34 - 7.16 (m, 12 H), 6.90 (dd,  $^4J_{\text{HH}} = 1.2$  Hz,  $^3J_{\text{HH}} = 7.8$  Hz, NArH<sup>c</sup>, 2 H), 4.52 - 4.43 (m, H<sup>g</sup>, 2 H), 4.2 (dd,  $^3J_{\text{HH}} = 8.6$  Hz,  $^2J_{\text{HH}} = 9.4$  Hz, H<sup>e</sup>, 2 H), 3.98 (dd,  $^3J_{\text{HH}} = 7.4$  Hz,  $^2J_{\text{HH}} = 9.4$  Hz, H<sup>f</sup>, 2 H), 3.17 (dd,  $^3J_{\text{HH}} = 5.4$  Hz,  $^2J_{\text{HH}} = 13.6$  Hz, CHHPh, 2 H), 2.72 (dd,  $^3J_{\text{HH}} = 8.6$  Hz,  $^2J_{\text{HH}} = 13.6$  Hz, CHHPh, 2 H).

$^1\text{H}$  NMR (400.1 MHz,  $\text{C}_6\text{D}_6$ , 293 K)  $\delta_{\text{H}}$  8.12 (dd,  $^4J_{\text{HH}} = 1.75$  Hz,  $^3J_{\text{HH}} = 7.89$  Hz, NArH<sup>d</sup>, 2 H), 7.52 (dd,  $^4J_{\text{HH}} = 0.73$  Hz,  $^3J_{\text{HH}} = 8.48$  Hz, NArH<sup>a</sup>, 2 H), 7.07 – 6.96 (m, 12 H), 6.76 (app. t,  $^3J_{\text{HH}} = 7.89$  Hz, NArH<sup>c</sup>, 2 H), 4.24 – 4.15 (m, H<sup>g</sup>, 2 H), 3.79 (dd,  $^3J_{\text{HH}} = 8.48$  Hz,  $^2J_{\text{HH}} = 8.19$  Hz, H<sup>e</sup>, 2 H), 3.64 (app. t,  $^2J_{\text{HH}} = 8.19$  Hz, H<sup>f</sup>, 2 H), 2.89 (dd,  $^3J_{\text{HH}} = 6.29$  Hz,  $^2J_{\text{HH}} = 13.45$  Hz, CHHPh, 2 H), 2.51 (dd,  $^3J_{\text{HH}} = 7.31$  Hz,  $^2J_{\text{HH}} = 13.45$  Hz, CHHPh, 2 H).

### 6.2.1.3 iPr-BOPA (2.1c)

$^1\text{H}$  NMR (400.1 MHz,  $\text{CDCl}_3$ , 293 K)  $\delta_{\text{H}}$  7.81 (dd,  $^4J_{\text{HH}} = 1.4$  Hz,  $^3J_{\text{HH}} = 7.8$  Hz, NArH<sup>d</sup>, 2 H), 7.40 (d,  $^3J_{\text{HH}} = 7.6$  Hz, NArH<sup>a</sup>, 2 H), 7.32 – 7.22 (m, NArH<sup>b</sup>, 2 H), 6.93 – 6.84 (m, NArH<sup>c</sup>, 2 H), 4.36 – 4.28 (m, H<sup>g</sup>, 2 H), 4.15 – 3.97 (m, H<sup>e</sup>/H<sup>f</sup>, 4 H), 1.84 – 1.71 (m,  $(\text{Me})_2\text{CH}$ , 2 H), 1.01 (d,  $^3J_{\text{HH}} = 6.6$  Hz,  $\text{MeCHMe}$ , 6 H), 0.91 (d,  $^3J_{\text{HH}} = 6.8$  Hz,  $\text{MeCHMe}$ , 6 H).

$^1\text{H}$  NMR (400.1 MHz,  $\text{C}_6\text{D}_6$ , 293 K)  $\delta_{\text{H}}$  8.12 (dd,  $^4J_{\text{HH}} = 1.61$  Hz,  $^3J_{\text{HH}} = 8.04$  Hz, NArH<sup>d</sup>, 2 H), 7.43 (d,  $^2J_{\text{HH}} = 8.19$  Hz, NArH<sup>a</sup>, 2 H), 6.96 (app. t,  $^3J_{\text{HH}} = 7.45$  Hz, NArH<sup>b</sup>, 2 H), 6.73 (app. t,  $^3J_{\text{HH}} = 7.31$  Hz, NArH<sup>c</sup>, 2 H), 3.98 – 3.88 (m, 4 H), 3.71 – 3.62 (m, 2 H), 1.60 – 1.49 (m, (Me)<sub>2</sub>CH, 2 H), 0.98 (d,  $^3J_{\text{HH}} = 6.72$  Hz, MeCHMe, 6 H), 0.77 (d,  $^3J_{\text{HH}} = 7.16$  Hz, MeCHMe, 6 H).

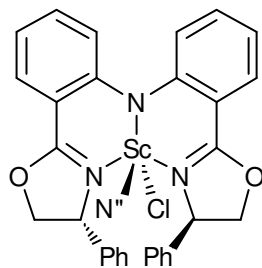
### 6.2.2 [Sc{N(SiMe<sub>3</sub>)<sub>2</sub>}Cl(THF)] (1)

A pentane solution (20 ml) of LiN(SiMe<sub>3</sub>)<sub>2</sub> (4.54 mmol) was added dropwise to a suspension of [ScCl<sub>3</sub>(THF)<sub>3</sub>] (2.72 mmol) in THF (20 mL) at 0 °C. The reaction mixture was left to warm to room temperature and stir overnight by which time all reactants had gone into solution. The solvent was removed under reduced pressure to yield a white solid. The scandium amide was extracted into pentane and recrystallised at – 20 °C to yield colourless prismatic crystals. Yield 78%;  $^1\text{H}$  NMR (400.1 MHz,  $\text{C}_6\text{D}_6$ , 293 K)  $\delta_{\text{H}}$  3.82 (4H, br s), 1.25 (4H, br s) 0.39 (36H, s) ppm;  $^{13}\text{C}\{^1\text{H}\}$  NMR (100.6 MHz,  $\text{C}_6\text{D}_6$ , 293 K)  $\delta_{\text{C}}$  62.6, 25.5, 4.0 ppm.

### 6.2.3 General procedure for [Sc(R-BOPA){N(SiMe<sub>3</sub>)<sub>2</sub>}Cl] (2a-c)

To a solution of [Sc{N(SiMe<sub>3</sub>)<sub>2</sub>}<sub>2</sub>Cl(THF)] in THF (20 ml) the BOPA ligand (1 eq.) in THF (10 ml) was added dropwise at 0 °C. The reaction mixture was stirred at 40 °C for 48 hours after which the solvent was removed under reduced pressure. The resulting yellow solid was washed with cold pentane (5 ml) and dried in *vacuo* to yield the complex (2a-c).





### 6.2.3.1 [Sc(Ph-BOPA){N(SiMe<sub>3</sub>)<sub>2</sub>}Cl] (2a) 82%

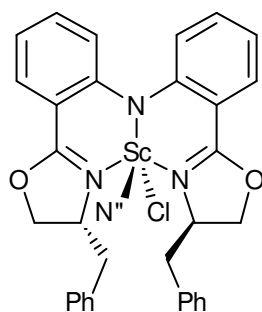
#### *exo* isomer

<sup>1</sup>H NMR (500.1 MHz, C<sub>6</sub>D<sub>6</sub>, 293 K) δ<sub>H</sub> 8.06 (dd, <sup>3</sup>J<sub>HH</sub> = 8.4 Hz, <sup>4</sup>J<sub>HH</sub> = 2.2 Hz, NArH<sup>d</sup>, 1 H), 7.84 (dd, <sup>3</sup>J<sub>HH</sub> = 8.0 Hz, <sup>4</sup>J<sub>HH</sub> = 1.6 Hz, NArH<sup>d</sup>, 1 H), 7.42 (d, <sup>3</sup>J<sub>HH</sub> = 7.7 Hz, *p*-C<sub>6</sub>H<sub>5</sub>, 2 H), 7.28 (d, <sup>3</sup>J<sub>HH</sub> = 8.2 Hz, NArH<sup>a</sup>, 1 H), 7.14 – 7.03 (m, 4 H), 6.95 (app. t, <sup>3</sup>J<sub>HH</sub> = 7.1 Hz, NArH<sup>b</sup>, 2 H), 6.83 – 6.77 (m, 5 H), 6.59 – 6.54 (m, NArH<sup>c</sup>, 2 H), 6.10 (dd, <sup>3</sup>J<sub>HH</sub> = 10.1 Hz, <sup>3</sup>J<sub>HH</sub> = 5.2 Hz, H<sup>g</sup>, 1 H), 6.00 (dd, <sup>3</sup>J<sub>HH</sub> = 9.6 Hz, <sup>3</sup>J<sub>HH</sub> = 3.6 Hz, H<sup>g</sup>, 1 H), 4.22 (app. t, <sup>3</sup>J<sub>HH</sub> = 8.7 Hz, H<sup>e</sup>, 1 H), 3.82 – 3.77 (m, H<sup>e</sup>/H<sup>f</sup>, 2 H), 3.58 (dd, <sup>2</sup>J<sub>HH</sub> = 9.6 Hz, <sup>3</sup>J<sub>HH</sub> = 1.4 Hz, H<sup>f</sup>, 1 H), 0.51 (s, N(SiMe<sub>3</sub>)<sub>2</sub>, 9 H), -0.33 (s, N(SiMe<sub>3</sub>)<sub>2</sub>, 9 H) ppm; <sup>13</sup>C{<sup>1</sup>H} NMR (100.6 MHz, C<sub>6</sub>D<sub>6</sub>, 293 K) δ<sub>C</sub> 169.0 (C=N), 168.8 (C=N), 156.0 (NArC<sup>m</sup>), 151.9 (NArC<sup>m</sup>), 141.8 (*ipso*-C<sub>6</sub>H<sub>5</sub>), 140.5 (*ipso*-C<sub>6</sub>H<sub>5</sub>), 134.5 (NArC<sup>k</sup>), 132.5 (NArC<sup>i</sup>), 130.3 (NArC<sup>i</sup>), 129.6 (NArC<sup>l</sup>), 129.3 (oxaz-ph), 129.3 (oxaz-ph), 128.8, 128.7, 126.2, 122.7, 119.3, 119.1 (NArC<sup>j</sup>), 116.0 (NArC<sup>j</sup>), 110.6 (NArC<sup>n</sup>), 76.1 (C<sup>p</sup>), 74.3 (C<sup>p</sup>), 70.7 (C<sup>q</sup>), 70.5 (C<sup>q</sup>), 5.8 (N(SiMeMe)<sub>2</sub>), 5.1 (N(SiMeMe)<sub>2</sub>) ppm.

#### *endo* isomer

<sup>1</sup>H NMR (500.1 MHz, C<sub>6</sub>D<sub>6</sub>, 293 K) δ<sub>H</sub> 8.04 (dd, <sup>3</sup>J<sub>HH</sub> = 8.04 Hz, <sup>4</sup>J<sub>HH</sub> = 2.05 Hz, NArH<sup>d</sup>, 2 H), 7.95 (br.d, <sup>3</sup>J<sub>HH</sub> = 8.19 Hz, *p*-C<sub>6</sub>H<sub>5</sub>, 2 H), 7.33 (br.d, <sup>3</sup>J<sub>HH</sub> = 8.48 Hz, NArH<sup>a</sup>, 2 H), 7.23-7.18 (m, 2 H), 7.14 – 7.10 (m, 4 H), 6.88 (dd, <sup>3</sup>J<sub>HH</sub> = 7.31 Hz, <sup>4</sup>J<sub>HH</sub> = 1.90 Hz, NArH<sup>b</sup>, 2 H), 6.67 (t, <sup>3</sup>J<sub>HH</sub> = 6.72 Hz, 2 H), 6.51 (t, <sup>3</sup>J<sub>HH</sub> = 8.77 Hz, NArH<sup>c</sup>, 2 H), 6.37-6.31 (m, H<sup>g</sup>, 1 H), 5.70 (dd, <sup>3</sup>J<sub>HH</sub> = 8.33 Hz, <sup>4</sup>J<sub>HH</sub> = 2.49 Hz, H<sup>g</sup>, 1 H), 4.45-4.35 (m, H<sup>e</sup>/H<sup>f</sup>, 2 H), 3.85 – 3.81 Hz (m, H<sup>e</sup>, 1 H), 3.72 – 3.67 (m, H<sup>f</sup>, 1 H), 0.29 (s, N(SiMe<sub>3</sub>)<sub>2</sub> 18 H); IR (ν cm<sup>-1</sup>) (KBr): 3058 (w), 3028 (w), 2961 (m), 2900 (w), 1624 (s) (C=N), 1608 (s) (C=N), 1580 (m), 1560 (w), 1539

(w), 1464 (s), 1431 (m), 1384 (m), 1322 (w), 1262 (s), 1227 (s), 1159 (m), 1074 (s), 1053 (m), 953 (w), 927 (w), 866 (w), 841 (m), 799 (m), 750 (s), 698 (s)  $\text{cm}^{-1}$ .



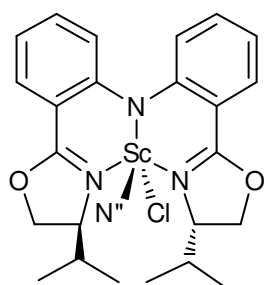
### 6.2.3.2 [Sc(Bn-BOPA){N(SiMe<sub>3</sub>)<sub>2</sub>}Cl] (2b) 80%

#### *exo* isomer

<sup>1</sup>H NMR (500.1 MHz, C<sub>6</sub>D<sub>6</sub>, 293 K)  $\delta_{\text{H}}$  8.00 (dd, <sup>4</sup>*J* = 1.6 Hz, <sup>3</sup>*J* = 8.0 Hz, NArH<sup>d</sup>, 1 H), 7.74 (dd, <sup>4</sup>*J*<sub>HH</sub> = 1.6 Hz, <sup>3</sup>*J*<sub>HH</sub> = 8.0 Hz, NArH<sup>d</sup>, 1 H), 7.38 (d, <sup>3</sup>*J*<sub>HH</sub> = 7.41 Hz, *p*-CH<sub>2</sub>C<sub>6</sub>H<sub>5</sub>, 1 H), 7.33 (d, <sup>3</sup>*J*<sub>HH</sub> = 8.2 Hz, *p*-CH<sub>2</sub>C<sub>6</sub>H<sub>5</sub>, 1 H), 7.14-6.94 (m, 4 H), 6.93-6.90 (m, *m*-CH<sub>2</sub>C<sub>6</sub>H<sub>5</sub>, 4 H), 6.82 (d, <sup>3</sup>*J*<sub>HH</sub> = 8.7 Hz, NArH<sup>a</sup>, 1 H), 6.75 (m, *o*-CH<sub>2</sub>C<sub>6</sub>H<sub>5</sub>, 2 H), 6.74 (m, *o*-CH<sub>2</sub>C<sub>6</sub>H<sub>5</sub>, 2 H), 6.56 (app. t, <sup>3</sup>*J*<sub>HH</sub> = 7.6 Hz, NArH<sup>c</sup>, 1 H), 5.61 (m, H<sup>g</sup>, 1 H), 5.24 (m, H<sup>g</sup>, 1 H), 4.41 (dd, <sup>2</sup>*J*<sub>HH</sub> = 12.9 Hz, <sup>3</sup>*J*<sub>HH</sub> = 2.7 Hz, CHHC<sub>6</sub>H<sub>5</sub>, 1 H), 3.92 (dd, <sup>2</sup>*J*<sub>HH</sub> = 9.3 Hz, <sup>3</sup>*J*<sub>HH</sub> = 4.3 Hz, H<sup>e</sup>, 1 H), 3.88 (d, <sup>2</sup>*J*<sub>HH</sub> = 9.0 Hz, H<sup>e</sup>, 1 H), 3.83 (d, <sup>2</sup>*J*<sub>HH</sub> = 9.0 Hz, H<sup>f</sup>, 1 H), 3.77 (app. t, <sup>2</sup>*J*<sub>HH</sub> = 9.3 Hz, H<sup>f</sup>, 1 H), 2.83 (app. t, <sup>2</sup>*J*<sub>HH</sub> = 12.5 Hz, CHHC<sub>6</sub>H<sub>5</sub>, 1 H), 2.81 (app. t, <sup>2</sup>*J*<sub>HH</sub> = 6.9 Hz, CHHC<sub>6</sub>H<sub>5</sub>, 1 H), 2.64 (dd, <sup>2</sup>*J*<sub>HH</sub> = 7.3 Hz, <sup>3</sup>*J*<sub>HH</sub> = 6.3 Hz, CHHC<sub>6</sub>H<sub>5</sub>, 1 H), 0.48 (s, N(SiMe<sub>3</sub>)<sub>2</sub>, 9 H), 0.06 (s, N(SiMe<sub>3</sub>)<sub>2</sub>, 9 H) ppm; <sup>13</sup>C{<sup>1</sup>H} NMR (100.6 MHz, C<sub>6</sub>D<sub>6</sub>, 293 K)  $\delta_{\text{C}}$  168.8 (C=N), 155.8 (NArC<sup>m</sup>), 152.0 (NArC<sup>m</sup>), 137.9 (*ipso* – CH<sub>2</sub>Ph), 136.0 (*ipso* – CH<sub>2</sub>Ph), 135.0 (NArC<sup>l</sup>), 134.1 (oxaz-ph or NArC<sup>j</sup>), 132.9 (oxaz-ph or NArC<sup>j</sup>), 130.3 (NArC<sup>i</sup>), 130.1 (NArC<sup>i</sup>), 129.2 (oxaz-ph), 128.8 (oxaz-ph or NArC<sup>j</sup>), 128.5 (oxaz-ph or NArC<sup>j</sup>), 128.3 (oxaz-ph or NArC<sup>j</sup>), 127.4 (NArC<sup>k</sup>), 126.8 (oxaz-ph or NArC<sup>j</sup>), 121.1 (NArC<sup>l</sup>), 120.7 (oxaz-ph or NArC<sup>j</sup>), 117.0 (NArC<sup>k</sup>), 115.9 (NArC<sup>n</sup>), 110.2 (NArC<sup>n</sup>), 72.2 (C<sup>p</sup>), 71.9 (C<sup>p</sup>), 70.3 (C<sup>q</sup>), 68.2 (C<sup>q</sup>), 42.6 (CH<sub>2</sub>Ph), 40.9 (CH<sub>2</sub>Ph), 5.7 (N(SiMe<sub>3</sub>)(SiMe<sub>3</sub>)), 5.6 (N(SiMe<sub>3</sub>)(SiMe<sub>3</sub>)) ppm.

**endo isomer**

$^1\text{H}$  NMR (500.1 MHz,  $\text{C}_6\text{D}_6$ , 293 K)  $\delta_{\text{H}}$  8.16 (d,  $^3J_{\text{HH}} = 8.0$  Hz,  $\text{NArH}^{\text{d}}$ , 2 H), 7.39 (dd,  $^3J_{\text{HH}} = 7.4$  Hz,  $p\text{-CH}_2\text{C}_6\text{H}_5$ , 2 H), 7.14-6.94 (m, 4 H), 6.93-6.90 (m,  $m\text{-CH}_2\text{C}_6\text{H}_5$ , 4 H), 6.86 (d,  $^3J_{\text{HH}} = 3.6$  Hz,  $\text{NArH}^{\text{c}}$ , 2 H), 6.64 (d,  $^3J_{\text{HH}} = 7.6$  Hz,  $o\text{-CH}_2\text{C}_6\text{H}_5$ , 4 H), 4.13 (app. t,  $^2J_{\text{HH}} = 9.6$  Hz,  $\text{H}^{\text{e}}$ , 2 H), 4.05 (m,  $\text{H}^{\text{g}}$ , 2 H), 3.59 (app. t,  $^2J_{\text{HH}} = 8.2$  Hz,  $\text{H}^{\text{f}}$ , 2 H), 3.29 (dd,  $^2J_{\text{HH}} = 12.6$  Hz,  $^3J_{\text{HH}} = 3.3$  Hz,  $\text{CHHC}_6\text{H}_5$ , 2 H), 2.50 (app. t,  $^2J_{\text{HH}} = 12.6$  Hz,  $\text{CHHC}_6\text{H}_5$ , 2 H), 0.72 (s,  $\text{N}(\text{SiMe}_3)_2$ , 18 H) ppm;  $^{13}\text{C}\{^1\text{H}\}$  NMR (100.6 MHz,  $\text{C}_6\text{D}_6$ , 293 K)  $\delta_{\text{C}}$  170.9 (C=N), 155.2 ( $\text{NArC}^{\text{m}}$ ), 136.5 ( $i\text{-CH}_2\text{Ph}$ ), 134.0 ( $\text{NArC}^{\text{l}}$ ), 132.0 ( $\text{NArC}^{\text{i}}$ ), 129.3 (oxaz-ph), 127.1 (oxaz-ph or  $\text{NArC}^{\text{j}}$ ), 125.2 (oxaz-ph or  $\text{NArC}^{\text{j}}$ ), 122.0 (oxaz-ph or  $\text{NArC}^{\text{j}}$ ), 117.8 ( $\text{NArC}^{\text{k}}$ ), 112.1 ( $\text{NArC}^{\text{n}}$ ), 73.0 ( $\text{C}^{\text{p}}$ ), 66.7 ( $\text{C}^{\text{q}}$ ), 42.2 ( $\text{CH}_2\text{Ph}$ ), 6.5 ( $\text{N}(\text{SiMe}_3)_2$ ) ppm; IR ( $\nu$   $\text{cm}^{-1}$ ) (KBr): 3419 (br s), 3058 (w), 3025 (w), 2957 (m), 1634 (m) (C=N), 1610 (m) (C=N), 1580 (m), 1520 (w), 1463 (s), 1432 (m), 1405 (w), 1389 (w), 1362 (w), 1315 (m), 1262 (s), 1225 (m), 1158 (m), 1084 (m), 1052 (m), 1030 (m), 967 (w), 836 (w), 803 (m), 747 (m), 701 (m)  $\text{cm}^{-1}$ ; Anal. Calcd for  $\text{ScC}_{38}\text{H}_{46}\text{N}_4\text{O}_2\text{Si}_2$  (727.38  $\text{g mol}^{-1}$ ): C 62.75, H 6.37, N 7.70. Found: C 62.58, H 6.46, N 7.68.

**6.2.3.3[Sc(iPr-BOPA){N(SiMe<sub>3</sub>)<sub>2</sub>}Cl] (2c) 75%****exo isomer**

$^1\text{H}$  NMR (500.1 MHz,  $\text{C}_6\text{D}_6$ , 293 K)  $\delta_{\text{H}}$  8.02 (d,  $^3J_{\text{HH}} = 8.0$  Hz,  $\text{NArH}^{\text{d}}$ , 1 H), 7.89 (dd,  $^3J_{\text{HH}} = 8.2$  Hz,  $^4J_{\text{HH}} = 1.4$  Hz,  $\text{NArH}^{\text{d}}$ , 1 H), 6.98 – 6.86 (m, 3 H), 6.77 – 6.59 (m, 2 H), 6.53 (app. t,  $^3J_{\text{HH}} = 7.4$  Hz,  $\text{NArH}^{\text{c}}$ , 1 H), 5.22 – 5.17 (m,  $\text{H}^{\text{g}}$ , 1 H), 4.83 – 4.78 (m,  $\text{H}^{\text{g}}$ , 1 H), 4.10 (app. t,  $^2J_{\text{HH}} = 10.1$  Hz,  $\text{H}^{\text{e}}$ , 1 H), 4.07 – 3.98 (m,  $\text{H}^{\text{e}}$ , 1 H), 3.94 – 3.87 (m,  $\text{H}^{\text{f}}$ , 1H), 3.80 (app. t,  $^2J_{\text{HH}} =$

9.6 Hz, H<sup>f</sup>, 1 H), 2.54 – 2.44 (m, (CH<sub>3</sub>)<sub>2</sub>CH, 1 H), 1.36 – 1.29 (m, (CH<sub>3</sub>)<sub>2</sub>CH, 1 H), 0.78 (d, <sup>3</sup>J<sub>HH</sub> = 7.1 Hz, MeCHMe, 3 H), 0.56 (s, N(SiMe<sub>3</sub>)(SiMe<sub>3</sub>), 9 H), 0.52 (d, <sup>3</sup>J<sub>HH</sub> = 7.1 Hz, MeCHMe, 3 H), 0.40 – 0.33 (m, MeCHMe, 6 H), 0.05 (s, N(SiMe<sub>3</sub>)(SiMe<sub>3</sub>), 9 H) ppm; <sup>13</sup>C{<sup>1</sup>H} NMR (100.6 MHz, C<sub>6</sub>D<sub>6</sub>, 293 K) δ<sub>C</sub> 168.8 (C=N), 167.7 (C=N), 158.3 (NArC<sup>m</sup>), 157.5 (NArC<sup>m</sup>), 133.9, 132.4, 130.6 (NArC<sup>i</sup>), 129.0, 127.5, 121.2, 118.9, 117.5 (NArC<sup>n</sup>), 117.4 (NArC<sup>j</sup>), 114.9 (NArC<sup>n</sup>), 71.7 (C<sup>p</sup>), 70.1 (C<sup>p</sup>), 68.7 (C<sup>q</sup>), 68.6 (C<sup>q</sup>), 31.1 ((CH<sub>3</sub>)<sub>2</sub>CH), 30.8 ((CH<sub>3</sub>)<sub>2</sub>CH), 20.0 (CH<sub>3</sub>CHCH<sub>3</sub>), 18.4 (CH<sub>3</sub>CHCH<sub>3</sub>), 15.2 (CH<sub>3</sub>CHCH<sub>3</sub>), 14.3 (CH<sub>3</sub>CHCH<sub>3</sub>), 6.1 (N(SiMe<sub>3</sub>)(SiMe<sub>3</sub>)), 5.3 (N(SiMe<sub>3</sub>)(SiMe<sub>3</sub>)) ppm.

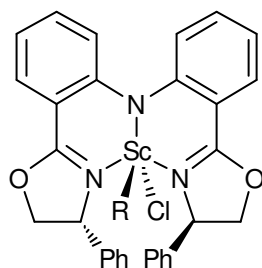
### **endo isomer**

<sup>1</sup>H NMR (500.1 MHz, C<sub>6</sub>D<sub>6</sub>, 293 K) δ<sub>H</sub> 8.11 (dd, <sup>3</sup>J<sub>HH</sub> = 8.5 Hz, <sup>4</sup>J<sub>HH</sub> = 1.7 Hz, NArH<sup>d</sup>, 1 H), 8.05 (dd, <sup>3</sup>J<sub>HH</sub> = 8.4 Hz, <sup>4</sup>J<sub>HH</sub> = 1.6 Hz, NArH<sup>d</sup>, 1 H), 7.98 (dd, <sup>3</sup>J<sub>HH</sub> = 8.0 Hz, <sup>4</sup>J<sub>HH</sub> = 1.6 Hz, NArH<sup>a</sup>, 1 H), 7.56 (dd, <sup>4</sup>J<sub>HH</sub> = 1.4 Hz, <sup>3</sup>J<sub>HH</sub> = 8.1 Hz, NArH<sup>a</sup>, 1 H), 7.08 (app. t, <sup>3</sup>J<sub>HH</sub> = 7.9 Hz, NArH<sup>b</sup> or NArH<sup>c</sup>, 1 H), 6.98 – 6.86 (m, NArH<sup>b</sup> or NArH<sup>c</sup>, 1 H), 6.77 – 6.59 (m, 2 H), 4.78 (m, H<sup>g</sup>, 1 H), 4.07 – 3.98 (m, 2 H), 3.94 – 3.87 (m, 2 H), 3.71 (app. t, <sup>2</sup>J<sub>HH</sub> = 9.6 Hz, H<sup>e</sup>, 1 H), 2.41 – 2.34 (m, (CH<sub>3</sub>)<sub>2</sub>CH, 1 H), 1.25 – 1.19 (m, (CH<sub>3</sub>)<sub>2</sub>CH, 1 H), 0.75 (s, N(SiMe<sub>3</sub>)(SiMe<sub>3</sub>), 9 H), 0.72 (d, <sup>3</sup>J<sub>HH</sub> = 7.6 Hz, MeCHMe, 3 H), 0.67 (d, <sup>3</sup>J<sub>HH</sub> = 6.6 Hz, MeCHMe, 3 H), 0.49 (s, N(SiMe<sub>3</sub>)(SiMe<sub>3</sub>), 9 H), 0.45 (d, <sup>3</sup>J<sub>HH</sub> = 6.6 Hz, MeCHMe 3 H), -0.02 (d, <sup>3</sup>J<sub>HH</sub> = 7.1 Hz, MeCHMe, 3 H) ppm; <sup>13</sup>C{<sup>1</sup>H} NMR (100.6 MHz, C<sub>6</sub>D<sub>6</sub>, 293 K) δ<sub>C</sub> 169.0 (C=N), 168.6 (C=N), 157.0 (NArC<sup>m</sup>), 155.6 (NArC<sup>m</sup>), 134.2 (NArC<sup>k</sup> or NArC<sup>j</sup>), 133.3, 131.8 (NArC<sup>i</sup>), 131.6, 126.6 (NArC<sup>k</sup> or NArC<sup>j</sup>), 121.3, 120.8, 120.7, 120.5 (NArC<sup>n</sup>), 119.7 (NArC<sup>n</sup>), 71.5 (C<sup>p</sup>), 70.0 (C<sup>p</sup>), 67.4 (C<sup>q</sup>), 66.9 (C<sup>q</sup>), 31.3 ((CH<sub>3</sub>)<sub>2</sub>CH), 29.8 ((CH<sub>3</sub>)<sub>2</sub>CH), 19.6 (CH<sub>3</sub>CHCH<sub>3</sub>), 18.7 (CH<sub>3</sub>CHCH<sub>3</sub>), 15.0 (CH<sub>3</sub>CHCH<sub>3</sub>), 14.5 (CH<sub>3</sub>CHCH<sub>3</sub>), 8.2 (N(SiMe<sub>3</sub>)(SiMe<sub>3</sub>)), 6.4 (N(SiMe<sub>3</sub>)(SiMe<sub>3</sub>)) ppm; IR (ν cm<sup>-1</sup>) (KBr): 2961 (s), 2907 (w), 2877 (w), 1617 (C=N), 1587 (w), 1563 (w), 1543 (w), 1483 (m), 1466 (s), 1432 (m), 1382 (m), 1322 (w), 1262 (s), 1227 (s), 1161 (m), 1097 (m), 1071 (s), 1047 (m), 1024 (m), 963 (w), 916 (w), 869 (w), 839 (w),

802 (s), 748 (m), 688 (w), 669 (w)  $\text{cm}^{-1}$ ; Anal. Calcd for  $\text{ScC}_{30}\text{H}_{46}\text{ClN}_4\text{O}_2\text{Si}_2$  ( $631.29 \text{ g mol}^{-1}$ ): C 57.08, H 7.34, N 8.87. Found: C 56.89, H 7.31, N 8.61.

### 6.2.4 General procedure for [Sc(R-BOPA)(OPhMe)Cl] (3a-c)

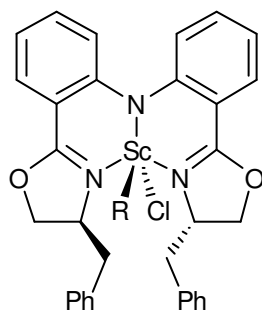
To a stirred solution of [Sc(R-BOPA)N(SiMe<sub>3</sub>)<sub>2</sub>Cl] (200 mg) in THF (15 mL), a solution of *p*-cresol (1 equiv.) in THF (5 mL) was added drop wise at 0 °C. The reaction mixture was left to stir at room temperature for 2 hours, after which the THF solution was concentrated under reduced pressure to 5 mL and pentane (20 mL) was subsequently added. The THF/pentane solution was stirred for 30 mins at -78 °C and the precipitate filtered and washed with cold pentane to yield a mixture of products, including **3a-c**.



#### 6.2.4.1 [Sc(Ph-BOPA)(OPhMe)Cl] (3a)

<sup>1</sup>H NMR (500.1 MHz, C<sub>6</sub>D<sub>6</sub>, 293 K)  $\delta_{\text{H}}$  8.09 (d, <sup>3</sup>*J*<sub>HH</sub> = 8.99 Hz, NArH<sup>d</sup>, 1 H), 8.04 (d, <sup>3</sup>*J*<sub>HH</sub> = 8.36 Hz, NArH<sup>d</sup>, 1 H), 7.48 (dd, <sup>4</sup>*J*<sub>HH</sub> = 1.73 Hz, <sup>3</sup>*J*<sub>HH</sub> = 7.72 Hz, 1 H), 7.35 (d, <sup>3</sup>*J*<sub>HH</sub> = 8.99 Hz, 1 H), 7.31 (t, <sup>3</sup>*J*<sub>HH</sub> = 7.72 Hz, 2 H), 7.19 (t, <sup>3</sup>*J*<sub>HH</sub> = 7.57 Hz, *o*-C<sub>6</sub>H<sub>5</sub>, 4 H), 7.05-6.99 (m, *p*-cresol, 2 H), 6.97 (d, <sup>3</sup>*J*<sub>HH</sub> = 7.57 Hz, *m*-C<sub>6</sub>H<sub>5</sub>, 4 H), 6.83-6.77 (m, *p*-cresol, 2 H), 6.76 (t, <sup>3</sup>*J*<sub>HH</sub> = 7.72 Hz, 1 H), 6.68 (d, <sup>3</sup>*J*<sub>HH</sub> = 8.20 Hz, 1 H), 6.62 (d, <sup>3</sup>*J*<sub>HH</sub> = 8.20 Hz, 1 H), 6.56 (t, <sup>3</sup>*J*<sub>HH</sub> = 8.36 Hz, NArH<sup>c</sup>, 1 H), 6.26 (d, <sup>3</sup>*J*<sub>HH</sub> = 7.41 Hz, H<sup>g</sup>, 2 H), 5.74 (dd, <sup>3</sup>*J*<sub>HH</sub> = 9.14 Hz, <sup>3</sup>*J*<sub>HH</sub> = 2.52 Hz, H<sup>g</sup>, 1 H), 4.67 (d, <sup>2</sup>*J*<sub>HH</sub> = 7.72 Hz, H<sup>e</sup>, 1 H), 3.58-3.47 (m, H<sup>e</sup>, 1 H), 3.46 (dd, <sup>2</sup>*J*<sub>HH</sub> = 7.72 Hz, <sup>3</sup>*J*<sub>HH</sub> = 3.00 Hz, H<sup>f</sup>, 1 H), 2.86 (t, <sup>2</sup>*J*<sub>HH</sub> = 8.67 Hz, H<sup>f</sup>, 1 H), 2.20 (s, cresol-Me, 3 H) ppm; <sup>13</sup>C{<sup>1</sup>H} NMR (100.6 MHz, C<sub>6</sub>D<sub>6</sub>, 293 K)  $\delta_{\text{C}}$  169.1 (C=N), 168.4 (C=N), 156.4 (NArC<sup>m</sup>),

145.7 (NArC<sup>m</sup>), 142.9, 142.7, 142.0 (*ipso*-C<sub>6</sub>H<sub>5</sub>), 140.8 (*ipso*-C<sub>6</sub>H<sub>5</sub>), 131.9, 131.2, 130.3, 129.7, 127.8, 127.5, 127.2, 127.0, 126.1, 125.8, 125.5, 124.8, 121.5, 121.3 (NArC<sup>j</sup>), 118.7, 117.3 (NArC<sup>j</sup>), 112.9 (NArC<sup>n</sup>), 112.6 (NArC<sup>n</sup>), 72.2 (C<sup>p</sup>), 71.8 (C<sup>p</sup>), 70.0 (C<sup>q</sup>), 69.2 (C<sup>q</sup>), 19.5 (C<sub>6</sub>H<sub>5</sub>Me) ppm.



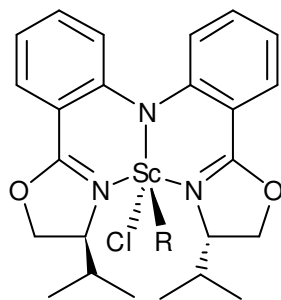
#### 6.2.4.2[Sc(Bn-BOPA)(OPhMe)Cl] (3b)

##### *exo* isomer

<sup>1</sup>H NMR (500.1 MHz, C<sub>6</sub>D<sub>6</sub>, 293 K) δ<sub>H</sub> 8.25 (d, <sup>3</sup>J<sub>HH</sub> = 7.41 Hz, NArH<sup>d</sup>, 1 H), 7.69 (d, <sup>3</sup>J<sub>HH</sub> = 8.99 Hz, NArH<sup>d</sup>, 1 H), 7.49 (d, <sup>3</sup>J<sub>HH</sub> = 8.36 Hz, *p*-cresol, 2 H), 7.27 (t, <sup>3</sup>J<sub>HH</sub> = 7.57 Hz, *p*-cresol, 2 H), 7.11 (t, <sup>3</sup>J<sub>HH</sub> = 7.73 Hz, NArH<sup>a</sup>, 1 H), 7.07 – 6.88 (m, 13 H), 6.70 (t, <sup>3</sup>J<sub>HH</sub> = 6.94 Hz, NArH<sup>a</sup>, 1 H), 6.61 (t, <sup>3</sup>J<sub>HH</sub> = 7.73 Hz, NArH<sup>c</sup>, 1 H), 5.25 (m, H<sup>g</sup>, 1 H), 5.00 (m, H<sup>g</sup>, 1 H), 4.26 (d, <sup>2</sup>J<sub>HH</sub> = 13.24 Hz, CHHC<sub>6</sub>H<sub>5</sub>, 1 H), 3.86 (d, <sup>2</sup>J<sub>HH</sub> = 10.40 Hz, H<sup>e</sup>, 1 H), 3.77 – 3.70 (m, H<sup>e</sup>/H<sup>f</sup>, 2 H), 3.41 – 3.31 (m, H<sup>f</sup>, 1 H), 3.19 (t, <sup>2</sup>J<sub>HH</sub> = 8.99 Hz, CHHC<sub>6</sub>H<sub>5</sub>, 1 H), 3.07 (t, <sup>3</sup>J<sub>HH</sub> = 7.57 Hz, CHHC<sub>6</sub>H<sub>5</sub>, 1 H), 2.26 (dd, <sup>2</sup>J<sub>HH</sub> = 13.24 Hz, <sup>3</sup>J<sub>HH</sub> = 7.73 Hz, CHHC<sub>6</sub>H<sub>5</sub>, 1 H), 2.05 (s, C<sub>6</sub>H<sub>5</sub>Me, 3 H) ppm; <sup>13</sup>C{<sup>1</sup>H} NMR (100.6 MHz, C<sub>6</sub>D<sub>6</sub>, 293 K) δ<sub>C</sub> 169.5 (C=N), 166.0 (C=N), 159.6 (NArC<sup>m</sup>), 152.4 (NArC<sup>m</sup>), 144.1, 138.7 (*i*-CH<sub>2</sub>C<sub>6</sub>H<sub>5</sub>), 132.4, 131.6 (NArC<sup>i</sup>), 130.1 (NArC<sup>i</sup>), 130.9, 129.9, 129.7, 128.9, 128.5, 128.3, 127.2 (NArC<sup>k</sup>), 126.9, 126.8, 126.5, 121.5, 119.0 (NArC<sup>k</sup>), 118.0 (NArC<sup>n</sup>), 114.0 (NArC<sup>n</sup>), 72.8 (C<sup>p</sup>), 70.4 (C<sup>p</sup>), 69.8 (C<sup>q</sup>), 68.8 (C<sup>q</sup>), 42.0 (CH<sub>2</sub>C<sub>6</sub>H<sub>5</sub>), 40.5 (CH<sub>2</sub>C<sub>6</sub>H<sub>5</sub>), 25.3 (C<sub>6</sub>H<sub>5</sub>Me) ppm.

**endo isomer**

$^1\text{H}$  NMR (500.1 MHz,  $\text{C}_6\text{D}_6$ , 293 K)  $\delta_{\text{H}}$  8.65 (d,  $^3J_{\text{HH}} = 7.41$  Hz,  $\text{NArH}^{\text{d}}$ , 1 H), 7.97 (d,  $^3J_{\text{HH}} = 7.88$  Hz,  $\text{NArH}^{\text{d}}$ , 1 H), 7.91 (d,  $^3J_{\text{HH}} = 7.73$  Hz,  $\text{NArH}^{\text{a}}$ , 1 H), 7.80 (d,  $^3J_{\text{HH}} = 7.73$  Hz, 2 H), 7.59 (d,  $^3J_{\text{HH}} = 8.67$  Hz, 1 H), 7.21 (t,  $^3J_{\text{HH}} = 8.67$  Hz, 1 H), 7.07 – 6.88 (m,  $m\text{-C}_6\text{H}_5$ , 4 H), 6.58 – 6.49 (m, 7 H), 6.42 (d,  $^3J_{\text{HH}} = 8.20$  Hz,  $o\text{-CH}_2\text{C}_6\text{H}_5$ , 4 H), 4.83 (m,  $\text{H}^{\text{g}}$ , 2 H), 4.61 (m,  $\text{H}^{\text{c}}$ , 2 H), 3.77 – 3.70 (m,  $\text{H}^{\text{f}}$ , 2 H), 3.27 (t,  $^2J_{\text{HH}} = 9.14$  Hz,  $\text{CHHC}_6\text{H}_5$ , 2 H), 2.56 (t,  $^2J_{\text{HH}} = 9.14$  Hz,  $\text{CHHC}_6\text{H}_5$ , 2 H), 2.10 (s,  $\text{C}_6\text{H}_5\text{Me}$ , 3 H) ppm;  $^{13}\text{C}\{^1\text{H}\}$  NMR (100.6 MHz,  $\text{C}_6\text{D}_6$ , 293 K)  $\delta_{\text{C}}$  167.8 (C=N), 165.7 (C=N), 147.1 ( $\text{NArC}^{\text{m}}$ ), 139.3, 132.8 ( $\text{NArC}^{\text{l}}$ ), 132.2 ( $\text{NArC}^{\text{l}}$ ), 131.8 ( $\text{NArC}^{\text{i}}$ ), 130.0 ( $\text{NArC}^{\text{i}}$ ), 129.6, 129.0, 128.7, 127.6, 127.5, 127.4, 122.6, 121.4 ( $\text{NArC}^{\text{k}}$ ), 118.6 ( $\text{NArC}^{\text{k}}$ ), 116.4 ( $\text{NArC}^{\text{n}}$ ), 71.4 ( $\text{C}^{\text{p}}$ ), 71.7 ( $\text{C}^{\text{p}}$ ), 69.0 ( $\text{C}^{\text{q}}$ ), 68.9 ( $\text{C}^{\text{q}}$ ), 41.7 ( $\text{CH}_2\text{C}_6\text{H}_5$ ), 41.3 ( $\text{CH}_2\text{C}_6\text{H}_5$ ), 20.7 ( $\text{C}_6\text{H}_5\text{Me}$ ) ppm.

**6.2.4.3[Sc(iPr-BOPA)(OPhMe)Cl] (3c)****exo isomer**

$^1\text{H}$  NMR (500.1 MHz,  $\text{C}_6\text{D}_6$ , 293 K)  $\delta_{\text{H}}$  8.04 (d,  $^3J_{\text{HH}} = 7.72$  Hz,  $\text{NArH}^{\text{d}}$ , 1 H), 7.92 (d,  $^3J_{\text{HH}} = 6.93$  Hz,  $\text{NArH}^{\text{d}}$ , 1 H), 7.84 (t,  $^3J_{\text{HH}} = 8.51$  Hz,  $\text{NArH}^{\text{a}}$ , 1 H), 7.03 (d,  $^3J_{\text{HH}} = 6.62$  Hz,  $\text{NArH}^{\text{a}}$ , 1 H), 6.97 (s,  $p\text{-cresol}$ , 4 H), 6.96 (t,  $^3J_{\text{HH}} = 8.20$  Hz,  $\text{NArH}^{\text{b}}$ , 1 H), 6.94 (t,  $^3J_{\text{HH}} = 8.96$  Hz,  $\text{NArH}^{\text{c}}$ , 1 H), 6.85 (d,  $^3J_{\text{HH}} = 9.46$  Hz,  $\text{NArH}^{\text{b}}$ , 1 H), 6.52 (t,  $^3J_{\text{HH}} = 8.04$  Hz,  $\text{NArH}^{\text{c}}$ , 1 H), 4.69-4.60 (m,  $\text{H}^{\text{g}}$ , 1 H), 4.38 (d,  $^3J_{\text{HH}} = 8.20$  Hz,  $\text{H}^{\text{g}}$ , 1 H), 3.87 (d,  $^2J_{\text{HH}} = 9.93$  Hz,  $\text{H}^{\text{c}}$ , 1 H), 3.85-3.71 (m,  $\text{H}^{\text{e}}/\text{H}^{\text{f}}$ , 2 H), 2.73 (t,  $^2J_{\text{HH}} = 9.93$  Hz,  $\text{H}^{\text{f}}$ , 1 H), 2.17 – 2.10 (m,  $(\text{CH}_3)_2\text{CH}$ , 1 H),

2.11 (s, C<sub>6</sub>H<sub>5</sub>Me, 3 H), 1.26-1.16 (m, (CH<sub>3</sub>)<sub>2</sub>CH, 1 H), 0.72 (d, <sup>3</sup>J<sub>HH</sub> = 7.09 Hz, MeCHMe, 3 H), 0.61 (d, <sup>3</sup>J<sub>HH</sub> = 5.68 Hz, MeCHMe, 3 H), 0.58- 0.47 (m, MeCHMe, 6 H) ppm; <sup>13</sup>C{<sup>1</sup>H} NMR (100.6 MHz, C<sub>6</sub>D<sub>6</sub>, 293 K) δ<sub>C</sub> 169.6 (C=N), 168.2 (C=N), 132.5 (NArC<sup>m</sup>), 131.4 (NArC<sup>m</sup>), 129.8, 129.6, 128.7, 128.7, 128.5, 127.7, 127.7, 127.0, 126.4, 125.1, 124.4, 124.1, 119.9 (NArC<sup>n</sup>), 118.9 (NArC<sup>n</sup>), 72.7 (C<sup>p</sup>), 70.8 (C<sup>p</sup>), 69.3 (C<sup>q</sup>), 65.2 (C<sup>q</sup>), 36.3 ((CH<sub>3</sub>)<sub>2</sub>CH), 33.5 ((CH<sub>3</sub>)<sub>2</sub>CH), 20.7 (MeCHMe), 18.9 (C<sub>6</sub>H<sub>5</sub>Me), 18.8 (MeCHMe), 14.7 (MeCHMe), 14.4 (MeCHMe) ppm.

#### *endo* isomer

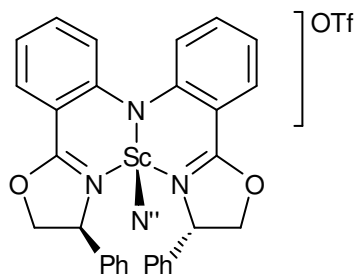
<sup>1</sup>H NMR (500.1 MHz, C<sub>6</sub>D<sub>6</sub>, 293 K) δ<sub>H</sub> 8.52 (d, <sup>3</sup>J<sub>HH</sub> = 9.30 Hz, NArH<sup>d</sup>, 1 H), 7.98 (d, <sup>3</sup>J<sub>HH</sub> = 9.30 Hz, NArH<sup>d</sup>, 1 H), 7.19 (t, <sup>3</sup>J<sub>HH</sub> = 3.94 Hz, NArH<sup>a</sup>, 1 H), 7.09 (t, <sup>3</sup>J<sub>HH</sub> = 9.30 Hz, *p*-cresol, 2 H), 6.96 (t, <sup>3</sup>J<sub>HH</sub> = 8.20 Hz, NArH<sup>b</sup>, 2 H), 6.85 (d, <sup>3</sup>J<sub>HH</sub> = 9.46 Hz, *p*-cresol, 2 H), 6.80 (d, <sup>3</sup>J<sub>HH</sub> = 8.04 Hz, NArH<sup>a</sup>, 1 H), 6.63 (t, <sup>3</sup>J<sub>HH</sub> = 6.62 Hz, NArH<sup>c</sup>, 1 H), 6.59 (t, <sup>3</sup>J<sub>HH</sub> = 8.04 Hz, NArH<sup>c</sup>, 1 H), 3.85-3.71 (m, H<sup>g</sup>, 1 H), 3.62-3.42 (m, H<sup>g</sup>/H<sup>e</sup>, 2 H), 3.52 (d, <sup>2</sup>J<sub>HH</sub> = 8.52 Hz, H<sup>e</sup>, 1 H), 3.39 (t, <sup>2</sup>J<sub>HH</sub> = 8.52 Hz, H<sup>f</sup>, 1 H), 2.95 (t, <sup>2</sup>J<sub>HH</sub> = 6.94 Hz, H<sup>f</sup>, 1 H), 2.67 - 2.55 (m, (CH<sub>3</sub>)<sub>2</sub>CH, 1 H), 2.39 - 2.28 (m, (CH<sub>3</sub>)<sub>2</sub>CH, 1 H), 2.09 (s, C<sub>6</sub>H<sub>5</sub>Me, 3 H), 0.58- 0.47 (m, MeCHMe, 6 H), 0.23 (d, <sup>3</sup>J<sub>HH</sub> = 9.93 Hz, MeCHMe, 3 H), -0.11 (d, <sup>3</sup>J<sub>HH</sub> = 8.51 Hz, MeCHMe, 3 H) ppm; <sup>13</sup>C{<sup>1</sup>H} NMR (100.6 MHz, C<sub>6</sub>D<sub>6</sub>, 293 K) δ<sub>C</sub> 163.2 (C=N), 131.2 (NArC<sup>m</sup>), 129.4, 128.2, 128.0, 127.9, 126.8, 126.1, 124.7, 124.4, 117.9 (NArC<sup>n</sup>), 71.7 (C<sup>p</sup>), 67.2 (C<sup>q</sup>), 33.4 ((CH<sub>3</sub>)<sub>2</sub>CH), 20.5 (C<sub>6</sub>H<sub>5</sub>Me), 19.0 (MeCHMe), 15.0 (MeCHMe) ppm.

#### 6.2.5 General procedure for [Sc(R-BOPA){N(SiMe<sub>3</sub>)<sub>2</sub>}]OTf (4a-c)

To a stirred solution of [Sc(R-BOPA){N(SiMe<sub>3</sub>)<sub>2</sub>}Cl] (200 mg) in toluene (10 ml) a solution of AgOTf (1 equiv.) in toluene (5 ml) was added drop-wise at 0 °C. The mixture was left to stir overnight after which a fine white precipitate had formed. The solvent was filtered and the



solid AgCl washed with toluene (5 ml x 2). The washings and filtrate were concentrated under reduced pressure and the resulting solid dried in *vacuo* to yield complexes **4a-c**.



### 6.2.5.1 [Sc(Ph-BOPA){N(SiMe<sub>3</sub>)<sub>2</sub>}]OTf (**4a**) 77%

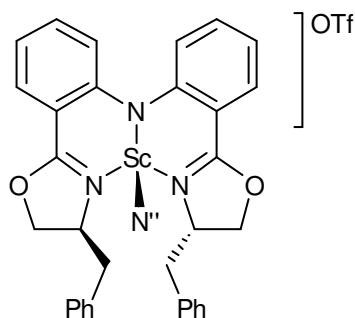
#### *exo* isomer

<sup>1</sup>H NMR (500.1 MHz, C<sub>6</sub>D<sub>6</sub>, 293 K) δ<sub>H</sub> 8.19 (d, <sup>3</sup>J<sub>HH</sub> = 7.72 Hz, NArH<sup>d</sup>, 2 H), 7.10 (d, <sup>3</sup>J<sub>HH</sub> = 7.41 Hz, NArH<sup>a</sup>, 2 H), 7.04 – 7.00 (m, 10 H), 6.99 (t, <sup>3</sup>J<sub>HH</sub> = 9.46 Hz, NArH<sup>b</sup>, 2 H), 6.71 (t, <sup>3</sup>J<sub>HH</sub> = 7.25 Hz, NArH<sup>c</sup>, 2 H), 4.56 (br t, <sup>3</sup>J<sub>HH</sub> = 8.83 Hz, H<sup>g</sup>, 2 H), 3.84 – 3.79 (br s, H<sup>e</sup>, 2 H), 3.66 – 3.59 (m, H<sup>f</sup>, 2 H), 0.08 (s, N(SiMe<sub>3</sub>)<sub>2</sub>, 18 H) ppm; <sup>13</sup>C{<sup>1</sup>H} NMR (100.6 MHz, C<sub>6</sub>D<sub>6</sub>, 293 K) δ<sub>C</sub> 171.7 (C=N), 152.6 (NArC<sup>m</sup>), 141.0 (*ipso*-C<sub>6</sub>H<sub>5</sub>), 134.6 (NArC<sup>i</sup>), 129.6, 128.5, 126.3, 120.5, 120.1, 116.4 (NArC<sup>j</sup>), 114.9 (q, <sup>1</sup>J<sub>CF</sub> = 311.7 Hz, CF<sub>3</sub>), 110.2 (NArC<sup>n</sup>), 76.8 (C<sup>p</sup>), 67.5 (C<sup>q</sup>), 2.6 (N(SiMe<sub>3</sub>)<sub>2</sub>) ppm; <sup>19</sup>F NMR (282.7 MHz, C<sub>6</sub>D<sub>6</sub>, 293 K) δ<sub>F</sub> -77.81 (s, CF<sub>3</sub>) ppm.

#### *endo* isomer

<sup>1</sup>H NMR (500.1 MHz, C<sub>6</sub>D<sub>6</sub>, 293 K) δ<sub>H</sub> 7.83 (dd, <sup>3</sup>J<sub>HH</sub> = 8.04 Hz, <sup>4</sup>J<sub>HH</sub> = 1.89 Hz, NArH<sup>d</sup>, 2 H), 7.39 (d, <sup>3</sup>J<sub>HH</sub> = 8.20 Hz, NArH<sup>a</sup>, 2 H), 7.04 – 7.00 (m, 10 H), 6.89 (t, <sup>3</sup>J<sub>HH</sub> = 7.88 Hz, NArH<sup>b</sup>, 2 H), 6.83 (d, <sup>3</sup>J<sub>HH</sub> = 8.36 Hz, NArH<sup>c</sup>, 2 H), 5.62 (dd, <sup>2</sup>J<sub>HH</sub> = 9.93 Hz, <sup>3</sup>J<sub>HH</sub> = 4.73 Hz, H<sup>g</sup>, 2 H), 4.16 (dd, <sup>2</sup>J<sub>HH</sub> = 9.30 Hz, <sup>3</sup>J<sub>HH</sub> = 8.99 Hz, H<sup>e</sup>, 2 H), 3.05 – 2.99 (m, H<sup>f</sup>, 2 H), 0.04 (s, N(SiMe<sub>3</sub>)<sub>2</sub>, 18 H) ppm; <sup>13</sup>C{<sup>1</sup>H} NMR (100.6 MHz, C<sub>6</sub>D<sub>6</sub>, 293 K) δ<sub>C</sub> 171.6 (C=N), 141.9 (NArC<sup>m</sup>), 132.2 (NArC<sup>i</sup>), 129.7, 128.6, 128.5, 127.7, 126.1, 119.4, 115.8 (NArC<sup>j</sup>), 114.3 (q, <sup>1</sup>J<sub>CF</sub> = 311.2 Hz, CF<sub>3</sub>), 110.4 (NArC<sup>n</sup>), 75.9 (C<sup>p</sup>), 68.2 (C<sup>q</sup>), 7.9 (N(SiMe<sub>3</sub>)<sub>2</sub>) ppm; <sup>19</sup>F NMR

(282.7 MHz, C<sub>6</sub>D<sub>6</sub>, 293 K)  $\delta_F$  -78.12 (s, CF<sub>3</sub>) ppm; IR ( $\nu$  cm<sup>-1</sup>) (KBr): 3064 (m), 3031 (m), 2961 (s), 2917 (m), 2850 (m), 1627 (m) (C=N), 1608 (s) (C=N), 1583 (m), 1557 (w), 1536 (w), 1493 (w), 1465 (s), 1429 (m), 1382 (m), 1318 (m), 1261 (s), 1228 (s), 1208 (m), 1161 (m) (S=O), 1074 (m), 1028 (s), 956 (w), 859 (m) cm<sup>-1</sup>; Anal. Calcd for ScC<sub>37</sub>H<sub>42</sub>F<sub>3</sub>N<sub>4</sub>O<sub>5</sub>SSi<sub>2</sub> (812.94 g mol<sup>-1</sup>): C 54.67, H 5.21, N 6.89. Found: C 54.29, H 5.57, N 6.92.



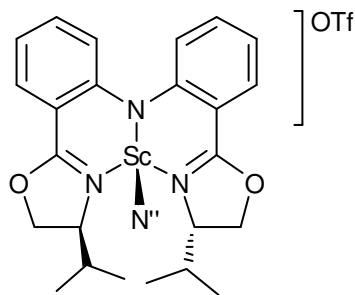
### 6.2.5.2 [Sc(Bn-BOPA){N(SiMe<sub>3</sub>)<sub>2</sub>}]OTf (4b) 82%

#### *exo* isomer

<sup>1</sup>H NMR (500.1 MHz, C<sub>6</sub>D<sub>6</sub>, 293 K)  $\delta_H$  8.00 (d, <sup>3</sup>J<sub>HH</sub> = 8.7 Hz, NArH<sup>d</sup>, 1 H), 7.74 (d, <sup>3</sup>J<sub>HH</sub> = 8.7 Hz, NArH<sup>d</sup>, 1 H), 7.39 (d, <sup>3</sup>J<sub>HH</sub> = 7.9 Hz, *o*-CH<sub>2</sub>C<sub>6</sub>H<sub>5</sub>, 2 H), 7.14 – 6.89 (m, 10 H), 6.78 – 6.66 (m, 4 H), 5.67 – 5.57 (m, H<sup>e</sup>, 1 H), 5.28 – 5.20 (m, H<sup>e</sup><sub>2</sub>, 1 H), 4.41 (br. d, <sup>2</sup>J<sub>HH</sub> = 13.6 Hz, CHHC<sub>6</sub>H<sub>5</sub>, 1 H), 4.12 – 4.05 (m, H<sup>e</sup>, 1 H), 3.89 – 3.83 (dd, <sup>3</sup>J<sub>HH</sub> = 8.5 Hz, <sup>2</sup>J<sub>HH</sub> = 17.6 Hz, H<sup>e</sup>/H<sup>f</sup>, 2 H), 3.81 – 3.73 (m, H<sup>f</sup>, 1 H), 2.90 – 2.74 (m, CHHC<sub>6</sub>H<sub>5</sub>, 2 H), 2.64 (dd, <sup>2</sup>J<sub>HH</sub> = 13.6 Hz, <sup>3</sup>J<sub>HH</sub> = 7.6 Hz, CHHC<sub>6</sub>H<sub>5</sub>, 1 H), 0.48 (s, N(SiMe<sub>3</sub>)(SiMe<sub>3</sub>), 9 H), 0.06 (s, N(SiMe<sub>3</sub>)(SiMe<sub>3</sub>), 9 H) ppm; <sup>13</sup>C{<sup>1</sup>H} NMR (100.6 MHz, C<sub>6</sub>D<sub>6</sub>, 293 K)  $\delta_C$  169.5 (C=N), 166.0 (C=N), 158.6 (NArC<sup>m</sup>), 155.8 (NArC<sup>m</sup>), 137.9, 136.5, 134.1, 134.0, 132.0 (NArC<sup>i</sup>), 130.3 (NArC<sup>j</sup>), 130.1, 129.3 (*ipso*-C<sub>6</sub>H<sub>5</sub>), 129.2 (*ipso*-C<sub>6</sub>H<sub>5</sub>), 127.1, 126.8, 122.4, 122.3, 121.5 (NArC<sup>l</sup>), 118.0 (NArC<sup>k</sup>), 115.3 (q, <sup>1</sup>J<sub>CF</sub> = 310.4 Hz, CF<sub>3</sub>), 114.0 (NArC<sup>n</sup>), 72.8 (C<sup>p</sup>), 70.4 (C<sup>p</sup>), 69.8 (C<sup>q</sup>), 68.8 (C<sup>q</sup>), 42.0 (CH<sub>2</sub>C<sub>6</sub>H<sub>5</sub>), 40.5 (CH<sub>2</sub>C<sub>6</sub>H<sub>5</sub>), 5.2 (N(SiMe<sub>3</sub>)<sub>2</sub>) ppm; <sup>19</sup>F NMR (282.8 MHz, C<sub>6</sub>D<sub>6</sub>, 293 K)  $\delta_F$  -76.51 (s, CF<sub>3</sub>) ppm.

**endo isomer**

$^1\text{H}$  NMR (500.1 MHz,  $\text{C}_6\text{D}_6$ , 293 K)  $\delta_{\text{H}}$  7.97 (d,  $^3J_{\text{HH}} = 7.7$  Hz,  $\text{NArH}^{\text{d}}$ , 1 H), 7.69 (d,  $^3J_{\text{HH}} = 7.7$  Hz,  $\text{NArH}^{\text{d}}$ , 1 H), 7.34 (d,  $^3J_{\text{HH}} = 10.1$  Hz,  $o\text{-CH}_2\text{C}_6\text{H}_5$ , 2 H), 7.14 – 6.89 (m, 10 H), 6.82 (d,  $^3J_{\text{HH}} = 9.3$  Hz,  $\text{NArH}^{\text{a}}$ , 1 H), 6.78– 6.66 (m, 2 H), 6.56 (app.t,  $^3J_{\text{HH}} = 7.1$  Hz, 1 H), 5.74 – 5.66 (m,  $\text{H}^{\text{g}}$ , 1 H), 5.18 – 5.10 (m,  $\text{H}^{\text{g}}$ , 1 H), 4.02 – 3.94 (m,  $\text{H}^{\text{e}}$ , 2 H), 3.94 – 3.90 (m,  $\text{H}^{\text{f}}$ , 2 H), 2.90 – 2.74 (m,  $\text{CHHC}_6\text{H}_5$ , 3 H), 2.56 (dd,  $^2J_{\text{HH}} = 15.1$  Hz,  $^3J = 7.7$  Hz,  $\text{CHHC}_6\text{H}_5$ , 1 H), 0.37 (s,  $\text{N}(\text{SiMe}_3)(\text{SiMe}_3)$ , 9 H), -0.03 (s,  $\text{N}(\text{SiMe}_3)(\text{SiMe}_3)$ , 9 H) ppm;  $^{13}\text{C}\{^1\text{H}\}$  NMR (100.6 MHz,  $\text{C}_6\text{D}_6$ , 293 K)  $\delta_{\text{C}}$  168.8 (C=N), 158.7 ( $\text{NArC}^{\text{m}}$ ), 154.1 ( $\text{NArC}^{\text{m}}$ ), 137.4, 134.5, 134.5, 132.0 ( $\text{NArC}^{\text{i}}$ ), 130.3, 130.2, 129.4, 128.7 ( $\text{NArC}^{\text{i}}$ ), 128.5, 128.5, 128.7, 127.3, 127.0, 123.2, 122.5, 122.0, 117.8 ( $\text{NArC}^{\text{k}}$  or  $\text{NArC}^{\text{j}}$ ), 114.9 (q,  $^1J_{\text{CF}} = 312.7$  Hz,  $\text{CF}_3$ ), 113.6 ( $\text{NArC}^{\text{n}}$ ), 110.8 ( $\text{NArC}^{\text{n}}$ ), 72.3 ( $\text{C}^{\text{p}}$ ), 72.2 ( $\text{C}^{\text{p}}$ ), 66.5 ( $\text{C}^{\text{q}}$ ), 65.8 ( $\text{C}^{\text{q}}$ ), 42.2 ( $\text{CH}_2\text{C}_6\text{H}_5$ ), 40.6 ( $\text{CH}_2\text{C}_6\text{H}_5$ ), 5.5 ( $\text{N}(\text{SiMe}_3)(\text{SiMe}_3)$ ), 5.2 ( $\text{N}(\text{SiMe}_3)(\text{SiMe}_3)$ ) ppm;  $^{19}\text{F}$  NMR (282.8 MHz,  $\text{C}_6\text{D}_6$ , 293 K)  $\delta_{\text{F}}$  – 78.00 (s,  $\text{CF}_3$ ) ppm; IR ( $\nu$   $\text{cm}^{-1}$ ) (KBr): 3445 (m), 3064 (w), 3031 (w), 2962 (s), 1615 (m) (C=N), 1583 (w), 1559 (w), 1540 (w), 1465 (m), 1431 (m), 1384 (s), 1325 (m), 1261 (s), 1231 (w), 1207 (w), 1160 (w) (S=O), 1094 (s), 1024 (s), 933 (w), 800 (s), 749 (m), 701 (m), 665 (w), 635 (m), 615 (w), 462 (w), 421 (w), 405 (w)  $\text{cm}^{-1}$ ; Anal. Calcd for  $\text{ScC}_{39}\text{H}_{46}\text{F}_3\text{N}_4\text{O}_5\text{SSi}_2$  (840.99  $\text{g mol}^{-1}$ ): C 55.70, H 5.51, N 6.66. Found: C 55.61, H 5.68, N 6.73.



### 6.2.5.3 [Sc(iPr-BOPA){N(SiMe<sub>3</sub>)<sub>2</sub>}]OTf (4c) 68%

#### *exo* isomer

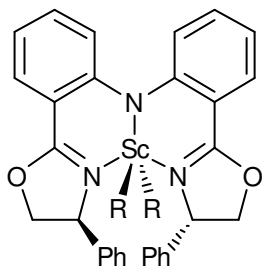
<sup>1</sup>H NMR (500.1 MHz, C<sub>6</sub>D<sub>6</sub>, 293 K) δ<sub>H</sub> 8.06 (d, <sup>3</sup>J<sub>HH</sub> = 7.7 Hz, NArH<sup>d</sup>, 1 H), 7.86 (d, <sup>3</sup>J<sub>HH</sub> = 8.0 Hz, NArH<sup>d</sup>, 1 H), 7.00 (d, <sup>3</sup>J<sub>HH</sub> = 6.3 Hz, NArH<sup>a</sup>, 1 H), 6.88 (app.t, <sup>3</sup>J<sub>HH</sub> = 7.7 Hz, NArH<sup>b</sup> or NArH<sup>c</sup>, 1 H), 6.76 – 6.70 (m, 2H), 6.61 (d, <sup>3</sup>J<sub>HH</sub> = 8.5 Hz, NArH<sup>a</sup>, 1 H), 6.55 (app.t, <sup>3</sup>J<sub>HH</sub> = 7.4 Hz, NArH<sup>b</sup> or NArH<sup>c</sup>, 1 H), 4.92 (dt, <sup>3</sup>J<sub>HH</sub> = 9.3 Hz, <sup>3</sup>J = 2.8 Hz, H<sup>g</sup>, 1 H), 4.65 (dt, <sup>3</sup>J<sub>HH</sub> = 9.0 Hz, <sup>3</sup>J<sub>HH</sub> = 3.8 Hz, H<sup>g</sup>, 1 H), 4.36 (app.t, <sup>2</sup>J<sub>HH</sub> = 9.0 Hz, H<sup>e</sup>, 1 H), 4.04 (dd, <sup>2</sup>J<sub>HH</sub> = 9.0 Hz, <sup>3</sup>J<sub>HH</sub> = 3.3 Hz, H<sup>f</sup>, 1 H), 3.86 (dd, <sup>2</sup>J<sub>HH</sub> = 9.8 Hz, <sup>3</sup>J<sub>HH</sub> = 3.6 Hz, H<sup>f</sup>, 1 H), 3.78 (app.t, <sup>2</sup>J<sub>HH</sub> = 9.0 Hz, H<sup>f</sup>, 1 H), 2.42 – 2.34 (m, (CH<sub>3</sub>)<sub>2</sub>CH, 1 H), 2.21 – 2.12 (m, (CH<sub>3</sub>)<sub>2</sub>CH, 1 H), 0.75 (d, <sup>3</sup>J<sub>HH</sub> = 7.1 Hz, MeCHMe, 3 H), 0.69 (d, <sup>3</sup>J<sub>HH</sub> = 6.8 Hz, MeCHMe, 3 H), 0.60 (d, <sup>3</sup>J<sub>HH</sub> = 7.4 Hz, MeCHMe, 3 H), 0.38 (s, N(SiMe<sub>3</sub>)(SiMe<sub>3</sub>), 9 H), 0.34 (d, <sup>3</sup>J<sub>HH</sub> = 7.1 Hz, MeCHMe, 3 H), -0.02 (s, N(SiMe<sub>3</sub>)(SiMe<sub>3</sub>), 9 H) ppm; <sup>13</sup>C{<sup>1</sup>H} NMR (100.6 MHz, C<sub>6</sub>D<sub>6</sub>, 293 K) δ<sub>C</sub> 170.2 (C=N), 164.7 (C=N), 158.6 (NArC<sup>m</sup>), 154.5 (NArC<sup>m</sup>), 134.3 (NArC<sup>k</sup> or NArC<sup>j</sup>), 133.9, 132.3 (NArC<sup>i</sup>), 131.4 (NArC<sup>i</sup>), 127.7 (NArC<sup>l</sup>), 121.8, 121.2 (NArC<sup>l</sup>), 118.5 (NArC<sup>k</sup> or NArC<sup>j</sup>), 117.1 (NArC<sup>n</sup>), 114.1 (q, <sup>1</sup>J<sub>CF</sub> = 312.2 Hz, CF<sub>3</sub>), 110.3 (NArC<sup>n</sup>), 71.6 (C<sup>p</sup>), 70.3 (C<sup>p</sup>), 69.6 (C<sup>q</sup>), 68.4 (C<sup>q</sup>), 30.9 ((CH<sub>3</sub>)<sub>2</sub>CH), 30.4 ((CH<sub>3</sub>)<sub>2</sub>CH), 19.3 (MeCHMe), 18.4 (MeCHMe), 14.3 (MeCHMe), 13.9 (MeCHMe), 5.3 (N(SiMe<sub>3</sub>)(SiMe<sub>3</sub>)), 5.0 (N(SiMe<sub>3</sub>)(SiMe<sub>3</sub>)) ppm; <sup>19</sup>F NMR (282.8 MHz, C<sub>6</sub>D<sub>6</sub>, 293 K) δ<sub>F</sub> -78.1 (CF<sub>3</sub>) ppm.

**endo isomer**

$^1\text{H}$  NMR (500.1 MHz,  $\text{C}_6\text{D}_6$ , 293 K)  $\delta_{\text{H}}$  8.02 (d,  $^3J_{\text{HH}} = 8.4$  Hz,  $\text{NArH}^{\text{d}}$ , 1 H), 7.89 (dd,  $^3J_{\text{HH}} = 8.2$  Hz,  $^4J_{\text{HH}} = 1.7$  Hz,  $\text{NArH}^{\text{d}}$ , 1 H), 7.03 (d,  $^3J_{\text{HH}} = 8.2$  Hz,  $\text{NArH}^{\text{a}}$ , 1 H), 7.01 – 6.98 (m, 1 H), 6.90 (app.t,  $^3J_{\text{HH}} = 6.9$  Hz,  $\text{NArH}^{\text{b}}$  or  $\text{NArH}^{\text{c}}$ , 1 H), 6.76 – 6.71 (m, 2 H), 6.53 (app.t,  $^3J_{\text{HH}} = 6.3$  Hz,  $\text{NArH}^{\text{b}}$  or  $\text{NArH}^{\text{c}}$ , 1 H), 5.23 – 5.17 (m,  $\text{H}^{\text{g}}$ , 1 H), 4.84 – 4.78 (m,  $\text{H}^{\text{g}}$ , 1 H), 3.95 – 3.88 (m,  $\text{H}^{\text{e}}/\text{H}^{\text{f}}$ , 3 H), 3.81 (app.t,  $^2J_{\text{HH}} = 9.3$  Hz,  $\text{H}^{\text{f}}$ , 1 H), 2.55-2.45 (m,  $(\text{CH}_3)_2\text{CH}$ , 2 H), 0.79 (d,  $^3J_{\text{HH}} = 7.6$  Hz,  $\text{MeCHMe}$ , 6 H), 0.75 (d,  $^3J_{\text{HH}} = 7.1$  Hz,  $\text{MeCHMe}$ , 6 H), 0.56 (s,  $\text{N}(\text{SiMe}_3)(\text{SiMe}_3)$ , 9 H), 0.05 (s,  $\text{N}(\text{SiMe}_3)(\text{SiMe}_3)$ , 9 H) ppm;  $^{13}\text{C}\{^1\text{H}\}$  NMR (100.6 MHz,  $\text{C}_6\text{D}_6$ , 293 K)  $\delta_{\text{C}}$  170.3 (C=N), 166.1 (C=N), 156.4 ( $\text{NArC}^{\text{m}}$ ), 156.1 ( $\text{NArC}^{\text{m}}$ ), 134.6 ( $\text{NArC}^{\text{k}}$  or  $\text{NArC}^{\text{j}}$ ), 134.2 ( $\text{NArC}^{\text{l}}$ ), 133.7, 131.8 ( $\text{NArC}^{\text{i}}$ ), 130.8 ( $\text{NArC}^{\text{i}}$ ), 128.5, 122.9, 121.9, 117.4 ( $\text{NArC}^{\text{n}}$ ), 112.3 (q,  $^1J_{\text{CF}} = 314.0$  Hz,  $\text{CF}_3$ ), 111.6 ( $\text{NArC}^{\text{n}}$ ), 71.7 ( $\text{C}^{\text{p}}$ ), 71.6 ( $\text{C}^{\text{p}}$ ), 68.5 ( $\text{C}^{\text{q}}$ ), 67.4 ( $\text{C}^{\text{q}}$ ), 30.8 ( $(\text{CH}_3)_2\text{CH}$ ), 30.3 ( $(\text{CH}_3)_2\text{CH}$ ), 19.3 ( $\text{MeCHMe}$ ), 18.2 ( $\text{MeCHMe}$ ), 15.2 ( $\text{MeCHMe}$ ), 14.8 ( $\text{MeCHMe}$ ), 6.1 ( $\text{N}(\text{SiMe}_3)(\text{SiMe}_3)$ ), 5.3 ( $\text{N}(\text{SiMe}_3)(\text{SiMe}_3)$ ) ppm;  $^{19}\text{F}$  NMR (282.8 MHz,  $\text{C}_6\text{D}_6$ , 293 K)  $\delta_{\text{F}}$  -77.3 ( $\text{CF}_3$ ) ppm; IR ( $\nu$   $\text{cm}^{-1}$ ) (KBr): 3063 (m), 3029 (m), 2958 (s), 2919 (m), 2853 (m), 1623 (m) (C=N), 1601 (s) (C=N), 1577 (m), 1560 (w), 1534 (w), 1493 (w), 1464 (s), 1429 (m), 1381 (m), 1322 (m), 1260 (s), 1225 (s), 1210 (m), 1164 (m) (S=O), 1072 (m), 1029 (s), 956 (w), 858 (m)  $\text{cm}^{-1}$ .

**6.2.6 General procedure for  $[\text{Sc}(\text{R-BOPA})(\text{CH}_2\text{SiMe}_2\text{Ph})_2]$  (**5a-c**)**

To a solution of  $[\text{Sc}(\text{CH}_2\text{SiMe}_2\text{Ph})_3(\text{THF})_2]$  (200 mg), in THF (10 ml) at 0 °C, R-BOPA (1 eq.) in THF (5 ml) was added dropwise. The reaction mixture was left to stir for 1 hour and the solvent was then removed under reduced pressure. The resulting thick oil was dissolved in hexane (7 ml) and cooled to -37 °C. The yellow solid was filtered and dried in *vacuo* to yield the complex (**5a-c**).



### 6.2.6.1 [Sc(Ph-BOPA)(CH<sub>2</sub>SiMe<sub>2</sub>Ph)<sub>2</sub>] (5a) 74%

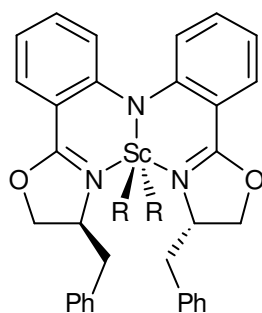
#### *exo* product

<sup>1</sup>H NMR (500.1 MHz, C<sub>6</sub>D<sub>6</sub>, 293 K) δ<sub>H</sub> 7.97 (dd, <sup>3</sup>J<sub>HH</sub> = 6.5 Hz, <sup>4</sup>J<sub>HH</sub> = 1.7 Hz, NArH<sup>d</sup>, 2 H), 7.58 (dd, <sup>3</sup>J<sub>HH</sub> = 1.4 Hz, <sup>3</sup>J<sub>HH</sub> = 6.5 Hz, *m*-SiC<sub>6</sub>H<sub>5</sub>, 4 H), 7.27 (app. t, <sup>3</sup>J<sub>HH</sub> = 7.5 Hz, *o*-SiC<sub>6</sub>H<sub>5</sub>, 4 H), 7.15 (t, <sup>3</sup>J<sub>HH</sub> = 7.5 Hz, *p*-SiC<sub>6</sub>H<sub>5</sub>, 2 H), 7.05 – 6.86 (m, 14 H), 6.66 (app. t, <sup>3</sup>J<sub>HH</sub> = 7.8 Hz, NArH<sup>c</sup>, 2 H), 5.24 (dd, <sup>3</sup>J<sub>HH</sub> = 5.5 Hz, <sup>3</sup>J<sub>HH</sub> = 3.0 Hz, H<sup>g</sup>, 2 H), 3.68 (m, H<sup>e</sup>/H<sup>f</sup>, 4 H), 0.02 (d, <sup>2</sup>J<sub>HH</sub> = 11.0 Hz, CH<sub>2</sub>SiMe<sub>2</sub>Ph, 2 H), -0.02 (s, CH<sub>2</sub>SiMe<sub>2</sub>Ph, 6 H), -0.14 (s, CH<sub>2</sub>SiMe<sub>2</sub>Ph, 6 H), -0.29 (d, <sup>2</sup>J<sub>HH</sub> = 11.0 Hz, CH<sub>2</sub>SiMe<sub>2</sub>Ph, 2 H) ppm; <sup>13</sup>C{<sup>1</sup>H} NMR (100.6 MHz, C<sub>6</sub>D<sub>6</sub>, 293 K) δ<sub>C</sub> 169.2 (C=N), 155.4 (NArC<sup>m</sup>), 146.5 (*i*-SiC<sub>6</sub>H<sub>5</sub>), 141.7 (*i*-C<sup>\*</sup>HC<sub>6</sub>H<sub>5</sub>), 133.9 (*m*-SiC<sub>6</sub>H<sub>5</sub>), 131.4 (NArC<sup>i</sup>), 129.2 (C<sup>k</sup> or C<sup>l</sup>), 129.1 (C<sup>k</sup> or C<sup>l</sup>), 128.1 (oxaz-C<sub>6</sub>H<sub>5</sub>), 128.1 (*p*-SiC<sub>6</sub>H<sub>5</sub>), 127.6 (*o*-SiC<sub>6</sub>H<sub>5</sub>), 126.6 (oxaz-C<sub>6</sub>H<sub>5</sub>), 124.8 (oxaz-C<sub>6</sub>H<sub>5</sub>), 114.7 (NArC<sup>n</sup>), 75.7 (C<sup>p</sup>), 68.7 (C<sup>q</sup>), 38.7 (CH<sub>2</sub>SiMe<sub>2</sub>Ph), 2.8 (CH<sub>2</sub>SiMe<sub>2</sub>Ph), 1.0 (CH<sub>2</sub>SiMe<sub>2</sub>Ph) ppm.

#### *exo* product

<sup>1</sup>H NMR (500.1 MHz, C<sub>6</sub>D<sub>6</sub>, 293 K) δ<sub>H</sub> 7.94 (dd, <sup>3</sup>J<sub>HH</sub> = 6.4 Hz, <sup>4</sup>J<sub>HH</sub> = 1.6 Hz, NArH<sup>d</sup>, 2 H), 7.54 (dd, <sup>3</sup>J<sub>HH</sub> = 1.5 Hz, <sup>3</sup>J<sub>HH</sub> = 6.5 Hz, *m*-SiC<sub>6</sub>H<sub>5</sub>, 4 H), 7.27 (app. t, <sup>3</sup>J<sub>HH</sub> = 7.5 Hz, *o*-SiC<sub>6</sub>H<sub>5</sub>, 4 H), 7.11 (t, <sup>3</sup>J<sub>HH</sub> = 7.5 Hz, *p*-SiC<sub>6</sub>H<sub>5</sub>, 2 H), 7.05 – 6.86 (m, 14 H), 6.71 (app. t, <sup>3</sup>J<sub>HH</sub> = 7.8 Hz, NArH<sup>c</sup>, 2 H), 4.73 (dd, <sup>3</sup>J<sub>HH</sub> = 5.5 Hz, <sup>3</sup>J<sub>HH</sub> = 4.5 Hz, H<sup>g</sup>, 2 H), 3.82 (dd, <sup>2</sup>J<sub>HH</sub> = 5.5 Hz, <sup>3</sup>J<sub>HH</sub> = 3.5 Hz, H<sup>e</sup>, 2 H), 3.70 (dd, <sup>2</sup>J = 6.5 Hz, <sup>3</sup>J<sub>HH</sub> = 2.0 Hz, H<sup>f</sup>, 2 H), 0.15 (s, CH<sub>2</sub>SiMe<sub>2</sub>Ph, 6 H), -0.08 (s, CH<sub>2</sub>SiMe<sub>2</sub>Ph, 6 H), -0.17 (d, <sup>2</sup>J<sub>HH</sub> = 11.5 Hz, CH<sub>2</sub>SiMe<sub>2</sub>Ph, 2 H), -0.75 (d, <sup>2</sup>J<sub>HH</sub> = 11.5 Hz, CH<sub>2</sub>SiMe<sub>2</sub>Ph, 2 H) ppm; <sup>13</sup>C{<sup>1</sup>H} NMR (100.6 MHz, C<sub>6</sub>D<sub>6</sub>, 293 K) δ<sub>C</sub> 169.1 (C=N),

156.3 (NArC<sup>m</sup>), 146.6 (*i*-SiC<sub>6</sub>H<sub>5</sub>), 140.3 (*i*-C<sup>\*</sup>HC<sub>6</sub>H<sub>5</sub>), 140.9 (*i*-C<sup>\*</sup>HC<sub>6</sub>H<sub>5</sub>), 134.4 (C<sup>k</sup> or C<sup>l</sup>), 134.0 (*m*-SiC<sub>6</sub>H<sub>5</sub>), 130.1 (NArC<sup>i</sup>), 129.2 (C<sup>k</sup> or C<sup>l</sup>), 128.9 (oxaz-C<sub>6</sub>H<sub>5</sub>), 128.7 (oxaz-C<sub>6</sub>H<sub>5</sub>), 127.9 (*o*-SiC<sub>6</sub>H<sub>5</sub>), 127.4 (*p*-SiC<sub>6</sub>H<sub>5</sub>), 126.4 (oxaz-C<sub>6</sub>H<sub>5</sub>), 119.2 (NArC<sup>j</sup>), 117.1 (NArC<sup>n</sup>), 76.0 (C<sup>p</sup>), 70.4 (C<sup>q</sup>), 39.1 (CH<sub>2</sub>SiMe<sub>2</sub>Ph), 2.3 (CH<sub>2</sub>SiMeMePh), 1.1 (CH<sub>2</sub>SiMeMePh) ppm; IR (ν cm<sup>-1</sup>) (KBr): 3064 (m), 3025 (m), 2961 (m), 2894 (m), 1611 (s) (C=N), 1559 (w), 1538 (w), 1494 (w), 1464 (m), 1431 (m), 1378 (w), 1323 (w), 1262 (m), 1248 (w), 1225 (m), 1157 (w), 1112 (w), 1070 (m), 1047 (w), 952 (w), 929 (w), 837 (m), 803 (m), 747 (m), 728 (w), 698 (s), 669 (w), 618 (w), 595 (w), 540 (w), 467 (w) cm<sup>-1</sup>; Anal. Calcd for ScC<sub>48</sub>H<sub>50</sub>N<sub>3</sub>O<sub>2</sub>Si<sub>2</sub> (802.06 g mol<sup>-1</sup>): C 71.88, H 6.28, N 5.24. Found: C 58.33, H 6.27, N 5.15.



### 6.2.6.2 [Sc(Bn-BOPA)(CH<sub>2</sub>SiMe<sub>2</sub>Ph)<sub>2</sub>] (5b) 78%

#### *exo* product

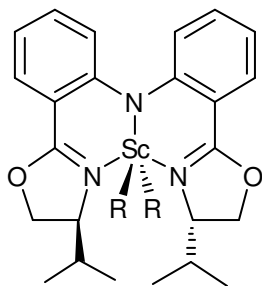
<sup>1</sup>H NMR (500.1 MHz, C<sub>6</sub>D<sub>6</sub>, 293 K) δ<sub>H</sub> 7.90 (dd, <sup>3</sup>J<sub>HH</sub> = 8.1 Hz, <sup>4</sup>J<sub>HH</sub> = 1.5 Hz, NArH<sup>d</sup>, 2 H), 7.61 (dd, <sup>3</sup>J<sub>HH</sub> = 1.5 Hz, <sup>3</sup>J<sub>HH</sub> = 6.4 Hz, *m*-SiC<sub>6</sub>H<sub>5</sub>, 4 H), 7.20 - 6.98 (m, 16 H), 6.92 (d, <sup>3</sup>J<sub>HH</sub> = 7.0 Hz, *o*-CH<sub>2</sub>Ph, 4 H), 6.63 (app. t, <sup>3</sup>J<sub>HH</sub> = 6.62 Hz, NArH<sup>c</sup>, 2 H), 4.60 (m, H<sup>g</sup>, 2 H), 3.89 (dd, <sup>2</sup>J<sub>HH</sub> = 5.1 Hz, <sup>3</sup>J<sub>HH</sub> = 3.6 Hz, H<sup>e</sup>, 2 H), 3.49 (m, H<sup>f</sup>, 2 H), 2.85 (dd, <sup>2</sup>J<sub>HH</sub> = 10.3 Hz, <sup>3</sup>J<sub>HH</sub> = 3.4 Hz, CHHPh, 2 H), 2.52 (dd, <sup>2</sup>J<sub>HH</sub> = 8.4 Hz, <sup>3</sup>J<sub>HH</sub> = 5.3 Hz, CHHPh, 2 H), 0.50 (d, <sup>2</sup>J<sub>HH</sub> = 11.4 Hz, CHHSiMe<sub>2</sub>Ph, 2 H), 0.38 (d, <sup>2</sup>J<sub>HH</sub> = 11.4 Hz, CHHSiMe<sub>2</sub>Ph, 2 H), 0.26 (s, CH<sub>2</sub>SiMeMePh, 6 H), 0.25 (s, CH<sub>2</sub>SiMeMePh, 6 H) ppm; <sup>13</sup>C{<sup>1</sup>H} NMR (125.8 MHz, C<sub>6</sub>D<sub>6</sub>, 293 K) δ<sub>C</sub> 168.7 (C=N), 155.0 (NArC<sup>m</sup>), 145.8 (*i*-SiC<sub>6</sub>H<sub>5</sub>), 136.4 (*i*-CH<sub>2</sub>Ph), 134.2 (NArC<sup>k</sup>),

134.0 (*m*-SiC<sub>6</sub>H<sub>5</sub>), 130.4 (NArC<sup>l</sup>), 129.1 (oxaz-ph or *p*-SiC<sub>6</sub>H<sub>5</sub>), 128.7 (oxaz-ph or *p*-SiC<sub>6</sub>H<sub>5</sub>), 128.1 (oxaz-ph or *p*-SiC<sub>6</sub>H<sub>5</sub>), 127.5 (*o*-SiC<sub>6</sub>H<sub>5</sub>), 127.0 (oxaz-Ph), 124.7 (NArC<sup>l</sup>), 119.1 (NArC<sup>j</sup>), 114.9 (NArC<sup>n</sup>), 71.2 (C<sup>p</sup>), 65.9 (C<sup>q</sup>), 40.8 (CH<sub>2</sub>PH), 39.2 (CH<sub>2</sub>SiMe<sub>2</sub>Ph), 3.0 (CH<sub>2</sub>SiMeMePh), 2.0 (CH<sub>2</sub>SiMeMePh) ppm.

### **endo product**

<sup>1</sup>H NMR (500.1 MHz, C<sub>6</sub>D<sub>6</sub>, 293 K) δ<sub>H</sub> 7.94 (dd, <sup>3</sup>J<sub>HH</sub> = 8.1 Hz, <sup>4</sup>J<sub>HH</sub> = 1.6 Hz, NArH<sup>d</sup>, 2 H), 7.61 (dd, <sup>3</sup>J<sub>HH</sub> = 1.5 Hz, <sup>3</sup>J<sub>HH</sub> = 6.4 Hz, *m*-SiC<sub>6</sub>H<sub>5</sub>, 4 H), 7.20 -6.98 (m, 18 H), 6.86 (d, <sup>3</sup>J<sub>HH</sub> = 8.4 Hz, NArH<sup>a</sup>, 2 H), 6.69 (app. t, <sup>3</sup>J<sub>HH</sub> = 8.0 Hz, NArH<sup>c</sup>, 2 H), 4.60 (m, H<sup>g</sup>, 2 H), 4.15 (dd, <sup>2</sup>J<sub>HH</sub> = 10.2 Hz, <sup>3</sup>J<sub>HH</sub> = 3.14 Hz, CH<sub>2</sub>Ph, 2 H), 3.83 (dd, <sup>2</sup>J<sub>HH</sub> = 6.9 Hz, <sup>3</sup>J<sub>HH</sub> = 1.8 Hz, H<sup>e</sup>, 2 H), 3.49 (m, H<sup>f</sup>, 2 H), 2.66 (dd, <sup>2</sup>J<sub>HH</sub> = 11.9 Hz, <sup>3</sup>J<sub>HH</sub> = 1.2 Hz, PhCH<sub>2</sub>, 2 H), 0.59 (d, <sup>2</sup>J<sub>HH</sub> = 11.5 Hz, CH<sub>2</sub>SiMe<sub>2</sub>Ph, 2 H), 0.45 (d, <sup>2</sup>J<sub>HH</sub> = 10.6 Hz, CH<sub>2</sub>SiMe<sub>2</sub>Ph, 2 H), 0.24 (s, CH<sub>2</sub>SiMeMePh, 6 H), 0.07 (s, CH<sub>2</sub>SiMeMePh, 6 H) ppm; <sup>13</sup>C{<sup>1</sup>H} NMR (125.8 MHz, C<sub>6</sub>D<sub>6</sub>, 293 K) δ<sub>C</sub> 169.0 (C=N), 155.5 (NArC<sup>m</sup>), 146.0 (*i*-SiC<sub>6</sub>H<sub>5</sub>), 137.4 (*i*-SiC<sub>6</sub>H<sub>5</sub>), 134.2 (NArC<sup>k</sup>), 133.6 (*m*-SiC<sub>6</sub>H<sub>5</sub>), 131.4 (NArC<sup>i</sup>), 129.4 (oxaz-ph or *p*-SiC<sub>6</sub>H<sub>5</sub>), 129.1 (oxaz-ph or *p*-SiC<sub>6</sub>H<sub>5</sub>), 128.3 (oxaz-ph or *p*-SiC<sub>6</sub>H<sub>5</sub>), 127.7 (*o*-SiC<sub>6</sub>H<sub>5</sub>), 127.2 (oxaz-Ph), 125.9 (NArC<sup>l</sup>), 119.3 (NArC<sup>j</sup>), 116.6 (NArC<sup>n</sup>), 72.4 (C<sup>p</sup>), 68.3 (C<sup>q</sup>), 42.6 (CH<sub>2</sub>Ph), 38.2 (CH<sub>2</sub>SiMe<sub>2</sub>Ph), 1.9 (CH<sub>2</sub>SiMeMePh), 1.8 (CH<sub>2</sub>SiMeMePh) ppm; IR (ν cm<sup>-1</sup>) (KBr): 3480 (s), 3416 (s), 3065 (w), 3021 (w), 2961 (w), 1636 (m) (C=N), 1617 (m) (C=N), 1577 (w), 1559 (w), 1540 (w), 1522 (w), 1507 (w), 1458 (m), 1430 (w), 1384 (w), 1319 (w), 1261 (m), 1228 (m), 1159 (w), 1091 (m), 1079 (m), 1051 (m), 1030 (m), 839 (m), 800 (m), 747 (m), 728 (w), 699 (m), 669 (w) cm<sup>-1</sup>; Anal. Calcd for ScC<sub>50</sub>H<sub>54</sub>N<sub>3</sub>O<sub>2</sub>Si<sub>2</sub> (830.11 g mol<sup>-1</sup>): C 72.34, H 6.56, N 5.06. Found: C 65.77, H 6.45, N 5.61.





### 6.2.6.3 [Sc(iPr-BOPA)(CH<sub>2</sub>SiMe<sub>2</sub>Ph)<sub>2</sub>] (5c) 69%

#### *exo* product

<sup>1</sup>H NMR (400.1 MHz, C<sub>6</sub>D<sub>6</sub>, 293 K) δ<sub>H</sub> 7.96 (dd, <sup>3</sup>J<sub>HH</sub> = 8.1 Hz, <sup>4</sup>J<sub>HH</sub> = 1.6 Hz, NArH<sup>d</sup>, 2 H), 7.61 (dd, <sup>3</sup>J<sub>HH</sub> = 7.9 Hz, <sup>3</sup>J<sub>HH</sub> = 1.7 Hz, *m*-SiC<sub>6</sub>H<sub>5</sub>, 4 H), 7.20 (d, <sup>3</sup>J<sub>HH</sub> = 1.9 Hz, *o*-SiC<sub>6</sub>H<sub>5</sub>, 4 H), 7.15 (m, *p*-SiC<sub>6</sub>H<sub>5</sub>, 2 H), 6.95 (dd, <sup>3</sup>J<sub>HH</sub> = 7.0 Hz, <sup>4</sup>J<sub>HH</sub> = 1.7 Hz, NArH<sup>b</sup>, 2 H), 6.82 (d, <sup>3</sup>J<sub>HH</sub> = 7.7 Hz, NArH<sup>a</sup>, 2 H), 6.63 (dd, <sup>3</sup>J = 7.0 Hz, <sup>4</sup>J<sub>HH</sub> = 1.1 Hz, NArH<sup>c</sup>, 2 H), 4.31 (m, H<sup>g</sup>, 2 H), 3.86 (dd, <sup>2</sup>J<sub>HH</sub> = 8.9 Hz, <sup>3</sup>J<sub>HH</sub> = 4.9 Hz, H<sup>e</sup>, 2 H), 3.60 (app. t, <sup>2</sup>J<sub>HH</sub> = 9.3 Hz, H<sup>f</sup>, 2 H), 2.20 (m, (CH<sub>3</sub>)<sub>2</sub>CH, 2 H), 0.47 (d, <sup>3</sup>J<sub>HH</sub> = 7.1 Hz, CH<sub>3</sub>CHCH<sub>3</sub>, 6 H), 0.44 (d, <sup>3</sup>J<sub>HH</sub> = 6.6 Hz, CH<sub>3</sub>CHCH<sub>3</sub>, 6 H), 0.30 (app. t, <sup>2</sup>J<sub>HH</sub> = 11.4 Hz, CH<sub>2</sub>SiMe<sub>2</sub>Ph, 4 H), 0.24 (s, CH<sub>2</sub>SiMeMePh, 6 H), 0.22 (s, CH<sub>2</sub>SiMeMePh, 6 H) ppm; <sup>13</sup>C{<sup>1</sup>H} NMR (125.8 MHz, C<sub>6</sub>D<sub>6</sub>, 293 K) δ<sub>C</sub> 167.9 (C=N), 155.0 (NArC<sup>m</sup>), 146.0 (*i*-SiC<sub>6</sub>H<sub>5</sub>), 133.9 (NArC<sup>k</sup>), 133.6 (*m*-SiC<sub>6</sub>H<sub>5</sub>), 131.3 (NArC<sup>i</sup>), 128.3 (*p*-SiC<sub>6</sub>H<sub>5</sub>), 127.7 (*o*-SiC<sub>6</sub>H<sub>5</sub>), 124.7 (NArC<sup>l</sup>), 118.9 (NArC<sup>j</sup>), 114.8 (NArC<sup>n</sup>), 69.9 (C<sup>q</sup>), 67.6 (C<sup>p</sup>), 38.2 (CH<sub>2</sub>SiMe<sub>2</sub>Ph), 30.8 ((CH<sub>3</sub>)<sub>2</sub>CH), 18.5 (MeMeCH), 13.7 (MeMeCH), 2.7 (CH<sub>2</sub>SiMeMePh), 1.9 (CH<sub>2</sub>SiMeMePh) ppm.

#### *endo* product

<sup>1</sup>H NMR (400.1 MHz, C<sub>6</sub>D<sub>6</sub>, 293 K) δ<sub>H</sub> 7.83 (dd, <sup>3</sup>J<sub>HH</sub> = 8.0 Hz, <sup>4</sup>J = 1.6 Hz, NArH<sup>d</sup>, 2 H), 7.56 (dd, <sup>3</sup>J<sub>HH</sub> = 7.9 Hz, <sup>4</sup>J<sub>HH</sub> = 1.5 Hz, *m*-SiC<sub>6</sub>H<sub>5</sub>, 4 H), 7.19 (d, <sup>3</sup>J<sub>HH</sub> = 2.4 Hz, *o*-SiC<sub>6</sub>H<sub>5</sub>, 2 H), 7.18 (d, <sup>3</sup>J<sub>HH</sub> = 2.2 Hz, *o*-SiC<sub>6</sub>H<sub>5</sub>, 2 H), 7.12 (t, <sup>3</sup>J<sub>HH</sub> = 1.5 Hz, *p*-SiC<sub>6</sub>H<sub>5</sub>, 1 H), 7.10 (t, <sup>3</sup>J<sub>HH</sub> = 2.7 Hz, *p*-SiC<sub>6</sub>H<sub>5</sub>, 1 H), 6.70 (dd, <sup>3</sup>J<sub>HH</sub> = 7.0 Hz, <sup>4</sup>J<sub>HH</sub> = 1.7 Hz, NArH<sup>b</sup>, 2 H), 6.89 (d, <sup>3</sup>J<sub>HH</sub> = 7.7 Hz, NArH<sup>a</sup>, 2 H), 6.65 (dd, <sup>3</sup>J<sub>HH</sub> = 7.1 Hz, <sup>4</sup>J<sub>HH</sub> = 1.1 Hz, NArH<sup>c</sup>, 2 H), 4.06 (m, H<sup>g</sup>,

2 H), 3.81 (dd,  $^2J_{\text{HH}} = 8.8$  Hz,  $^3J_{\text{HH}} = 3.4$  Hz, H<sup>e</sup>, 2 H), 3.40 (dd,  $^3J_{\text{HH}} = 8.8$  Hz,  $^4J_{\text{HH}} = 1.4$  Hz, H<sup>f</sup>, 2 H), 2.78 (m, (CH<sub>3</sub>)<sub>2</sub>CH, 2 H), 0.82 (d,  $^3J_{\text{HH}} = 6.7$  Hz, CH<sub>3</sub>CHCH<sub>3</sub>, 6 H), 0.56 (d,  $^3J_{\text{HH}} = 7.0$  Hz, CH<sub>3</sub>CHCH<sub>3</sub>, 6 H), 0.18 (s, CH<sub>2</sub>SiMeMePh, 6 H), 0.16 (app. t,  $^2J_{\text{HH}} = 11.8$  Hz, CH<sub>2</sub>SiMe<sub>2</sub>Ph, 4 H), -0.06 (s, CH<sub>2</sub>SiMeMePh, 6 H) ppm;  $^{13}\text{C}\{^1\text{H}\}$  NMR (125.8 MHz, C<sub>6</sub>D<sub>6</sub>, 293 K)  $\delta_{\text{C}}$  168.7 (C=N), 155.5 (NArC<sup>m</sup>), 146.3 (*i*-SiC<sub>6</sub>H<sub>5</sub>), 134.2 (NArC<sup>k</sup>), 133.8 (*m*-SiC<sub>6</sub>H<sub>5</sub>), 130.0 (NArC<sup>i</sup>), 129.1 (*p*-SiC<sub>6</sub>H<sub>5</sub>), 127.4 (*o*-SiC<sub>6</sub>H<sub>5</sub>), 126.0 (NArC<sup>l</sup>), 119.2 (NArC<sup>j</sup>), 117.1 (NArC<sup>n</sup>), 71.7 (C<sup>q</sup>), 67.7 (C<sup>p</sup>), 38.5 (CH<sub>2</sub>SiMe<sub>2</sub>Ph), 30.4 ((CH<sub>3</sub>)<sub>2</sub>CH), 19.4 (MeCHMe), 14.0 (MeCHMe), 2.2 (CH<sub>2</sub>SiMeMePh), 1.4 (CH<sub>2</sub>SiMeMePh) ppm; IR ( $\nu$  cm<sup>-1</sup>) (KBr): 3451 (br m), 3068 (w), 3051 (w), 2957 (s), 2900 (w), 2871 (w), 1617 (s) (C=N), 1590 (w), 1563 (w), 1543 (m), 1523 (w), 1486 (w), 1459 (s), 1429 (m), 1375 (m), 1315 (m), 1261 (s), 1228 (s), 1154 (m), 1107 (m), 1067 (s), 1047 (s), 1030 (s), 967 (m), 839 (m), 799 (s), 749 (m), 725 (w), 698 (w), 675 (w), 591 (w) cm<sup>-1</sup>; Anal. Calcd for ScC<sub>42</sub>H<sub>54</sub>N<sub>3</sub>O<sub>2</sub>Si<sub>2</sub> (734.02 g mol<sup>-1</sup>): C 68.72, H 7.42, N 5.72. Found: C 68.64, H 7.46, N 5.81.

## 6.2.7 NMR scale general procedure for

### [Sc(R-BOPA)CH<sub>2</sub>SiMe<sub>2</sub>Ph][B(C<sub>6</sub>F<sub>5</sub>)<sub>4</sub>] (6a-c)

To a solution of **5** (0.0105 mmol) in bromobenzene (0.3 ml) a solution of [Ph<sub>3</sub>C][B(C<sub>6</sub>F<sub>5</sub>)<sub>4</sub>] (1 eq.) in bromobenzene (0.3 ml) was added dropwise to form a red solution.

#### 6.2.7.1 [Sc(Ph-BOPA)CH<sub>2</sub>SiMe<sub>2</sub>Ph][B(C<sub>6</sub>F<sub>5</sub>)<sub>4</sub>] (6a)

$^1\text{H}$  NMR (400.1 MHz, C<sub>6</sub>D<sub>5</sub>Br, 293 K)  $\delta_{\text{H}}$  7.66 (d,  $^3J_{\text{HH}} = 7.25$  Hz, NArH<sup>d</sup>, 2 H), 7.61 (d,  $^3J_{\text{HH}} = 7.26$  Hz, *m*-SiC<sub>6</sub>H<sub>5</sub>, 2 H), 7.11 – 7.07 (m, 6 H), 7.08 – 7.05 (m, 2 H), 6.86 – 6.81 (m, 3 H), 6.68 (m, 4 H), 6.43 (t,  $^3J_{\text{HH}} = 7.41$  Hz, NArH<sup>c</sup>, 2 H), 6.10 (d,  $^3J_{\text{HH}} = 8.67$  Hz, NArH<sup>a</sup>, 2 H), 5.85 (d,  $^3J_{\text{HH}} = 8.67$  Hz, H<sup>g</sup>, 2 H), 4.20 (dd,  $^2J_{\text{HH}} = 11.35$  Hz,  $^3J_{\text{HH}} = 5.68$  Hz, H<sup>e</sup>, 2 H), 3.85 –

3.79 (m, H<sup>f</sup>, 2 H), -0.05 (s, CH<sub>2</sub>SiMeMePh, 3 H), -0.10 (d, <sup>2</sup>J<sub>HH</sub> = 8.35 Hz, CHHSiMe<sub>2</sub>Ph, 1 H), -0.13 (d, <sup>2</sup>J<sub>HH</sub> = 8.36 Hz, CHHSiMe<sub>2</sub>Ph, 1 H) -0.34 (s, CH<sub>2</sub>SiMeMePh, 3 H) ppm; <sup>13</sup>C{<sup>1</sup>H} NMR (125.8 MHz, C<sub>6</sub>D<sub>5</sub>Br, 293 K) δ<sub>C</sub> 169.4 (C=N), 152.3 (NArC<sup>m</sup>), 148.7 (d, <sup>1</sup>J<sub>CF</sub> = 247 Hz, C<sub>6</sub>F<sub>5</sub>), 148.2 (*i*-C<sub>6</sub>F<sub>5</sub>), 146.3 (*i*-SiC<sub>6</sub>H<sub>5</sub>), 142.5 (*i*-C\*HC<sub>6</sub>H<sub>5</sub>), 138.6 (d, <sup>1</sup>J<sub>CF</sub> = 233.4 Hz, C<sub>6</sub>F<sub>5</sub>), 136.2 (d, <sup>1</sup>J<sub>CF</sub> = 241.2 Hz, C<sub>6</sub>F<sub>5</sub>), 132.0 (*m*-C<sub>6</sub>H<sub>5</sub>), 130.6 (NArC<sup>i</sup>), 130.4, 130.2, 128.7, 128.6, 127.7, 127.0, 126.6, 126.5, 126.4, 125.3, 121.3, 120.8 (NArC<sup>n</sup>), 72.3 (C<sup>p</sup>), 69.6 (C<sup>q</sup>), 0.03 (CH<sub>2</sub>SiMe<sub>2</sub>Ph), -2.3 (CH<sub>2</sub>SiMe<sub>2</sub>Ph) ppm; <sup>11</sup>B NMR (96.4 MHz, C<sub>6</sub>D<sub>5</sub>Br, 293 K) δ<sub>B</sub> -17.01 (s, 1 B) ppm; <sup>19</sup>F NMR (282.8 MHz, C<sub>6</sub>D<sub>5</sub>Br, 293 K) δ<sub>F</sub> -131.21 (s, 2 F), -161.73 (s, 1 F), -165.52 (s, 2 F) ppm.

### 6.2.7.2 [Sc(Bn-BOPA)CH<sub>2</sub>SiMe<sub>2</sub>Ph][B(C<sub>6</sub>F<sub>5</sub>)<sub>4</sub>] (6b)

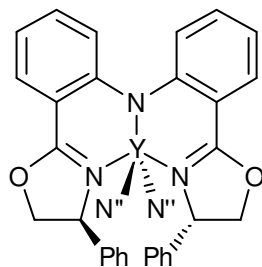
<sup>1</sup>H NMR (400.1 MHz, C<sub>6</sub>D<sub>5</sub>Br, 293 K) δ<sub>H</sub> 7.51 (d, <sup>3</sup>J<sub>HH</sub> = 8.16 Hz, NArH<sup>d</sup>, 2 H), 7.11 – 7.07 (m, 7 H), 7.08 – 7.05 (m, 2 H), 6.86 – 6.81 (m, 6 H), 6.96 (t, <sup>3</sup>J<sub>HH</sub> = 8.71 Hz, NArH<sup>b</sup>, 2 H), 6.64 (t, <sup>3</sup>J<sub>HH</sub> = 7.61 Hz, NArH<sup>c</sup>, 2 H), 6.42 (d, <sup>3</sup>J<sub>HH</sub> = 8.71 Hz, NArH<sup>a</sup>, 2 H), 4.11- 4.02 (m, H<sup>g</sup>, 2 H), 3.89 – 3.79 (m, H<sup>e</sup>, 2 H), 3.64 (t, <sup>3</sup>J<sub>HH</sub> = 8.80 Hz, H<sup>f</sup>, 2 H), 2.42 (dd, <sup>2</sup>J<sub>HH</sub> = 13.11 Hz, <sup>3</sup>J<sub>HH</sub> = 7.70 Hz, CHHPh, 2 H), 2.23 – 2.12 (m, CHHPh, 2 H), -0.31 (s, CHHSiMe<sub>2</sub>Ph, 1 H), -0.34 (s, CH<sub>2</sub>SiMe<sub>2</sub>Ph, 6 H), -0.49 (s, CHHSiMe<sub>2</sub>Ph, 1 H) ppm; <sup>13</sup>C{<sup>1</sup>H} NMR (125.8 MHz, C<sub>6</sub>D<sub>5</sub>Br, 293 K) δ<sub>C</sub> 174.4 (C=N), 156.3 (NArC<sup>m</sup>), 150.0 (*i*-C<sub>6</sub>F<sub>5</sub>), 147.4 (d, <sup>1</sup>J<sub>CF</sub> = 245.3 Hz, C<sub>6</sub>F<sub>5</sub>), 145.0 (*i*-SiC<sub>6</sub>H<sub>5</sub>), 138.4 (d, <sup>1</sup>J<sub>CF</sub> = 232.5 Hz, C<sub>6</sub>F<sub>5</sub>), 135.6 (d, <sup>1</sup>J<sub>CF</sub> = 241.9 Hz, C<sub>6</sub>F<sub>5</sub>), 138.6 (*i*-C\*HC<sub>6</sub>H<sub>5</sub>), 136.3, 134.6, 134.0, 132.5 (*m*-SiC<sub>6</sub>H<sub>5</sub>), 131.7, 131.3, 130.1 (NArC<sup>i</sup>), 127.7, 126.9, 123.6, 123.1 (NArC<sup>n</sup>), 75.4 (C<sup>p</sup>), 68.3 (C<sup>q</sup>), 41.3 (CH<sub>2</sub>Ph), 0.0 (CH<sub>2</sub>SiMe<sub>2</sub>Ph), -0.1 (CH<sub>2</sub>SiMe<sub>2</sub>Ph) ppm; <sup>11</sup>B NMR (96.4 MHz, C<sub>6</sub>D<sub>5</sub>Br, 293 K) δ<sub>B</sub> -17.10 (s, 1 B) ppm; <sup>19</sup>F NMR (282.8 MHz, C<sub>6</sub>D<sub>5</sub>Br, 293 K) δ<sub>F</sub> -131.06 (s, 2 F), -161.62 (s, 1 F), -165.48 (s, 2 F) ppm.

**6.2.7.3 [Sc(iPr-BOPA)CH<sub>2</sub>SiMe<sub>2</sub>Ph][B(C<sub>6</sub>F<sub>5</sub>)<sub>4</sub>] (6c)**

<sup>1</sup>H NMR (400.1 MHz, C<sub>6</sub>D<sub>5</sub>Br, 293 K) δ<sub>H</sub> 7.60 (d, <sup>3</sup>J<sub>HH</sub> = 7.72 Hz, NArH<sup>d</sup>, 2 H), 6.93 (t, <sup>3</sup>J<sub>HH</sub> = 7.09 Hz, NArH<sup>b</sup>, 2 H), 6.90 – 6.87 (m, 3 H), 6.86 (t, <sup>3</sup>J<sub>HH</sub> = 7.88 Hz, NArH<sup>c</sup>, 2 H), 6.82 – 6.78 (m, 2 H), 6.73 (m, NArH<sup>a</sup>, 2 H), 4.23 – 3.68 (m, 6 H), 0.47 – 0.25 (m, (CH<sub>3</sub>)<sub>2</sub>CH, 2 H), 0.05 (s, MeCHMe, 3 H), -0.27 (s, CH<sub>2</sub>SiMe<sub>2</sub>Ph, 6 H), -0.33 (s, MeCHMe, 3 H), -0.49 (s, CH<sub>2</sub>SiMe<sub>2</sub>Ph, 2 H) ppm; <sup>13</sup>C{<sup>1</sup>H} NMR (125.8 MHz, C<sub>6</sub>D<sub>5</sub>Br, 293 K) δ<sub>C</sub> 173.0 (C=N), 150.0 (NArC<sup>m</sup>), 147.4 (*i*-C<sub>6</sub>F<sub>5</sub>), 145.0 (d, <sup>1</sup>J<sub>CF</sub> = 244.3 Hz, C<sub>6</sub>F<sub>5</sub>), 138.9 (*i*-SiC<sub>6</sub>H<sub>5</sub>), 138.6 (d, <sup>1</sup>J<sub>CF</sub> = 233.2 Hz, C<sub>6</sub>F<sub>5</sub>), 134.6 (d, <sup>1</sup>J<sub>CF</sub> = 242.1 Hz, C<sub>6</sub>F<sub>5</sub>), 134.4, 133.0, 132.5 (*m*-SiC<sub>6</sub>H<sub>5</sub>), 131.2 (NArC<sup>i</sup>), 128.9, 128.8, 126.9, 123.1 (NArC<sup>n</sup>), 111.1, 72.2 (C<sup>p</sup>), 66.6 (C<sup>q</sup>), 31.3 ((CH<sub>3</sub>)<sub>2</sub>CH), 20.1 (MeCHMe), 15.2 (MeCHMe), 0.0 (CH<sub>2</sub>SiMe<sub>2</sub>Ph), -2.5 (CH<sub>2</sub>SiMe<sub>2</sub>Ph) ppm; <sup>11</sup>B NMR (96.4 MHz, C<sub>6</sub>D<sub>5</sub>Br, 293 K) δ<sub>B</sub> -16.96 (s, 1 B) ppm; <sup>19</sup>F NMR (282.8 MHz, C<sub>6</sub>D<sub>5</sub>Br, 293 K) δ<sub>F</sub> -131.32 (s, 2 F), -161.68 (s, 1 F), -165.54 (s, 2 F) ppm.

**6.2.8 General procedure for [Y(R-BOPA){N(SiMe<sub>3</sub>)<sub>2</sub>]<sub>2</sub>] (7a-c)**

To a solution of [Y{N(SiMe<sub>3</sub>)<sub>2</sub>]<sub>3</sub>] (200 mg) in THF (20 ml) the BOPA ligand (1 eq.) in THF (10 ml) was added dropwise. The reaction mixture was stirred at 40 °C for 48 hours after which the solvent was removed under reduced pressure. The resulting yellow solid was washed with cold pentane (5 ml) and dried in *vacuo* to yield the complex (7a-c).



### 6.2.8.1 [Y(Ph-BOPA){N(SiMe<sub>3</sub>)<sub>2</sub>}<sub>2</sub>] (7a) 79%

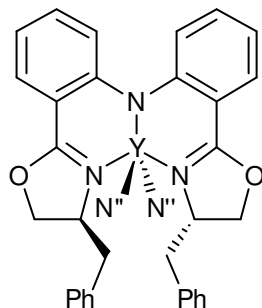
#### *exo* isomer

<sup>1</sup>H NMR (500.1 MHz, C<sub>6</sub>D<sub>6</sub>, 293 K) δ<sub>H</sub> 8.06 (dd, <sup>3</sup>J<sub>HH</sub> = 8.2 Hz, <sup>4</sup>J<sub>HH</sub> = 1.6 Hz, NArH<sup>d</sup>, 2 H), 7.04 – 6.93 (m, 14 H), 6.63 (app.t, <sup>3</sup>J<sub>HH</sub> = 8.2 Hz, NArH<sup>c</sup>, 2 H), 5.65 – 5.60 (m, H<sup>g</sup>, 2 H), 4.28 (app.t, <sup>2</sup>J<sub>HH</sub> = 8.5 Hz, H<sup>e</sup>, 2 H), 3.83 (dd, <sup>2</sup>J<sub>HH</sub> = 8.4 Hz, <sup>3</sup>J<sub>HH</sub> = 2.5 Hz, H<sup>f</sup>, 2 H), 0.36 (s, N(SiMe<sub>3</sub>)(SiMe<sub>3</sub>), 18 H), 0.09 (s, N(SiMe<sub>3</sub>)(SiMe<sub>3</sub>), 18 H) ppm, <sup>13</sup>C{<sup>1</sup>H} NMR (100.6 MHz, C<sub>6</sub>D<sub>6</sub>, 293 K) δ<sub>C</sub> 170.6 (C=N), 156.9 (NArC<sup>m</sup>), 140.6 (*i*-C<sub>6</sub>H<sub>5</sub>), 134.0 (NArC<sup>k</sup> or NArC<sup>l</sup>), 132.3 (NArC<sup>i</sup>), 129.7 (NArC<sup>k</sup> or NArC<sup>l</sup>), 129.0 (oxaz-ph), 127.2 (oxaz-ph), 126.3 (oxaz-ph), 118.4 (NArC<sup>j</sup>), 115.5 (NArC<sup>n</sup>), 75.2 (C<sup>p</sup>), 69.5 (C<sup>q</sup>), 6.1 (N(SiMe<sub>3</sub>)(SiMe<sub>3</sub>)), 4.8 (N(SiMe<sub>3</sub>)(SiMe<sub>3</sub>)) ppm.

#### *endo* isomer

<sup>1</sup>H NMR (500.1 MHz, C<sub>6</sub>D<sub>6</sub>, 293 K) δ<sub>H</sub> 8.09 (dd, <sup>3</sup>J<sub>HH</sub> = 7.89 Hz, <sup>4</sup>J<sub>HH</sub> = 1.46 Hz, NArH<sup>d</sup>, 2 H), 7.78 (d, <sup>3</sup>J<sub>HH</sub> = 8.04 Hz, 2 H), 7.04 – 6.93 (m, 14 H), 6.54 (app.t, <sup>3</sup>J<sub>HH</sub> = 7.89 Hz, NArH<sup>c</sup>, 2 H), 5.95 – 5.86 (m, H<sup>g</sup>, 1 H), 5.77 – 5.69 (m, H<sup>g</sup>, 1 H), 4.08 (app.t, <sup>2</sup>J<sub>HH</sub> = 8.04 Hz, H<sup>e</sup>, 1 H), 3.76 (dd, <sup>2</sup>J<sub>HH</sub> = 10.48 Hz, <sup>3</sup>J<sub>HH</sub> = 8.04 Hz, H<sup>f</sup>, 2 H), 3.49 (app.t, <sup>2</sup>J<sub>HH</sub> = 10.23 Hz, H<sup>e</sup>, 1 H), 0.36 (s, N(SiMe<sub>3</sub>)(SiMe<sub>3</sub>), 18 H), 0.09 (s, N(SiMe<sub>3</sub>)(SiMe<sub>3</sub>), 18 H) ppm; IR (ν cm<sup>-1</sup>) (KBr): 3461 (m), 3061 (w), 3028 (w), 2962 (s), 2900 (m), 1635 (m) (C=N), 1614 (m) (C=N), 1582 (m), 1558 (w), 1535 (m), 1494 (w), 1461 (m), 1430 (m), 1379 (w), 1359 (w), 1325 (w), 1261

(s), 1224 (w), 1159 (w), 1097 (s), 1060 (s), 1027 (s), 953 (w), 936 (w), 842 (m), 802 (s), 747 (m), 698 (m), 665 (w), 595 (w), 540 (w)  $\text{cm}^{-1}$ .



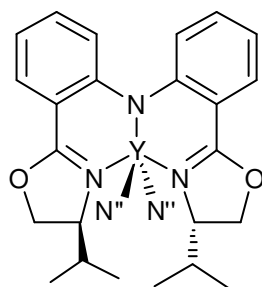
### 6.2.8.2 [Y(Bn-BOPA){N(SiMe<sub>3</sub>)<sub>2</sub>}<sub>2</sub>] (7b) 77%

<sup>1</sup>H NMR (500.1 MHz, C<sub>6</sub>D<sub>6</sub>, 293 K)  $\delta_{\text{H}}$  7.99 (dd, <sup>3</sup>J<sub>HH</sub> = 8.2 Hz, <sup>4</sup>J<sub>HH</sub> = 1.6 Hz, NArH<sup>d</sup>, 2 H), 7.14 – 7.08 (m, 10 H), 7.04 - 6.98 (m, NArH<sup>a</sup> and NArH<sup>b</sup>, 4 H), 6.62 (app.t, <sup>3</sup>J<sub>HH</sub> = 7.3 Hz, NArH<sup>c</sup>, 2 H), 5.19-5.11 (m, H<sup>g</sup>, 2 H), 4.01 (app.t, <sup>2</sup>J<sub>HH</sub> = 9.1 Hz, H<sup>e</sup>, 2 H), 3.86 (dd, <sup>2</sup>J<sub>HH</sub> = 8.4 Hz, <sup>3</sup>J<sub>HH</sub> = 6.0 Hz, H<sup>f</sup>, 2 H), 3.61 (dd, <sup>2</sup>J<sub>HH</sub> = 14.0 Hz, <sup>3</sup>J<sub>HH</sub> = 3.9 Hz, CHHP<sub>2</sub>, 2 H), 2.75 (dd, <sup>2</sup>J<sub>HH</sub> = 14.0 Hz, <sup>3</sup>J<sub>HH</sub> = 9.1 Hz, CHHP<sub>2</sub>, 2 H), 0.47 (s, N(SiMe)(SiMe), 18 H), 0.16 (s, N(SiMe)(SiMe), 18 H) ppm; <sup>13</sup>C{<sup>1</sup>H} NMR (100.6 MHz, C<sub>6</sub>D<sub>6</sub>, 293 K)  $\delta_{\text{C}}$  170.0 (C=N), 157.3 (NArC<sup>m</sup>), 136.9 (*i*-C<sub>6</sub>H<sub>5</sub>), 133.8 (NArC<sup>k</sup> or NArC<sup>l</sup>), 133.1 (NArC<sup>i</sup>), 129.4 (NArC<sup>k</sup> or NArC<sup>l</sup>), 129.4 (oxaz-ph), 127.4 (oxaz-ph), 127.3 (oxaz-ph), 118.8 (NArC<sup>j</sup>), 116.4 (NArC<sup>n</sup>), 70.8 (C<sup>p</sup>), 67.3 (C<sup>q</sup>), 42.6 (CH<sub>2</sub>Ph), 7.7 (N(SiMe<sub>3</sub>)(SiMe<sub>3</sub>)), 6.3 (N(SiMe<sub>3</sub>)(SiMe<sub>3</sub>)) ppm.

#### *endo* isomer

<sup>1</sup>H NMR (500.1 MHz, C<sub>6</sub>D<sub>6</sub>, 293 K)  $\delta_{\text{H}}$  8.05 (dd, <sup>3</sup>J<sub>HH</sub> = 8.19 Hz, <sup>4</sup>J<sub>HH</sub> = 1.61 Hz, NArH<sup>d</sup>, 2 H), 7.69 (dd, <sup>3</sup>J<sub>HH</sub> = 8.33 Hz, <sup>4</sup>J<sub>HH</sub> = 1.61 Hz, NArH<sup>b</sup>, 2 H), 7.14 – 7.08 (m, 10 H), 6.78 (d, <sup>3</sup>J<sub>HH</sub> = 8.77 Hz, NArH<sup>a</sup>, 2 H), 6.56 (app.t, <sup>3</sup>J<sub>HH</sub> = 7.60 Hz, NArH<sup>c</sup>, 2 H), 4.97- 4.86 (m, H<sup>g</sup>, 2 H), 4.19 (dd, <sup>2</sup>J<sub>HH</sub> = 13.00 Hz, <sup>3</sup>J<sub>HH</sub> = 3.36 Hz, H<sup>e</sup>, 2 H), 3.76 (d, <sup>2</sup>J<sub>HH</sub> = 9.21 Hz, H<sup>f</sup>, 2 H), 3.69 (dd, <sup>2</sup>J<sub>HH</sub> = 9.06 Hz, CHHP<sub>2</sub>, 2 H), 2.83 (dd, <sup>2</sup>J<sub>HH</sub> = 12.13 Hz, CHHP<sub>2</sub>, 2 H), 0.36 (s,

$\text{N}(\text{SiMe})_2(\text{SiMe})$ , 18 H), 0.28 (s,  $\text{N}(\text{SiMe})_2(\text{SiMe})$ , 18 H) ppm; IR ( $\nu \text{ cm}^{-1}$ ) (KBr): 3448 (m), 2959 (s), 2897 (m), 1624 (s) (C=N), 1559 (w), 1537 (m), 1481 (w), 1464 (s), 1427 (s), 1363 (w), 1321 (m), 1260 (s), 1220 (s), 1159 (m), 1089 (m), 1048 (s), 976 (m), 864 (w), 821 (m), 807 (m), 749 (m), 669 (w), 609 (w), 542 (w), 517 (w), 471 (w), 452 (w), 440 (w), 419 (w)  $\text{cm}^{-1}$ ; Anal. Calcd for  $\text{YC}_{44}\text{H}_{64}\text{Si}_4\text{N}_5\text{O}_2$  (896.26  $\text{g mol}^{-1}$ ): C 58.96, H 7.20, N 7.81. Found: C 59.69, H 7.46, N 7.14.



### 6.2.8.3 [Y(iPr-BOPA){N(SiMe<sub>3</sub>)<sub>2</sub>}<sub>2</sub>] (7c) 68%

<sup>1</sup>H NMR (500.1 MHz, C<sub>6</sub>D<sub>6</sub>, 293 K)  $\delta_{\text{H}}$  8.05 (dd, <sup>3</sup> $J_{\text{HH}} = 8.5$  Hz, <sup>4</sup> $J_{\text{HH}} = 1.3$  Hz, NArH<sup>d</sup>, 2 H), 6.94 (dd, <sup>3</sup> $J_{\text{HH}} = 8.3$  Hz, <sup>4</sup> $J_{\text{HH}} = 1.6$  Hz, NArH<sup>a</sup>, 2 H), 6.91 (app.t, <sup>3</sup> $J_{\text{HH}} = 8.3$  Hz, NArH<sup>b</sup>, 2 H), 6.60 (app.t, <sup>3</sup> $J_{\text{HH}} = 8.5$  Hz, NArH<sup>c</sup>, 2 H), 4.75 – 4.68 (m, H<sup>g</sup>, 2 H), 3.98 (d, <sup>3</sup> $J_{\text{HH}} = 6.4$  Hz, H<sup>e</sup>/H<sup>f</sup>, 4 H), 2.28 – 2.16 (m, (CH<sub>3</sub>)<sub>2</sub>CH, 2 H), 0.68 (d, <sup>3</sup> $J_{\text{HH}} = 7.0$  Hz, MeCHMe, 6 H), 0.61 (d, <sup>3</sup> $J_{\text{HH}} = 6.9$  Hz, MeCHMe, 6 H), 0.09 (s, N(SiMe<sub>3</sub>)<sub>2</sub>, 36 H) ppm; <sup>13</sup>C{<sup>1</sup>H} NMR (100.6 MHz, C<sub>6</sub>D<sub>6</sub>, 293 K)  $\delta_{\text{C}}$  169.4 (C=N), 157.2 (NArC<sup>m</sup>), 133.8 (NArC<sup>k</sup>), 132.5 (NArC<sup>i</sup>), 126.9 (NArC<sup>l</sup>), 118.5 (NArC<sup>j</sup>), 115.7 (NArC<sup>n</sup>), 71.1 (C<sup>p</sup>), 66.8 (C<sup>q</sup>), 30.4 ((CH<sub>3</sub>)<sub>2</sub>CH), 19.2 (MeCHMe), 14.5 (MeCHMe), 2.7 (N(SiMe<sub>3</sub>)(SiMe<sub>3</sub>)), 2.7 (N(SiMe<sub>3</sub>)(SiMe<sub>3</sub>)) ppm.

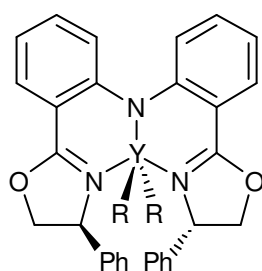
#### *endo isomer*

<sup>1</sup>H NMR (500.1 MHz, C<sub>6</sub>D<sub>6</sub>, 293 K)  $\delta_{\text{H}}$  8.08 (dd, <sup>3</sup> $J_{\text{HH}} = 7.89$  Hz, <sup>4</sup> $J_{\text{HH}} = 1.02$  Hz, NArH<sup>d</sup>, 2 H), 7.76 (dd, <sup>3</sup> $J_{\text{HH}} = 6.43$  Hz, NArH<sup>a</sup>, 2 H), 7.02 (app.t, <sup>3</sup> $J_{\text{HH}} = 7.89$  Hz, NArH<sup>b</sup>, 2 H), 6.54 (app.t, <sup>3</sup> $J_{\text{HH}} = 7.89$  Hz, NArH<sup>c</sup>, 2 H), 4.53 – 4.45 (m, H<sup>g</sup>, 2 H), 3.71 – 3.64 (m, H<sup>e</sup>/H<sup>f</sup>, 4 H),

2.74 – 2.64 (m, (CH<sub>3</sub>)<sub>2</sub>CH, 2 H), 0.48 (d, <sup>3</sup>J<sub>HH</sub> = 6.43 Hz, MeCHMe, 6 H), 0.46 (d, <sup>3</sup>J<sub>HH</sub> = 6.29 Hz, MeCHMe, 6 H), 0.09 (s, N(SiMe<sub>3</sub>)(SiMe<sub>3</sub>), 36 H) ppm; IR (ν cm<sup>-1</sup>) (KBr): 3446 (br w), 2960 (s), 2897 (m), 2877 (w), 1626 (s) (C=N), 1587 (w), 1559 (w), 1537 (m), 1479 (m), 1464 (s), 1427 (s), 1357 (w), 1322 (m), 1260 (s), 1221 (s), 1159 (m), 1097 (m), 1048 (s), 976 (w), 866 (w), 804 (m), 750 (m), 665 (w), 595 (w), 540 (w), 518 (w), 442 (w), 419 (w) cm<sup>-1</sup>.

### 6.2.9 General procedure for [Y(R-BOPA)(CH<sub>2</sub>SiMe<sub>2</sub>Ph)<sub>2</sub>] (8a-c)

To a pentane (10 mL) solution of [Y(CH<sub>2</sub>SiMe<sub>2</sub>Ph)<sub>3</sub>(THF)<sub>2</sub>] (200 mg) at 0 °C the R-BOPA ligand (1 equiv.) was added dropwise in a THF solution (20 ml). The solution was allowed to warm to room temperature and stirred for a further 2 hours, after which volatiles were removed under reduced pressure. The resulting orange oil was dissolved in the minimum amount of THF (~5 mL), and pentane added (20 mL). The mixture was then cooled to -78 °C and stirred for 30 minutes, after which a yellow precipitate had formed. The precipitate was filtered and washed with cold pentane and subsequently dried in *vacuo* to yield complexes (8a-c).



#### 6.2.9.1 [Y(Ph-BOPA)(CH<sub>2</sub>SiMe<sub>2</sub>Ph)<sub>2</sub>] (8a) 74%

*exo* isomer

<sup>1</sup>H NMR (500.1 MHz, C<sub>6</sub>D<sub>6</sub>, 293 K) δ<sub>H</sub> 7.90 (dd, <sup>3</sup>J<sub>HH</sub> = 8.0 Hz, <sup>4</sup>J<sub>HH</sub> = 1.1 Hz, NArH<sup>d</sup>, 2 H), 7.59 (d, <sup>3</sup>J<sub>HH</sub> = 6.9 Hz, *m* - SiC<sub>6</sub>H<sub>5</sub>, 4 H), 7.29 – 7.17 (m, 4 H), 7.14 – 6.97 (m, 6 H), 6.95

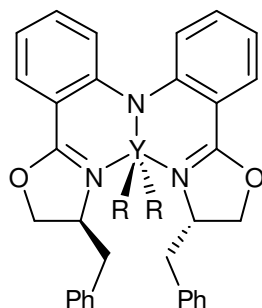


(app.t,  $^3J_{\text{HH}} = 7.4$  Hz, *p* – SiC<sub>6</sub>H<sub>5</sub>, 4 H), 6.90 (app.t,  $^3J_{\text{HH}} = 8.2$  Hz, oxaz-ph, 4 H), 6.85 (d,  $^3J_{\text{HH}} = 8.5$  Hz, NArH<sup>a</sup>, 2 H), 6.64 (app.t,  $^3J_{\text{HH}} = 7.3$  Hz, NArH<sup>c</sup>, 2 H), 5.00 (dd,  $^3J_{\text{HH}} = 9.1$  Hz,  $^3J_{\text{HH}} = 4.6$  Hz, H<sup>g</sup>, 2 H), 3.82 (app.t,  $^2J_{\text{HH}} = 9.3$  Hz, H<sup>e</sup>, 2 H), 3.65 (dd,  $^2J_{\text{HH}} = 8.5$  Hz,  $^3J_{\text{HH}} = 5.4$  Hz, H<sup>f</sup>, 2 H), 0.15 (s, CH<sub>2</sub>SiMeMePh, 6 H), -0.02 (s, CH<sub>2</sub>SiMeMePh, 6 H), -0.54 (dd,  $^2J_{\text{HH}} = 11.3$  Hz,  $^2J_{\text{HY}} = 2.7$  Hz, CHHSiMe<sub>2</sub>Ph, 2 H), -0.93 (dd,  $^2J_{\text{HH}} = 11.3$  Hz,  $^2J_{\text{HY}} = 2.7$  Hz, CHHSiMe<sub>2</sub>Ph, 2 H) ppm;  $^{13}\text{C}\{^1\text{H}\}$  NMR (100.6 MHz, C<sub>6</sub>D<sub>6</sub>, 293 K)  $\delta_{\text{C}}$  169.6 (C=N), 156.1 (NArC<sup>m</sup>), 147.0 (*i* – SiC<sub>6</sub>H<sub>5</sub>), 141.2 (*i* – oxaz-ph), 134.5 (*m* – SiC<sub>6</sub>H<sub>5</sub>), 133.8 (NArC<sup>l</sup>), 133.6 (NArC<sup>k</sup>), 131.9 (NArC<sup>i</sup>), 129.3 (*p* – SiC<sub>6</sub>H<sub>5</sub>), 129.1, 128.8, 127.6, 126.7, 118.6 (NArC<sup>j</sup>), 114.9 (NArC<sup>n</sup>), 75.5 (C<sup>p</sup>), 68.3 (C<sup>q</sup>), 35.0 (d,  $^1J_{\text{CY}} = 38.2$  Hz, CH<sub>2</sub>SiMe<sub>2</sub>Ph), 3.4 (CH<sub>2</sub>SiMeMePh), 1.9 (CH<sub>2</sub>SiMeMePh) ppm.

#### **endo isomer**

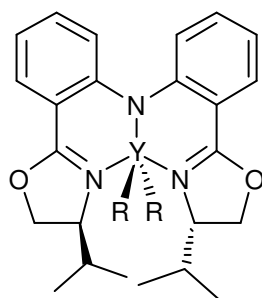
$^1\text{H}$  NMR (500.1 MHz, C<sub>6</sub>D<sub>6</sub>, 293 K)  $\delta_{\text{H}}$  7.95 (d,  $^3J_{\text{HH}} = 8.2$  Hz, NArH<sup>d</sup>, 2 H), 7.55 (d,  $^3J_{\text{HH}} = 6.9$  Hz, *m* – SiC<sub>6</sub>H<sub>5</sub>, 4 H), 7.29 – 7.17 (m, 4 H), 7.14 – 6.97 (m, 8 H), 6.95 (app.t,  $^3J_{\text{HH}} = 7.4$  Hz, *p* – SiC<sub>6</sub>H<sub>5</sub>, 4 H), 6.90 (app.t,  $^3J_{\text{HH}} = 8.2$  Hz, oxaz-ph, 4 H), 6.70 (app.t,  $^3J_{\text{HH}} = 6.9$  Hz, NArH<sup>c</sup>, 2 H), 4.37 (dd,  $^3J_{\text{HH}} = 10.4$  Hz,  $^3J_{\text{HH}} = 7.6$  Hz, H<sup>g</sup>, 2 H), 3.82 (app.t,  $^2J_{\text{HH}} = 10.1$  Hz, H<sup>e</sup>, 2 H), 3.74 (app.t,  $^2J_{\text{HH}} = 8.0$  Hz, H<sup>f</sup>, 2 H), 0.25 (s, CH<sub>2</sub>SiMeMePh, 6 H), 0.02 (s, CH<sub>2</sub>SiMeMePh, 6 H), -0.86 (dd,  $^2J_{\text{HH}} = 11.0$  Hz,  $^2J_{\text{HY}} = 2.4$  Hz, CHHSiMe<sub>2</sub>Ph, 2 H), -1.17 (dd,  $^2J_{\text{HH}} = 11.0$  Hz,  $^2J_{\text{HY}} = 2.7$  Hz, CHHSiMe<sub>2</sub>Ph, 2 H) ppm;  $^{13}\text{C}\{^1\text{H}\}$  NMR (100.6 MHz, C<sub>6</sub>D<sub>6</sub>, 293 K)  $\delta_{\text{C}}$  170.9 (C=N), 153.7 (NArC<sup>m</sup>), 146.8 (*i* – SiC<sub>6</sub>H<sub>5</sub>), 140.4 (*i* – oxaz-ph), 134.1 (*m* – SiC<sub>6</sub>H<sub>5</sub>), 134.0 (NArC<sup>l</sup>), 131.1 (NArC<sup>i</sup>), 130.8 (NArC<sup>k</sup>), 130.4 (*p* – SiC<sub>6</sub>H<sub>5</sub>), 128.6, 127.5, 127.4, 125.8, 125.2, 125.1, 118.8 (NArC<sup>j</sup>), 113.9 (NArC<sup>n</sup>), 75.8 (C<sup>p</sup>), 69.3 (C<sup>q</sup>), 33.7 (d,  $^1J_{\text{CY}} = 37.4$  Hz, CH<sub>2</sub>SiMe<sub>2</sub>Ph), 2.8 (CH<sub>2</sub>SiMeMePh), -0.9 (CH<sub>2</sub>SiMeMePh) ppm; IR ( $\nu$  cm<sup>-1</sup>) (KBr): 3067 (m), 3023 (w), 2956 (s), 2898 (m), 1632 (w) (C=N), 1609 (s) (C=N), 1578 (m), 1562 (m), 1534 (w), 1461 (s), 1434 (m), 1380 (m), 1319 (m), 1262 (m), 1248 (s), 1225 (s), 1205 (m), 1154 (m), 1111 (m), 1070 (s), 1037 (w), 956 (m), 837 (s), 743 (m), 696 (s) cm<sup>-1</sup>;

Anal. Calcd for  $\text{YC}_{48}\text{H}_{50}\text{N}_3\text{O}_2\text{Si}_2$  (846.01 g mol<sup>-1</sup>): C 68.15, H 5.96, N 4.97. Found: C 63.38, H 5.83, N 5.54.



### 6.2.9.2 [Y(Bn-BOPA)(CH<sub>2</sub>SiMe<sub>2</sub>Ph)<sub>2</sub>] (8b) 77%

<sup>1</sup>H NMR (500.1 MHz, C<sub>6</sub>D<sub>6</sub>, 293 K) δ<sub>H</sub> 7.88 (d, <sup>3</sup>J<sub>HH</sub> = 8.04 Hz, NArH<sup>d</sup>, 2 H), 7.66 (d, <sup>3</sup>J<sub>HH</sub> = 7.25 Hz, *m*-SiC<sub>6</sub>H<sub>5</sub>, 4 H), 7.07 – 6.96 (m, 18 H), 6.89 (d, <sup>3</sup>J<sub>HH</sub> = 6.62 Hz, *p*-SiC<sub>6</sub>H<sub>5</sub>, 2 H), 6.65 – 6.57 (m, NArH<sup>c</sup>, 2 H), 4.44 – 4.35 (m, H<sup>g</sup>, 2 H), 3.80 (d, <sup>3</sup>J<sub>HH</sub> = 7.25 Hz, H<sup>e</sup>, 2 H), 3.55 (t, <sup>3</sup>J<sub>HH</sub> = 8.83 Hz, H<sup>f</sup>, 2 H), 2.73 (d, <sup>2</sup>J<sub>HH</sub> = 14.50 Hz, CHHC<sub>6</sub>H<sub>5</sub>, 2 H), 2.45 (dd, <sup>2</sup>J<sub>HH</sub> = 13.87 Hz, <sup>3</sup>J<sub>HH</sub> = 8.04 Hz, CHHC<sub>6</sub>H<sub>5</sub>, 2 H), 0.37 (s, CH<sub>2</sub>SiMe<sub>2</sub>Ph, 6 H), 0.35 (s, CH<sub>2</sub>SiMe<sub>2</sub>Ph, 6 H), -0.04 (d, <sup>2</sup>J<sub>HH</sub> = 11.50 Hz, CHHSiMe<sub>2</sub>Ph, 2 H), -0.19 (d, <sup>2</sup>J<sub>HH</sub> = 11.50 Hz, CHHSiMe<sub>2</sub>Ph, 2 H) ppm; <sup>13</sup>C{<sup>1</sup>H} NMR (100.6 MHz, C<sub>6</sub>D<sub>6</sub>, 293 K) δ<sub>C</sub> 169.3 (C=N), 155.8 (NArC<sup>m</sup>), 146.5 (*i*-SiC<sub>6</sub>H<sub>5</sub>), 141.6 (*i*-oxaz-ph), 134.4 (*m*-SiC<sub>6</sub>H<sub>5</sub>), 133.8 (NArC<sup>l</sup>), 133.6 (NArC<sup>i</sup>), 132.0 (NArC<sup>k</sup>), 129.9 (*p*-SiC<sub>6</sub>H<sub>5</sub>), 129.1, 128.8, 127.1, 125.7, 118.7 (NArC<sup>j</sup>), 114.9 (NArC<sup>n</sup>), 71.2 (C<sup>p</sup>), 65.4 (C<sup>q</sup>), 41.0 (CH<sub>2</sub>C<sub>6</sub>H<sub>5</sub>), 34.5 (d, <sup>1</sup>J<sub>HH</sub> = 39.4 Hz, CH<sub>2</sub>SiMe<sub>2</sub>Ph), 3.5 (CH<sub>2</sub>SiMe<sub>2</sub>Ph), 2.8 (CH<sub>2</sub>SiMe<sub>2</sub>Ph) ppm; IR (ν cm<sup>-1</sup>) (KBr): 3061.4 (m), 3023.8 (m), 2957 (m), 2920 (m), 2899 (m), 2854 (w), 1608 (s) (C=N), 1580 (m), 1557 (w), 1535 (m), 1497 (w), 1462 (s), 1428 (s), 1376 (m), 1318 (m), 1260 (s), 1222 (s), 1159 (m), 1109 (m), 1079 (m), 1058 (m), 1035 (m), 969 (w), 928 (w), 836 (m), 807 (m), 746 (m), 723 (m), 699 (s) cm<sup>-1</sup>; Anal. Calcd for  $\text{YC}_{50}\text{H}_{54}\text{N}_3\text{O}_2\text{Si}_2$  (874.06 g mol<sup>-1</sup>): C 68.71, H 6.23, N 4.81. Found: C 63.29, H 5.87, N 5.39.



### 6.2.9.3 [Y(iPr-BOPA)(CH<sub>2</sub>SiMe<sub>2</sub>Ph)<sub>2</sub>] (8c) 64%

#### *exo* isomer

<sup>1</sup>H NMR (500.1 MHz, C<sub>6</sub>D<sub>6</sub>, 293 K) δ<sub>H</sub> 7.92 (dd, <sup>3</sup>J<sub>HH</sub> = 8.4 Hz, <sup>4</sup>J<sub>HH</sub> = 1.9 Hz, NArH<sup>d</sup>, 2 H), 7.68 (dd, <sup>3</sup>J<sub>HH</sub> = 8.0 Hz, <sup>4</sup>J<sub>HH</sub> = 1.4 Hz, *m*-SiC<sub>6</sub>H<sub>5</sub>, 4 H), 7.25 – 7.16 (m, 6 H), 6.96 (app.t, <sup>3</sup>J<sub>HH</sub> = 7.9 Hz, NArH<sup>b</sup>, 2 H), 6.78 (d, <sup>3</sup>J<sub>HH</sub> = 8.7 Hz, NArH<sup>a</sup>, 2 H), 6.61 (app.t, <sup>3</sup>J<sub>HH</sub> = 7.7 Hz, NArH<sup>c</sup>, 2 H), 4.17 – 4.11 (m, H<sup>g</sup>, 2 H), 3.77 (dd, <sup>2</sup>J<sub>HH</sub> = 8.74 Hz, <sup>3</sup>J<sub>HH</sub> = 4.3 Hz, H<sup>e</sup>, 2 H), 3.60 (app.t, <sup>2</sup>J<sub>HH</sub> = 9.5 Hz, H<sup>f</sup>, 2 H), 2.09 – 2.00 (m, (CH<sub>3</sub>)<sub>2</sub>CH, 2 H), 0.44 (d, <sup>3</sup>J<sub>HH</sub> = 6.8 Hz, CH<sub>3</sub>CHCH<sub>3</sub>, 6 H), 0.41 (d, <sup>3</sup>J<sub>HH</sub> = 6.5 Hz, CH<sub>3</sub>CHCH<sub>3</sub>, 6 H), 0.34 (s, SiMeMePh, 6 H), 0.33 (s, SiMeMePh, 6 H), -0.13 (dd, <sup>2</sup>J<sub>HH</sub> = 10.9 Hz, <sup>2</sup>J<sub>HY</sub> = 2.7 Hz, CHHSiMe<sub>2</sub>Ph, 2 H), -0.28 (dd, <sup>2</sup>J<sub>HH</sub> = 11.4 Hz, <sup>2</sup>J<sub>HY</sub> = 2.4 Hz, CHHSiMe<sub>2</sub>Ph, 2 H) ppm; <sup>13</sup>C{<sup>1</sup>H} NMR (100.6 MHz, C<sub>6</sub>D<sub>6</sub>, 293 K) δ<sub>C</sub> 168.6 (C=N), 155.6 (NArC<sup>m</sup>), 146.6 (*i* – SiC<sub>6</sub>H<sub>5</sub>), 134.4 (NArC<sup>k</sup>), 133.8 (*m* – SiC<sub>6</sub>H<sub>5</sub>), 131.8 (NArC<sup>i</sup>), 129.1 (*p* – SiC<sub>6</sub>H<sub>5</sub>), 127.4 (*o* – SiC<sub>6</sub>H<sub>5</sub>), 125.6 (NArC<sup>l</sup>), 118.6 (NArC<sup>j</sup>), 114.8 (NArC<sup>n</sup>), 69.6 (C<sup>p</sup>), 67.6 (C<sup>q</sup>), 33.5 (d, <sup>1</sup>J<sub>CY</sub> = 37.4 Hz, CH<sub>2</sub>SiMe<sub>2</sub>Ph), 31.4 ((CH<sub>3</sub>)<sub>2</sub>CH), 18.5 (MeCHMe), 13.9 (MeCHMe), 3.4 (CH<sub>2</sub>SiMeMePh), -1.1 (CH<sub>2</sub>SiMeMePh) ppm.

#### *endo* isomer

<sup>1</sup>H NMR (500.1 MHz, C<sub>6</sub>D<sub>6</sub>, 293 K) δ<sub>H</sub> 8.18 (dd, <sup>3</sup>J<sub>HH</sub> = 7.73 Hz, <sup>4</sup>J<sub>HH</sub> = 1.73 Hz, H, 2 H), 7.56 (br.d, <sup>3</sup>J<sub>HH</sub> = 6.78 Hz, *m*-SiC<sub>6</sub>H<sub>5</sub>, 4 H), 7.25 – 7.16 (m, 6 H), 6.96 (app.t, <sup>3</sup>J<sub>HH</sub> = 7.25 Hz, NArH<sup>b</sup>, 2 H), 6.84 (d, <sup>3</sup>J<sub>HH</sub> = 8.67 Hz, NArH<sup>a</sup>, 2 H), 6.64 (app.t, <sup>3</sup>J<sub>HH</sub> = 7.72 Hz, NArH<sup>c</sup>, 2 H),

3.97 – 3.92 (m, H<sup>g</sup>, 2 H), 3.89 (dd,  $^2J_{\text{HH}} = 9.30$  Hz,  $^3J_{\text{HH}} = 3.45$  Hz, H<sup>e</sup>, 2 H), 3.31 (app.t,  $^2J_{\text{HH}} = 9.14$  Hz, H<sup>f</sup>, 2 H), 1.80 – 1.71 (m, (CH<sub>3</sub>)<sub>2</sub>CH, 2 H), 0.50 (d,  $^3J_{\text{HH}} = 6.20$  Hz, CH<sub>3</sub>CHCH<sub>3</sub>, 6 H), 0.48 (d,  $^3J_{\text{HH}} = 6.31$  Hz, CH<sub>3</sub>CHCH<sub>3</sub>, 6 H), 0.31 (s, SiMeMePh, 6 H), 0.06 (s, SiMeMePh, 6 H), -0.13 (dd,  $^2J_{\text{HH}} = 10.9$  Hz,  $^2J_{\text{HY}} = 2.7$  Hz, CHHSiMe<sub>2</sub>Ph, 2 H), -0.28 (dd,  $^2J_{\text{HH}} = 11.4$  Hz,  $^2J_{\text{HY}} = 2.4$  Hz, CHHSiMe<sub>2</sub>Ph, 2 H) ppm; IR ( $\nu$  cm<sup>-1</sup>) (KBr): 3064 (m), 3054 (w), 2959 (s), 2902 (m), 2871 (m), 1617 (s) (C=N), 1589 (m), 1560 (m), 1539 (m), 1484 (m), 1461 (s), 1429 (s), 1372 (m), 1316 (m), 1261 (s), 1245 (w), 1223 (m), 1159 (m), 1148 (m), 1115 (m), 1063 (m), 1050 (m), 969 (m), 925 (w) cm<sup>-1</sup>; Anal. Calcd for YC<sub>42</sub>H<sub>54</sub>N<sub>3</sub>O<sub>2</sub>Si<sub>2</sub> (777.97 g mol<sup>-1</sup>): C 64.84, H 7.00, N 5.40. Found: C 64.69, H 7.07, N 5.38.

## 6.2.10 NMR scale General procedure for

### [Y(R-BOPA)CH<sub>2</sub>SiMe<sub>2</sub>Ph][B(C<sub>6</sub>F<sub>5</sub>)<sub>4</sub>] (9a-c)

To a solution of **8** (0.0105 mmol) in bromobenzene (0.30 ml) a solution of [Ph<sub>3</sub>C][B(C<sub>6</sub>F<sub>5</sub>)<sub>4</sub>] (1 eq.) in bromobenzene (0.30 ml) was added dropwise to form a red solution.

#### 6.2.10.1 [Y(Ph-BOPA)CH<sub>2</sub>SiMe<sub>2</sub>Ph][B(C<sub>6</sub>F<sub>5</sub>)<sub>4</sub>] (9a)

<sup>1</sup>H NMR (400.1 MHz, C<sub>6</sub>D<sub>5</sub>Br, 293 K)  $\delta_{\text{H}}$  7.60 (d,  $^3J_{\text{HH}} = 9.45$  Hz, NArH<sup>d</sup>, 2 H), 6.91 – 6.83 (m, 13 H), 6.76 (t,  $^3J_{\text{HH}} = 5.50$  Hz, *p*-SiC<sub>6</sub>H<sub>5</sub>, 2 H), 6.70 (t,  $^3J_{\text{HH}} = 11.10$  Hz, NArH<sup>c</sup>, 2 H), 6.61 (br d,  $^3J_{\text{HH}} = 7.43$  Hz, NArH<sup>b</sup>, 2 H), 6.09 (d,  $^3J_{\text{HH}} = 11.00$  Hz, NArH<sup>a</sup>, 2 H), 4.78 – 4.66 (m, H<sup>g</sup>, 2 H), 4.46 (t,  $^2J_{\text{HH}} = 10.45$  Hz, H<sup>e</sup>, 2 H), 4.02 (t,  $^2J_{\text{HH}} = 7.34$  Hz, H<sup>f</sup>, 2 H), 0.06 (s, CH<sub>2</sub>SiMeMePh, 3 H), 0.03 (d,  $^2J_{\text{HH}} = 9.26$  Hz, CHHSiMe<sub>2</sub>Ph, 1 H), -0.29 (d,  $^2J_{\text{HH}} = 11.10$  Hz, CHHSiMe<sub>2</sub>Ph, 1 H), -0.34 (s, CH<sub>2</sub>SiMeMePh, 3 H) ppm; <sup>13</sup>C{<sup>1</sup>H} NMR (125.8 MHz, C<sub>6</sub>D<sub>5</sub>Br, 293 K)  $\delta_{\text{C}}$  164.0 (C=N), 150.7 (NArC<sup>m</sup>), 150.0 (*i*-SiC<sub>6</sub>H<sub>5</sub>), 148.6 (*i*-C<sub>6</sub>F<sub>5</sub>) 145.0, 140.4, 136.6, 134.4 (*m*-SiC<sub>6</sub>H<sub>5</sub>), 131.5, 130.1, 128.8 (*p*-SiC<sub>6</sub>H<sub>5</sub>), 128.4, 127.7, 126.7, 126.4, 125.4, 123.1,

120.2 (NArC<sup>j</sup>), 111.2 (NArC<sup>n</sup>), 72.2 (C<sup>p</sup>), 68.7 (C<sup>q</sup>), 33.9 (d,  $^1J_{\text{CY}} = 39.5$  Hz,  $\underline{\text{C}}\text{H}_2\text{SiMe}_2\text{Ph}$ ), 0.0 ( $\underline{\text{C}}\text{H}_2\text{SiMeMePh}$ ), -0.1 ( $\underline{\text{C}}\text{H}_2\text{SiMeMePh}$ ) ppm;  $^{11}\text{B}$  NMR (96.4 MHz,  $\text{C}_6\text{D}_5\text{Br}$ , 293 K)  $\delta_{\text{B}}$  -17.3 (s, 1 B) ppm;  $^{19}\text{F}$  NMR (282.8 MHz,  $\text{C}_6\text{D}_5\text{Br}$ , 293 K)  $\delta_{\text{F}}$  -131.3 (s, 2 F), -161.3 (s, 1 F), -165.3 (s, 1 F) ppm.

### 6.2.10.2 [Y(Bn-BOPA)CH<sub>2</sub>SiMe<sub>2</sub>Ph][B(C<sub>6</sub>F<sub>5</sub>)<sub>4</sub>] (9b)

$^1\text{H}$  NMR (400.1 MHz,  $\text{C}_6\text{D}_5\text{Br}$ , 293 K)  $\delta_{\text{H}}$  7.50 (dd,  $^3J_{\text{HH}} = 8.35$  Hz,  $^4J_{\text{HH}} = 1.56$  Hz, NArH<sup>d</sup>, 2 H), 7.12 (dd,  $^3J_{\text{HH}} = 7.34$  Hz,  $^4J_{\text{HH}} = 1.83$  Hz, *o*-SiC<sub>6</sub>H<sub>5</sub>, 2 H), 6.96 (t,  $^3J_{\text{HH}} = 7.98$  Hz,  $^4J_{\text{HH}} = 1.56$  Hz, *m*-SiC<sub>6</sub>H<sub>5</sub>, 2 H), 6.93 (t,  $^3J_{\text{HH}} = 6.88$  Hz, oxaz-ph, 4 H), 6.91 – 6.86 (m, 5 H), 6.84 – 6.78 (m, 4 H), 6.60 (t,  $^3J_{\text{HH}} = 7.70$  Hz, NArH<sup>c</sup>, 2 H), 6.43 (d,  $^3J_{\text{HH}} = 8.84$  Hz, NArH<sup>a</sup>, 2 H), 4.02 – 3.95 (m, H<sup>e</sup>, 2 H), 3.86 – 3.82 (m, H<sup>e</sup>/H<sup>f</sup>, 4 H), 2.39 (dd,  $^2J_{\text{HH}} = 13.02$  Hz,  $^3J_{\text{HH}} = 6.88$  Hz, CHHC<sub>6</sub>H<sub>5</sub>, 2 H), 2.08 (dd,  $^2J_{\text{HH}} = 12.93$  Hz,  $^3J_{\text{HH}} = 8.16$  Hz, CHHC<sub>6</sub>H<sub>5</sub>, 2 H), 0.00 (s,  $\underline{\text{C}}\text{H}_2\text{SiMeMePh}$ , 3 H), -0.33 (s,  $\underline{\text{C}}\text{H}_2\text{SiMeMePh}$ , 3 H), -0.53 (dd,  $^2J_{\text{HH}} = 11.74$  Hz,  $^2J_{\text{HY}} = 3.30$  Hz,  $\underline{\text{C}}\text{HHSiMe}_2\text{Ph}$ , 2 H), -1.08 (dd,  $^2J_{\text{HH}} = 11.37$  Hz,  $^2J_{\text{HY}} = 2.80$  Hz,  $\underline{\text{C}}\text{HHSiMe}_2\text{Ph}$ , 2 H) ppm;  $^{13}\text{C}\{^1\text{H}\}$  NMR (125.8 MHz,  $\text{C}_6\text{D}_5\text{Br}$ , 293 K)  $\delta_{\text{C}}$  169.3 (C=N), 155.3 (NArC<sup>m</sup>), 150.1 (*i*-C<sub>6</sub>F<sub>5</sub>), 147.4 (*i*-SiC<sub>6</sub>H<sub>5</sub>), 145.1 (*i*-oxaz-ph), 136.5, 134.7 (*m*-SiC<sub>6</sub>H<sub>5</sub>), 134.5, 134.0 (NArC<sup>l</sup>), 131.8, 131.2, 129.9, 129.5, 129.0, 129.0 (*p*-SiC<sub>6</sub>H<sub>5</sub>), 128.8, 127.0, 126.7, 121.7 (NArC<sup>n</sup>), 73.8 (C<sup>p</sup>), 68.0 (C<sup>q</sup>), 41.6 ( $\underline{\text{C}}\text{H}_2\text{Ph}$ ), 32.4 (d,  $^2J_{\text{CY}} = 40.9$  Hz,  $\underline{\text{C}}\text{H}_2\text{SiMe}_2\text{Ph}$ , 2 H), 0.1 ( $\underline{\text{C}}\text{H}_2\text{SiMeMePh}$ ), 0.0 ( $\underline{\text{C}}\text{H}_2\text{SiMeMePh}$ ) ppm;  $^{11}\text{B}$  NMR (96.4 MHz,  $\text{C}_6\text{D}_5\text{Br}$ , 293 K)  $\delta_{\text{B}}$  -16.9 (s, 1 B) ppm;  $^{19}\text{F}$  NMR (282.8 MHz,  $\text{C}_6\text{D}_5\text{Br}$ , 293 K)  $\delta_{\text{F}}$  -131.4 (s, 2 F), -161.4 (s, 1 F), -165.4 (s, 2 F) ppm.

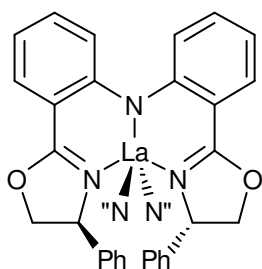
### 6.2.10.3 [Y(*i*Pr-BOPA)CH<sub>2</sub>SiMe<sub>2</sub>Ph][B(C<sub>6</sub>F<sub>5</sub>)<sub>4</sub>] (9c)

$^1\text{H}$  NMR (400.1 MHz,  $\text{C}_6\text{D}_5\text{Br}$ , 293 K)  $\delta_{\text{H}}$  7.54 (d,  $^3J_{\text{HH}} = 8.35$  Hz, NArH<sup>d</sup>, 2 H), 6.94 (t,  $^3J_{\text{HH}} = 7.70$  Hz, *o*-SiC<sub>6</sub>H<sub>5</sub>, 2 H), 6.83 (d,  $^3J_{\text{HH}} = 6.05$  Hz, *p*-SiC<sub>6</sub>H<sub>5</sub>, 1 H), 6.81 (m, 4 H), 6.59 (t,

$^3J_{\text{HH}} = 7.70$  Hz, NArH<sup>c</sup>, 2 H), 6.41 (d,  $^3J_{\text{HH}} = 8.25$  Hz, NArH<sup>a</sup>, 2 H), 3.94 – 3.81 (m, 6 H), 1.41 – 1.26 (m, (CH<sub>3</sub>)<sub>2</sub>CH, 2 H), 0.39 (d,  $^3J_{\text{HH}} = 4.49$  Hz, MeCHMe, 6 H), 0.20 (d,  $^3J_{\text{HH}} = 6.14$  Hz, MeCHMe, 6 H), -0.12 (d,  $^2J_{\text{HH}} = 11.09$  Hz,  $^2J_{\text{HY}} = 2.80$  Hz, CHHSiMe<sub>2</sub>Ph, 2 H), -0.33 (s, CH<sub>2</sub>SiMe<sub>2</sub>Ph, 6 H), -0.88 (d,  $^2J_{\text{HH}} = 11.09$  Hz,  $^2J_{\text{HY}} = 2.80$  Hz, CHHSiMe<sub>2</sub>Ph, 2 H) ppm;  $^{13}\text{C}\{^1\text{H}\}$  NMR (125.8 MHz, C<sub>6</sub>D<sub>5</sub>Br, 293 K)  $\delta_{\text{C}}$  169.7 (C=N), 150.0 (NArC<sup>m</sup>), 145.0 (*i*-C<sub>6</sub>F<sub>5</sub>), 138.6 (*i*-SiC<sub>6</sub>H<sub>5</sub>), 136.7, 134.9, 134.6, 134.4 (*m*-SiC<sub>6</sub>H<sub>5</sub>), 129.9, 129.4, 128.9, 126.9, 123.1, 121.9, 112.3 (NArC<sup>n</sup>), 67.4 (C<sup>p</sup>), 64.9 (C<sup>q</sup>), 33.2 ((CH<sub>3</sub>)<sub>2</sub>CH), 32.7 (d,  $^1J_{\text{CY}} = 38.2$  Hz, CH<sub>2</sub>SiMe<sub>2</sub>Ph), 32.0 (MeCHMe), 15.6 (MeCHMe), 0.0 (CH<sub>2</sub>SiMe<sub>2</sub>Ph), -0.1 (CH<sub>2</sub>SiMe<sub>2</sub>Ph) ppm;  $^{11}\text{B}$  NMR (96.4 MHz, C<sub>6</sub>D<sub>5</sub>Br, 293 K)  $\delta_{\text{B}}$  -16.8 (s, 1 B) ppm;  $^{19}\text{F}$  NMR (282.8 MHz, C<sub>6</sub>D<sub>5</sub>Br, 293 K)  $\delta_{\text{F}}$  -131.3 (s, 2 F), -161.4 (s, 1 F), -165.3 (s, 2 F) ppm.

### 6.2.11 General procedure for [La(R-BOPA)(N(SiMe<sub>3</sub>)<sub>2</sub>)<sub>2</sub>] (10a-c)

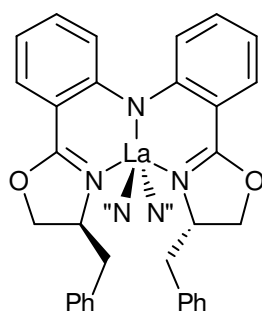
A dry THF solution (10 mL) of R-BOPA (1 eq.) was added drop-wise to a dry pentane solution (20 mL) of [La{N(SiMe<sub>3</sub>)<sub>2</sub>}<sub>3</sub>] (200 mg). The reaction mixture was left to stir for 2 hours and subsequently volatiles were removed under reduced pressure. The resulting yellow solid was washed with cold pentane (-76 °C) and left to dry in *vacuo* for 2 hours to yield **10a-c** as yellow solids.



#### 6.2.11.1 [La(Ph-BOPA)(N(SiMe<sub>3</sub>)<sub>2</sub>)<sub>2</sub>] (10a) 85 %

$^1\text{H}$  NMR (500.1 MHz, C<sub>6</sub>D<sub>6</sub>, 293 K)  $\delta_{\text{H}}$  8.06 (dd,  $^3J_{\text{HH}} = 6.5$  Hz,  $^4J_{\text{HH}} = 1.7$  Hz, NArH<sup>d</sup>, 2 H), 7.04 (ddd,  $^3J_{\text{HH}} = 5.4$  Hz,  $^4J_{\text{HH}} = 1.7$  Hz, NArH<sup>b</sup>, 2 H), 7.00 – 6.94 (m, 10 H), 6.79 (d,  $^3J_{\text{HH}} =$

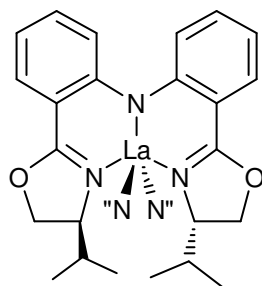
8.4 Hz, NArH<sup>a</sup>, 2 H), 6.65 (dd,  $^3J_{\text{HH}} = 6.0$  Hz,  $^4J_{\text{HH}} = 1.1$  Hz, NArH<sup>c</sup>, 2 H), 5.56 (dd,  $^3J_{\text{HH}} = 9.0$  Hz,  $^4J_{\text{HH}} = 3.2$  Hz, H<sup>g</sup>, 2 H), 4.23 (app.t,  $^3J_{\text{HH}} = 8.7$  Hz, H<sup>e</sup>, 2 H), 3.83 (dd,  $^4J_{\text{HH}} = 2.8$  Hz,  $^3J_{\text{HH}} = 8.7$  Hz, H<sup>f</sup>, 2 H), 0.10 (br s, N(SiMe<sub>3</sub>)<sub>2</sub>, 36 H) ppm;  $^{13}\text{C}\{^1\text{H}\}$  NMR (100.6 MHz, C<sub>6</sub>D<sub>6</sub>, 293 K)  $\delta_{\text{C}}$  169.5 (C=N), 156.0 (NArC<sup>m</sup>), 141.1 (*i*-C<sup>\*</sup>HC<sub>6</sub>H<sub>5</sub>), 134.3 (NArC<sup>k</sup>), 132.6 (NArC<sup>i</sup>), 129.1 (oxaz – C<sub>6</sub>H<sub>5</sub>), 128.3 (oxaz – C<sub>6</sub>H<sub>5</sub>), 127.0 (oxaz – C<sub>6</sub>H<sub>5</sub>), 126.3 (NArC<sup>l</sup>), 118.3 (NArC<sup>j</sup>), 115.5 (NArC<sup>n</sup>), 74.7 (C<sup>p</sup>), 69.5 (C<sup>q</sup>), 4.9 (N(SiMe<sub>3</sub>)<sub>2</sub>) ppm; IR ( $\nu$  cm<sup>-1</sup>) (KBr): 3453 (br m), 3055 (w), 3025 (w), 2955 (m), 2892 (m), 1633 (m) (C=N), 1606 (s) (C=N), 1579 (m), 1556 (w), 1533 (w), 1459 (s), 1429 (m), 1368 (w), 1338 (w), 1260 (s), 1223 (s), 1208 (m), 1157 (m), 1067 (m), 1040 (m), 991 (m), 821 (s), 746 (s), 695 (s), 664 (w), 594 (w) cm<sup>-1</sup>; Anal. Calcd for LaC<sub>42</sub>H<sub>60</sub>Si<sub>4</sub>N<sub>5</sub>O<sub>2</sub> (918.21 g mol<sup>-1</sup>): C 54.94, H 6.59, N 7.63. Found: C 54.82, H 6.45, N 7.67.



#### 6.2.11.2 [La(Bn-BOPA)(N(SiMe<sub>3</sub>)<sub>2</sub>)<sub>2</sub>] (10b) 82%

$^1\text{H}$  NMR (500.1 MHz, C<sub>6</sub>D<sub>6</sub>, 293 K)  $\delta_{\text{H}}$  8.00 (dd,  $^3J_{\text{HH}} = 8.4$  Hz,  $^4J_{\text{HH}} = 1.4$  Hz, NArH<sup>d</sup>, 2 H), 7.13-7.05 (m, CHC<sub>6</sub>H<sub>5</sub>, 10 H), 7.04-6.99 (m, NArH<sup>b</sup>, NArH<sup>a</sup>, 4 H), 6.62 (dd,  $^3J_{\text{HH}} = 6.5$  Hz,  $^4J_{\text{HH}} = 1.3$  Hz, NArH<sup>c</sup>, 2 H), 5.04 – 4.95 (m, H<sup>g</sup>, 2 H), 3.98 – 3.90 (m, H<sup>e</sup>/H<sup>f</sup>, 4 H), 3.42 (dd,  $^2J_{\text{HH}} = 13.9$  Hz,  $^3J_{\text{HH}} = 4.1$  Hz, CHHC<sub>6</sub>H<sub>5</sub>, 2 H), 2.62 (dd,  $^2J_{\text{HH}} = 13.9$  Hz,  $^3J_{\text{HH}} = 3.8$  Hz, CHHC<sub>6</sub>H<sub>5</sub>, 2 H), 0.30 (s, N(SiMe<sub>3</sub>)<sub>2</sub>, 36 H) ppm;  $^{13}\text{C}\{^1\text{H}\}$  NMR (100.6 MHz, C<sub>6</sub>D<sub>6</sub>, 293 K)  $\delta_{\text{C}}$  169.2 (C=N), 156.3 (NArC<sup>m</sup>), 136.6 (*i*-CH<sub>2</sub>C<sub>6</sub>H<sub>5</sub>), 134.0 (NArC<sup>k</sup> or NArC<sup>l</sup>), 132.5 (NArC<sup>i</sup>), 129.5 (CH<sub>2</sub>C<sub>6</sub>H<sub>5</sub>), 129.1 (CH<sub>2</sub>C<sub>6</sub>H<sub>5</sub>), 127.3 (CH<sub>2</sub>C<sub>6</sub>H<sub>5</sub>), 126.9 (NArC<sup>k</sup> or NArC<sup>l</sup>), 118.4 (NArC<sup>j</sup>), 115.8 (NArC<sup>n</sup>), 70.4 (C<sup>p</sup>), 67.1 (C<sup>q</sup>), 41.2 (CH<sub>2</sub>C<sub>6</sub>H<sub>5</sub>), 5.4 (N(SiMe<sub>3</sub>)<sub>2</sub>) ppm; IR ( $\nu$

cm<sup>-1</sup>) (KBr): 3450 (br w), 3061 (w), 3028 (w), 2954 (s), 2894 (m), 1626 (s) (C=N), 1606 (s) (C=N), 1583 (m), 1560 (w), 1536 (m), 1496 (w), 1462 (s), 1425 (m), 1368 (w), 1318 (m), 1257 (s), 1216 (s), 1181 (w), 1159 (m), 1048 (m), 980 (m), 930 (m), 823 (s), 747 (s), 698 (m), 664 (w), 595 (w) cm<sup>-1</sup>; Anal. Calcd for LaC<sub>44</sub>H<sub>64</sub>Si<sub>4</sub>N<sub>5</sub>O<sub>2</sub> (946.26 g mol<sup>-1</sup>): C 55.85, H 6.82, N 7.40. Found: C 55.74, H 6.91, N 7.28.



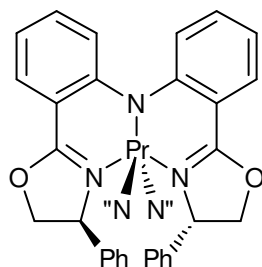
### 6.2.11.3 [La(ipr-BOPA)(N(SiMe<sub>3</sub>)<sub>2</sub>)<sub>2</sub>] (10c) 76%

<sup>1</sup>H NMR (500.1 MHz, C<sub>6</sub>D<sub>6</sub>, 293 K) δ<sub>H</sub> 8.03 (dd, <sup>3</sup>J<sub>HH</sub> = 8.4 Hz, <sup>4</sup>J<sub>HH</sub> = 1.7 Hz, NArH<sup>d</sup>, 2 H), 6.96 (dd, <sup>3</sup>J<sub>HH</sub> = 6.2 Hz, <sup>4</sup>J<sub>HH</sub> = 1.7 Hz, NArH<sup>b</sup>, 2 H), 6.80 (d, <sup>3</sup>J<sub>HH</sub> = 8.4 Hz, NArH<sup>a</sup>, 2 H), 6.61 (dd, <sup>3</sup>J<sub>HH</sub> = 6.9 Hz, <sup>4</sup>J<sub>HH</sub> = 0.9 Hz, NArH<sup>c</sup>, 2 H), 4.72 – 4.65 (m, H<sup>g</sup>, 2 H), 3.98 – 3.93 (m, H<sup>e</sup>/H<sup>f</sup>, 4 H), 2.18 – 2.08 (m, (CH<sub>3</sub>)<sub>2</sub>CH, 2 H), 0.66 (d, <sup>3</sup>J<sub>HH</sub> = 6.9 Hz, MeCHMe, 6 H), 0.56 (d, <sup>3</sup>J<sub>HH</sub> = 6.9 Hz, MeCHMe, 6 H), 0.23 (s, N(SiMe<sub>3</sub>)<sub>2</sub>, 36 H) ppm; <sup>13</sup>C{<sup>1</sup>H} NMR (100.6 MHz, C<sub>6</sub>D<sub>6</sub>, 293 K) δ<sub>C</sub> 168.4 (C=N), 156.3 (NArC<sup>m</sup>), 133.9 (NArC<sup>k</sup>), 132.4 (NArC<sup>i</sup>), 126.7 (NArC<sup>l</sup>), 118.2 (NArC<sup>j</sup>), 115.4 (NArC<sup>n</sup>), 70.9 (C<sup>p</sup>), 66.4 (C<sup>q</sup>), 30.8 ((CH<sub>3</sub>)<sub>2</sub>CH), 18.8 (MeCHMe), 13.9 (MeCHMe), 5.1 (N(SiMe<sub>3</sub>)<sub>2</sub>) ppm; IR (ν cm<sup>-1</sup>) (KBr): 3443 (br m), 2957 (m), 2900 (w), 1625 (m) (C=N), 1609 (s) (C=N), 1586 (m), 1556 (w), 1533 (w), 1460 (s), 1426 (m), 1372 (w), 1322 (w), 1259 (s), 1218 (s), 1161 (m), 1048 (m), 984 (m), 822 (m), 745 (m), 664 (w) cm<sup>-1</sup>; Anal. Calcd for LaC<sub>36</sub>H<sub>64</sub>Si<sub>4</sub>N<sub>5</sub>O<sub>2</sub> (850.17 g mol<sup>-1</sup>): C 50.86, H 7.59, N 8.24. Found: C 50.98, H 7.47, N 8.19.



### 6.2.12 General procedure for [Ln(R-BOPA)(N(SiMe<sub>3</sub>)<sub>2</sub>)<sub>2</sub>] (11-13a-c) Ln = Pr (11), Nd (12), Sm (13)

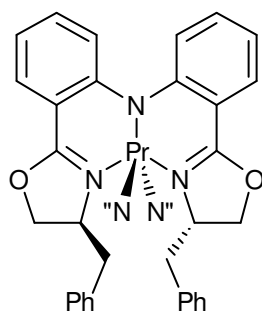
A dry THF solution (10 mL) of R-BOPA (1 eq.) was added drop-wise to a dry pentane solution (20 mL) of [Ln{N(SiMe<sub>3</sub>)<sub>2</sub>}<sub>3</sub>] (200 mg). The reaction mixture was left to stir overnight and subsequently volatiles were removed under reduced pressure. The resulting yellow solid was washed with cold pentane (-76 °C) and left to dry in *vacuo* for 2 hours to yield (11-13a-c) as yellow solids.



#### 6.2.12.1 [Pr(Ph-BOPA)(N(SiMe<sub>3</sub>)<sub>2</sub>)<sub>2</sub>] (11a) 87%

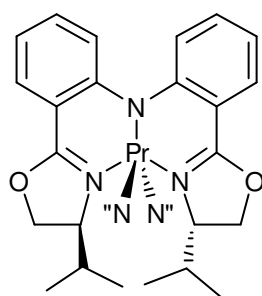
<sup>1</sup>H NMR (400.1 MHz, C<sub>6</sub>D<sub>6</sub>, 293 K) δ<sub>H</sub> 35.03 (br d, <sup>3</sup>J<sub>HH</sub> = 5.16 Hz, 2 H), 19.17 (t, <sup>3</sup>J<sub>HH</sub> = 5.16 Hz, 2 H), 16.40 (d, <sup>3</sup>J<sub>HH</sub> = 8.31 Hz, 2 H), 14.66 (t, <sup>3</sup>J<sub>HH</sub> = 7.17 Hz, 2 H), 3.63 (br s, 2 H), -2.63 (t, <sup>3</sup>J<sub>HH</sub> = 7.17 Hz, 2 H), -4.32 (t, <sup>3</sup>J<sub>HH</sub> = 7.17 Hz, *o*-oxazPh or *m*-oxazPh, 4 H), -7.04 (br s, 2 H), -8.68 (s, N(SiMe<sub>3</sub>)<sub>2</sub>, 36 H), -10.10 (d, <sup>3</sup>J<sub>HH</sub> = 7.17 Hz, 2 H), -17.12 (d, <sup>3</sup>J<sub>HH</sub> = 9.47 Hz, *o*-oxazPh or *m*-oxazPh, 4 H) ppm; <sup>13</sup>C{<sup>1</sup>H} NMR (100.6 MHz, C<sub>6</sub>D<sub>6</sub>, 293 K) δ<sub>C</sub> 168.5 (C=N), 146.0, 135.4, 126.4, 118.6, 111.8, 68.3, 31.6, 24.8, 24.2, 15.4, 5.7, 1.0, 0.8 ppm; IR (ν cm<sup>-1</sup>) (KBr): 2961 (s), 2897 (m), 1638 (w) (C=N), 1608 (m) (C=N), 1580 (m), 1557 (w), 1537 (w), 1462 (m), 1430 (m), 1334 (w), 1321 (w), 1261 (s), 1226 (w), 1182 (w), 1153 (m), 1096 (s), 1070 (s), 1020 (s), 937 (m), 868 (m), 804 (s), 761 (m), 746 (m), 691 (w), 660 (m), 597 (m) cm<sup>-1</sup>.

1.



### 6.2.12.2 [Pr(Bn-BOPA)(N(SiMe<sub>3</sub>)<sub>2</sub>)<sub>2</sub>] (11b) 86%

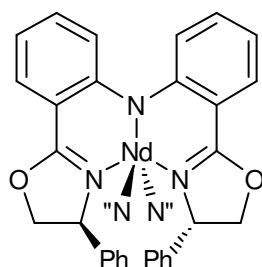
<sup>1</sup>H NMR (400.12 MHz, C<sub>6</sub>D<sub>6</sub>, 293 K) δ<sub>H</sub> 24.04 (br s, 2 H), 16.90 (br s, 2 H), 13.55 (br s, 2 H), 13.16 (br s, 2 H), 3.10 (t, <sup>3</sup>J<sub>HH</sub> = 6.88 Hz, 2 H), 2.07 (t, <sup>3</sup>J<sub>HH</sub> = 5.74 Hz, *m*-oxazPh or *o*-oxazPh, 4 H), -7.93 (d, <sup>3</sup>J<sub>HH</sub> = 7.17 Hz, *m*-oxazPh or *o*-oxazPh, 4 H), -8.70 (s, N(SiMe<sub>3</sub>)<sub>2</sub>, 36 H), -11.09 (br s, 2 H), -15.12 (br s, 2 H), -36.10 (s, 2 H), -39.46 (s, 2 H), -57.11 (s, 2 H) ppm; <sup>13</sup>C{<sup>1</sup>H} NMR (100.6 MHz, C<sub>6</sub>D<sub>6</sub>, 293 K) δ<sub>C</sub> 168.2 (C=N), 147.4, 140.9, 127.9, 121.6, 121.2, 115.4, 114.5, 68.0, 31.6, 24.5, 22.7, 14.0, 5.6, 0.2 ppm; IR (ν cm<sup>-1</sup>) (KBr): 2956 (s), 2894 (m), 1629 (m) (C=N), 1612 (w) (C=N), 1557 (w), 1535 (m), 1497 (w), 1462 (s), 1425 (m), 1370 (w), 1358 (w), 1315 (m), 1261 (s), 1217 (w), 1185 (w), 1159 (w), 1096 (s), 1047 (s), 1015 (s), 998 (s), 935 (m), 862 (m), 826 (s), 761 (m), 697 (w), 677 (w), 661 (w), 597 (m) cm<sup>-1</sup>.



### 6.2.12.3 [Pr(iPr-BOPA)(N(SiMe<sub>3</sub>)<sub>2</sub>)<sub>2</sub>] (11c) 80%

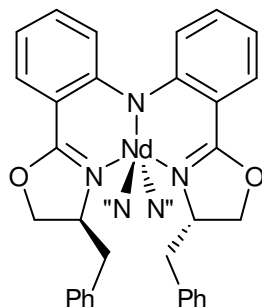
<sup>1</sup>H NMR (400.1 MHz, C<sub>6</sub>D<sub>6</sub>, 293 K) δ<sub>H</sub> 27.85 (d, <sup>3</sup>J<sub>HH</sub> = 6.88 Hz, 2 H), 17.64 (t, <sup>3</sup>J<sub>HH</sub> = 6.88 Hz, 2 H), 15.07 (d, <sup>3</sup>J<sub>HH</sub> = 7.74 Hz, 2 H), 14.10 (t, <sup>3</sup>J<sub>HH</sub> = 6.88 Hz, 2 H), -8.37 (d, <sup>3</sup>J<sub>HH</sub> = 5.16 Hz, 2 H), -8.59 (s, N(SiMe<sub>3</sub>)<sub>2</sub>, 36 H), -11.70 (d, <sup>3</sup>J<sub>HH</sub> = 6.02 Hz, 2 H), -15.58 (s, MeCHMe, 6

H), -22.60 (s, MeCHMe, 6 H), -36.72 (br s, 2 H), -66.61 (s, 2 H) ppm;  $^{13}\text{C}\{^1\text{H}\}$  NMR (100.6 MHz,  $\text{C}_6\text{D}_6$ , 293 K)  $\delta_{\text{C}}$  203.0, 170.4, 156.6, 149.8, 143.7, 131.2, 120.0, 115.1, 69.9, 65.5, 51.5, 19.0, 8.1 ppm; IR ( $\nu \text{ cm}^{-1}$ ) (KBr): 3061 (w), 2959 (s), 2899 (m), 2873 (m), 1609 (s) (C=N), 1586 (m), 1560 (m), 1536 (m), 1477 (m), 1462 (s), 1429 (s), 1370 (m), 1323 (m), 1260 (s), 1220 (s), 1160 (s), 1090 (m), 1064 (s), 1050 (s), 1021 (m), 971 (s), 934 (w), 862 (m), 839 (m), 822 (s), 747 (m), 694 (w), 665 (m), 596 (w)  $\text{cm}^{-1}$ ; Anal. Calcd for  $\text{PrC}_{36}\text{H}_{64}\text{N}_5\text{O}_2\text{Si}_4$  (852.18 g  $\text{mol}^{-1}$ ): C 50.74, H 7.57, N 8.22. Found: C 50.89, H 7.62, N 8.17.



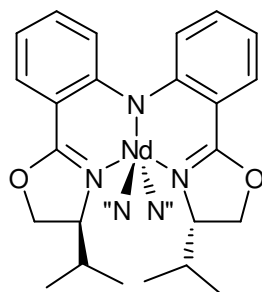
#### 6.2.12.4 [Nd(Ph-BOPA)(N(SiMe<sub>3</sub>)<sub>2</sub>)<sub>2</sub>] (12a) 80%

$^1\text{H}$  NMR (400.1 MHz,  $\text{C}_6\text{D}_6$ , 293 K)  $\delta_{\text{H}}$  20.23 (br d,  $^3J_{\text{HH}} = 4.02$  Hz, 2 H), 14.24 (d,  $^3J_{\text{HH}} = 5.74$  Hz, 2 H), 13.78 (br s, 2 H), 11.48 (t,  $^3J_{\text{HH}} = 5.74$  Hz, 2 H), 1.20 (t,  $^3J_{\text{HH}} = 7.74$  Hz, 2 H), 0.09 (t,  $^3J_{\text{HH}} = 6.88$  Hz, 2 H), -0.96 (br s, *o*-oxazPh or *m*-oxazPh, 4 H), -3.60 (br d,  $^3J_{\text{HH}} = 5.45$  Hz, *o*-oxazPh or *m*-oxazPh, 4 H), -5.95 (br s, N(SiMe<sub>3</sub>)<sub>2</sub>, 36 H), -8.29 (d,  $^3J_{\text{HH}} = 7.17$  Hz, 2 H), -22.71 (br s, 2 H) ppm;  $^{13}\text{C}\{^1\text{H}\}$  NMR (150.9 MHz,  $\text{C}_6\text{D}_6$ , 293 K)  $\delta_{\text{C}}$  179.7, 166.8, 154.4, 146.0, 145.7, 141.1, 140.8, 126.5, 119.0, 118.0, 113.5, 107.2, 73.2, 5.7 ppm; IR ( $\nu \text{ cm}^{-1}$ ) (KBr): 2963 (s), 2913 (m), 2852 (m), 1635 (m) (C=N), 1609 (m) (C=N), 1581 (w), 1534 (w), 1461 (m), 1430 (m), 1261 (s), 1221 (m), 1157 (m), 1092 (s), 1022 (s), 953 (w), 799 (s), 749 (m), 698 (m)  $\text{cm}^{-1}$ ; Anal. Calcd for  $\text{NdC}_{42}\text{H}_{60}\text{N}_5\text{O}_2\text{Si}_4$  (923.54 g  $\text{mol}^{-1}$ ): C 54.62, H 6.55, N 7.58. Found: C 54.43, H 6.66, N 7.53.



### 6.2.12.5 [Nd(Bn-BOPA)(N(SiMe<sub>3</sub>)<sub>2</sub>)<sub>2</sub>] (12b) 76%

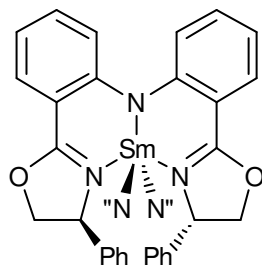
<sup>1</sup>H NMR (400.1 MHz, C<sub>6</sub>D<sub>6</sub>, 293 K) δ<sub>H</sub> 14.46 (d, <sup>3</sup>J<sub>HH</sub> = 4.45 Hz, 2 H), 12.41 (br s, 2 H), 11.87 (br d, <sup>3</sup>J<sub>HH</sub> = 8.32 Hz, 2 H), 10.31 (t, <sup>3</sup>J<sub>HH</sub> = 8.32 Hz, 2 H), 4.92 (t, <sup>3</sup>J<sub>HH</sub> = 8.03 Hz, 2 H), 4.40 (t, <sup>3</sup>J<sub>HH</sub> = 7.74 Hz, *o*-oxazPh or *m*-oxazPh, 4 H), 0.75 (br s, 2 H), -1.08 (d, <sup>3</sup>J<sub>HH</sub> = 8.89 Hz, *o*-oxazPh or *m*-oxazPh, 4 H), -2.96 (d, <sup>3</sup>J<sub>HH</sub> = 6.60 Hz, 2 H), -5.72 (br d, <sup>3</sup>J<sub>HH</sub> = 7.74 Hz, 2 H), -5.93 (br s, N(SiMe<sub>3</sub>)<sub>2</sub> 36 H), -17.92 (s, 2 H), -21.95 (s, 2 H), -32.5 (s, 2 H) ppm; <sup>13</sup>C{<sup>1</sup>H} NMR (150.9 MHz, C<sub>6</sub>D<sub>6</sub>, 293 K) δ<sub>C</sub> 160.4, 157.4, 143.1, 141.7, 136.2, 132.2, 131.3, 128.6, 124.9, 124.7, 123.6, 121.2, 68.8, 8.7, 5.6 ppm; IR (ν cm<sup>-1</sup>) (KBr): 3064 (w), 3030 (w), 2962 (s), 2902 (m), 1608 (m) (C=N), 1584 (m), 1558 (w), 1536 (w), 1497 (w), 1462 (m), 1428 (m), 1375 (w), 1323 (w), 1261 (s), 1221 (m), 1182 (w), 1160 (m), 1095 (s), 1021 (s), 975 (m), 933 (m), 863 (m), 801 (s), 747 (m), 700 (m), 665 (m), 598 (w) cm<sup>-1</sup>; Anal. Calcd for NdC<sub>44</sub>H<sub>64</sub>N<sub>5</sub>O<sub>2</sub>Si<sub>4</sub> (951.60 g mol<sup>-1</sup>): C 55.54, H 6.78, N 7.36. Found: C 55.38, H 6.75, N 7.28.



### 6.2.12.6 [Nd(iPr-BOPA)(N(SiMe<sub>3</sub>)<sub>2</sub>)<sub>2</sub>] (12c) 84%

<sup>1</sup>H NMR (400.1 MHz, C<sub>6</sub>D<sub>6</sub>, 293 K) δ<sub>H</sub> 16.42 (d, <sup>3</sup>J<sub>HH</sub> = 7.46 Hz, 2 H), 13.04 (d, <sup>3</sup>J<sub>HH</sub> = 7.74 Hz, 2 H), 12.75 (br t, <sup>3</sup>J<sub>HH</sub> = 6.02 Hz, 2 H), 10.72 (t, <sup>3</sup>J<sub>HH</sub> = 6.88 Hz, 2 H), -1.62 (br d, <sup>3</sup>J<sub>HH</sub> =

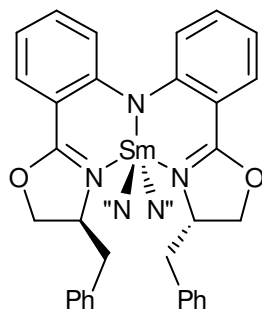
6.88 Hz, 2 H), -3.90 (d,  $^3J_{\text{HH}} = 7.17$  Hz, 2 H), -5.96 (s,  $\text{N}(\text{SiMe}_3)_2$  36 H), -9.17 (s, MeCHMe, 6 H), -12.83 (s, MeCHMe, 6 H), -20.34 (s, 2 H), -39.29 (s, 2 H) ppm;  $^{13}\text{C}\{^1\text{H}\}$  NMR (150.9 MHz,  $\text{C}_6\text{D}_6$ , 293 K)  $\delta_{\text{C}}$  166.2, 162.4, 147.0, 143.2, 138.2, 135.7, 125.3, 65.4, 28.0, 24.8 5.7, -1.2, -3.4 ppm; IR ( $\nu$   $\text{cm}^{-1}$ ) (KBr): 3056 (w), 2959 (s), 2897 (m), 1609 (s) (C=N), 1584 (m), 1559 (m), 1537 (m), 1481 (m), 1462 (s), 1429 (m), 1371 (m), 1326 (w), 1260 (s), 1220 (m), 1160 (m), 1092 (m), 1065 (s), 1048 (s), 1018 (s), 968 (s), 863 (m), 838 (s), 823 (s), 810 (m), 747 (m), 687 (w), 664 (m), 597 (m)  $\text{cm}^{-1}$ ; Anal. Calcd for  $\text{NdC}_{36}\text{H}_{64}\text{N}_5\text{O}_2\text{Si}_4$  (855.51  $\text{g mol}^{-1}$ ): C 50.54, H 7.54, N 8.19. Found: C 50.39, H 7.46, N 8.09.



### 6.2.12.7 [Sm(Ph-BOPA)(N(SiMe<sub>3</sub>)<sub>2</sub>)<sub>2</sub>] (13a) 86%

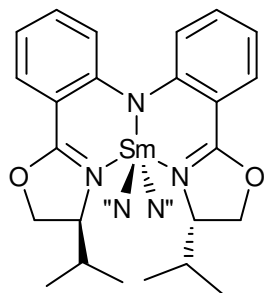
$^1\text{H}$  NMR (400.1 MHz,  $\text{C}_6\text{D}_6$ , 293 K)  $\delta_{\text{H}}$  10.16 (dd,  $^3J_{\text{HH}} = 8.04$  Hz,  $^4J_{\text{HH}} = 1.90$  Hz, 2 H), 9.37 (d,  $^3J_{\text{HH}} = 8.04$  Hz, 2 H), 7.86 (t,  $^3J_{\text{HH}} = 7.75$  Hz,  $^4J_{\text{HH}} = 1.46$  Hz, 2 H), 7.81 (t,  $^3J_{\text{HH}} = 7.89$  Hz, 2 H), 5.55 (t,  $^3J_{\text{HH}} = 7.16$  Hz, 2 H), 5.39 (t,  $^3J_{\text{HH}} = 7.89$  Hz, *o*-oxazPh or *m*-oxazPh, 4 H), 5.10 (t,  $^3J_{\text{HH}} = 8.48$  Hz, 2 H), 4.16 (d,  $^3J_{\text{HH}} = 7.89$  Hz, *o*-oxazPh or *m*-oxazPh, 4 H), 3.23 (d,  $^3J_{\text{HH}} = 8.33$  Hz, 2 H), 1.88 (d,  $^3J_{\text{HH}} = 8.04$  Hz, 2 H), 0.09 (s,  $\text{N}(\text{SiMe}_3)_2$ , 36 H) ppm;  $^{13}\text{C}\{^1\text{H}\}$  NMR (100.6 MHz,  $\text{C}_6\text{D}_6$ , 293 K)  $\delta_{\text{C}}$  174.5, 166.8, 135.4, 132.1, 126.7, 126.0, 123.1, 119.6, 73.4, 64.7, 25.2, 22.7, 14.0, 2.3 ppm; IR ( $\nu$   $\text{cm}^{-1}$ ) (KBr): 3061 (w), 3030 (w), 2959 (s), 2899 (m), 1635 (m) (C=N), 1608 (s) (C=N), 1577 (m), 1554 (w), 1537 (m), 1494 (w), 1461 (s), 1430 (s), 1373 (m), 1338 (w), 1321 (w), 1261 (s), 1219 (m), 1182 (w), 1156 (m), 1099 (s), 1070 (s), 1047 (s), 1021 (s), 986 (m), 974 (m), 819 (s), 804 (s), 746 (m), 698 (m), 668 (w), 605 (w)  $\text{cm}^{-1}$

<sup>1</sup>; Anal. Calcd for SmC<sub>42</sub>H<sub>60</sub>N<sub>5</sub>O<sub>2</sub>Si<sub>4</sub> (929.66 g mol<sup>-1</sup>): C 54.26, H 6.51, N 7.53. Found: C 54.11, H 6.56, N 7.43.



### 6.2.12.8 [Sm(Bn-BOPA)(N(SiMe<sub>3</sub>)<sub>2</sub>)<sub>2</sub>] (13b) 83%

<sup>1</sup>H NMR (400.1 MHz, C<sub>6</sub>D<sub>6</sub>, 293 K) δ<sub>H</sub> 9.02 (dd, <sup>3</sup>J<sub>HH</sub> = 8.17 Hz, <sup>4</sup>J<sub>HH</sub> = 1.72 Hz, 2 H), 8.49 (d, <sup>3</sup>J<sub>HH</sub> = 8.46 Hz, 2 H), 7.54 (t, <sup>3</sup>J<sub>HH</sub> = 7.89 Hz, <sup>4</sup>J<sub>HH</sub> = 1.72 Hz, 2 H), 7.36 (t, <sup>3</sup>J<sub>HH</sub> = 7.60 Hz, 2 H), 6.75 – 6.71 (m, 8 H), 5.96 – 5.92 (m, *o*-oxazPh or *m*-oxazPh, 4 H), 3.87 (t, <sup>3</sup>J<sub>HH</sub> = 8.75 Hz, 2 H), 2.84 (dd, <sup>2</sup>J<sub>HH</sub> = 8.89 Hz, <sup>3</sup>J<sub>HH</sub> = 5.74 Hz, 2 H), 1.24 (dd, <sup>2</sup>J<sub>HH</sub> = 10.90, <sup>3</sup>J<sub>HH</sub> = 7.46 Hz, 2 H), 0.88 (t, <sup>3</sup>J<sub>HH</sub> = 6.88 Hz, 2 H), 0.09 (s, N(SiMe<sub>3</sub>)<sub>2</sub>, 36 H) ppm; <sup>13</sup>C{<sup>1</sup>H} NMR (100.6 MHz, C<sub>6</sub>D<sub>6</sub>, 293 K) δ<sub>C</sub> 173.5 (C=N), 148.3, 141.2, 130.3, 121.4, 121.3, 115.0, 68.4, 31.6, 24.7, 22.7, 14.0, 5.8, 0.8, 0.3 ppm; IR (ν cm<sup>-1</sup>) (KBr): 3067 (w), 3029 (w), 2957 (s), 2899 (m), 1610 (m) (C=N), 1583 (m), 1560 (w), 1534 (m), 1494 (w), 1463 (m), 1428 (m), 1375 (m), 1323 (m), 1260 (s), 1249 (s), 1223 (m), 1185 (m), 1160 (m), 1096 (s), 1044 (s), 1018 (s), 988 (s), 940 (m), 865 (s), 828 (s), 807 (s), 769 (m), 749 (m), 694 (w), 674 (w), 659 (m), 602 (m) cm<sup>-1</sup>.



### 6.2.12.9 [Sm(iPr-BOPA)(N(SiMe<sub>3</sub>)<sub>2</sub>)<sub>2</sub>] (13c) 78%

<sup>1</sup>H NMR (500.1 MHz, C<sub>6</sub>D<sub>6</sub>, 293 K) δ<sub>H</sub> 9.63 (d, <sup>3</sup>J<sub>HH</sub> = 8.36 Hz, 2 H), 8.84 (d, <sup>3</sup>J<sub>HH</sub> = 8.36 Hz, 2 H), 7.63 (t, <sup>3</sup>J<sub>HH</sub> = 7.09 Hz, 2 H), 7.58 (t, <sup>3</sup>J<sub>HH</sub> = 7.25 Hz, 2 H), 4.43 (t, <sup>3</sup>J<sub>HH</sub> = 8.83 Hz, 2 H), 3.21 (d, <sup>3</sup>J<sub>HH</sub> = 8.36 Hz, 2 H), 1.87 (br d, <sup>3</sup>J<sub>HH</sub> = 7.88 Hz, 2 H), 0.09 (d, <sup>3</sup>J<sub>HH</sub> = 2.05 Hz, 2 H), -1.09 (br d, <sup>3</sup>J<sub>HH</sub> = 6.15 Hz, MeCHMe 6 H), -1.58 (br s, N(SiMe<sub>3</sub>)<sub>2</sub>, 36 H), -1.83 (br d, <sup>3</sup>J<sub>HH</sub> = 5.83 Hz, MeCHMe 6 H) ppm; <sup>13</sup>C{<sup>1</sup>H} NMR (125.8 MHz, C<sub>6</sub>D<sub>6</sub>, 293 K) δ<sub>C</sub> 170 (C=N), 157.3, 133.5, 133.4, 127.2, 119.2, 118.2, 65.5, 63.7, 15.19, 9.62, 4.74, 0.84 ppm; IR (ν cm<sup>-1</sup>) (KBr): 3064 (w), 2959 (s), 2899 (m), 1609 (s) (C=N), 1583 (m), 1559 (m), 1537 (m), 1517 (w), 1483 (m), 1462 (s), 1429 (m), 1372 (m), 1323 (m), 1289 (w), 1260 (s), 1220 (s), 1182 (w), 1160 (m), 1096 (m), 1066 (s), 1050 (s), 1021 (s), 986 (m), 957 (s), 865 (m), 823 (s), 769 (m), 747 (m), 712 (w), 688 (w), 665 (m), 602 (m) cm<sup>-1</sup>; Anal. Calcd for SmC<sub>36</sub>H<sub>64</sub>N<sub>5</sub>O<sub>2</sub>Si<sub>4</sub> (861.63 g mol<sup>-1</sup>): C 50.18, H 7.49, N 8.13. Found: C 49.96, H 7.51, N 8.08.

### 6.2.13 General procedure for Li(R-BOPA) (14a-c)

To a pentane suspension of R-BOPA (0.820 mmol) at -78 °C, <sup>t</sup>BuLi (0.82 mmol) was added dropwise. The reaction mixture was allowed to warm slowly and left overnight to stir at room temperature after which the solution was concentrated under reduced pressure and cooled to -78 °C. The resulting suspension was filtered, and the precipitate dried under vacuo to yield (14a-c) as a light yellow solid.

**6.2.13.1 Li(Ph-BOPA) (14a) 78%*****exo* isomer**

$^1\text{H}$  NMR (500.1 MHz,  $\text{C}_6\text{D}_6$ , 293 K)  $\delta_{\text{H}}$  8.19 (d,  $^3J_{\text{HH}} = 7.72$  Hz,  $\text{NArH}^{\text{d}}$ , 2 H), 7.87 (d,  $^3J_{\text{HH}} = 8.51$  Hz,  $\text{NArH}^{\text{a}}$ , 2 H), 7.12-7.05 (m, 6 H), 6.77 (t,  $^3J_{\text{HH}} = 7.41$  Hz,  $\text{NArH}^{\text{b}}$ , 2 H), 6.72 (t,  $^3J_{\text{HH}} = 7.57$  Hz,  $\text{NArH}^{\text{c}}$ , 2 H), 4.32 (dd,  $^3J_{\text{HH}} = 9.46$  Hz,  $^3J_{\text{HH}} = 8.51$  Hz,  $\text{H}^{\text{g}}$ , 2 H), 4.03 (m,  $\text{H}^{\text{e}}/\text{H}^{\text{f}}$ , 4 H) ppm;  $^{13}\text{C}\{^1\text{H}\}$  NMR (100.6 MHz,  $\text{C}_6\text{D}_6$ , 293 K)  $\delta_{\text{C}}$  167.7 (C=N), 143.2 ( $\text{NArC}^{\text{m}}$ ), 132.5 (*i*- $\text{C}^*\text{HC}_6\text{H}_5$ ), 132.4 ( $\text{NArC}^{\text{i}}$ ), 131.6, 128.3, 127.7, 126.7, 125.5, 120.4, 114.5 ( $\text{NArC}^{\text{n}}$ ), 74.0 ( $\text{C}^{\text{p}}$ ), 69.3 ( $\text{C}^{\text{q}}$ ) ppm.

***endo* isomer**

$^1\text{H}$  NMR (500.1 MHz,  $\text{C}_6\text{D}_6$ , 293 K)  $\delta_{\text{H}}$  8.18 (dd,  $^3J_{\text{HH}} = 8.04$  Hz,  $^4J_{\text{HH}} = 1.89$  Hz,  $\text{NArH}^{\text{d}}$ , 2 H), 7.00-6.91 (m, 6 H), 6.69-6.62 (m, 8 H), 6.52 (d,  $^3J_{\text{HH}} = 7.57$  Hz,  $\text{NArH}^{\text{c}}$ , 2 H), 3.89 (dd,  $^3J_{\text{HH}} = 8.67$  Hz,  $^3J_{\text{HH}} = 8.51$  Hz,  $\text{H}^{\text{g}}$ , 2 H), 3.67-3.60 (m,  $\text{H}^{\text{e}}/\text{H}^{\text{f}}$ , 4 H) ppm;  $^{13}\text{C}\{^1\text{H}\}$  NMR (100.6 MHz,  $\text{C}_6\text{D}_6$ , 293 K)  $\delta_{\text{C}}$  162.5 (C=N), 142.5 ( $\text{NArC}^{\text{m}}$ ), 131.8 (*i*- $\text{C}^*\text{HC}_6\text{H}_5$ ), 128.8 ( $\text{NArC}^{\text{i}}$ ), 128.4, 128.1, 127.9, 127.6, 126.7, 117.4, 115.7 ( $\text{NArC}^{\text{n}}$ ), 73.0 ( $\text{C}^{\text{p}}$ ), 67.8 ( $\text{C}^{\text{q}}$ ) ppm; IR ( $\nu$   $\text{cm}^{-1}$ ) (KBr): 3055 (w), 3025 (w), 2957 (w), 2917 (w), 2897 (w), 1633 (s) (C=N), 1613 (s) (C=N), 1558 (w), 1532 (m), 1492 (w), 1460 (s), 1430 (s), 1360 (w), 1341 (m), 1295 (w), 1260 (m), 1224 (s), 1203 (m), 1159 (m), 1138 (w), 1063 (m), 1038 (m), 952 (m), 922 (w), 877 (w), 822 (w), 745 (s), 695 (s), 665 (w), 599 (w), 539 (m), 511 (w)  $\text{cm}^{-1}$ ; Anal. Calcd for  $\text{LiC}_{30}\text{H}_{24}\text{N}_3\text{O}_2$  (465.47  $\text{g mol}^{-1}$ ): C 77.41, H 5.20, N 9.03. Found: C 77.54, H 5.14, N 8.98.

**6.2.13.2 Li(Bn-BOPA) (14b) 80%*****exo* isomer**

$^1\text{H}$  NMR (500.1 MHz,  $\text{C}_6\text{D}_6$ , 293 K)  $\delta_{\text{H}}$  8.16 (dd,  $^3J_{\text{HH}} = 8.20$  Hz,  $^4J_{\text{HH}} = 1.73$  Hz,  $\text{NArH}^{\text{d}}$ , 2 H), 7.31 (dd,  $^3J_{\text{HH}} = 8.51$  Hz,  $^4J_{\text{HH}} = 0.91$  Hz,  $\text{NArH}^{\text{a}}$ , 2 H), 7.14-7.10 (m, 2 H), 7.06-7.01 (m, 6 H), 6.87 (d,  $^3J_{\text{HH}} = 7.25$  Hz, 2 H), 6.70 (d,  $^3J_{\text{HH}} = 7.57$  Hz,  $\text{NArH}^{\text{b}}$ , 2 H), 6.55 (app. t,  $^3J_{\text{HH}} =$



7.57 Hz,  $^4J_{\text{HH}} = 1.10$  Hz, NArH<sup>c</sup>, 2 H), 3.78 (dd,  $^3J_{\text{HH}} = 8.83$  Hz,  $^3J_{\text{HH}} = 8.20$  Hz, H<sup>g</sup>, 2 H), 3.55 (t,  $^2J_{\text{HH}} = 8.04$  Hz, H<sup>e</sup>/H<sup>f</sup>, 4 H), 2.97 (dd,  $^2J_{\text{HH}} = 13.56$  Hz,  $^3J_{\text{HH}} = 3.94$  Hz, CHHPPh, 2 H), 2.27 (dd,  $^2J_{\text{HH}} = 13.24$  Hz,  $^3J_{\text{HH}} = 3.96$  Hz, CHHPPh, 2 H) ppm;  $^{13}\text{C}\{^1\text{H}\}$  NMR (100.6 MHz, C<sub>6</sub>D<sub>6</sub>, 293 K)  $\delta_{\text{C}}$  166.4 (C=N), 157.0 (NArC<sup>m</sup>), 137.7 (*i*-C<sub>6</sub>H<sub>5</sub>), 132.3, 131.7, 129.4, 128.6, 128.3, 127.9, 126.7, 115.8 (NArC<sup>n</sup>), 70.3 (C<sup>p</sup>), 66.1 (C<sup>q</sup>), 41.9 (CH<sub>2</sub>Ph) ppm.

#### **endo isomer**

$^1\text{H}$  NMR (500.1 MHz, C<sub>6</sub>D<sub>6</sub>, 293 K)  $\delta_{\text{H}}$  8.19 (dd,  $^3J_{\text{HH}} = 8.20$  Hz,  $^4J_{\text{HH}} = 1.73$  Hz, NArH<sup>d</sup>, 2 H), 7.81 (d,  $^3J_{\text{HH}} = 8.67$  Hz, NArH<sup>a</sup>, 2 H), 7.14-7.10 (m, 2 H), 7.06-7.01 (m, 6 H), 6.97 (d,  $^3J_{\text{HH}} = 7.41$  Hz, 2 H), 6.93 (d,  $^3J_{\text{HH}} = 7.25$  Hz, NArH<sup>b</sup>, 2 H), 6.66 (app. t,  $^3J_{\text{HH}} = 7.25$  Hz,  $^4J_{\text{HH}} = 1.10$  Hz, NArH<sup>c</sup>, 2 H), 3.82 (t,  $^3J_{\text{HH}} = 8.83$  Hz, H<sup>g</sup>, 2 H), 3.45 (t,  $^2J_{\text{HH}} = 7.41$  Hz, H<sup>e</sup>, 2 H), 3.33 (m, 4 H), 2.11 (dd,  $^2J_{\text{HH}} = 12.77$  Hz,  $^3J_{\text{HH}} = 5.20$  Hz, CHHPPh, 2 H) ppm;  $^{13}\text{C}\{^1\text{H}\}$  NMR (100.6 MHz, C<sub>6</sub>D<sub>6</sub>, 293 K)  $\delta_{\text{C}}$  163.2 (C=N), 143.9 (NArC<sup>m</sup>), 132.4 (NArC<sup>i</sup>), 131.7, 128.9, 128.9, 126.5, 126.2, 125.3, 120.6, 114.4 (NArC<sup>n</sup>), 70.8 (C<sup>p</sup>), 65.7 (C<sup>q</sup>), 41.7 (CH<sub>2</sub>Ph) ppm; IR ( $\nu$  cm<sup>-1</sup>) (KBr): 3055 (w), 3025 (w), 2957 (w), 2892 (w), 1624 (s) (C=N), 1557 (w), 1536 (m), 1497 (w), 1462 (s), 1424 (m), 1358 (m), 1317 (m), 1258 (m), 1216 (m), 1159 (m), 1138 (w), 1041 (m), 979 (w), 930 (w), 872 (w), 844 (w), 823 (w), 747 (m), 721 (w), 698 (m), 664 (w), 583 (w), 541 (w), 510 (w) cm<sup>-1</sup>; Anal. Calcd for LiC<sub>32</sub>H<sub>28</sub>N<sub>3</sub>O<sub>2</sub> (493.52 g mol<sup>-1</sup>): C 77.88, H 5.72, N 8.51. Found: C 77.93, H 5.83, N 8.62.

#### **6.2.13.3 Li(iPr-BOPA) (14c) 75%**

##### **exo isomer**

$^1\text{H}$  NMR (500.1 MHz, C<sub>6</sub>D<sub>6</sub>, 293 K)  $\delta_{\text{H}}$  8.24 (d,  $^3J_{\text{HH}} = 8.20$  Hz, NArH<sup>d</sup>, 2 H), 7.05 (d,  $^3J_{\text{HH}} = 8.67$  Hz, NArH<sup>a</sup>, 2 H), 6.95 (t,  $^3J_{\text{HH}} = 7.41$  Hz, NArH<sup>b</sup>, 2 H), 6.56 (t,  $^3J_{\text{HH}} = 7.41$  Hz, NArH<sup>c</sup>, 2 H), 3.82 (t,  $^3J_{\text{HH}} = 8.67$  Hz, H<sup>g</sup>, 2 H), 3.66 (t,  $^2J_{\text{HH}} = 8.19$  Hz, H<sup>e</sup>, 2 H), 2.83 – 2.75 (m, H<sup>f</sup>, 2 H), 1.73-1.67 (m, (CH<sub>3</sub>)<sub>2</sub>CH, 2 H), 0.56 (app.t,  $^3J_{\text{HH}} = 5.83$  Hz, (CH<sub>3</sub>)<sub>2</sub>CH, 6 H) ppm;  $^{13}\text{C}\{^1\text{H}\}$

NMR (100.6 MHz, C<sub>6</sub>D<sub>6</sub>, 293 K)  $\delta_C$  162.0 (C=N), 147.9 (NArC<sup>m</sup>), 135.2, 130.5, 130.2, 116.6, 114.1 (NArC<sup>n</sup>), 68.8 (C<sup>p</sup>), 64.5 (C<sup>q</sup>), 29.3 ((CH<sub>3</sub>)<sub>2</sub>CH), 18.0 (MeCHMe), 13.7 (MeCHMe) ppm.

### **endo isomer**

<sup>1</sup>H NMR (500.1 MHz, C<sub>6</sub>D<sub>6</sub>, 293 K)  $\delta_H$  8.16 (d, <sup>3</sup>J<sub>HH</sub> = 7.88 Hz, NArH<sup>d</sup>, 2 H), 7.84 (d, <sup>3</sup>J<sub>HH</sub> = 8.99 Hz, NArH<sup>a</sup>, 2 H), 7.10 (t, <sup>3</sup>J<sub>HH</sub> = 7.41 Hz, NArH<sup>b</sup>, 2 H), 6.63 (t, <sup>3</sup>J<sub>HH</sub> = 8.20 Hz, NArH<sup>c</sup>, 2 H), 3.76 (t, <sup>3</sup>J<sub>HH</sub> = 7.40 Hz, H<sup>g</sup>, 2 H), 3.59 (t, <sup>3</sup>J<sub>HH</sub> = 7.88 Hz, H<sup>e</sup>, 2 H), 3.55 – 3.45 (m, H<sup>f</sup>, 2 H), 0.97-0.90 (m, (CH<sub>3</sub>)<sub>2</sub>CH, 2 H), 0.67 (d, <sup>3</sup>J<sub>HH</sub> = 6.93 Hz, MeCHMe, 3 H), 0.56 (d, <sup>3</sup>J<sub>HH</sub> = 6.93 Hz, MeCHMe, 3 H) ppm; <sup>13</sup>C{<sup>1</sup>H} NMR (100.6 MHz, C<sub>6</sub>D<sub>6</sub>, 293 K)  $\delta_C$  164.3 (C=N), 147.6 (NArC<sup>m</sup>), 134.9, 131.0, 127.5, 119.0, 113.2 (NArC<sup>n</sup>), 69.1 (C<sup>p</sup>), 64.4 (C<sup>q</sup>), 28.3 ((CH<sub>3</sub>)<sub>2</sub>CH), 17.5 (MeCHMe), 17.5 (MeCHMe) ppm; IR ( $\nu$  cm<sup>-1</sup>) (KBr): 2958 (m), 2904 (w), 2874 (w), 1626 (s) (C=N), 1582 (w), 1559 (w), 1537 (m), 1516 (w), 1464 (s), 1426 (m), 1388 (w), 1362 (m), 1320 (m), 1259 (m), 1218 (m), 1159 (m), 1048 (m), 975 (w), 916 (w), 874 (w), 846 (w), 821 (w), 748 (m), 683 (w), 665 (w), 596 (w), 541 (w), 410 (w) cm<sup>-1</sup>; Anal. Calcd for LiC<sub>24</sub>H<sub>28</sub>N<sub>3</sub>O<sub>2</sub> (397.44 g mol<sup>-1</sup>): C 72.53, H 7.10, N 10.57. Found: C 72.35, H 7.15, N 10.47.

## **6.3 Chapter 3**

### **6.3.1 General procedure for hydroamination catalysis**

In a dinitrogen filled glovebox [Ln(R-BOPA)R'<sub>2</sub>] (0.5 mmol) was dissolved in C<sub>6</sub>D<sub>6</sub> (0.5 mL). To this solution was added the corresponding amino olefin (0.5 mmol). The solution was transferred to a J. Young Teflon valve equipped NMR tube and sealed. All catalyst reactions were monitored *via* <sup>1</sup>H NMR periodically to monitor conversion (conversion was determined from notable resonances in the spectra corresponding to the pyrrolidine product). Upon conversion ceasing, a solution of (R)-(-)-*O*-acetylmandelic acid (0.51 mmol) dissolved in a minimal amount of CDCl<sub>3</sub> was added to the reaction mixture producing the diastereomeric

salts. The resulting enantiomeric excess (e.e) were then determined from  $^1\text{H}$  NMR spectroscopy.

## 6.4 Chapter 4

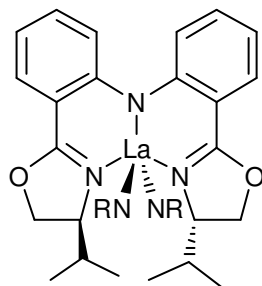
### 6.4.1 General Procedure for Solution Polymerisation of *rac*-LA

*rac*-LA (4.00 mmol) was added to a solution of initiator (0.04 mmol) in THF (4 mL). 0.1 mL aliquots were drawn periodically and quenched with wet THF (5 mL). Volatiles were removed under reduced pressure to leave behind the polymer residue. Samples were analysed by GPC, MALDI-ToF-MS and  $^1\text{H}$  NMR ( $\text{CDCl}_3$ ) spectroscopy.

## 6.5 Chapter 5

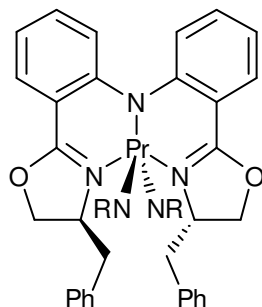
### 6.5.1 General Procedure for $[\text{Ln}(\text{R-BOPA})(\text{NHCH}_2\text{C}(\text{Ph})_2\text{C}_3\text{H}_7)_2]$ Ln = Nd, Pr, La (Complexes 15-17)

A dry hexane solution (1.eq) of 2,2'-diphenyl-aminopentane was added drop-wise to a dry hexane solution (20 mL) of  $[\text{Ln}(\text{R-BOPA})\{\text{N}(\text{SiMe}_3)_2\}_2]$ . The reaction mixture was left to stir overnight, filtered and subsequently volatiles were removed under reduced pressure. The resulting yellow solid was washed with cold pentane ( $-76\text{ }^\circ\text{C}$ ) and left to dry in *vacuo* for 2 hours to yield (**15-17**) as yellow solids.



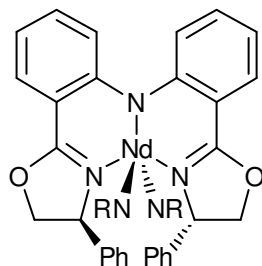
### 6.5.1.1 [La(iPr-BOPA)(NHCH<sub>2</sub>C(Ph)<sub>2</sub>C<sub>3</sub>H<sub>7</sub>)<sub>2</sub>] (15) 55%

<sup>1</sup>H NMR (500.1 MHz, C<sub>6</sub>D<sub>6</sub>, 293 K) δ<sub>H</sub> 8.11 (dd, <sup>3</sup>J<sub>HH</sub> = 7.98 Hz, <sup>4</sup>J<sub>HH</sub> = 1.74 Hz, NArH<sup>d</sup>, 2 H), 7.74 (d, <sup>3</sup>J<sub>HH</sub> = 8.71 Hz, NArH<sup>a</sup>, 2 H), 7.14 – 6.99 (m, 22 H), 6.59 (t, <sup>3</sup>J<sub>HH</sub> = 7.88 Hz, NArH<sup>c</sup>, 2 H), 3.95 (d, <sup>3</sup>J<sub>HH</sub> = 7.61 Hz, H<sup>g</sup>, 2 H), 3.90 – 3.81 (m, 4 H), 3.78 (t, <sup>2</sup>J<sub>HH</sub> = 11.37 Hz, H<sup>e</sup>, 2 H), 3.70 – 3.61 (m, 6 H), 2.20 – 2.06 (m, 4 H), 1.47 – 1.33 (m, (CH<sub>3</sub>)<sub>2</sub>CH, 2 H), 1.04 – 0.92 (m, 8 H), 0.65 (d, <sup>3</sup>J<sub>HH</sub> = 7.61 Hz, MeCHMe, 6 H), 0.57 (d, <sup>3</sup>J<sub>HH</sub> = 6.05 Hz, MeCHMe, 6 H) ppm; <sup>13</sup>C{<sup>1</sup>H} NMR (150.9 MHz, C<sub>6</sub>D<sub>6</sub>, 293 K) δ<sub>H</sub> 165.7 (C=N), 155.7 (NArC<sup>m</sup>), 145.8 (*i*-NHRC<sub>6</sub>H<sub>5</sub>), 132.6 (NArC<sup>k</sup>), 130.8, 130.4, 127.3, 125.4, 124.7, 118.7 (NArC<sup>j</sup>), 112.6 (NArC<sup>n</sup>), 70.9 (C<sup>p</sup>), 66.6 (C<sup>q</sup>), 45.2 (Ph<sub>2</sub>CNHR), 31.4 ((CH<sub>3</sub>)<sub>2</sub>CH), 17.7 (MeCHMe), 16.5 (NHCH<sub>2</sub>R), 15.4 (C<sub>2</sub>H<sub>5</sub>CH<sub>2</sub>NHR), 13.6 (MeCHMe), 4.6 (MeCH<sub>2</sub>NHR), 3.6 (MeNHR) ppm; IR (ν cm<sup>-1</sup>) (KBr): 3087 (m), 3057 (m), 3030 (m), 2963 (s), 2930 (m), 2874 (m), 1645 (s), 1635 (s) (C=N), 1618 (m) (C=N), 1577 (m), 1521 (m), 1457 (s), 1362 (m), 1313 (m), 1261 (s), 1221 (w), 1159 (m), 1093 (s), 1032 (s), 1016 (s), 938 (m), 870 (w), 821 (m), 797 (s) cm<sup>-1</sup>; Anal. Calcd for LaC<sub>58</sub>H<sub>68</sub>N<sub>5</sub>O<sub>2</sub> (1006.10 g mol<sup>-1</sup>): C 69.24, H 6.81, N 6.96. Found: C 68.78, H 7.46, N 6.89.



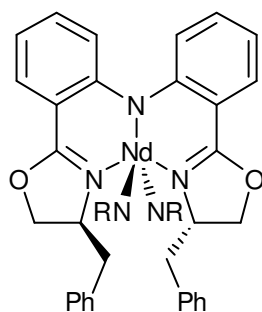
### 6.5.1.2 [Pr(Bn-BOPA)(NHCH<sub>2</sub>C(Ph)<sub>2</sub>C<sub>3</sub>H<sub>7</sub>)<sub>2</sub>] (16) 67%

<sup>1</sup>H NMR (400.1 MHz, C<sub>6</sub>D<sub>6</sub>, 293 K) δ<sub>H</sub> 49.40 (d, <sup>3</sup>J<sub>HH</sub> = 6.88 Hz, 2 H), 44.87 (d, <sup>3</sup>J<sub>HH</sub> = 6.88 Hz, 2 H), 44.4 (d, <sup>3</sup>J<sub>HH</sub> = 7.20 Hz, 2 H), 23.7 (t, <sup>3</sup>J<sub>HH</sub> = 6.75 Hz, 2 H), 16.7 (br s, 4 H), 13.4 (t, <sup>3</sup>J<sub>HH</sub> = 6.75 Hz, 2 H), 13.0 (br s, 2 H), 11.08 (br s, 4 H), 10.3 (br s, 4 H), 8.19 (d, <sup>3</sup>J<sub>HH</sub> = 7.57 Hz, 4 H) 5.08 (br s, 4 H), 4.43 (br s, 4 H), 3.14 (br s, HNR-Me, 6 H), 2.99 (d, <sup>3</sup>J<sub>HH</sub> = 7.57 Hz, 2 H), -0.49 (br s, 2 H), -1.72 (d, <sup>3</sup>J<sub>HH</sub> = 6.45 Hz, 2 H), -3.85 (br s, 4 H), -4.26 (br s, 2 H), -10.67 (d, <sup>3</sup>J<sub>HH</sub> = 6.45 Hz, 2 H), -33.27 (d, <sup>3</sup>J<sub>HH</sub> = 5.49 Hz, 2 H) ppm; <sup>13</sup>C{<sup>1</sup>H} NMR (150.9 MHz, C<sub>6</sub>D<sub>6</sub>, 293 K) δ<sub>H</sub> 163.4 (C=N), 144.3, 142.0, 138.5, 137.4, 129.4, 128.7, 123.5, 122.3, 121.6, 120.3, 119.5, 116.4, 115.2, 67.7, 64.1, 54.3, 50.9, 40.5, 48.8, 27.0, 15.5, 10.4 ppm; IR (ν cm<sup>-1</sup>) (KBr): 3087 (m), 3061 (m), 3025 (m), 2959 (s), 2871 (m), 1950 (w), 1880 (w), 1804 (w), 1652 (w) (C=N), 1601 (m) (C=N), 1560 (w), 1534 (w), 1496 (m), 1469 (w), 1456 (w), 1445 (m), 1408 (w), 1378 (w), 1261 (s), 1181 (m), 1159 (w), 1097 (s), 1021 (s), 933 (m), 856 (m), 812 (s) cm<sup>-1</sup>.



### 6.5.1.3 [Nd(Ph-BOPA)(NHCH<sub>2</sub>C(Ph)<sub>2</sub>C<sub>3</sub>H<sub>7</sub>)<sub>2</sub>] (17a) 71%

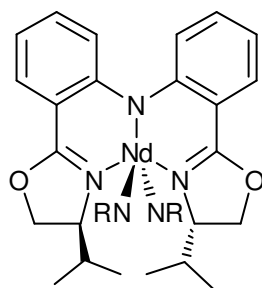
<sup>1</sup>H NMR (400.1 MHz, C<sub>6</sub>D<sub>6</sub>, 293 K) δ<sub>H</sub> 20.02 (br s, 2 H), 14.08 (d, <sup>3</sup>J<sub>HH</sub> = 8.03 Hz, 2 H), 13.6 (br s, 2 H), 11.33 (t, <sup>3</sup>J<sub>HH</sub> = 5.59 Hz, 2 H), 8.58 (br s, 4 H), 7.10 (br s, 4 H), 7.01 (br s, HNR-Me, 6 H), 1.11 (t, <sup>3</sup>J<sub>HH</sub> = 7.89 Hz, 2 H), 0.05 (br s, 4 H), -0.05 (br s, 4 H), -1.06 (br s, 2 H), -1.58 (br s, 4 H), -1.64 (br s, 2 H), -3.68 (d, <sup>3</sup>J<sub>HH</sub> = 4.73 Hz, 2 H), -3.87 (br s, 20 H), -8.23 (d, <sup>3</sup>J<sub>HH</sub> = 6.45 Hz, 2 H) ppm; <sup>13</sup>C{<sup>1</sup>H} NMR (150.9 MHz, C<sub>6</sub>D<sub>6</sub>, 293 K) δ<sub>C</sub> 178.5, 165.7, 145.5, 141.6, 140.6, 136.8, 134.8, 121.2, 120.5, 119.3, 118.3, 117.1, 116.3, 114.3, 107.8, 73.4, 48.4, 38.6, 29.8, 17.6, 14.6, -0.9 ppm; IR (ν cm<sup>-1</sup>) (KBr): 3057 (m), 3027 (m), 2959 (s), 2876 (m), 1637 (m) (C=N), 1604 (s) (C=N), 1583 (m), 1534 (w), 1496 (s), 1456 (m), 1442 (m), 1372 (w), 1337 (w), 1316 (m), 1261 (s), 1224 (m), 1156 (m), 1098 (m), 1032 (m), 837 (m), 822 (m), 798 (s) cm<sup>-1</sup>; Anal. Calcd for NdC<sub>64</sub>H<sub>64</sub>N<sub>5</sub>O<sub>2</sub> (1079.47 g mol<sup>-1</sup>): C 71.21, H 5.98, N 6.49. Found: C 70.69, H 6.05, N 6.25.



### 6.5.1.4 [Nd(Bn-BOPA)(NHCH<sub>2</sub>C(Ph)<sub>2</sub>C<sub>3</sub>H<sub>7</sub>)<sub>2</sub>] (17b) 69%

<sup>1</sup>H NMR (400.1 MHz, C<sub>6</sub>D<sub>6</sub>, 293 K) δ<sub>H</sub> 14.16 (br s, 2 H), 12.13 (br s, 2 H), 11.60 (d, <sup>3</sup>J<sub>HH</sub> = 6.88 Hz, 2 H), 10.04 (br s, 2 H), 7.10 (s, 4 H), 6.68 (d, <sup>3</sup>J<sub>HH</sub> = 6.02 Hz, 4 H), 6.62 (br s, 4 H),

4.70 (t,  $^3J_{\text{HH}} = 7.60$  Hz, 2 H), 4.18 (t,  $^3J_{\text{HH}} = 6.88$  Hz, 4 H), 0.60 (br s, 20 H), 0.25 (br s, HNR-Me, 6 H), -1.25 (d,  $^3J_{\text{HH}} = 6.74$  Hz, 4 H), -2.96 (br s, 2 H), -3.10 (br s, 2 H), -5.89 (br d,  $^3J_{\text{HH}} = 5.31$  Hz, 2 H), -17.99 (br s, 2 H), -22.00 (br s, 2 H), -32.49 (br s, 2 H) ppm;  $^{13}\text{C}\{^1\text{H}\}$  NMR (125.8 MHz,  $\text{C}_6\text{D}_6$ , 293 K)  $\delta_{\text{C}}$  166.3, 155.8, 147.4, 137.5, 131.1, 130.3, 127.6, 127.5, 127.4, 126.1, 124.7, 120.2, 119.2, 113.0, 69.1, 66.1, 50.8, 41.0, 37.5, 16.2, 13.4, 0.0, -0.1, -0.3 ppm; IR ( $\nu$   $\text{cm}^{-1}$ ) (KBr): 3087 (m), 3063 (m), 3027 (m), 2962 (s), 2874 (m), 1652 (m), 1635 (m) (C=N), 1601 (m) (C=N), 1560 (m), 1534 (m), 1496 (m), 1457 (m), 1445 (w), 1321 (w), 1261 (s), 1219 (m), 1183 (w), 1156 (w), 1096 (s), 1022 (s), 930 (m), 864 (m), 800 (s)  $\text{cm}^{-1}$ ; Anal. Calcd for  $\text{NdC}_{66}\text{H}_{68}\text{N}_5\text{O}_2$  (1107.52 g  $\text{mol}^{-1}$ ): C 71.57, H 6.19, N 6.32. Found: C 70.89, H 6.21, N 6.36.



#### 6.5.1.5 [Nd(*i*Pr-BOPA)(NHCH<sub>2</sub>C(Ph)<sub>2</sub>C<sub>3</sub>H<sub>7</sub>)<sub>2</sub>] (17c) 66%

$^1\text{H}$  NMR (400.1 MHz,  $\text{C}_6\text{D}_6$ , 293 K)  $\delta_{\text{H}}$  16.44 (d,  $^3J_{\text{HH}} = 7.17$  Hz, 2 H), 12.99 (d,  $^3J_{\text{HH}} = 8.17$  Hz, 2 H), 12.71 (br s, 2 H), 10.66 (t,  $^3J_{\text{HH}} = 7.17$  Hz, 2 H), 5.64 (br s, HNR-Me, 6 H), 3.04 (br s, 20 H), 0.48 (d,  $^3J_{\text{HH}} = 7.17$  Hz, 2 H), -0.05 (s, 4 H), -1.8 (br s, 4 H), -4.14 (d,  $^3J_{\text{HH}} = 6.02$  Hz, 4 H), -4.34 (br s, 2 H), -5.41 (br s, 2 H), -9.41 (s, MeCHMe, 6 H), -13.12 (s, MeCHMe, 6 H), -20.23 (br s, 2 H), -20.76 (br s, 2 H) ppm;  $^{13}\text{C}\{^1\text{H}\}$  NMR (150.9 MHz,  $\text{C}_6\text{D}_6$ , 293 K)  $\delta_{\text{C}}$  165.2, 154.5, 141.1, 136.2, 133.7, 129.8, 128.3, 123.4, 117.8, 115.5, 112.1, 67.8, 63.3, 30.5, 28.3, 17.0, 15.6, 16.6, 12.7, 3.5, -5.4 ppm; IR ( $\nu$   $\text{cm}^{-1}$ ) (KBr): 3087 (w), 3057 (m), 3025 (m), 2960 (s), 2903 (m), 2871 (w), 1652 (m), 1635 (m) (C=N), 1615 (m) (C=N), 1574 (m), 1560 (m), 1534 (m), 1507 (m), 1457 (s), 1432 (m), 1364 (m), 1318 (m), 1260 (s), 1221 (m), 1181 (m),

1156 (m), 1092 (m), 1054 (m), 1019 (s), 967 (m), 933 (m), 869 (m), 844 (m), 800 (s)  $\text{cm}^{-1}$ ;

Anal. Calcd for  $\text{NdC}_{58}\text{H}_{68}\text{N}_5\text{O}_2$  ( $1011.43 \text{ g mol}^{-1}$ ): C 68.87, H 6.78, N 6.92. Found: C 68.42, H 6.50, N 6.72.



## 6.6 References for Chapter 6

- 1 H. L. W. Hoegy and A. Rudin, *J. Polym. Sci., Part A: Polym. Chem.*, 1972, **10**, 217.
- 2 I. Barakat, P. Dubois, R. Jérôme, and P. Teyssié, *J. Polym. Sci., Part A: Polym. Chem.*, 1993, **31**, 505.
- 3 J. R. Dorgan, S. B. Hait, M. H. Hutchinson, J. Janzen, D. M. Knauss, and B. R. Limoges, *J. Polym. Sci., Part B: Polym. Phys.*, 2005, **43**, 3100.
- 4 E. C. Alyea, D. C. Bradley, and R. G. Copperthwaite, *J. Chem. Soc. Dalt*, 1972, 1580.
- 5 D. J. H. Emslie, W. E. Piers, M. Parvez, and R. McDonald, *Organometallics*, 2002, **21**, 4226.
- 6 D. C. Bradley, J. S. Ghotra, and F. A. Hart, *J. C. S. Dalton*, 1973, 1021.
- 7 M. R. Gagné, C. L. Stern, and T. J. Marks, *J. Am. Chem. Soc.*, 1992, **114**, 275.

# APPENDICES

**Appendix A - Crystallographic data**

**[Sc{N(SiMe<sub>3</sub>)<sub>2</sub>}<sub>2</sub>Cl(THF)] (1)****Crystal data and structure refinement**

Empirical formula	C <sub>16</sub> H <sub>42</sub> Cl <sub>1</sub> N <sub>2</sub> O <sub>1</sub> Sc <sub>1</sub> Si <sub>4</sub>	
Formula weight	471.28	
Crystal description	colourless prism	
Crystal size	0.25 x 0.15 x 0.08 mm	
Temperature	150 K	
Crystal system	Triclinic	
Space group	P -1	
Unit cell dimensions	a = 8.386(2) Å	α = 106.24(3) °
	b = 11.674(2) Å	β = 93.66(3) °
	c = 15.807(3) Å	γ = 108.04(3) °
Reflections for cell refinement	9301	
Range in theta	1.360 to 27.519 °	
Volume, Z	1393.3(6) Å <sup>3</sup> , 2	
Density (calculated)	1.123 mg/m <sup>3</sup>	
Absorption coefficient	0.540 mm <sup>-1</sup>	
F(000)	508	
Diffractometer type	Area	
Wavelength	0.71073 Å	
Scan type	phi & omega scans	
Theta range for data collection	1.36 to 27.52 °	
Index ranges	-10 ≤ h ≤ 10, -15 ≤ k ≤ 14, 0 ≤ l ≤ 20	
Reflections collected	9301	
Independent reflections	6353 [R(merge) = 0.072]	
Observed reflections	3614 [I > 3σ(I)]	
Absorption correction	Multi-scan (T <sub>min</sub> = 0.90, T <sub>max</sub> = 0.90)	
Structure solution by	direct and Fourier difference maps	
Hydrogen atom location	Calculated	
Hydrogen atom treatment	Constrained riding model	
Refinement method	Full-matrix least-squares on F <sup>2</sup>	
Weighting scheme	calculated	

Data / restraints / parameters	6329 / 12 / 236
Goodness-of-fit on F2	0.9723
Final R indices [ $I > 3 \sigma(I)$ ]	$R_1 = 0.0745$ , $R_w = 0.2052$
Final maximum delta/sigma	0.000495
Largest diff. peak and hole	1.29 and -1.17 e. $\text{\AA}^{-3}$

## 2. Bond lengths ( $\text{\AA}$ ) and angles ( $^\circ$ )

Sc(1)-Cl(1)	2.381(2)	Sc(1)-O(1)	2.136(3)
Sc(1)-N(1)	2.055(3)	Sc(1)-N(2)	2.037(3)
Si(1)-N(1)	1.732(4)	Si(1)-C(1)	1.864(5)
Si(1)-C(2)	1.866(4)	Si(1)-C(3)	1.864(5)
Si(2)-N(1)	1.728(4)	Si(2)-C(4)	1.867(4)
Si(2)-C(5)	1.871(5)	Si(2)-C(6)	1.854(5)
Si(3)-N(2)	1.725(4)	Si(3)-C(7)	1.866(5)
Si(3)-C(8)	1.865(4)	Si(3)-C(9)	1.883(5)
Si(4)-N(2)	1.730(4)	Si(4)-C(10)	1.866(5)
Si(4)-C(11)	1.879(5)	Si(4)-C(12)	1.867(5)
O(1)-C(13)	1.475(5)	O(1)-C(17)	1.475(5)
C(13)-C(14)	1.476(7)	C(14)-C(15)	1.571(13)
C(14)-C(16)	1.325(11)	C(15)-C(17)	1.462(11)
C(16)-C(17)	1.590(12)		
Cl(1)-Sc(1)-O(1)	95.52(10)	Cl(1)-Sc(1)-N(1)	114.46(11)
O(1)-Sc(1)-N(1)	97.51(12)	Cl(1)-Sc(1)-N(2)	108.42(10)
O(1)-Sc(1)-N(2)	109.59(14)	N(1)-Sc(1)-N(2)	126.03(14)
N(1)-Si(1)-C(1)	110.4(2)	N(1)-Si(1)-C(2)	114.9(2)
C(1)-Si(1)-C(2)	106.5(2)	N(1)-Si(1)-C(3)	111.4(2)
C(1)-Si(1)-C(3)	107.9(3)	C(2)-Si(1)-C(3)	105.3(3)
N(1)-Si(2)-C(4)	113.8(2)	N(1)-Si(2)-C(5)	109.7(2)
C(4)-Si(2)-C(5)	106.1(2)	N(1)-Si(2)-C(6)	112.1(2)
C(4)-Si(2)-C(6)	107.4(2)	C(5)-Si(2)-C(6)	107.4(2)
N(2)-Si(3)-C(7)	113.2(2)	N(2)-Si(3)-C(8)	113.6(2)

## Appendix

C(7)-Si(3)-C(8)	108.3(2)	N(2)-Si(3)-C(9)	108.4(2)
C(7)-Si(3)-C(9)	106.4(2)	C(8)-Si(3)-C(9)	106.6(2)
N(2)-Si(4)-C(10)	110.3(2)	N(2)-Si(4)-C(11)	113.1(2)
C(10)-Si(4)-C(11)	108.8(3)	N(2)-Si(4)-C(12)	111.6(2)
C(10)-Si(4)-C(12)	107.5(2)	C(11)-Si(4)-C(12)	105.1(2)
Sc(1)-O(1)-C(13)	126.9(3)	Sc(1)-O(1)-C(17)	123.7(2)
C(13)-O(1)-C(17)	109.1(3)	Sc(1)-N(1)-Si(1)	117.6(2)
Sc(1)-N(1)-Si(2)	119.4(2)	Si(1)-N(1)-Si(2)	123.0(2)
Sc(1)-N(2)-Si(4)	125.7(2)	Sc(1)-N(2)-Si(3)	110.7(2)
Si(4)-N(2)-Si(3)	121.8(2)	O(1)-C(13)-C(14)	105.7(4)
C(13)-C(14)-C(15)	106.5(5)	C(13)-C(14)-C(16)	106.8(6)
C(14)-C(15)-C(17)	102.2(8)	C(14)-C(16)-C(17)	107.9(8)
O(1)-C(17)-C(15)	106.2(5)	C(16)-C(17)-O(1)	99.6(5)

**[Nd(Ph-BOPA){NSiMe<sub>3</sub>}<sub>2</sub>]<sub>2</sub> (12a)****Crystal data and structure refinement.**

Empirical formula	C <sub>42</sub> H <sub>60</sub> N <sub>5</sub> NdO <sub>2</sub> Si <sub>4</sub>
Formula weight	923.55
Temperature	100(2) K
Wavelength	0.71073 Å
Crystal system, space group	Monoclinic, C2
Unit cell dimensions	$a = 21.7130(15)$ Å $\alpha = 90^\circ$ $b = 10.0823(7)$ Å $\beta = 105.315(7)^\circ$ $c = 21.2984(14)$ Å $\gamma = 90^\circ$
Volume	4497.0(5) Å <sup>3</sup>
Z, Calculated density	4, 1.364 Mg/m <sup>3</sup>
Absorption coefficient	1.301 mm <sup>-1</sup>
F(000)	1916
Crystal size	0.08 × 0.05 × 0.02 mm
Theta range for data collection	3.09 to 27.48 °
Limiting indices	-28 ≤ h ≤ 28, -13 ≤ k ≤ 11, -27 ≤ l ≤ 27
Reflections collected / unique	16161 / 9297 [R(int) = 0.0342]
Completeness to theta = 27.48	99.5 %
Absorption correction	Semi-empirical from equivalents
Max. and min. transmission	0.9745 and 0.9031
Refinement method	Full-matrix least-squares on F <sup>2</sup>
Data / restraints / parameters	9297 / 1 / 499
Goodness-of-fit on F <sup>2</sup>	1.111
Final R indices [I > 2σ(I)]	R <sub>1</sub> = 0.0313, wR <sub>2</sub> = 0.0710
R indices (all data)	R <sub>1</sub> = 0.0344, wR <sub>2</sub> = 0.0766
Absolute structure parameter	-0.002(9)
Largest diff. peak and hole	0.797 and -0.716 e.Å <sup>-3</sup>

**2. Bond lengths (Å) and angles (°)**

Nd(1)-N(5)	2.332(3)	Nd(1)-N(4)	2.360(3)
Nd(1)-N(1)	2.415(3)	Nd(1)-N(2)	2.535(4)
Nd(1)-N(3)	2.551(3)	Nd(1)-Si(3)	3.4236(10)
Si(1)-N(4)	1.710(4)	Si(1)-C(32)	1.852(5)
Si(1)-C(31)	1.869(5)	Si(1)-C(33)	1.879(4)
Si(2)-N(4)	1.714(4)	Si(2)-C(36)	1.857(5)
Si(2)-C(35)	1.881(4)	Si(2)-C(34)	1.886(4)
Si(3)-N(5)	1.698(4)	Si(3)-C(42)	1.866(4)
Si(3)-C(40)	1.871(5)	Si(3)-C(41)	1.882(5)
Si(4)-N(5)	1.714(4)	Si(4)-C(38)	1.865(4)
Si(4)-C(39)	1.873(5)	Si(4)-C(37)	1.873(5)
O(1)-C(7)	1.344(4)	O(1)-C(8)	1.443(6)
O(2)-C(22)	1.380(5)	O(2)-C(23)	1.443(5)
N(1)-C(1)	1.376(5)	N(1)-C(16)	1.397(4)
N(2)-C(7)	1.283(5)	N(2)-C(9)	1.504(5)
N(3)-C(22)	1.302(5)	N(3)-C(24)	1.478(5)
C(1)-C(2)	1.411(6)	C(1)-C(6)	1.424(5)
C(2)-C(3)	1.370(6)	C(3)-C(4)	1.388(5)
C(4)-C(5)	1.366(6)	C(5)-C(6)	1.403(6)
C(6)-C(7)	1.444(6)	C(8)-C(9)	1.532(6)
C(9)-C(10)	1.499(6)	C(10)-C(15)	1.375(6)
C(10)-C(11)	1.388(6)	C(11)-C(12)	1.370(6)
C(12)-C(13)	1.388(7)	C(13)-C(14)	1.364(7)
C(14)-C(15)	1.394(6)	C(16)-C(21)	1.415(6)
C(16)-C(17)	1.416(6)	C(17)-C(18)	1.369(5)
C(18)-C(19)	1.405(6)	C(19)-C(20)	1.372(6)
C(20)-C(21)	1.411(5)	C(21)-C(22)	1.442(5)
C(23)-C(24)	1.525(5)	C(24)-C(25)	1.509(6)
C(25)-C(26)	1.375(7)	C(25)-C(30)	1.383(6)
C(26)-C(27)	1.373(7)	C(27)-C(28)	1.379(9)
C(28)-C(29)	1.363(11)	C(29)-C(30)	1.363(8)



## Appendix

N(5)-Nd(1)-N(4)	117.50(12)	N(5)-Nd(1)-N(1)	110.03(11)
N(4)-Nd(1)-N(1)	132.39(11)	N(5)-Nd(1)-N(2)	128.78(12)
N(4)-Nd(1)-N(2)	82.03(11)	N(1)-Nd(1)-N(2)	70.12(11)
N(5)-Nd(1)-N(3)	90.45(11)	N(4)-Nd(1)-N(3)	106.12(11)
N(1)-Nd(1)-N(3)	69.97(11)	N(2)-Nd(1)-N(3)	131.50(11)
N(5)-Nd(1)-Si(3)	26.60(9)	N(4)-Nd(1)-Si(3)	128.73(9)
N(1)-Nd(1)-Si(3)	95.63(8)	N(2)-Nd(1)-Si(3)	103.40(8)
N(3)-Nd(1)-Si(3)	106.83(7)	N(4)-Si(1)-C(32)	112.7(2)
N(4)-Si(1)-C(31)	109.66(19)	C(32)-Si(1)-C(31)	107.8(2)
N(4)-Si(1)-C(33)	114.74(19)	C(32)-Si(1)-C(33)	105.8(2)
C(31)-Si(1)-C(33)	105.7(2)	N(4)-Si(2)-C(36)	114.4(2)
N(4)-Si(2)-C(35)	109.55(18)	C(36)-Si(2)-C(35)	107.8(2)
N(4)-Si(2)-C(34)	115.5(2)	C(36)-Si(2)-C(34)	103.3(2)
C(35)-Si(2)-C(34)	105.6(2)	N(5)-Si(3)-C(42)	113.6(2)
N(5)-Si(3)-C(40)	114.4(2)	C(42)-Si(3)-C(40)	106.7(2)
N(5)-Si(3)-C(41)	107.69(19)	C(42)-Si(3)-C(41)	108.6(3)
C(40)-Si(3)-C(41)	105.3(2)	N(5)-Si(3)-Nd(1)	37.96(12)
C(42)-Si(3)-Nd(1)	126.31(14)	C(40)-Si(3)-Nd(1)	125.90(13)
C(41)-Si(3)-Nd(1)	69.73(14)	N(5)-Si(4)-C(38)	113.14(19)
N(5)-Si(4)-C(39)	114.1(2)	C(38)-Si(4)-C(39)	104.8(2)
N(5)-Si(4)-C(37)	109.48(18)	C(38)-Si(4)-C(37)	109.0(2)
C(39)-Si(4)-C(37)	105.9(2)	C(7)-O(1)-C(8)	107.0(3)
C(22)-O(2)-C(23)	105.1(3)	C(1)-N(1)-C(16)	116.8(3)
C(1)-N(1)-Nd(1)	130.8(2)	C(16)-N(1)-Nd(1)	112.1(3)
C(7)-N(2)-C(9)	107.2(3)	C(7)-N(2)-Nd(1)	123.4(3)
C(9)-N(2)-Nd(1)	121.8(3)	C(22)-N(3)-C(24)	106.4(3)
C(22)-N(3)-Nd(1)	113.7(3)	C(24)-N(3)-Nd(1)	138.3(2)
Si(1)-N(4)-Si(2)	122.46(19)	Si(1)-N(4)-Nd(1)	119.27(18)
Si(2)-N(4)-Nd(1)	118.24(17)	Si(3)-N(5)-Si(4)	123.8(2)
Si(3)-N(5)-Nd(1)	115.43(19)	Si(4)-N(5)-Nd(1)	120.72(18)
N(1)-C(1)-C(2)	121.6(3)	N(1)-C(1)-C(6)	121.0(4)
C(2)-C(1)-C(6)	117.3(4)	C(3)-C(2)-C(1)	121.9(4)
C(2)-C(3)-C(4)	120.4(4)	C(5)-C(4)-C(3)	119.2(4)
C(4)-C(5)-C(6)	122.2(4)	C(5)-C(6)-C(1)	118.8(4)

## Appendix

C(5)-C(6)-C(7)	117.2(3)	C(1)-C(6)-C(7)	124.0(4)
N(2)-C(7)-O(1)	116.7(4)	N(2)-C(7)-C(6)	128.0(3)
O(1)-C(7)-C(6)	115.2(3)	O(1)-C(8)-C(9)	104.1(3)
C(10)-C(9)-N(2)	114.4(3)	C(10)-C(9)-C(8)	113.3(4)
N(2)-C(9)-C(8)	101.9(3)	C(15)-C(10)-C(11)	118.6(4)
C(15)-C(10)-C(9)	118.9(4)	C(11)-C(10)-C(9)	122.4(4)
C(12)-C(11)-C(10)	120.6(4)	C(11)-C(12)-C(13)	120.6(5)
C(14)-C(13)-C(12)	119.2(5)	C(13)-C(14)-C(15)	120.2(5)
C(10)-C(15)-C(14)	120.7(4)	N(1)-C(16)-C(21)	122.5(4)
N(1)-C(16)-C(17)	120.2(4)	C(21)-C(16)-C(17)	117.3(3)
C(18)-C(17)-C(16)	121.7(4)	C(17)-C(18)-C(19)	120.0(4)
C(20)-C(19)-C(18)	120.3(4)	C(19)-C(20)-C(21)	120.1(4)
C(20)-C(21)-C(16)	120.5(4)	C(20)-C(21)-C(22)	118.0(4)
C(16)-C(21)-C(22)	121.2(3)	N(3)-C(22)-O(2)	115.1(3)
N(3)-C(22)-C(21)	129.1(4)	O(2)-C(22)-C(21)	115.7(3)
O(2)-C(23)-C(24)	103.0(3)	N(3)-C(24)-C(25)	111.5(3)
N(3)-C(24)-C(23)	101.8(3)	C(25)-C(24)-C(23)	112.6(3)
C(26)-C(25)-C(30)	117.5(4)	C(26)-C(25)-C(24)	123.6(4)
C(30)-C(25)-C(24)	118.7(5)	C(27)-C(26)-C(25)	121.2(5)
C(26)-C(27)-C(28)	120.1(6)	C(29)-C(28)-C(27)	119.3(5)
C(30)-C(29)-C(28)	120.4(5)	C(29)-C(30)-C(25)	121.6(6)

**[Sm(Ph-BOPA){NSiMe<sub>3</sub>}<sub>2</sub>]<sub>2</sub> (13a)****Crystal data and structure refinement.**

Empirical formula	C <sub>42</sub> H <sub>60</sub> N <sub>5</sub> O <sub>2</sub> Si <sub>4</sub> Sm
Formula weight	929.66
Temperature	100(2)
Wavelength	0.71075 Å
Crystal system, space group	Monoclinic, C2
Unit cell dimensions	$a = 21.7225(11)$ Å $\alpha = 90^\circ$ $b = 10.0865(3)$ Å $\beta = 105.020(10)^\circ$ $c = 21.249(2)$ Å $\gamma = 90^\circ$
Volume	4496.6(5) Å <sup>3</sup>
Z, Calculated density	4, 1.373 Mg/m <sup>3</sup>
Absorption coefficient	1.452 mm <sup>-1</sup>
F(000)	1924
Crystal size	0.15 × 0.09 × 0.04 mm
$\theta$ range for data collection	3.11 to 27.48 °
Limiting indices	-28 ≤ h ≤ 25, -12 ≤ k ≤ 13, -25 ≤ l ≤ 27
Reflections collected / unique	30002 / 10248 [R(int) = 0.0312]
Completeness to $\theta = 27.48$	99.8%
Absorption correction	Semi-empirical from equivalents
Max. and min. transmission	0.9442 and 0.8116
Refinement method	Full-matrix least-squares on F <sup>2</sup>
Data / restraints / parameters	10248 / 1 / 499
Goodness-of-fit on F <sup>2</sup>	1.068
Final R indices [I > 2σ(I)]	R <sub>1</sub> = 0.0202, wR <sub>2</sub> = 0.0439
R indices (all data)	R <sub>1</sub> = 0.0216, wR <sub>2</sub> = 0.0453
Absolute structure parameter	-0.008(4)
Largest diff. peak and hole	0.394 and -0.494 e.Å <sup>-3</sup>

**2. Bond lengths [Å] and angles [°].**

Sm(1)-N(4)	2.3007(19)	Sm(1)-N(5)	2.3430(19)
Sm(1)-N(1)	2.3874(18)	Sm(1)-N(3)	2.5062(18)
Sm(1)-N(2)	2.5286(19)	Sm(1)-Si(1)	3.4105(7)
Si(1)-N(4)	1.713(2)	Si(1)-C(32)	1.869(3)
Si(1)-C(33)	1.869(2)	Si(1)-C(31)	1.885(3)
Si(2)-N(4)	1.713(2)	Si(2)-C(35)	1.872(3)
Si(2)-C(34)	1.877(3)	Si(2)-C(36)	1.881(3)
Si(3)-N(5)	1.7093(19)	Si(3)-C(38)	1.873(3)
Si(3)-C(37)	1.874(3)	Si(3)-C(39)	1.894(3)
Si(4)-N(5)	1.710(2)	Si(4)-C(40)	1.864(3)
Si(4)-C(41)	1.867(2)	Si(4)-C(42)	1.875(3)
O(1)-C(7)	1.362(3)	O(1)-C(8)	1.451(3)
O(2)-C(22)	1.354(3)	O(2)-C(23)	1.447(3)
N(1)-C(16)	1.374(3)	N(1)-C(1)	1.407(3)
N(2)-C(7)	1.296(3)	N(2)-C(9)	1.483(3)
N(3)-C(22)	1.289(3)	N(3)-C(24)	1.494(3)
C(1)-C(2)	1.407(3)	C(1)-C(6)	1.415(3)
C(2)-C(3)	1.370(3)	C(3)-C(4)	1.397(3)
C(4)-C(5)	1.373(3)	C(5)-C(6)	1.403(3)
C(6)-C(7)	1.451(3)	C(8)-C(9)	1.525(3)
C(9)-C(10)	1.518(3)	C(10)-C(15)	1.376(4)
C(10)-C(11)	1.384(4)	C(11)-C(12)	1.385(4)
C(12)-C(13)	1.370(5)	C(13)-C(14)	1.372(6)
C(14)-C(15)	1.369(4)	C(16)-C(21)	1.414(3)
C(16)-C(17)	1.417(3)	C(17)-C(18)	1.376(3)
C(18)-C(19)	1.392(3)	C(19)-C(20)	1.372(3)
C(20)-C(21)	1.409(3)	C(21)-C(22)	1.452(3)
C(23)-C(24)	1.519(4)	C(24)-C(25)	1.511(3)
C(25)-C(30)	1.381(3)	C(25)-C(26)	1.388(3)
C(26)-C(27)	1.385(3)	C(27)-C(28)	1.388(4)
C(28)-C(29)	1.377(4)	C(29)-C(30)	1.392(3)

N(4)-Sm(1)-N(5)	115.92(6)	N(4)-Sm(1)-N(1)	109.92(7)
N(5)-Sm(1)-N(1)	134.10(6)	N(4)-Sm(1)-N(3)	128.44(7)
N(5)-Sm(1)-N(3)	82.30(6)	N(1)-Sm(1)-N(3)	71.07(6)
N(4)-Sm(1)-N(2)	89.77(6)	N(5)-Sm(1)-N(2)	106.42(6)
N(1)-Sm(1)-N(2)	70.70(6)	N(3)-Sm(1)-N(2)	133.20(6)
N(4)-Sm(1)-Si(1)	26.93(5)	N(5)-Sm(1)-Si(1)	127.54(5)
N(1)-Sm(1)-Si(1)	95.15(5)	N(3)-Sm(1)-Si(1)	102.94(5)
N(2)-Sm(1)-Si(1)	106.40(5)	N(4)-Si(1)-C(32)	114.42(11)
N(4)-Si(1)-C(33)	113.62(12)	C(32)-Si(1)-C(33)	106.61(12)
N(4)-Si(1)-C(31)	107.83(11)	C(32)-Si(1)-C(31)	105.44(12)
C(33)-Si(1)-C(31)	108.49(15)	N(4)-Si(1)-Sm(1)	37.47(6)
C(32)-Si(1)-Sm(1)	125.93(9)	C(33)-Si(1)-Sm(1)	126.27(8)
C(31)-Si(1)-Sm(1)	70.37(8)	N(4)-Si(2)-C(35)	113.43(10)
N(4)-Si(2)-C(34)	109.82(11)	C(35)-Si(2)-C(34)	108.54(12)
N(4)-Si(2)-C(36)	114.49(12)	C(35)-Si(2)-C(36)	104.22(12)
C(34)-Si(2)-C(36)	105.87(13)	N(5)-Si(3)-C(38)	109.74(11)
N(5)-Si(3)-C(37)	114.35(12)	C(38)-Si(3)-C(37)	107.98(13)
N(5)-Si(3)-C(39)	115.26(11)	C(38)-Si(3)-C(39)	105.92(12)
C(37)-Si(3)-C(39)	102.97(13)	N(5)-Si(4)-C(40)	112.77(11)
N(5)-Si(4)-C(41)	110.27(10)	C(40)-Si(4)-C(41)	107.19(12)
N(5)-Si(4)-C(42)	114.91(11)	C(40)-Si(4)-C(42)	105.52(12)
C(41)-Si(4)-C(42)	105.64(12)	C(7)-O(1)-C(8)	105.35(17)
C(22)-O(2)-C(23)	106.39(18)	C(16)-N(1)-C(1)	116.88(18)
C(16)-N(1)-Sm(1)	130.00(15)	C(1)-N(1)-Sm(1)	112.81(13)
C(7)-N(2)-C(9)	106.10(19)	C(7)-N(2)-Sm(1)	114.63(15)
C(9)-N(2)-Sm(1)	137.93(14)	C(22)-N(3)-C(24)	107.28(19)
C(22)-N(3)-Sm(1)	121.97(15)	C(24)-N(3)-Sm(1)	122.88(14)
Si(1)-N(4)-Si(2)	122.60(11)	Si(1)-N(4)-Sm(1)	115.60(9)
Si(2)-N(4)-Sm(1)	121.78(10)	Si(3)-N(5)-Si(4)	122.38(11)
Si(3)-N(5)-Sm(1)	119.29(10)	Si(4)-N(5)-Sm(1)	118.32(9)
C(2)-C(1)-N(1)	119.8(2)	C(2)-C(1)-C(6)	117.8(2)
N(1)-C(1)-C(6)	122.4(2)	C(3)-C(2)-C(1)	121.5(2)
C(2)-C(3)-C(4)	120.4(2)	C(5)-C(4)-C(3)	119.5(2)
C(4)-C(5)-C(6)	121.0(2)	C(5)-C(6)-C(1)	119.8(2)

## Appendix

C(5)-C(6)-C(7)	118.6(2)	C(1)-C(6)-C(7)	121.3(2)
N(2)-C(7)-O(1)	116.0(2)	N(2)-C(7)-C(6)	128.7(2)
O(1)-C(7)-C(6)	115.3(2)	O(1)-C(8)-C(9)	102.64(18)
N(2)-C(9)-C(10)	111.96(19)	N(2)-C(9)-C(8)	101.75(19)
C(10)-C(9)-C(8)	111.7(2)	C(15)-C(10)-C(11)	118.6(2)
C(15)-C(10)-C(9)	118.8(2)	C(11)-C(10)-C(9)	122.5(2)
C(10)-C(11)-C(12)	119.9(3)	C(13)-C(12)-C(11)	120.8(3)
C(12)-C(13)-C(14)	119.1(3)	C(15)-C(14)-C(13)	120.5(3)
C(14)-C(15)-C(10)	121.1(3)	N(1)-C(16)-C(21)	121.9(2)
N(1)-C(16)-C(17)	121.1(2)	C(21)-C(16)-C(17)	116.8(2)
C(18)-C(17)-C(16)	121.7(2)	C(17)-C(18)-C(19)	121.0(2)
C(20)-C(19)-C(18)	118.7(2)	C(19)-C(20)-C(21)	121.6(2)
C(20)-C(21)-C(16)	120.1(2)	C(20)-C(21)-C(22)	117.0(2)
C(16)-C(21)-C(22)	122.9(2)	N(3)-C(22)-O(2)	116.3(2)
N(3)-C(22)-C(21)	128.9(2)	O(2)-C(22)-C(21)	114.77(19)
O(2)-C(23)-C(24)	104.4(2)	N(3)-C(24)-C(25)	113.7(2)
N(3)-C(24)-C(23)	102.56(19)	C(25)-C(24)-C(23)	112.9(2)
C(30)-C(25)-C(26)	118.9(2)	C(30)-C(25)-C(24)	118.8(2)
C(26)-C(25)-C(24)	122.1(2)	C(27)-C(26)-C(25)	120.3(2)
C(26)-C(27)-C(28)	120.3(2)	C(29)-C(28)-C(27)	119.7(2)
C(28)-C(29)-C(30)	119.7(2)	C(25)-C(30)-C(29)	121.0(2)

**Appendix B - Publications from this thesis**

Near-IR luminescent neodymium complexes:  
spectroscopic probes for hydroamination catalysis†

Stacey D. Bennett, Simon J. A. Pope and Benjamin D. Ward\*

Cite this: *Chem. Commun.*, 2013, **49**, 6072Received 19th April 2013,  
Accepted 24th May 2013

DOI: 10.1039/c3cc42923g

www.rsc.org/chemcomm

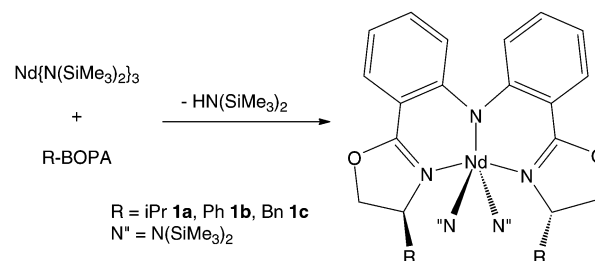
Neodymium complexes bearing the sensitising bis(oxazolinyphenyl)amine (BOPA) ligands have been prepared, and analysed spectroscopically under both catalytic and *pseudo*-catalytic conditions with respect to the intramolecular hydroamination of an aminoalkene, providing a direct means of monitoring binding events and relative space around the metal centre.

Rare-earth metal complexes have many applications in catalysis, including hydroamination.<sup>1</sup> The presence of partially occupied, low-lying 4f orbitals also gives them unique spectroscopic properties. The formally forbidden f–f transitions are notably sharp compared to many other fluorescence systems, and the long near-IR wavelength provides an emission profile that is largely free from environmentally emissive ‘pollution’.<sup>2</sup>

The spectroscopic fingerprint of a luminescent lanthanide ion (*i.e.* spectral profile and lifetime of f-centred emission) is uniquely sensitive to the local coordination environment.<sup>3</sup> In particular, the lifetime provides information on the relative shielding of the ion from bound and unbound proximate quenchers, such as O–H, N–H and C–H oscillators,<sup>4</sup> present in solvents, (bound) substrates, ligand architectures, and/or the proximity of stereodirecting groups. This parameter may therefore provide reportage on the space at the metal centre in which catalytic reactions take place, and may provide critical information relating to the short-lived species that lie beyond the detection limit of many other analytical techniques.<sup>5</sup>

Our goal in this study was to use the luminescent properties of Nd(III) to probe the intricate nature of chiral complexes, providing information that cannot be obtained using other spectroscopic techniques, and to relate this information to their behaviour in hydroamination/cyclisation catalysis.

The bis(oxazolinyphenyl)amine (BOPA) series of ligands<sup>6</sup> are able to efficiently sensitise the metal-centred excited states of neodymium,

Scheme 1 Preparation of [Nd(R-BOPA)(N(SiMe<sub>3</sub>)<sub>2</sub>)<sub>2</sub>] **1a–c**.

such that the resultant near-IR photophysical properties can be used to probe the complexes under conditions relevant to catalytic reactions. In their anionic form, these ligands possess conjugated amides coordinated to the lanthanide in an ideal position to aid investigations into the luminescence properties of the species.

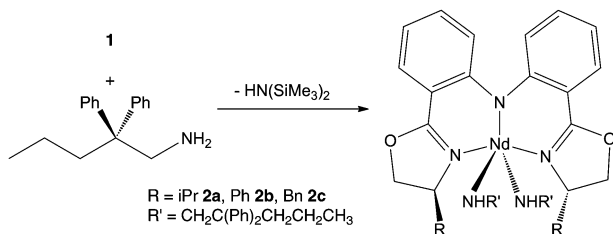
The protio-ligands react with the neodymium precursor [Nd{N(SiMe<sub>3</sub>)<sub>2</sub>}<sub>3</sub>] to afford the five-coordinate complexes [Nd(R-BOPA){N(SiMe<sub>3</sub>)<sub>2</sub>}<sub>2</sub>] (R = *i*Pr **1a**, Ph **1b**, Bn **1c**) (Scheme 1). The <sup>1</sup>H NMR data of the paramagnetic complexes were found to give relatively sharp signals with an expected reduction in fine structure and an increase in chemical shift range (*ca.* 20 to –40 ppm).<sup>7</sup> The overall molecular symmetry, number of resonances, and their relative intensity are fully consistent with the proposed structures. The resonance attributed to the two equivalent N(SiMe<sub>3</sub>)<sub>2</sub> ligands is a distinctive, large singlet in the range of –5.96 to –5.93 ppm. The structure of [Nd(Ph-BOPA){N(SiMe<sub>3</sub>)<sub>2</sub>}<sub>2</sub>] **1b** has been confirmed by X-ray crystallography; X-ray data are included in the ESI.†<sup>8</sup>

Complexes **1a–c** were employed in the catalytic hydroamination of aminoalkenes (*vide infra*). The catalyst resting state for this reaction (*i.e.* a tethered amidoalkene) is well understood,<sup>9</sup> but cannot be isolated owing to the intramolecular nature of the reaction. Therefore model complexes were prepared that suppress the catalytic turnover by removing the C=C from the substrate. The resulting complexes were prepared using the *pseudo* substrate 2,2'-diphenyl-aminopentane, to afford [Nd(R-BOPA){NHCH<sub>2</sub>C(Ph)<sub>2</sub>Pr'}<sub>2</sub>] (R = *i*Pr **2a**, Ph **2b**, Bn **2c**) according to Scheme 2. The <sup>1</sup>H NMR data of complexes **3a–c** showed similar features to the spectra of **1a–c** in terms of the overall C<sub>2</sub> symmetry of the complexes. In comparison to the data obtained for

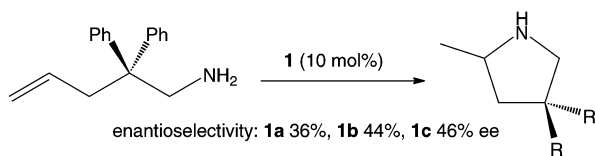
School of Chemistry, Cardiff University, Main Building, Park Place, Cardiff CF10 3AT, UK. E-mail: WardBD@Cardiff.ac.uk; Fax: +44 (0)29 208 74030; Tel: +44 (0)29 208 70302

† Electronic supplementary information (ESI) available: Full experimental procedures, crystal, computational and characterising data for all new complexes. CCDC 903609. For ESI and crystallographic data in CIF or other electronic format see DOI: 10.1039/c3cc42923g





**Scheme 2** Preparation of  $[\text{Nd}(\text{R-BOPA})(\text{NHCH}_2\text{C}(\text{Ph})_2\text{Pr})]_2$  **2a-c**.



**Scheme 3** Catalytic hydroamination using  $[\text{Nd}(\text{R-BOPA})(\text{N}(\text{SiMe}_3)_2)_2]$ .

complexes **1a-c** the signal assigned to the silylamide co-ligands was absent from the spectra of **2a-c**.

The spectroscopic analysis of these complexes can only provide adequate information relating to their catalytic performance if supported by a clear demonstration of their implementation in the catalytic reaction being studied. Consequently, complexes **1a-c** were employed in the hydroamination/cyclisation of 2,2'-diphenyl-amino-pent-4-ene in toluene- $d_8$  using 10 mol% catalyst at 25 °C (Scheme 3).<sup>10</sup> All reactions proceeded to quantitative conversion and with moderate enantioselectivities. The phenyl and benzyl derivatives **1b** and **1c** gave essentially identical enantiomeric excesses of 44–46%, whereas the isopropyl congener **1a** gave a lower level of selectivity (36%). These moderate levels of selectivity can be reasonably explained by the presence of two isomeric forms of the complexes (which the luminescence studies would suggest pertain during the catalytic reaction and that have been identified computationally, *vide infra*), particularly where one of the components moves the stereodirecting groups away from the expected site of alkene insertion.

Solutions of **1a-c** (toluene,  $10^{-4}$  M,  $\text{N}_2$  atmosphere) were investigated from a photophysical standpoint and are described as dual emissive. Irradiation ( $\lambda_{\text{ex}} = 485$  nm) induced visible emission from the complexes, typically characterised by a broad, unstructured luminescence band peaking between 500–510 nm with a small associated Stokes' shift (*ca.* 1000  $\text{cm}^{-1}$ ).<sup>11</sup> The precise positioning of the band and the fluorescence lifetime (5.0, 4.6 and 4.5 ns, for  $\text{R} = \text{iPr}$ ,  $\text{Ph}$  and  $\text{Bn}$  respectively) were subtly dependent on the specific composition of the ligand. The diphenylamine anion is known to be non-emissive,<sup>12</sup> and therefore the visible fluorescence was attributed to a ligand-centred excited state with a contributing charge transfer (N-to- $\pi^*$ ) component originating from the deprotonated/coordinated amide bridge-head.

Irradiation of solutions **1a-c** at 445 nm also induced sensitised near-IR emission from each of the Nd(III) complexes, with characteristic bands attributed to the  ${}^4\text{F}_{3/2}\text{-}{}^4\text{I}_{9/2}$ ,  ${}^4\text{F}_{3/2}\text{-}{}^4\text{I}_{11/2}$  and  ${}^4\text{F}_{3/2}\text{-}{}^4\text{I}_{13/2}$  transitions. The corresponding lifetime measurements were also obtained ( $\lambda_{\text{em}} = 1055$  nm) and are shown in Table 1; the magnitude of the values are consistent with Nd(III)-centred emission, and each profile fitted reasonably well to a bi-exponential decay yielding two distinct lifetime values. These data suggest that each of the

**Table 1** Lifetime measurements for  $[\text{Nd}(\text{R-BOPA})(\text{N}(\text{SiMe}_3)_2)_2]$  and related complexes (toluene,  $\text{N}_2$ ;  $\lambda_{\text{ex}} = 355$  nm;  $\lambda_{\text{em}} = 1055$  nm)

Compound	Lifetimes ( $\tau$ )/ns		
	+2,2-Diphenyl-aminopentane	+2,2-Diphenyl-aminopentene	
<b>1a</b>	148, 621 (70%)	111, 267 (59%) ( <b>2a</b> )	—
<b>1b</b>	129, 677 (90%)	71, 165 (90%) ( <b>2b</b> )	—
<b>1c</b>	41, 308 (80%)	41, 182 (93%) ( <b>2c</b> )	81, 252 (85%)

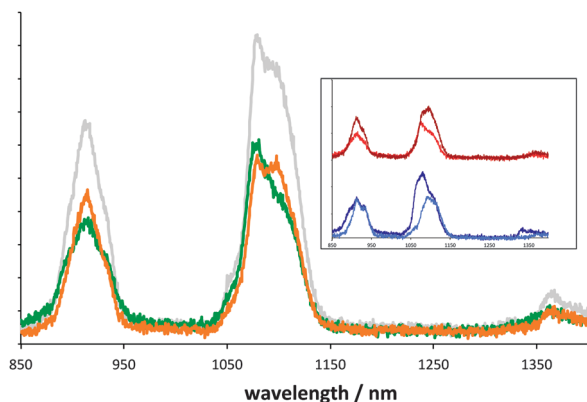
complexes  $[\text{Nd}(\text{R-BOPA})(\text{N}(\text{SiMe}_3)_2)_2]$  (**1a-c**) exists in (at least) two distinct environments. The fact that the analytical and NMR data suggest a single pure complex suggests that these species are likely to be interconverting isomers.

The lifetimes of the two species are remarkably different, and suggest that the main component represents a well-shielded Nd(III) centre, possibly representative of the X-ray structure. The second component (10–30% relative weighting) has a significantly shorter lifetime and suggests a species that is more readily quenched (*i.e.* by proximate C–H oscillators), possibly arising from a ligand conformation that renders the metal more accessible to solvent molecules. The lifetimes for the isopropyl and phenyl derivatives **1a** and **1b** are similar, suggesting a comparable environment around the Nd(III) centre, whereas the lifetimes for the benzyl derivative **1c** are shorter, implying less effective shielding. This may originate in the greater flexibility of a benzyl (at the methylene group) relative to phenyl and isopropyl groups, which are generally more rigid.

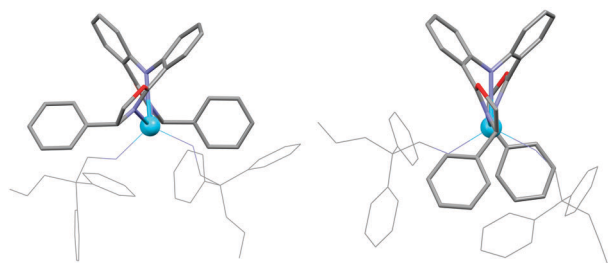
Importantly, the relative intensity of the emission bands of Nd(III) are known to be sensitive to the local coordination environment,<sup>3,13</sup> suggesting that changes in either ligand type or ligand arrangement will modulate the emission profile of a luminescent Nd(III) complex. In this context, addition of the saturated *pseudo*-substrate (2,2'-diphenyl-aminopentane) to form **2a-c**, subsequently showed a definitive and measurable change in spectral emission profile (in terms of peak position, profile and integrated intensity, Fig. 1), as well as significant alterations in Nd(III) lifetime. Such observations are clearly indicative of changes in the coordination environment and thus consistent with the bis(trimethylsilyl)amide ligands exchanging with the 2,2'-diphenyl-aminopentane ligands, establishing that coordination to the Nd(III) must occur *via* the terminal amino group of the *pseudo*-substrate. The dominant lifetime components for **2a-c** are significantly shortened compared to **1a-c** and consistent with a ligand substitution that would introduce N–H oscillators into the coordination sphere and reduce the steric crowding at Nd(III).

During the catalytic hydroamination reaction, the proposed cyclised intermediate is coordinated to Nd(III) *via* a methylene unit.<sup>9</sup> Therefore the actual catalytic substrate, 2,2'-diphenyl-amino-pent-4-ene, was also used with **2c** and, again, revealed modulation of the emission profile and shortening of the dominant lifetime component to 252 ns. Again, these observations are consistent with a substrate binding event, but one that is distinct from the *pseudo*-substrate. The lifetime data for this mixture can therefore be differentiated from both the free complex (**1c**) and the speciation of the saturated substrate analogue (**2c**).

The identity of the two components of **2a-c** (and by extension **1a-c**) was probed by calculating the structures of the La(III) congeners; the structures of **La-2b** are shown in Fig. 2.



**Fig. 1** Near-IR luminescence spectra ( $10^{-4}$  M toluene,  $\lambda_{\text{ex}}$  445 nm). Main: **1c** (green), **2c** (orange), **1c** + 2,2'-diphenyl-amino-pentene (grey). Inset: comparison **1a/2a** (light blue/dark blue) and **1b/2b** (red/brown).



**Fig. 2** Calculated *exo* (left) and *endo* (right) isomers of **La-2b**.

Calculations suggest that each of the complexes exist in two energetically accessible forms, each with a different sense of helical twist in the diphenyl backbone of the BOPA ligands, giving both *exo* and *endo* isomers with respect to the orientation of the stereodirecting groups. The *exo* isomer is consistent with the X-ray data, and is computationally favoured. It can be seen from Fig. 2 that the metal centre in the *endo* isomer is significantly less shielded than the *exo* isomer, and would therefore be more accessible to solvent molecules, accounting for the observed difference in the lifetimes of the two components. Additionally, the relative steric encumbrance of the stereodirecting group is evident, showing that the isopropyl offers the least steric demand and therefore is expected to give less energetic distinction between the isomeric forms, as observed experimentally by luminescence spectroscopy (Table 1).

The *exo* isomer of a given ligand derivative places the stereodirecting groups in the equatorial plane of the coordination sphere, shielding the metal centre to a greater extent than the *endo* isomer, which possesses a significant space that is largely unaffected by the ligand periphery (*i.e.* stereodirecting group). The *exo* isomer therefore possesses a better-defined chiral space at the coordination sphere, and is more likely to efficiently transfer chiral information to the catalytic substrates. We propose therefore that the relative proportion of these isomers is likely to be a significant contributor to the effectiveness of these complexes to evoke stereoselectivity in catalysis. The experimental data, showing that a higher proportion of the *exo* isomer is found for the catalyst that generates the highest enantiomeric excess,

supports this theory; however this does not contradict the effects of varying the size of the stereodirecting group. Rather, these studies show evidence of additional processes taking place at the molecular level that contribute to the overall effect of controlling stereoselectivity in catalysis.

The photophysics of luminescent neodymium complexes have been used to directly probe the metal species in the catalytic system, with emission profiles before, during, and after giving distinct luminescence signatures. The luminescence studies indicate the presence of different conformations of the complex in solution that are not apparent using NMR spectroscopy and X-ray crystallography. We propose that the presence of these conformations is a key aspect for explaining the relative stereocontrol offered by the different catalyst derivatives.

We thank Cardiff University (Endowment Fellowship to SDB and access to computing facilities "ARCCA"), the Leverhulme Trust, and the EPSRC crystallographic service for support.

## Notes and references

- (a) B. D. Ward and L. H. Gade, *Chem. Commun.*, 2012, **48**, 10587; (b) S. Hong and T. J. Marks, *Acc. Chem. Res.*, 2004, **37**, 673; (c) G. A. Molander and J. A. C. Romero, *Chem. Rev.*, 2002, **102**, 2161; (d) Z. Hou and Y. Wakatsuki, *Coord. Chem. Rev.*, 2002, **231**, 1.
- J.-C. G. Bünzli and S. V. Eliseeva, *Chem. Sci.*, 2013, **4**, 1939.
- (a) J.-C. G. Bünzli, A.-S. Chauvin, H. K. Kim, E. Dieters and S. V. Eliseeva, *Coord. Chem. Rev.*, 2010, **254**, 2623; (b) S. Faulkner, S. J. A. Pope and B. P. Burton-Pye, *Appl. Spectrosc. Rev.*, 2005, **40**, 1.
- (a) W. D. Horrocks Jr. and D. R. Sudnick, *Acc. Chem. Res.*, 1981, **14**, 384; (b) E. G. Moore, A. P. S. Samuel and K. N. Raymond, *Acc. Chem. Res.*, 2009, **42**, 542; (c) A. Beeby, I. M. Clarkson, R. S. Dickins, S. Faulkner, D. Parker, L. Royle, A. S. de Sousa, J. A. G. Williams and M. Woods, *J. Chem. Soc., Perkin Trans. 2*, 1999, 493.
- (a) X. Zhu, W.-K. Wong, W.-Y. Wong and X. Yang, *Eur. J. Inorg. Chem.*, 2011, 4651; (b) B. K. McMahon and T. Gunnlaugsson, *J. Am. Chem. Soc.*, 2012, **134**, 10725; (c) W. Chen, B. D. Wright and Y. Pang, *Chem. Commun.*, 2012, **48**, 3824.
- (a) H. A. McManus and P. J. Guiry, *J. Org. Chem.*, 2002, **67**, 8566; (b) S.-F. Lu, D.-M. Du, S.-W. Zhang and J. Xu, *Tetrahedron: Asymmetry*, 2004, **15**, 3433; (c) H. A. McManus, P. G. Cozzi and P. J. Guiry, *Adv. Synth. Catal.*, 2006, **348**, 551; (d) T. Inagaki, L. T. Phong, A. Furuta, J.-I. Ito and H. Nishiyama, *Chem.-Eur. J.*, 2010, **16**, 3090.
- (a) L. Lukešová, B. D. Ward, S. Bellemín-Lapponnaz, H. Wadepohl and L. H. Gade, *Dalton Trans.*, 2007, 920; (b) L. Lukešová, B. D. Ward, S. Bellemín-Lapponnaz, H. Wadepohl and L. H. Gade, *Organometallics*, 2007, **26**, 4652.
- X-ray data were collected by the EPSRC National Crystallographic Service: S. J. Coles and P. A. Gale, *Chem. Sci.*, 2012, **3**, 683.
- (a) M. R. Gagnè, C. L. Stern and T. J. Marks, *J. Am. Chem. Soc.*, 1992, **114**, 275; (b) Y. Li and T. J. Marks, *J. Am. Chem. Soc.*, 1996, **118**, 9295; (c) A. Motta, G. Lanza, I. L. Fragalà and T. J. Marks, *Organometallics*, 2004, **23**, 4097.
- For selected examples of asymmetric hydroamination catalysis using lanthanides see: (a) Y. Li and T. J. Marks, *Acc. Chem. Res.*, 2004, **37**, 673; (b) S. Hong, S. Tian, M. V. Metz and T. J. Marks, *J. Am. Chem. Soc.*, 2003, **125**, 14768; (c) P. N. O'Shaughnessy and P. Scott, *Tetrahedron: Asymmetry*, 2003, **14**, 1979; (d) P. N. O'Shaughnessy, P. D. Knight, C. Morton, K. M. Gillespie and P. Scott, *Chem. Commun.*, 2003, 1770; (e) P. N. O'Shaughnessy, K. M. Gillespie, P. D. Knight, I. J. Munslow and P. Scott, *Dalton Trans.*, 2004, 2251.
- For a comprehensive and authoritative review of issues relating to fluorescence see J. R. Lakowitz, *Principles of Fluorescence Spectroscopy*, Springer, New York, third edn, 2006.
- N. Chattopadhyay, A. Samanta, T. Kundu and M. Chowdhury, *J. Photochem. Photobiol., A*, 1989, **48**, 61.
- S. J. A. Pope, B. P. Burton-Pye, R. Berridge, T. Khan, P. J. Skabara and S. Faulkner, *Dalton Trans.*, 2006, 2907.